

STELLAR X-RAY POLARIMETRY FROM

THE ARIEL-V SATELLITE

by

Robert A. Gowen, B.Sc., M.Sc.

A thesis submitted to the
University of Leicester
for the degree of
Doctor of Philosophy

1977

X-ray Astronomy Group,
Physics Department,
University of Leicester.

UMI Number: U641561

All rights reserved

INFORMATION TO ALL USERS

The quality of this reproduction is dependent upon the quality of the copy submitted.

In the unlikely event that the author did not send a complete manuscript and there are missing pages, these will be noted. Also, if material had to be removed, a note will indicate the deletion.



UMI U641561

Published by ProQuest LLC 2015. Copyright in the Dissertation held by the Author.
Microform Edition © ProQuest LLC.

All rights reserved. This work is protected against
unauthorized copying under Title 17, United States Code.



ProQuest LLC
789 East Eisenhower Parkway
P.O. Box 1346
Ann Arbor, MI 48106-1346

THESIS
548748
3 5 78



x753009225

TO

MUM AND DAD

ABSTRACT

X-ray polarisation observations from the Ariel-V satellite are described. Notably, an upper limit to the X-ray polarisation of Sco X-1 was produced, more sensitive than previous results had managed to achieve, and for which constraints could be placed upon models for the X-ray emission mechanism.

Analysis of the data provided strong empirical confirmation of the desirability for future polarimeters to incorporate some previously proposed design features. These include utilisation of focusing methods to allow a smaller detector, and hence a reduced background level; increased area of collection, so that much weaker X-ray sources may be usefully observed; and also sufficiently accurate pointing, narrow f.o.v. and a capability for simultaneous measurement of more than one component of linear polarisation, all to suppress possible spurious modulations. It would be expected that the advantages obtained by following the advocated design features would result in a polarimeter sufficiently sensitive to be able to measure X-ray polarisation from weak X-ray sources, and to achieve accuracies that have not yet been remotely approached.

Characteristics of a Bragg crystal instrument capable of a sufficient degree of broad band X-ray polarimetry to test for the existence of a fast rotating black hole in the Cyg X-1 system, are also described.

Finally, the need for X-ray polarisation measurements throughout the field of current X-ray astronomy is illuminated.

ACKNOWLEDGMENTS

I would like to stress that the successful launch of a satellite experiment is a collaborative undertaking, and take this opportunity to thank all those, most of whom I do not know, involved with the planning, satellite construction, launch and continuing post launch operations, and for the finance of such an adventure.

The spectrometer/polarimeter experiment was also a collaborative undertaking, and rather than have this work represent just a fragment of that project, I have brought together as much information as possible so that a clear overall picture could be obtained in one volume. For this reason I would like to acknowledge much work described here which has been accomplished by other members of the Leicester X-ray astronomy group. In particular, Dr. Dave Adams, Dr. Brin Cooke and Prof. Ken Pounds for their early work in planning this experiment, and those, Dr. Brin Cooke, Mr. Arthur Rate, Mr. John Spragg, Dr. Martin Ricketts, Dr. Bill Parkes, Dr. Kenton Evans, and the engineering staff for construction and calibration of the experiment. I am also grateful to Dr. Anthony Peacock for his basic description of the instrument, upon which the description presented in § 3.2 is largely based, and for early guidance with the polarimetry data analysis.

I thank Mr. Gavin Eadie, Dr. Martin Turner, Dr. Clive Page, Dr. Russell Silk and Mr. John Lee for much of the basic programming tasks without which the raw data from the satellite would still be in complicated code.

For much of the early polarimeter analysis I acknowledge again Dr. Martin Ricketts and Dr. Anthony Peacock; and for analysis of the A0620-00 data, included here for completeness, Drs. Richard Griffiths and Martin Ricketts; and again Richard for helpful discussion concerned with interpretation of the polarisation results.

Clarifying and useful discussions have also been undertaken with Dr. Kenton Evans, Prof. Beeby, Dr. Dave Adams, Dr. Martin Turner, Mr. Jim Morris of the computer department, and my supervisor, Dr. Brin Cooke.

I am also very grateful for the support and encouragement given me in completing this work by my parents, Dr. Brin Cooke and Dr. Martin Turner.

Finally, I would like to acknowledge those who I have in error omitted, and also, with pleasure, a charming typist Mrs. Norma Corby.

CONTENTS

	Page
Acknowledgments	
§ 1 INTRODUCTION	1
§ 2 REVIEW OF X-RAY ASTRONOMY AND POLARIMETRY	3
2.1 X-ray Astronomy	4
2.2 X-ray Polarimetry	21
§ 3 THE ARIEL-V SATELLITE AND POLARISATION EXPERIMENT	35
3.1 The Ariel-V Satellite	36
3.2 The Spectrometer/Polarimeter Experiment	43
§ 4 DATA ANALYSIS	63
4.1 Leicester General Data Handling and Analysis System	65
4.2 Polarimeter Data Analysis	77
§ 5 OBSERVATIONS AND RESULTS	196
5.1 Observing Program	197
5.2 Some Preliminary Observation Results	199
5.3 1975 Sco X-1 Polarisation Search	209
5.4 Crab Nebula Polarisation Observation	229
5.5 A0620-00 (Mon X-1) Polarisation Search	247
5.6 1976 Sco X-1 Polarisation Search	253
§ 6 CONCLUSIONS	270
6.1 Recent Results	271
6.2 Ariel-V Polarimeter Performance	287
6.3 Future X-ray Polarimetry	301
References	307

§ 1 INTRODUCTION

The blanket of atmosphere that surrounds the Earth not only shields us from harmful cosmic rays, but also from vast amounts of information flooding across the universe. A small portion of this information in the form of light, filters down through the atmosphere and can be detected by our eyes. This light, plus a few meteorites, had, since the beginnings of astronomy (well over 2000 years ago), and until very recently, supplied all our knowledge of the cosmos surrounding our birthplace in space.

Astronomy, by means of viewing X-rays originating from sources beyond Earth is one such very recent new field, as instruments have to be carried above most of the Earth's atmosphere using balloons, rockets or satellites. Since 1948, with the first detection of X-rays from our Sun, and the discovery 14 years later of the first extra-solar X-ray source, the number of detected celestial X-ray sources has increased rapidly. Just previous to the launch of the Ariel-V satellite in 1974, about 160 celestial X-ray sources had been discovered, and now in 1977 they number over 200. The X-rays had been shown to originate from discrete sources within our galaxy; from other galaxies; clusters of galaxies; and from sources out to the believed most distant objects yet discovered in our universe, the quasars.

These celestial X-ray sources had become associated with the modern hypothesised exotic physical objects, neutron stars and black holes - for which confirmation of their existence is of current prime importance to our understanding of our universe and the physical laws which it appears to obey. In particular, the properties of black holes are linked intimately to general relativity, which we currently believe holds major importance in describing space, time and gravitation.

X-ray astronomy has already played an important role in detecting X-ray sources having properties, at present, consistent only with the existence of such exotic objects.

Before launch of the Ariel-V satellite, most of the information obtained concerning X-ray emission from these objects and the other X-ray sources, had been via intensity, time variation, positional and spectral studies. For only two extra-solar sources had X-ray polarisation studies been performed, and these of severely limited sensitivity. Thus, for the vast majority of the presently known X-ray sources such X-ray polarisation measurements are desired, and would be expected to provide much valuable information. In particular, for X-ray emission associated with the black holes and neutron stars high degrees of X-ray polarisation had been predicted, sufficient to provide strong evidence for distinguishing between these and other known objects. For these cases, therefore, X-ray polarisation measurements potentially hold great importance.

The Ariel-V spectrometer/polarimeter would be the first device carried on board a satellite designed to detect X-ray polarisation from extra-solar sources. Previous to the launch of this satellite the extra-solar X-ray polarisation measurements had been made from rocket flights - for which the short flight durations severely limited the X-ray collecting ability, hence limiting the possible sensitivity of the observations. A satellite polarimeter would provide much longer observing times and therefore the possibility of observing many sources at much greater sensitivities.

§ 2	<u>REVIEW OF X-RAY ASTRONOMY AND POLARIMETRY</u>	
		Page No.
§ 2.1	X-RAY ASTRONOMY	4
	1. Early Results	4
	2. Development to December 1970	4
	3. Status by approximately the Ariel-V launch date: October 1974	4
§ 2.2	POLARIMETRY	21
	1. Non X-Ray Polarimetry	21
	2. X-Ray Polarimetry	21

§ 2.1 X-RAY ASTRONOMY

§ 2.1.1 Early Results

Extra-terrestrial X-rays were first detected in 1948 by Burnight (1949) from a rocket flight of a simple X-ray camera. The origin of these X-rays was our Sun.

Fourteen years later, in 1962, a rocket was flown by the American Science and Engineering (A.S.E.) group (Giacconi et al., 1962) with the intention of detecting fluorescent X-rays from the Moon, and also to search the sky for other possible X-ray sources. The fluorescent X-rays from the Moon were expected to arise from solar X-rays impinging upon the lunar surface. However, while no lunar, fluorescent X-rays were detected, X-rays were discovered arriving from the general direction of the galactic centre.

Two further flights in October 1962 and June 1963 by the same A.S.E. group (Gursky et al., 1963) again detected the X-ray source in the direction of the galactic centre and found two more sources, one in the direction of the Crab Nebula. Data from a rocket flight intermediate to the two above mentioned A.S.E. flights, in April, 1963, (Bowyer et al., 1964), revealed one outstanding source located in the constellation Scorpius about 20° away from the galactic centre, and another source, about one-eighth as bright, coincident with the Crab Nebula.

The strong Scorpius X-ray source was almost certainly the same as that first source discovered by Giacconi et al., (1962), and which we now know as Sco X-1. The source coincident with the Crab Nebula almost certainly corresponds to another strong X-ray source now known as Tau X-1 or the Crab Nebula.

§ 2.1.2 Development to December 1970

By the end of 1970 over 30 cosmic X-ray sources had been detected, together with a diffuse background flux of X-radiation having a degree of isotropy that indicated a major part originates well beyond the limits of

our galaxy (see Pounds 1970, Gould 1967, Friedman 1969). The majority of the detected sources were located in the sky close to the Milky Way, strongly suggesting that they belong to our galaxy. Of those 30 or so X-ray sources, about 8 had been reasonably identified with optical celestial sources (see Pounds 1970, Hiltner and Mook 1970).

Notably, Sco X-1 was identified with a variable, blue star of 12-13'th magnitude, and X-rays were definitely detected from the supernova remnant "Crab Nebula" associated with the source Tau X-1. Also, two extragalactic objects, namely the peculiar galaxy in Virgo, M87, and the L.M.C. (Large Magellanic Cloud) galaxy, each had an X-ray source associated with them.

The luminosity of a 'typical' galactic X-ray source was estimated to range from 10^{36} to 10^{37} ergs s^{-1} at X-ray wavelengths (see Pounds 1970). This is far more than would be expected from a stellar source such as the Sun. The Sun emits only $\approx 10^{33}$ ergs s^{-1} over the complete electromagnetic spectrum, and of this only 10^{-4} % or less, is emitted in the X-ray region (Vaiana 1974, Gibson 1973).

Concerning development of the theory of the X-ray emission (see Pounds 1970), for the Crab Nebula there was already good evidence that both the radio flux and polarised optical continuum originate by synchrotron radiation from relativistic electrons spiralling along the nebula's magnetic field lines. The intensity and spectral distribution at X-ray wavelengths also pointed strongly towards the same explanation for the production of the X-ray flux. It was discovered in 1969 that about 10% of the Crab X-ray flux originates from a 33 millisecond radio pulsar (NP0532) lying close to the centre of the nebula. This pulsar, which is believed to be a neutron star formed from the original supernova explosion in 1054 A.D. and rotating at the 33 millisecond period of the pulses, was observed to be slowing down at approximately the rate required to generate the total 10^{37} ergs s^{-1} power

output of the Crab Nebula.

An alternative thermal emission mechanism for the production of X-rays from supernova remnants had also been proposed. The X-rays would be generated by conversion to heat of the energy released in the initial stellar explosion. Absence of polarised optical emission from two weak X-ray sources, which could be associated with the supernova remnants Tycho Brahe and Cassiopeia A, made them likely candidates for such a thermal model.

The spectra of Sco X-1 and the X-ray source Cygnus X-2 indicated, though not absolutely conclusively, a thermal origin for their radiation. This was further supported in the case of Sco X-1 where absence of polarisation in the optical band was reported (Hiltner et al., 1967). The X-radiation from Sco X-1 had been observed to vary and also the optical and radio emission of its counterpart (see Hiltner and Mook 1970). Models for thermal X-ray emission involved clouds of hot gas (perhaps at $\approx 5 \times 10^6$ °K), and energy generation by gravitational collapse. Models of gas being pulled onto the surface of a dense companion star in a binary system had also been proposed.

Variable X-ray stars were also discovered, e.g. Cen X-2; and 'X-ray Novas' were discussed.

The estimated energy emission from the nearby galaxy L.M.C. was $\approx 4 \times 10^{38}$ erg s⁻¹, compatible with simply the model of a galaxy like our own emitting X-rays as just the sum of all the individual X-ray stars. The total X-ray emission from our galaxy, a typical large spiral type, was estimated at a few 10^{39} erg s⁻¹. The total emission from the peculiar galaxy M87, however, was estimated to be $\approx 10^{43}$ erg s⁻¹ - some 10^4 times greater than that for our galaxy. Synchrotron radiation from a giant generator within the jet was proposed for the X-ray emission process of this object.

The final X-ray emission category, the diffuse isotropic X-ray background, if assumed to be the simple sum of emission from normal galaxies like our own, was found to be insufficient by a factor of 100. Other components considered for the origin of the diffuse X-ray emission included contributions from abnormally high extra-galactic X-ray emitters such as M87, or from intergalactic X-ray production (via, notably, Compton scattering of high energy cosmic electrons with low energy photons, or bremsstrahlung emission from a hot intergalactic gas) (see Gould 1967, Friedman 1969, Pounds 1970). Considerations of these theories had also been linked to cosmological models of the universe, depending as they might be expected to, on the large scale distribution in space, time and velocity, of sources and matter in the universe.

Thus, by the end of 1970, several possible and some promising, though often speculative, explanations existed for emission mechanisms concerning the origins of the observed high celestial X-ray fluxes.

§ 2.1.3 Status by approximately the Ariel-V launch date: October 1974

During December 1970 the Uhuru (SAS-A) satellite was launched. This was the first satellite devoted totally to X-ray astronomy (Gursky and Schwartz 1974, p.27). By virtue simply of the much longer observing time available to a satellite experiment compared with rocket and balloon flights, much weaker X-ray sources could be observed than previously, and the study of behaviour of X-ray sources as a function of time over a wide range of timescales could be made. Results from this satellite dominated observational X-ray astronomy to about 1975.

By 1974, a third Uhuru (3U) catalogue of X-ray sources had been published containing 161 sources observed in the first 125 days of the satellite's operation (Giacconi et al., 1974).

This satellite had surveyed 85% of the sky down to a sensitivity

of 2×10^{-10} erg cm⁻² s⁻¹, or better, in the 2-6 keV range. The intensity of the sources range from 2×10^4 cts s⁻¹ for Sco X-1 to 1.3 cts s⁻¹ for 3U1237-07, as observed with the Uhuru instruments in the 2 to 6 keV range. (1 Uhuru ct s⁻¹ \approx 1.7×10^{-11} erg cm⁻² s⁻¹) (Giacconi 1974).

The positions of the 161 X-ray sources over the sky, as illustrated in Fig. 2.1.1 confirmed the earlier distribution where the majority of the sources are concentrated in the direction of the Milky Way. The sources along the galactic plane were generally found to be much more intense than those at high galactic latitude, which is not expected if the high latitude sources belong to the local galaxy. In that case, the high latitude sources should be closer and hence brighter than those in the plane. The fact that on average the high latitude sources are fainter is taken to indicate that the majority of them are of extra-galactic origin. A plot of the number of sources N which have an intensity greater than a certain value S , against s , (i.e. a log N , log S plot) see Fig. 2.1.2, shows clearly the difference between the high and the low latitude sources. Except for the tail at high intensities, which is interpreted as being probably due to a spread in the intrinsic luminosity of the sources (see Giacconi 1974), the low latitude sources show a weak dependence of N on S , as expected for a disk or spiral arm population. The high latitude sources, however, show a steep dependence of N on S , as expected from a spherical distribution of sources.

The number of X-ray sources considered to be identified with optical objects had risen to about 34 (see Table 2.1.3).

Of the 64 sources listed in the 3rd Uhuru catalogue having $|b| > 20^\circ$, Sco X-1 and Her X-1 are considered to be known galactic sources, and 19 others to be associated with extra-galactic objects.

The remaining weak and unidentified 43 sources are known to have a latitude distribution completely consistent with isotropy indicating an

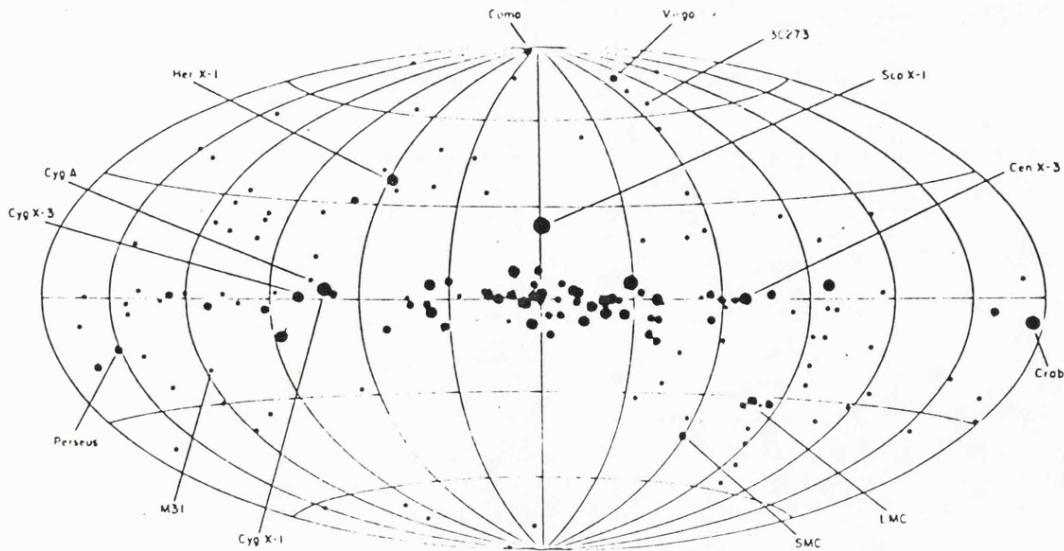


Fig. 2.1.1: A map of the X-ray sky in galactic coordinates derived from the 3U Catalog. The location of each X-ray source is approximately shown. The size of the dots is proportionate to the logarithm of the intensity. Several of the sources of outstanding astrophysical interest are shown (from Giacconi 1974).

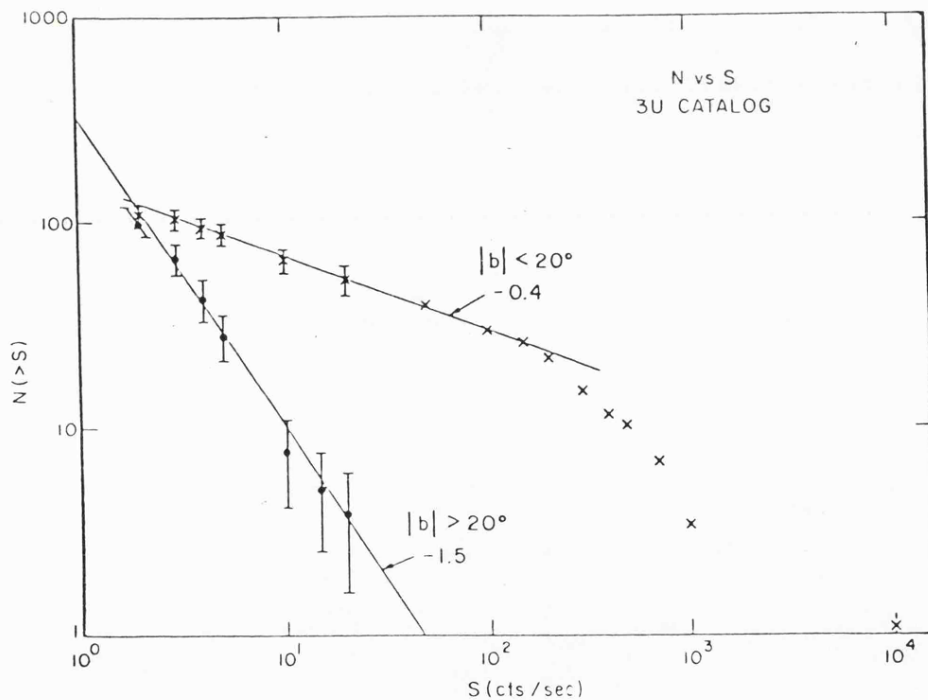


Fig. 2.1.2: A plot of the integral number of sources of intensity greater than S is plotted as a function of intensity S . The information is derived from the 3U Catalog. The number of sources is corrected for sky coverage. The errors represent statistical errors only. The sources are divided into two groups: one is galactic latitude $|b| > 20^\circ$; the other is galactic latitude $|b| < 20^\circ$. The intensities are measured in Uhuru units (from Giacconi 1974).

3U0021 + 42	M 31
3U0022 + 63	TYCHO SNR
3U0115 -- 73	SANDULEAK 160 SMC
3U0254 + 14	Abell 401 (Cluster)
3U0316 + 41	Abell 426 (Perseus Cluster)
3U0521 -- 72	Large Magellanic Cloud
3U0527 -- 05	M 42
3U0531 + 21	Crab Nebula
3U0532 -- 66	} Large Magellanic Cloud
3U0539 -- 64	
3U0540 -- 69	
3U082 -- 042	Pup A
3U0833 -- 45	Vela X
3U0900 -- 40	HD 77581
3U0901 -- 09	Abell 754 (Cluster)
3U1044 -- 30	Abell 1060 (Cluster)
3U1118 -- 60	Cen X-3
3U1144 + 19	Abell 1367
3U1207 + 30	NGC 4151
3U1224 + 02	3C273
3U1228 + 12	Virgo Cluster (M 87)
3U1231 + 07	IC 3576
3U1247 -- 41	NGC 4696 (Cluster)
3U1257 + 28	Abell 1656 (Coma Cluster)
3U1322 -- 42	NGC 5128 (Cen A)
3U1551 + 15	Hercules Cluster
3U1617 -- 15	Sco X-1
3U1653 + 35	HZ H1-R
3U1700 -- 37	HD 153919
3U1706 + 78	Abell 2256 (Cluster)
3U1956 + 35	HD 226868 (Cyg X-1)
3U1957 + 40	Cyg A = 3C 405
3U2142 + 38	Cyg X-2
3U2321 + 58	Cas A

Table 2.1.3: Identified X-ray sources (from Giacconi 1974)

extragalactic origin. However, it is also considered a possibility that these sources may belong to a local galactic population less than a few hundred parsecs away.

Owing to the increase in number of X-ray sources and identifications during this period, it had become apparent that similarities existed between certain X-ray sources or their optical counterparts. Then, discussion of X-ray sources in groups, as well as individual sources, had become much more meaningful.

Three general categorisations of the main features of the X-ray sky could be made from which sub-categories emerge.

- i) Galactic X-ray sources.
- ii) Extra-galactic X-ray sources.
- iii) The diffuse X-ray background.

i) Galactic X-ray Sources

The 3U catalogue lists about 100 sources which have $|b| < 20^\circ$ for which most are thought to belong to the Galaxy. There are 16 firm identifications with galactic objects and approximately an equal number which are considered to be probably correct. Of the firmly identified sources, 1 is associated with the galactic centre, 7 with super-nova remnants, 6 with binary stars and 2 with irregular variable stars which are also thought to possibly be members of binary systems.

About 40 X-ray sources are listed in the third Uhuru catalogue which are not identified with SNR's and which have been observed to vary on a time scale of days or less. One of these is extragalactic, in the Small Magellanic Cloud. The remaining sources are concentrated in the galactic plane with a median latitude of about 2° .

Twenty-four sources are located in the direction of the galactic centre, of which at least 7 show large, non-varying, low energy cut-offs in

their X-ray spectra. It is believed that if these cut-offs can be attributed to interstellar absorption then the sources must lie near the galactic centre. These sources will then have an intrinsic X-ray luminosity of in the 2 - 6 keV range of the order of 10^{38} erg s⁻¹, more than an order of magnitude greater than that of the 'spiral arm' galactic sources. Giacconi (1974) states that, although this may be a fundamental difference between the galactic centre and spiral arm sources, he believes it more likely not to be so. Members of each group show similarity in spectra and time variability, including binary nature, making it appear more likely that the difference in brightness may be due to differences in the characteristics of the binary systems, perhaps the nature of the primary component. Giacconi gives an estimate of the minimum and maximum luminosities of these sources as on the order of 10^{36} to 10^{38} erg s⁻¹, and that their total number in the galaxy is about 100.

In addition to these above sources, transient X-ray sources have appeared at locations where no source was previously known, become among the brightest X-ray sources in a matter of days, and then in a few months gradually faded away. These sources, when strong, have been observed to exhibit large fluctuations in intensity on a time scale of seconds. About 4 such sources, Cen X-2, Cen X-4, 2U1735-28 and 2U1543-47 (Giacconi 1974, Tananbaum and Tucker 1974), were detected in the 5 year period 1966-1971. No evidence for repetitive outbursts from these transient sources was obtained. Although the intensity versus time behaviour for these objects could be seen as suggestive of a nova, the frequency of the outbursts and lack of a bright optical object was taken to argue against this interpretation of their nature.

Two classes of objects which have become firmly associated with some of the galactic X-ray sources are (a) Supernova remnants, and (b) binary stars.

(a) Supernova Remnants (SNR's)

By 1975, from both rocket and Uhuru satellite measurements, about 12 supernova remnants had been observed either firmly or tentatively (see Table 2.1.4) (Gorenstein 1974). They had also been classified into 2 groups according to the age of the remnants. The young remnants (age less than a thousand years) have relatively hard spectra and X-ray diameters of the order of a few parsecs. Examples of the young remnants include Casseopeia A (Cas A), the Crab Nebula, SN1006 (a tentative X-ray source at this time (Gorenstein 1974)) and Tycho's Nova. The Crab Nebula, Tycho's Nova and also Cas A are detectable as intense X-ray sources above 2 keV.

The old remnants (age greater than a few thousand years) have soft spectra and X-ray diameters of the order of tens of parsecs. Examples of some old remnants include the Cygnus Loop and the Vela X-ray Nebula. The soft spectra are such that almost all the observable emission occurs below 2 keV.

The X-ray emission from almost all the SNR's is thought to arise from a hot gas produced by the interaction of the expanding supernova shell with the interstellar medium. With this model, the harder X-ray spectra are obtained from the younger SNR's when the temperature of the gas in the shock front of the supernova shell is high, and later as this gas cools the obtained spectra will be softer (Gorenstein and Tucker 1974).

Also, in addition to the X-ray pulsar discovered in the Crab Nebula before 1970, evidence had also been obtained of X-ray emission from a 89 ms pulsar associated with the Vela SNR.

(b) Binary Stars

About 6 X-ray sources had been firmly identified with binary star systems (of which 1 is extra-galactic, SMC X-1, located in the small

Table 2.1.4: X-ray Emitting Supernova Remnants (from Gorenstein and Tucker 1974).

Object	l	II	b	II	Distance (kpc)	Radio diameter (pc)	3U Name	Confidence of Identification
1. Tycho SN 1572	120.1 ^o	+ 1.4 ^o			3	5.8	0022+63	Certain
2. Crab Nebula	184.6	- 5.8			1.7	2.5	0531+22	Certain
3. PSR 0531+21	184.6	- 5.8			1.7		0531+22	Certain
4. IC 443	189.0	+ 3.0			19	19	0601+21	Probable
5. PSR 611+21	189.0	+ 3.0			1.5		?	Possible
6. Pup A	260.4	- 3.4			1.2	19.4	0821-42	Certain
7. Vela X-ray Nebula	263	- 3			0.46	27	0832-45	Certain
8. PSR 0833-45	263	- 3			0.46		0832-45	Probable
9. Lupus Loop	330	+15			0.8	60.7		Probable
10. SN 1006	372.6	+14.5			4.9	42.6		Possible
11. MSH 15-52A	320.4	- 1.4			5.4	22.0	1509-58	Possible
12. MSH 1811-17 (GX 13+1)	13.4	+ 0.1			9.8	19.0	1811-17	Possible
13. Cygnus Loop	73.6	- 8.6			0.8	31		Certain
14. Cas A	111.7	- 2.1			3.4	4.0	2321+58	Certain
15. North Polar Spur	330	20			0.1-0.2	170-340		Probable

Magellanic Cloud) (see Tananbaum and Tucker 1974, Giacconi 1974). These are displayed in Fig. 2.1.5. The X-ray data in support of the binary nature of these sources includes eclipse features and positional coincidence with optical binary systems. These sources have luminosities in the range $10^{36} - 10^{38} \text{ erg s}^{-1}$ in the 2 - 6 keV region, and a flat spectrum similar to that produced by radiation from a hot gas having a temperature in the range 50 - 500 million degrees. The spectra of the eclipsing sources show a variable low energy cut-off. Also fast, and in some cases periodic, intensity variations on a time scale of seconds or less are observed.

The X-ray production mechanism for these binary stars is believed to consist of accretion of matter from one of the stars to the other, a mechanism known before the launch of the Uhuru satellite in December 1970. Generally, three types of stellar objects are considered for which sufficiently high temperature plasmas can be achieved in the accretion process to produce the required X-ray fluxes. These are degenerate dwarf stars, neutron stars, and black holes.

Variation in the mass accretion rate can explain the variable, low energy cut-offs observed in the X-ray spectrum. Periodic variations of the order of seconds in X-ray intensity, which are observed in sources Her X-1 and Cen X-3, can be explained by accretion onto a neutron star which is rotating. Accretion onto a pulsating degenerate dwarf is also considered possible for these systems, though less favourably (Tananbaum and Tucker 1974). Cyg X-1, which has been observed to fluctuate on time-scales from seconds down to milliseconds, has a companion star whose mass is great enough ($\geq 3 M_{\odot}$) so that it is considered very likely to be a black hole.

It has also been suggested that many, if not all, compact, X-ray, galactic sources may be members of binary systems (Tananbaum and Tucker 1974) where an efficient mechanism, in accretion, exists for the production

Table 2.1.5:1) Firmly Identified Binary X-ray Sources (from Tananbaum and Tucker 1974; Giacconi 1974; Bahcall 1975; Gottlieb, Wright and Liller 1975; Gursky 1975).

X-ray Name	Other	Binary Period	Optical Companion	b	Remarks
1. 3U1956+35	Cyg X-1 HDE 226868	5.6 days	9 mag 0.97Ib	3°	Very short and long time scale variations
2. 1118-60	Cen X-3 Krzeminski	2.1 days	13 mag B0Ib-III	0°	4.8 sec X-ray pulse period
3. 0900-40	Vela XR-1 HD77581	8.9 days	6 mag B0.5Ib	+ 4°	Variations on tenths of seconds to hours
4. 1700-37	HD153919	3.4 days	6 mag 07f	2°	Variations on tenths of secs to minutes and longer
5. 0115-37	SMC X-1 Sk 160	3.9 days	13 mag B0Ib		Extended lows
6. 1653+35	Her X-1 HZ Her	1.7 days	15m late A	+38°	HZ-Her. 1.2 sec pulse period. 35d period
<u>ii) Other X-ray source binary candidates</u>					
7. 1017-15	Sco X-1	0.8 days	blue 12-13 mag	+24°	variability over minutes. Slow (~10 min-hour) flares
8. 2030+40	Cyg X-3	0.2 days		+ 1°	Heavily obscured, seen only $\lambda \geq 1 \mu$. Variability in terms of minutes
9. 2142+38	Cyg X-2	?	14 mag G	-11°	Variability in times of minutes

of the X-ray fluxes.

ii) Extragalactic X-ray Sources

The identified extragalactic sources can be divided into 3 main groups; (a) Normal galaxies, (b) Exotic extragalactic sources, and (c) Clusters of galaxies.

(a) Normal Galaxies

This group includes those galaxies where the X-ray emission is thought to be just the integrated output of all the individual stellar sources in the galaxy concerned. The X-ray luminosities measured are around 10^{39} erg s⁻¹.

The ratio of the X-ray emission to the total amount of light emitted at all wavelengths is $\frac{L_x}{L_{\text{rad}}} \approx 10^{-5}$, showing the relative very weak X-ray emission (Giacconi 1974).

The galaxies in this group include the SMC, LMC, M31 which is the Andromeda Nebula, and our own galaxy (Giacconi 1974, Kellogg 1974).

The X-ray luminosities of all the other 3U sources identified with extragalactic objects are much higher than those of the normal galaxies, and range from 10^{42} to 10^{46} erg s⁻¹ in the 1 - 10 keV range. The ratio of the X-ray to optical luminosity (L_x/L_{opt}) is also much larger.

(b) Exotic Extragalactic Objects

This group includes radio galaxies, a Seyfert galaxy and a quasar (Q.S.O., Quasi Stellar Object). The observed Seyfert galaxy is NGC4151, and quasar is 3C273. The radio galaxy Cen A (NGC5128) is considered to be observed in X-rays with a high degree of confidence and Cyg A with a lower degree of confidence (Giacconi 1974, Kellogg 1973, 1974, Sargent 1973, Burbidge 1973, Longair and Willmore 1974). (Much more doubt exists as to the observation of X-rays from two other radio galaxies, Her A

and Pic A (see Sargent 1973, Burbidge 1973, Giacconi et al., 1974).

For the sources identified with individual galaxies a definite low energy cut-off in the X-ray spectrum is measured (see Giacconi 1973, 1974) corresponding to an amount of absorbing material which, generally, if it was supposed to exist uniformly throughout something like the total sizes of the galaxies involved, would be prohibitively large (Giacconi 1973). For this reason the low energy cut-offs are taken to indicate that the emission arises from small central regions within these extragalactic objects.

(c) Clusters of Galaxies

This class of X-ray sources resulted from the Uhuru satellite sky survey (Kellogg, 1974). About 20 sources have been identified with clusters (see Table 2.1.6), and luminosities range from approximately 10^{43} to 10^{45} erg s⁻¹. Extended sizes are observed without any cut-off in the X-ray spectrum. This lack of cut-off has been taken to imply that the emission does not arise from a collection of individual sources within the cluster, but rather from an extended low density region. Extended optical and radio halos, which have been observed in cluster sources, occur in overlapping regions of space with the X-ray emission and this has been taken to suggest that it is a single medium from which the various radiations are produced. The X-ray emission is centred on active galaxies when present, as in the Virgo and Perseus Clusters. Theories concerning the origin of the cluster X-ray emission include, thermal emission from a hot intra-cluster gas, and non-thermal, inverse Compton, emission from relativistic electrons interacting with the cosmic microwave background. Hot intra-cluster gas models involve total masses of gas comparable with the observed mass of the galaxies in the clusters, at a temperature of about 10^8 °K. Gas heating mechanisms include; energy output from active galaxies; infall of gas from outside the cluster; and supersonic motion of

Table 2.1.6: Cluster X-ray Sources (from Kellog 1974).

Abell Number (1)	D,R (2)	3U Name (3)	R_x (4)	ΔR_x (5)	z (6)	ΔV (7)	Remarks (8)
A. Abell cluster sources							
262	1,0	0151+36	2.4	0.4	0.0168		Radio source
376	3,0		2.8	1.6	0.0437		
401	3,2	0254+13	3.4	0.3			Radio source
426	0,2	0316+41	47.4	0.6	0.0183	2410	Radio source, Perseus cluster
496	3,1		2.5	0.7			Radio source
576	2,1		2.6	0.7	0.0404		
754	3,2	0901-09	4.4	0.8	0.0537		Radio source
1060	0,1	1044-30	2.2	0.8	0.0094		
1367	1,2	1144+19	3.6	0.3	0.0205		Radio source, 3C264
1656	1,2	1257+28	14.8	0.3	0.023	1800	Radio source, Coma cluster
2052	3,0		6.7	0.7	0.0351		Radio source
2079	3,1		3.4	1.0			Radio source
2151	1,2	1551+15	2.1	0.5	0.0360	1090	Radio source
2199	1,2	1639+40	4.0	0.6	0.0309	1530	Radio source
2256	3,2	1706+78	3.2	0.3			Radio source
2319	3,1	1921+43	6.3	0.6	0.0549		
2666	1,0	2346+26	7.0	1.2	0.0273		
B. Other cluster sources							
3C 129		0446+44	5.5	0.9			
Virgo (M87)		1228+12	21.7	0.3		1000	3C 274, Virgo cluster
Cen (NGC 4696)		1247-41	5.9	0.4		1530	MSH 12-45, Cen cluster
Cyg A		1957+40	5.1	1.4			3C 405

Key: D,R are Abell Distance and Richness Class. R_x is Uhuru count rate cts s^{-1} (2-6 keV). ΔR_x is standard deviation on R_x . z is redshift in units of c . ΔV is velocity dispersion = $\sqrt{3}$ times projected dispersion in units of km s^{-1} . Possible identifications with strong radio sources are listed by 3C or MSH number.

the galaxies through the gas.

iii) The Diffuse X-ray Background

This feature of the X-ray sky and its degree of isotropy, indicating that a major portion of this emission is of extragalactic origin, was known previously to the launch of the Uhuru satellite (see § 2.1.2).

Between 1 and 100 keV the background is known to be remarkably isotropic to within a few percent. The 1 - 10 keV intensity is $\approx 10^{-8}$ erg cm⁻² s⁻¹ sr⁻¹, comparable to the mean intensity of the night sky due to discrete sources (see Giacconi 1974). However, the background below 1 keV is not isotropic, though interpretation is made difficult by the presence of strong interstellar absorption at these energies. It is considered that a good case can be made for a galactic origin of a large part of this soft X-ray background.

Three possibilities for the origin of the diffuse X-ray background are given in a review by Peterson (1975). These include Compton scattering of intergalactic electrons on the 3⁰K radiation, an $\approx 7 \times 10^7$ °K intergalactic medium of sufficient density to close the universe, or simply the summed flux from the, as yet, unresolved sources. It appears not too unlikely that the contribution from the unresolved extragalactic sources will, at least, contribute a significant portion of the isotropic, background flux.

§ 2.2 POLARIMETRY

Whilst X-rays were first detected from the Sun in 1948 and the first non-solar, celestial X-ray source was discovered in 1962, X-ray polarisation studies of celestial sources did not begin until comparatively recently, in 1968. Up to the time of launch of the Ariel-V satellite in October 1974 only 5 reports had been presented concerning X-ray polarisation of non-solar X-ray sources.

Several authors have stressed the potential usefulness and importance of X-ray polarisation measurements, notably Novick (1974, 1975) and Rees (1975) with easily readable reviews.

The review presented here attempts to represent the general state of X-ray polarimetry just previous to the time at which most of the Ariel-V polarimetry analysis was being performed (that is \approx 1975).

§ 2.2.1 Non X-ray Polarimetry

A short list of selected principle events concerning the historical development of polarimetry, taken mainly from Gehrels (1974), is presented in Table 2.2.1.

§ 2.2.2 X-ray Polarimetry

Studies of polarisation of celestial sources at X-ray wavelengths can be divided conveniently into two sections,

- i) Solar X-ray polarimetry
- ii) Non-solar X-ray polarimetry.

Up to October 1974 a total of only 8 X-ray polarisation observations had been reported and these are listed in Table 2.2.2. They were composed of 3 solar observations and 5 of non-solar X-ray sources.

i) Solar X-ray Polarimetry

Novick (1974) stresses the complexity of solar X-ray phenomena,

Table 2.2.1: Non X-ray Polarimetry (from Gehrels 1974, except where stated)

- a) General
- 1669 Erasmus Bartholinus, in Denmark, discovered double refraction with Iceland spar, although he was not aware of the polarisation.
- 1812 Sir David Brewster discovered the relation between refractive index and the polarising angle (Brewster's Law).
- 1845 Michael Faraday discovered the rotation of the plane of polarisation of linearly polarised light traversing certain media parallel to magnetic field lines.
- 1852 Sir George G. Stokes described the four Stokes parameters.
- b) Application to Astronomy
- 1809 D.F.J. Arago discovered that light from the sunlit sky is partially polarised. Observed polarisation from 2 comets and from the Moon.
- 1858 E. Liais discovered that light from the solar corona is partially linearly polarised.
- 1872 Lord Rosse discovered some polarisation of light from Venus (see also Coffeen and Hanson 1974).
- 1942 Yngre Ohman found polarisation in galaxy M31 (Andromeda Nebula).
- 1949 J.S. Hall and W.A. Hiltner discovered linear interstellar polarisation, and subsequently published extensive catalogues concerning polarised starlight.
- 1954 V.A. Dombrovskij discovered large optical polarisation from the Crab Nebula predicted from synchrotron radiation a year before by I.S. Shklovskij (see also Shklovskij 1960).
- 1957 C.H. Mayer, T.P. McCullough, and R.M. Sloanaker detected radio polarisation from the Crab Nebula. They were also the first to measure polarisation of an extragalactic radio source in 1962.
- 1959 Strong wavelength dependence was found for the linear polarisation of planets, stars and nebulae.
- 1962 N.M. Shakhovskoj found variable polarisation in early type eclipsing binary β Lyr.
- 1970 James C. Kemp discovered circular polarisation in radiation from a white dwarf star. This stimulated a variety of similar findings for planets, stars and nebulae.

Table 2.2.2: Observations of X-ray Polarisation from Celestial sources, up to October 1974.

(1)	<u>SOLAR</u>	Authors & Ref.	Group	Rocket/ Satellite	Polarimeter	Obs. date	Object Observed	Result/Energy Range
1.		Tindo, I.P. et al. (1970)	Lebedev phys. Inst. of USSR Moscow	Satellite Interkosmos 1	Scattering	Oct. 1969	3 flares	$p = 0.4 \pm 0.2$ at 90% confidence/ 12 - 20 keV
2.		Tindo, I.P. et al. (1972)	"	Satellite Interkosmos 4	Scattering	Oct. Nov. 1970	3 flares	$p = 0.12$ to $0.21/6 - 25$ keV
3.		Underwood, J.H. & Neupert, R.M. (1974)	NASA GSFC	Satellite OSO-7	Scattering	Launch Sept. 1971		No results to this time (Nov. 1973) since data believed to be influenced by instrument effects/15 - 40 keV
(1)	<u>NON-SOLAR</u>							
1.		Anzari, J.R.P. et al. (1969)	Columbia U.S.A.	Rocket	Scattering	July 1968	Sco X-1	$p \leq 20\%$ at 3- σ confidence/ $\sim 6 - 18$ keV
2.		Wolff, R.S. et al. (1970)	"	Rocket	Scattering	March 1969	Crab Nebula	$p < 27\%$ at 90% confidence/ $\sim 5.5 - 22$ keV
3.		Kestenbaum et al. (1971)	"	Rocket	Bragg Crystal	April 1970	Sco X-1	p (north-south direction only) = $-1.74 \pm 3.4\%$ $\sim 2.4 - 2.9$ keV
4.		Novick, R. et al. (1972)	"	Rocket	2 { 1) Scattering (1) Bragg Crystal	Feb. 1971	Crab Nebula	$p = 15 \pm 5.2\%$ at position angle $156^\circ \pm 10^\circ$ from combining result with that of Wolff, R.S. above/(1) ~ 7 to 17 keV, (11) $\sim 2.0 - 3.2$ keV
5.		Fertelsdorf, R. et al. (1973)	"	Rocket (same flight as 4 above)		Feb. 1971	Crab Pulsar	$p = 12 \pm 65\%$ at $110 \pm 160^\circ$

and discusses the high energy solar flare events which require polarimetry for their elucidation. He states that there is an abundance of evidence which shows that the early phase of flares involve non-thermal electron distributions, and that the X-rays are often emitted in short impulsive bursts which have strong temporal correlation with similar burst phenomena in the microwave region. Also, the X-ray spectra in these bursts are characterized by a power law, which as the flare develops and the burst decreases in intensity, gradually takes on a thermal character. In addition, Novick states that it has been suggested that the X-ray and microwave bursts are caused by a non-thermal high energy electron flux that is guided by the local magnetic field in the active region. In this model the microwave bursts occur by synchrotron radiation from the motion of the electrons about the magnetic field lines, and the strong circular and linear polarisation expected for this synchrotron process has been observed. In the same model, the X-rays result by linear bremsstrahlung emission, caused by the high energy electrons, travelling along the magnetic field lines, impacting with the ambient gas. Under these conditions strong linear X-ray polarisation is predicted. The sign of the polarisation changes with energy; at low energy the electric vector of the emitted photons is transverse to the direction of electron motion (sign denoted as +ve, see Clarke 1974, p. 47), whereas at higher energies it is in the plane of scattering (sign denoted as -ve). Fig. 2.2.3 shows two examples of detailed predictions made for this emission process for a variety of viewing angles.

If the above model is correct and the linear bremsstrahlung process is the cause of the X-ray emission, then observationally it can be tested (Novick 1974) against the possibility of synchrotron emission. For synchrotron radiation the polarisation should be energy independent and not change sign as predicted for the linear bremsstrahlung process.

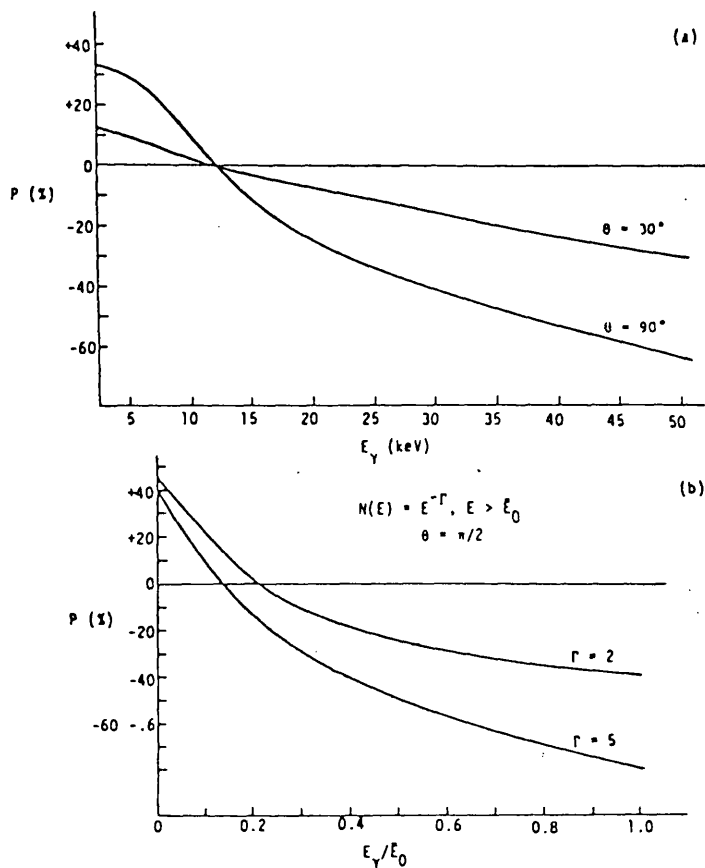


Fig. 2.2.3(a) Polarization of bremsstrahlung as a function of the photon energy E_γ for two viewing angles θ relative to the direction of the electron flux. Electron energy $E_0 = 100$ keV (Korchak, 1967), (from Novick 1975).

(b) X-ray polarization as a function of energy for bremsstrahlung from a power-law distribution of electrons $N(E)$. The viewing angle is 90° (Korchak, 1967), (from Novick 1975).

Also, for synchrotron radiation a moderate degree of circular polarisation may be expected (Angel 1974), whereas only pure linear polarisation is expected from the linear bremsstrahlung process (Novick 1974). However, as it appears that an X-ray circular polarisation analyser is difficult to construct (Novick 1974) it is likely that energy dependence will be the major distinguishing factor between these two processes.

Of the 3 solar X-ray polarisation observations, 2 were reported by Tindo et al. (1970, 1971) of the Lebedev physical institute of Moscow. The first report (1970) concerned a Thomson scattering polarimeter flown on the Intercosmos 1 satellite where 3 solar flares were observed during October 1969. An average polarisation from $\approx (0.6 - 1 \text{ \AA})^{\circ}$ (12.4 - 20.6 keV) of $40 \pm 20\%$ was detected at the rising, initial phase and also at a second maximum of intensity. The second report (1971) concerned observations of a further 3 solar flares during October/November 1970, from a Thomson scattering instrument onboard the intercosmos 4 satellite. From these observations, made in a similar energy range of $\approx (0.5 - 2) \text{ \AA}^{\circ}$ (6.2 - 25 keV), the existence of polarisation in the initial phase of the X-ray bursts was confirmed. It was also reported that the polarisation could be observed for a few minutes up to 10 minutes, and that an increase of polarisation occurred also during secondary maxima. Underwood and Neupert (1974) of the N.A.S.A. Goddard Space Flight Centre had flown a small scattering polarimeter on board the OSO-7 satellite, and reported one event, although they believe it was strongly affected by instrument problems.

Novick (1974) states that, although the present X-ray polarisation data supports the model for linear bremsstrahlung emission from solar flares, further verification for the existence of this polarisation is required, and the energy dependence of the polarisation is yet to be determined. Also noted is that as the present polarimeters view the entire

solar disk, in the future it will be necessary to improve the spatial resolution of the instruments.

A future polarisation experiment (reported by Novick (1974) from a personal communication of 1972), consists of 2 small polarimeters scheduled to be flown on the forthcoming DOD Solrad missions by the solar physics group at the U.S. Naval Research Laboratory.

ii) Non-Solar X-ray Polarimetry

Before the launch of the Ariel-V satellite in October 1974, X-ray polarisation observations of non-solar celestial objects had included only the 2 galactic sources Sco X-1 and the Crab Nebula. (These observations are summarized in Table 2.2.2).

Discussion of X-ray polarimetry concerned with the non-solar celestial sources can therefore be conveniently divided into 3 parts:-

- (a) Sco X-1
- (b) The Crab Nebula
- (c) Other sources, galactic and extragalactic.

Also, it will be possible to interpret X-ray polarisation observations of these extra-solar objects in terms of intrinsic source properties since interstellar grains are not expected to produce significant X-ray polarisation (Novick 1974).

(a) Sco X-1

For Sco X-1, which is thought to be a thermal emitter, polarised emission would not normally be expected. However, if the source is not spherically symmetric as would be the case for a binary system involving emission from an accretion disk, and a large amount of internal scattering occurs, then polarisation of up to about 7% could be expected (Angel 1969). Also, as Sco X-1 is known to be a flaring source, then these flares may be polarized (Angel et al. 1969). Thus, good reasons exist for expecting a slight degree of polarisation from Sco X-1.

The first X-ray polarisation observation of Sco X-1 was reported by the Columbia group (Angel et al. 1969), who flew a Thomson scattering polarimeter onboard an Aerobee 150 rocket in July 1968. The spectral range of this instrument was about 6 to 18 keV. As expected, no positive indication of polarisation was detected, lending weight to the already held general belief of a thermal bremsstrahlung emission process. An upper limit of 20% to the degree of X-ray polarisation at ≈ 3 sigma confidence was produced, complementing the already known absence of appreciable optical polarisation of this source (Hiltner et al. 1967) ($\approx 0.7\%$ optical polarisation was measured, for which an interstellar origin was considered).

A second report of an X-ray polarisation measurement of Sco X-1, also by the Columbia group, was reported by Kestenbaum et al. (1971). This measurement was a byproduct of a spectral line search with a Bragg crystal instrument, and gave a result only relevant to polarisation in a North-South direction. The degree of linear polarisation in this direction was measured as $p_x = -1.7 \pm 3.4\%$ for the energy range ≈ 2.4 to 2.9 keV, which may be interpreted as an upper limit of $\approx 12\%$ at 3-confidence. This result was somewhat lower, for this North-South direction, than the previous 20% upper limit obtained at the higher energy range of the lithium polarimeter.

No further X-ray polarisation measurements of Sco X-1, up to the time of the launch of the Ariel-V satellite, were reported. However, it was clearly realised that further more accurate X-ray polarisation measurements could be useful in determining the nature of Sco X-1 (Novick 1974), especially if a positive indication of polarisation associated with a non-spherical source, possibly a binary system, could be obtained.

(b) The Crab Nebula

Previous to the X-ray polarisation observations of this galactic

supernova remnant, it was already generally accepted that the continuum emission was produced by synchrotron radiation (Novick et al. 1972). Measurements of the spectral shape and of the polarisation of the optical and radio emissions were consistent with this hypothesis. Furthermore, the X-ray spectrum appeared to be a natural extension of the lower frequency spectrum. However, it was known that the shape of the continuum spectrum does not uniquely determine the X-ray emission process. Sartori and Morrison (1967) had presented a 2 temperature unpolarised thermal model sufficient to explain the existing X-ray spectra. A positive detection of X-ray polarisation in this object, consistent with the optical and radio results, would then be taken as proof against the thermal model, and as proof of synchrotron emission.

Two observations had been made before October 1974 with the intention of detecting X-ray polarisation from the Crab Nebula, both from rocket flights by the New York Columbia group.

The first flight, which occurred during March 1969, involved a Thomson scattering device, and succeeded in producing an upper limit of $\approx 27\%$ polarisation at 3-sigma confidence for the energy range $\approx (5.5$ to 22) keV (Wolff et al. 1970). The second flight in February 1971, included two instruments, one Thomson scattering device, sensitive in the range $\approx (7$ to 17) keV, and a Bragg crystal polarimeter, sensitive in the range $\approx (2.0$ to 3.2) keV. The results from this flight, when combined with that of the previous flight, resulted in a positive detection of X-ray polarisation amounting to $15.4 \pm 5.2\%$ at a position angle of $156^\circ \pm 10^\circ$, in excellent agreement with the optical polarisation when averaged over the X-ray emitting region of the Nebula (Novick et al. 1972). Thus, the Crab Nebula became the first X-ray source to have a confirmed emission mechanism (Novick 1974).

Novick (1974) notes that this confirmation of the X-ray synchrotron

emission for the Crab Nebula posed new problems, since it implied that the synchrotron electron spectrum extends to 6×10^4 GeV if the Nebula magnetic field is 10^{-4} gauss. Then, since the radiative lifetime for such electrons is a fraction of a year, they must either be continuously generated by the pulsar (see § 2.1) or continuously accelerated within the Nebula, and models for both of these methods appear to have serious difficulties. It was noted that a proposed continuous acceleration mechanism seemed to be ruled out by the failure of Landstreet and Angel (1971) to find the circular polarisation predicted for that process; and that continuous injection of 6×10^4 GeV electrons appears impossible, since in the high magnetic field (10^{12} gauss) of the pulsar, the electrons lose their energy by either synchrotron or curvature radiation before they escape from the neighbourhood of the pulsar.

An average optical polarisation of 7% at a position angle of 98° has been observed from the emission of the Crab pulsar NPO532 (Kristian et al. 1970). If X-ray polarisation in the main pulse is observed comparable to that in the optical band, then the presently held view that the optical and X-ray emission processes are the same may be confirmed (Novick 1974). Data from the second flight on the Crab Nebula was analysed by Berthelsdorf et al. (1973) for X-ray polarisation of the pulsar emission, though unfortunately no significant result could be obtained because of poor statistics. A degree of polarisation of $12 \pm 65\%$ at a position angle of $110 \pm 150^\circ$ was obtained, certainly of insufficient accuracy to confirm that the optical and X-ray emission processes are identical.

(c) Other Sources, Galactic and Extragalactic

Although no polarisation measurements had been performed on the X-rays from these objects prior to the launch of Ariel-V, such observations

would be of interest for many of these sources (Novick 1974, Rees 1975).

Galactic Sources

For binary X-ray sources, such as Her X-1 and Cen X-3, which are believed to contain rotating neutron stars, various models predict the pulsed X-ray emission to exhibit high degrees of polarisation (Rees 1975, Gnedin and Sunyaev 1974). Linear and circular polarisations of up to perhaps 100% may be reached. The polarisation may also be expected to vary with the pulse phase. Tsuruta (1974), in considering models for the pulsed emission from Her X-1, proposed X-ray polarisation measurements as a method for distinguishing between a degenerate pulsating/rotating white dwarf or the more favoured model of a rotating neutron star, as the compact companion. Tsuruta's calculations strongly indicate, if the predicted variation of linear and circular polarisation through the pulsed emission is detected according to the "pencil" beam model of a rotating neutron star, that the white dwarf model should then be abandoned. She also notes that such a result would mean that emission according to the "fan" beam model for a spinning neutron star, in the case of Her X-1, should also be ruled out. In the case of the Crab pulsar, though not in a binary system, it has already been found that the optical polarisation vector rotates through an angle of roughly 180° during the pulse (Kristian et al. 1970, Wampler et al. 1969), and this has been taken as strong evidence for the magnetic rotator, pulsar model. Furthermore, observation of circular polarisation in a number of white dwarf stars has shown that some highly evolved stars have large magnetic fields, supporting the soundness of the basic view of the magnetic neutron star model of pulsars (see Novick 1974). For binary stars, Novick (1974) also states that determination of the position angle of the polarisation may provide a clue to the orbital inclination of the binary system. A value i for the orbital inclination is then linked to the "mass function" for the

binary system $\left[\frac{M^3 \sin^3 i}{(M + m)^2} \right]$ essential for determining the masses of the two stars, where it was noted that this had not been determined in a convincing way for any eclipsing sources. Angel's (1969) calculations, from the degree of X-ray polarisation measured, can lead to limits being placed on either the orbital inclination or shape of the accretion disk involved in the binary system. Rees (1975) states that for accretion onto a black hole in a binary system, the "standard" Shakura-Sunyaev disk model predicts linear polarisation of around 10% over the whole X-ray band and that the polarisation (electric) vector lies in the plane of the disk. Rees also implies that this model may be applicable to Cyg X-1, for which there is strong evidence that the compact companion is a black hole, although any deviations from the above predicted, polarisation behaviour would suggest a less straightforward disc structure. Rees also notes many uncertainties and inadequacies in the "standard" disk model; so that polarisation measurements would be of still greater importance, insofar as they will enable checks to be made on the model's validity and for identifying those aspects that require modification. Rees also mentions that variation of polarisation around the orbital period may be observed in hard X-ray emission, where this is caused by reflection of X-rays off the non-compact star in a close binary system. He lists Sco X-1 and Cyg X-3 as possible candidates for this effect. X-ray polarisation may also be observed from flare events on Sco X-1 and Cyg X-1 and from the short lived "flare" stars, if linear bremsstrahlung contributes significantly to the emission process (Novick 1974).

The expected importance of X-ray polarisation measurements from supernova remnants as a class of objects, rather than just the Crab Nebula, does not appear to have attracted individual attention in the literature. However, Cas A, which exhibits a power law spectrum, is a good candidate for X-ray polarisation measurements so that its strongly

indicated synchrotron emission mechanism may be confirmed (Novick 1975).

Extragalactic Sources

Novick (1974) states that identifications have been made for the extragalactic sources NGC1275 (Perseus A), NGC4151 (Seyfert galaxy), M87 (NGC4486, 3C274), NGC5128 and 3C273 (quasar), and that the nature of the X-ray emission mechanism from these objects is still obscure. Both thermal and non-thermal models have been proposed.

Polarised optical radiation has been observed in the jet of M87, the giant elliptical galaxy in the Virgo Cluster. Individual knots in the jet have been observed to have polarisations of about 20%, indicating synchrotron emission. Depending upon the relative intensities of these knots, it is predicted that integrated polarisation of perhaps 5 to 10% should be expected for X-rays emitted in the jet.

Radio polarisation observations of small diameter variable sources have shown that, although sources like Perseus A (NGC1275) and the quasar 3C273 have small net polarisations (2%), the variable components have rather large polarisations (10 - 20%).

Novick notes that for some of these objects strong infrared emission may deplete the high energy electrons by Compton-type processes, in which case not much X-ray emission by the synchrotron process would occur, but that it is by no means clear that this happens in all or most of the sources.

X-ray polarisation observations of these objects would provide information about the radiation mechanism, and, if positive results are obtained, could give much information on the compact sources that are probably responsible for the energetics of radio galaxies and quasars.

Thus, it is clear that X-ray polarisation measurements hold importance for deciding between emission mechanisms, detecting weaknesses or confirming strengths in emission theories, and in simply gathering

information where existing theory is almost totally lacking or underdeveloped.

Finally, it is noted that Novick (1974) has discussed various types of X-ray polarimeters in addition to the scattering and Bragg crystal reflection types mentioned here, and described a further X-ray polarimeter (a high sensitivity focusing Bragg crystal type) scheduled to be flown on the U.S. satellite OSO I. This satellite was also launched successfully, during June 1975 (Weisskopf et al. 1976), approximately 8 months after the launch of Ariel-V.

§ 3	<u>THE ARIEL-V SATELLITE AND POLARISATION EXPERIMENT</u>	
		Page No.
§ 3.1	THE ARIEL-V SATELLITE	36
1.	Introduction and General Parameters	36
2.	The Experiments	38
3.	Satellite Data Handling from the Experiments	38
4.	Transmission of Data to Ground Stations	40
5.	The Orbital Clock and Sector Generator	40
6.	The Experiment Command Registers	41
7.	Background Radiation Monitors	42
§ 3.2	THE SPECTROMETER/POLARIMETER EXPERIMENT	43
1.	General Description	43
2.	The Honeycomb Collimator	45
3.	The Crystal Panels - and Calibration	45
4.	The Detectors - and Background Rejection Techniques	51
5.	Experiment Modes - and Satellite Handling of Data	58
6.	Command Register	61

§ 3.1 THE ARIEL-V SATELLITE

§ 3.1.1 Introduction and General Parameters

The program for this satellite had its beginnings in discussion between senior Science Research Council staff and N.A.S.A. headquarters staff at the launch of the Ariel III satellite in May 1967. The project satellite name before launch was UK-5, in common with previous satellites in the UK series for which the names are changed to 'Ariel' after launch. The scientific objective for the UK-5 satellite was the study of cosmic X-ray sources.

By the 15th October 1974, the satellite had been transported to the Italian San Maro range situated in the Indian Ocean just off the coast of Kenya, mounted to an American Scout B rocket, and was ready for launch.

The satellite was successfully launched that day, achieving the nominal orbital parameters set out in the Flight Qualification Review (1973). Injection was made into a nearly circular equatorial orbit of altitude 550×503 km at an inclination of 2.9° to the equator. The orbital period was ≈ 97 minutes. An artist's illustration of the satellite, an approximately cylindrical object about 1 m in diameter and length and weighing about 300 lbs, is depicted in Fig. 3.1.1.

As the satellite power was provided by solar cells, sufficient power to operate the experiments occurred only during ≈ 60 minutes of the orbital period. For this reason the experiments were switched off as the satellite entered the 'night' portion of the orbit. Spin-axis stabilisation and pointing were both achieved by the use of pulsing jets employing propane gas. The propane tank contained sufficient fuel at launch for spin-rate maintenance (of ≈ 10 r.p.m.) and altitude manoeuvres of 6000 degrees in steps of up to 20 degrees. Earth albedo

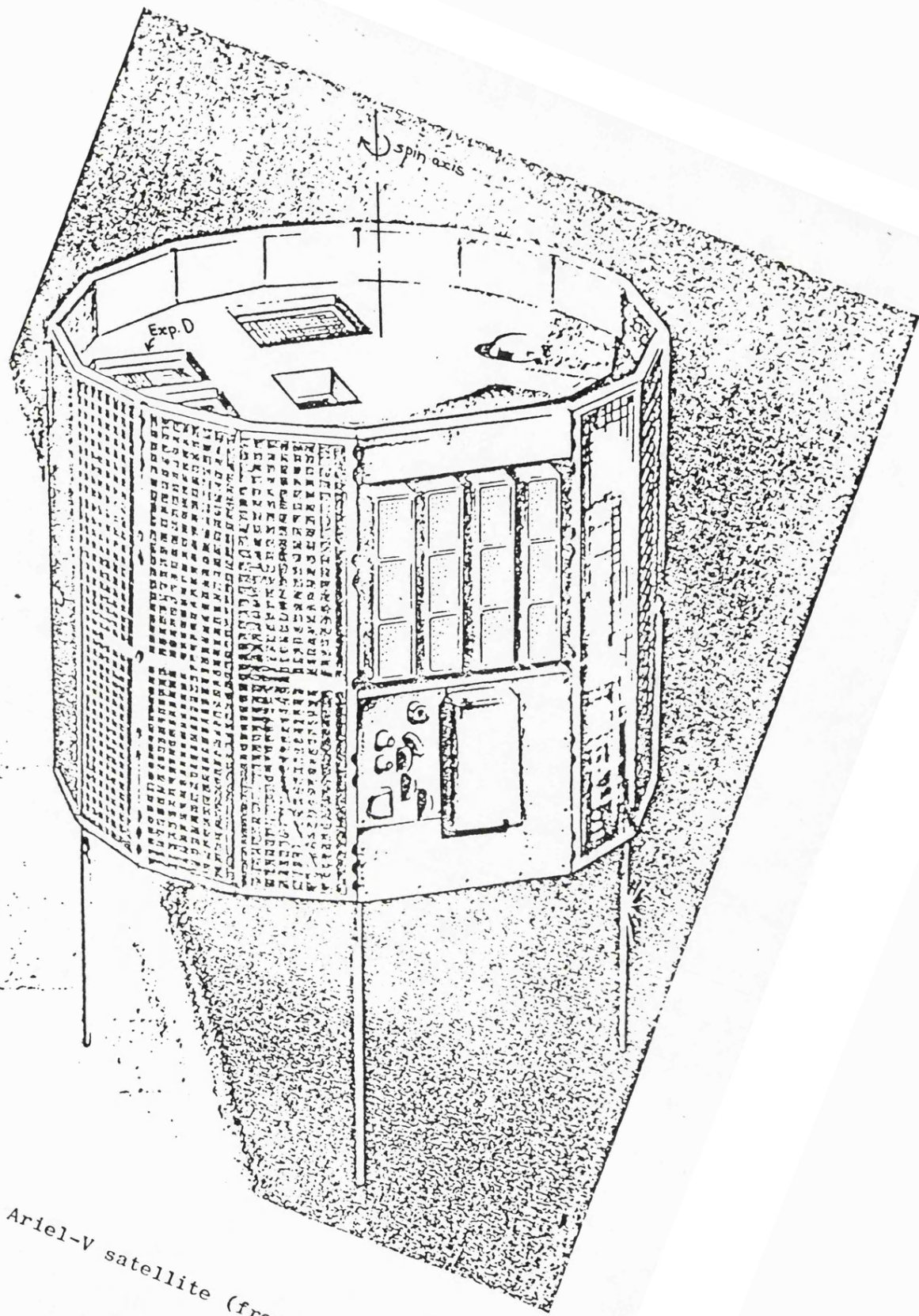


Fig. 3.1.1: The Ariel-V satellite (from Peacock 1975)

and Sun sensors were employed to give an overall attitude accuracy of $\pm \frac{1}{2}^\circ$. Spin-axis drift was minimised by the operation of a Dipole Cancellation Magnetorquer (D.C.M.) to $\leq 0.1^\circ \text{ orbit}^{-1}$. Limitations on pointing spin-axis directions were imposed by power constraints, because of the solar cells, to greater than 45° from the Sun or anti-Sun directions.

The minimum lifetime specified for the satellite was four months, though one year was considered a desirable aim. The satellite was still functioning effectively after 12,000 orbits, more than 2 years since launch.

§ 3.1.2 The Experiments

Six experiments were contained in the spacecraft and these are listed in Table 3.1.2. Four experiments were designed to view along the spin-axis, and two to scan the sky as the satellite spins.

The overall scientific objectives of the 6 experiments were as follows:-

- i) A survey at X-ray wavelengths of the whole sky.
- ii) Accurate position determination and spectra for specific sources.
- iii) The study of sources with pulsed emission.
- iv) The study and search for binary X-ray sources.
- v) Detection of transient X-ray sources.
- vi) Polarisation and emission line studies of specific sources.

§ 3.1.3 Satellite Data Handling from the Experiments

Data handling from the experiments incorporated two 4096 word, 8 bit, core stores each servicing 3 experiments.

Data from the satellite housekeeping encoder and background monitor hardware (see § 3.1.7) shared one of the core stores with data

Experiment	Research Group	Experiment Definition	Field of View FWHM Degrees	Energy Range (keV)	Mission
A	Mullard Space Science Laboratory	Rotation Modulation Collimator with Associated Star tracker	17	0.3 - 30	To position X-ray sources to within 5 mins of arc
B	Leicester University	Collimated Proportional Counter System	10 x 0.75	1.5 - 20	Sky Survey
C	Mullard Space Science Laboratory	Proportional Counter with 128 channels of Pulse height information	3.5 x 3.5	2 - 30	Detailed study of X-ray Source Spectra
D	Leicester University	Bragg Crystal Spectrometer / Polarimeter	7.5	2 - 8	Polarization and Emission line studies
F	Imperial College	Caesium Iodide Scintillator with active Collimator	8.0	20 - 2000	High energy Spectral Studies
G	Goddard Space Flight Centre	Two Pin-hole Cameras	360	3 - 6	All Sky Monitor

Table 3.1.2: Ariel-V Payload Summary (from Peacock 1975)

from experiments A, C and G. Experiments B, D and F shared the other core store.

Each source of data was allocated a 4 bit address, and these were interrogated in turn by a scanner. If an experiment detected an event, it interrupted the scanner demanding a service. Relevant information was then connected to what was known as "the data highway" forming a unique core store address. The number contained by that address was then incremented by one.

§ 3.1.4 Transmission of Data to Ground Stations

Data stored in the satellite on-board core stores was normally read out at one orbit intervals, on command, to ground stations of the N.A.S.A. STADAN network. The ground stations used were at Quito in South America and at the Ascension Islands in the Atlantic Ocean.

To enable the accuracy of the data transmission link to the satellite to be determined for each ground station pass, the satellite was commanded to read down the data three times. (Later on in the transmission system at the U.K. control centre, comparison of these 3 readouts were used to give a data quality percentage to each orbit's data. This allowed the experimenter the possibility of discrimination against possible bad data).

§ 3.1.5 The Orbital Clock and Sector Generator

These facilities provided by the satellite allowed the time of a detected event from an experiment to be recorded, and also the rotation orientation of the satellite to be known at that time.

The orbit clock was reset automatically after a command dump of the satellite's orbit data. It counted into a 12 bit register connected to the data handling system, allowing testing of various significant bits so that new core store allocations could be made for data collected at

different intervals. Thus, this 12 bit register could be used to separate sections of integrated data and hence select a desired time resolution for an experiment. This facility could be used for the study of time varying sources, for rejecting sections of data having high background levels or where the Earth has occulted an experiment's view to an X-ray source.

The sector generator operated to divide the 360° rotation of the satellite into 1024 equal separate divisions (or sectors). The rotation angle at any particular time was given by a 10 bit binary number. The start sector was determined every revolution by the arrival of a pulse from the Sun-sensor equipment. To ensure adequate accuracy a spin-period count from which the sector number is derived was updated every 64 seconds. Similarly, as for the orbit clock register, choice of various significant bits of the sector generator binary number allowed separation of data into various sized rotation angle blocks. This was obviously important for the scanning experiments where each rotation section implied that a different portion of the sky was being viewed; and also, for example, the polarisation experiment where the principle of detection of polarisation depends upon recording different count rates for different rotation segments (see § 4.2).

Control of time and rotation angle (sector) resolution was determined by the state of the command registers (see § 3.1.6) provided for each individual experiment.

§ 3.1.6 The Experiment Command Registers

Each experiment was provided with a multi-bit shift register which contained information defining the experiment state. This information was defined by the experimenter, and was transmitted to the satellite from a ground station during a ground station pass.

Thus the command register provided a link allowing the experimenter control of his experiment. Choice of time, sector resolution or hardware experiment mode, re-calibration or switch off of faulty components could be made during each ground station pass.

§ 3.1.7 Background Radiation Monitors

The satellite was also provided with a background monitor and rejection system, from counters in Experiments C and D. These counters were used as a measure against contamination of experiment X-ray data by spurious background counts during the passage of the spacecraft through areas of high intensity radiation, notably over the South Atlantic anomaly. When the background level passed a threshold count rate, a signal was transmitted to all the experiments (i.e. a flag was set) enabling a choice of inhibiting or restarting data collection. The threshold count level was independent for both the experiment C and D counters, and could be adjusted by ground command. As it was necessary to know the total observing time, if count rates were to be calculated, the orbit times at which the spacecraft entered and left the high flux region were recorded in the core store.

§ 3.2 THE SPECTROMETER/POLARIMETER EXPERIMENT

This experiment, known as experiment D, was one of the two experiments supplied by the Leicester group. It was situated in the aft region of the spacecraft so that its field of view was directed along the pointing axis of the satellite (see Fig. 3.1.1).

Information concerning a general description of the instrument was taken from the UK-5 Flight Qualification Review (1973), Griffiths et al. (1976), and Peacock (1975). Further information concerning calibration of the crystals was taken from Evans et al. (1976, 1977a and 1977b).

§ 3.2.1 General Description

The instrument is illustrated in Fig. 3.2.1, and is of the Bragg crystal type. X-rays entered the instrument through a honeycomb collimator mounted directly above 2 plane crystal assemblies. Bragg reflected X-rays from these crystals were then detected by 2 proportional counter detectors sensitive in the energy range 2-10 keV. Pulses from the proportional counters were fed through a single channel pulse height analyzer, and other electronics, designed to reduce events due to background effects. Finally, accepted events were then fed into the satellite data handling system which channeled them into storage.

Each crystal panel was constructed with a drive, so that independent movement to one of 62 Bragg reflection angles in the range 25° to 65° could be made.

All parts of the instrument were enclosed in a rectangular framework containing a stiff intermediate floor on which the crystal pivots and drives were mounted and from which the experiment electronics and high voltage supplies were suspended. Crystal drive was accomplished using a MoS_2 lubricated, low friction ball-screw, driven by a geared

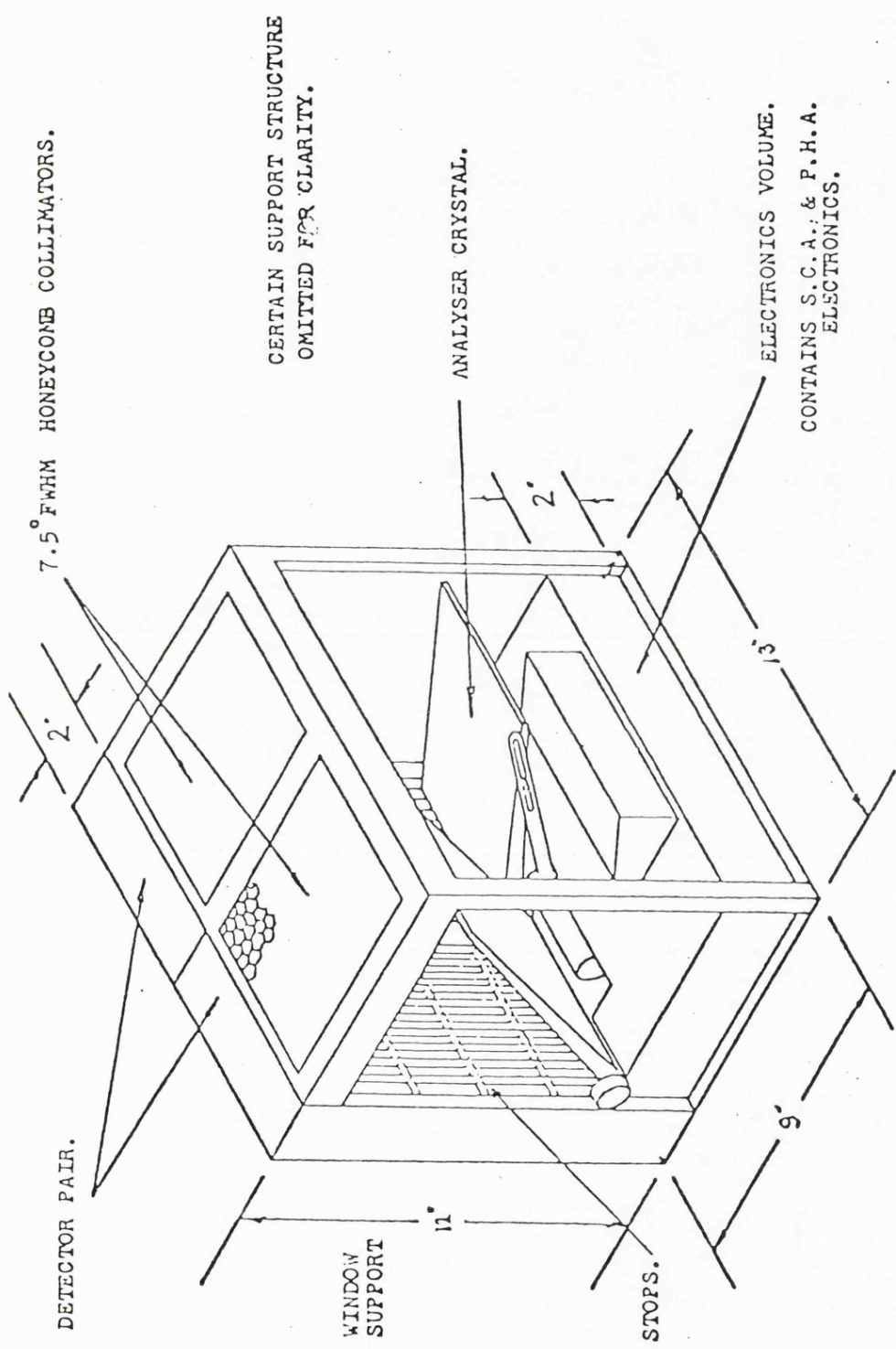


Fig. 3.2.1: The Ariel-V Spectrometer/Polarimeter (from Peacock 1975)

stepping motor. All bearings were space proven. Prevention of damage to the bearings during launch was accomplished by edge clamping each crystal assembly with pneumatically operated rubber pads. After launch the pressure was released by a commandable valve.

§ 3.2.2 The Honeycomb Collimator

This restricted the field of view of the instrument to 7.5° at full width half maximum, thus acting to reduce counts from the diffuse X-ray background and to help prevent multiple X-ray sources being viewed simultaneously. The collimator also prevented sky radiation from falling directly onto the detectors without having been reflected by the crystal.

The transmission $T(\Delta)$ to X-rays by this fabricated aluminium collimator is given by the expression

$$T(\Delta) = 0.81 \left(1 - \frac{\Delta}{7.5} \right) \quad (1)$$

where Δ represents the angle at which the X-ray source being viewed is offset from the satellite spin-axis.

§ 3.2.3 The Crystal Panels - and Calibration

It is Bragg reflection of X-rays off the crystals which is polarisation dependent (the mathematical analysis is conducted in § 4.2), and therefore the sensitivity of the instrument depends on the crystal reflecting area and the amount of reflection. Also, if the detected count rates are to be converted into incident photon flux allowing the sensitivity of the instrument to known X-ray sources to be estimated, then the reflection characteristics of the crystal panels must be known.

One of the crystal panels was composed of an assembly of graphite crystals (002 planes) and the other of lithium fluoride crystals (200). The panel areas, crystal thicknesses and interplanar distances

for the two crystal assemblies are given in Table 3.2.2.

Table 3.2.2

Characteristic	LIF (200)	Graphite (002)
Area A_0 cm ²	234	234
Thickness cm	2.5×10^{-2}	1.5×10^{-1}
interplanar distance $2d$ Å	4.0267	6.708

The separation distance d between the crystal planes, together with the Bragg angle θ_B between the incident X-ray direction and plane of the crystal area, determines the wavelength for which Bragg reflection occurs, according to the following formula

$$n \lambda = 2d \sin \theta_B \quad (2)$$

where n specifies the order of reflection. As $E = h\nu$ and $c = \nu\lambda$ for photons, (2) can be rewritten in terms of energy selection as follows:-

$$E = \frac{n hc}{2d \sin \theta_B} \left(\frac{1}{10^3 e} \right) \text{ keV} \quad (3)$$

where h is Planck's constant (joule s), c is the velocity of light (ms^{-1}), e is the electron charge (coulombs) and d is measured in metres. Then, the different Bragg angle settings made possible by the movable crystal, allows variation of the X-ray energy detected by the instrument. (This feature was designed for line emission searches, since polarisation studies are optimised at $\theta_B = 45^\circ$. See § 4.2).

However, for a real crystal, reflection of monochromatic X-rays does not just occur at the Bragg angle θ_B , but is spread out over a small range of angles. This spread determines the energy resolution (or effective bandwidth) of the crystal.

If a monochromatic parallel beam of intensity I_0 is incident on a plane crystal which is large enough to accept the entire beam, and the angle of incidence θ is uniformly scanned, then the intensity of the reflected beam $I(\theta)$ traces a profile known as the "Rocking Curve", with the total number of reflected photons equal to ϵ . The fraction of the total incident beam reflected at angle θ is given by

$$\frac{I(\theta)}{I_0} \equiv R(\theta) \quad (4)$$

The PEAK REFLECTIVITY occurs at the Bragg angle for the incident radiation $\theta = \theta_B$, and is given by the expression

$$R_{\max} = R(\theta_B) = \frac{I(\theta_B)}{I_0} \quad (5)$$

The HALF WIDTH $D(\theta)$ is the full width at half maximum of the Rocking Curve profile about the peak reflectivity, thus providing a measure of the effective bandwidth for the crystal.

The total recorded counts is given by

$$\epsilon = \int I(\theta) \frac{d\theta}{\omega} \quad (6)$$

where ω is the scan rate expressed in radians s^{-1} .

Thus,

$$\frac{\epsilon \omega}{I_0} = \int \frac{I(\theta)}{I_0} d\theta = \int R(\theta) d\theta \equiv R_c \quad (7)$$

where R_c is known as the INTEGRATED REFLECTIVITY of the crystal and is normally expressed in units of radians. R_c is the area under the reflectivity versus angle curve and from (7) it can be seen that as ϵ , the total number of reflected photons, increases then R_c increases in proportion. Thus a larger value of R_c means that more photons will be reflected so that the effectiveness of the instrument to polarisation will be increased.

For many crystals the half width and the integrated reflectivity are much greater than would be expected for perfect crystals using diffraction theory. The mosaic structure of the crystals explains this phenomena. Many small crystals domains within a large crystal structure are orientated slightly differently. The increase in half width follows immediately. The increase in integrated reflectivity follows because incident X-rays penetrate several of the mosaic components, and therefore have several chances to be reflected.

For polarisation studies the maximum integrated reflectivity is desired. However, high resolution was required for use of the instrument in searches for line emission where the half width is required to be narrow. For the Ariel-V crystals this meant a compromise, resulting in an estimated reduction of the maximum integrated reflectivity by a factor of 2 (Evans et al. 1977), with a corresponding drop in sensitivity for polarisation studies.

Both R_c and $D(\theta)$ are, in practice, a function of energy.

Also, in practice, for polarisation observations, it is not a monochromatic beam of X-rays which is observed by scanning θ , but usually a continuum with θ held constant. In this case the expression for the total number of photons reflected differs from (6) (Evans and Leigh, 1976), and becomes:

$$\frac{\epsilon}{T} = \frac{1}{E_{ph(\theta)}} \int_0^{\infty} I(\theta, \lambda) R(\theta, \lambda) d\lambda = \frac{I(\theta, \lambda_{\theta}) \lambda_{\theta} \cot \theta R_c}{E_{ph(\theta)}} \quad (8)$$

where $\frac{I(\theta, \lambda)}{E_{ph}}$ (9)

is the continuum intensity (ph λ^{-1} cm⁻² s⁻¹), T is the observing time (s), E_{ph} is the energy of a single photon (keV), the subscript θ refers to the Bragg angle θ such that $n\lambda = 2d \sin \theta$, and R_c still emerges as the calibration factor for the crystals. Equation

(8) then, knowing R_c , allows calculations of the sensitivity of the instrument as a polarimeter under realistic conditions where the intensity of the X-ray source is given by (9).

Each of the Ariel-V crystal assemblies consisted of 6 smaller crystals fixed on a plate, and the values of R_c for the individual crystal pieces are given in Table 3.2.3 for various line radiation sources.

Table 3.2.3

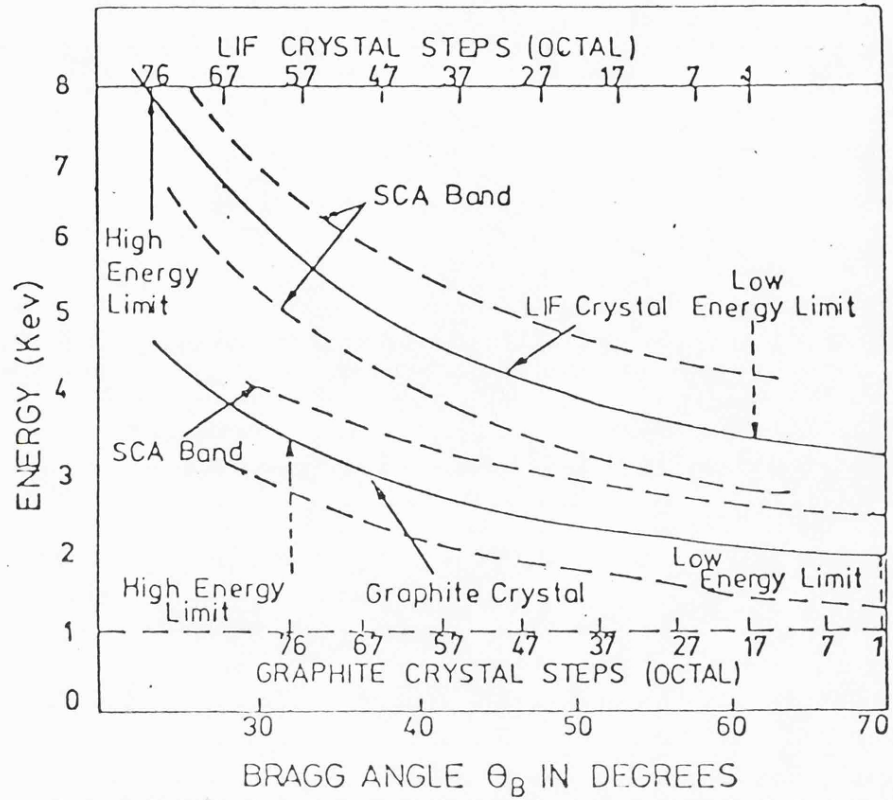
Graphite (002)			
Line Source	Wavelength λ \AA	Energy (keV)	$R_c \times 10^4$ rads
P $k\alpha$	6.158	2.0	9.22
Nb $k\alpha$	5.713	2.1	7.49
Ru $k\alpha$	4.830	2.5	5.68
K $k\alpha$	3.742	3.3	7.411
Ca $k\alpha$	3.360	3.7	9.21
LiF (200)			
Line Source	Wavelength λ \AA	Energy (keV)	$R_c \times 10^4$ rads
Ca $k\alpha$	3.36	3.7	3.1
Ti $k\alpha$	2.75	9.5	2.1
Fe $k\alpha$	1.9	6.4	2.5

The half width value will be broader than the values of individual crystals when assembled on the plate, due to misalignments. The typical values found for the assembled plates were $\approx 27'$ for graphite at 2.0 keV and $11.4'$ for the LiF assemblage at 3.7 keV. The variation of R_c with Bragg angle is shown in Fig. 3.2.4 for both crystal plate assemblages.

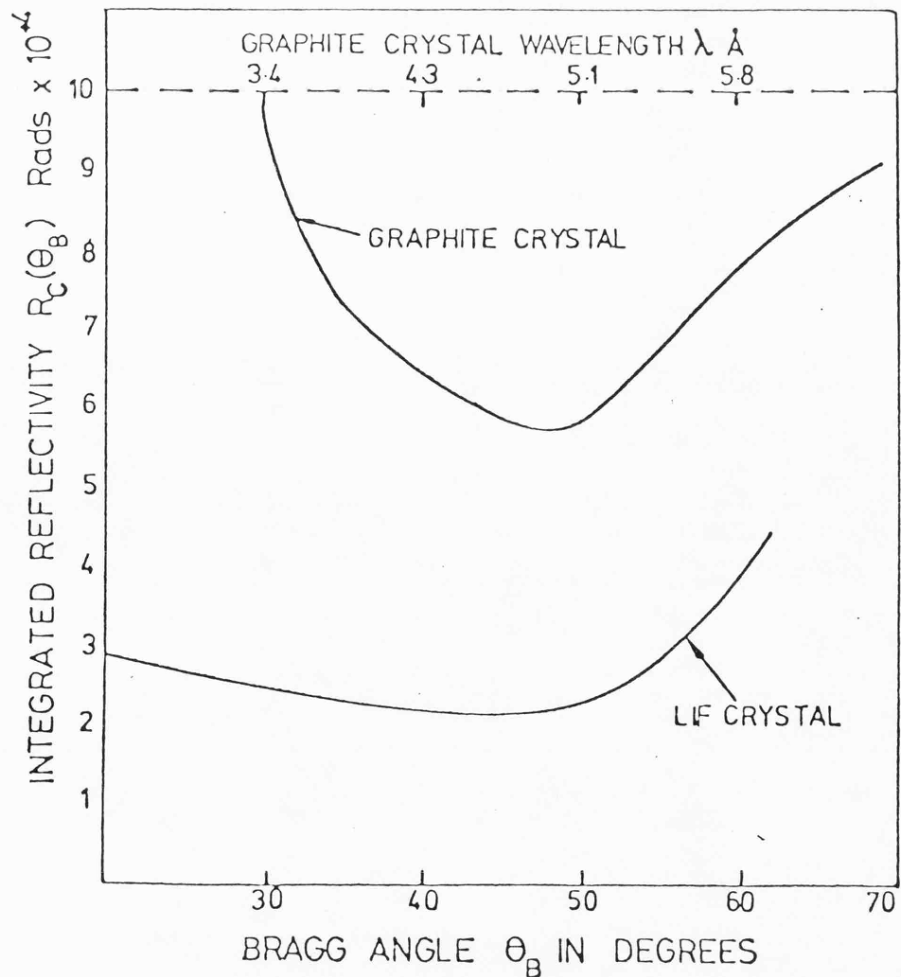
R_c also depends on the polarisation characteristics of the incident test beam, and for accurate polarisation measurements, calibration

Fig. 3.2.4: (from Peacock 1975)

a) SCA Bands and Crystal Positions



b) Variation of Integrated Reflectivity with Bragg Angle



of this variation of R_c is required. A plot of the variation of R_c as the instrument is rotated about the line of sight to a plane polarised test beam, keeping the angle of incidence θ_B constant, will show the sensitivity to polarisation. This sensitivity is evaluated to determine a modulation factor m for the instrument. However, the Ariel-V instrument was designed for use only at Bragg angles θ_B close to 45° where the modulation factor is confidently expected to be near unity, and calibration was considered not to be required within the accuracy limitations of the instrument under estimated observing conditions. (A more detailed discussion of the theoretical considerations for the determination of m , and its variation with Bragg angle, are given in § 4.2.2).

The total number of photons reflected also depends upon the area of the crystal assemblies, and is clearly a function of the incident Bragg angle, and of the form

$$A(\theta_B) = A_0 \sin \theta_B \quad (10)$$

However, this area is further reduced by various mechanical stops, and the complete function is shown graphically in Fig. 3.2.6a for the general range of Bragg angles appropriate to both crystals.

§ 3.2.4 The Detectors - and Background Rejection Techniques

The physical characteristics of the two proportional counters, employed to detect the Bragg reflected X-rays, are summarised in Table 3.2.5.

The efficiency of any one detector is given by the expression

$$\text{eff}(E) = \exp\left(-\frac{t\omega}{\lambda\omega}\right) \left(1 - \exp\left(-\frac{tg}{\lambda g}\right)\right) \quad (11)$$

where $t\omega$ = window thickness, tg = gas depth, $\lambda\omega$ = absorption mean

free path in the window and similarly λg for the gas.

Table 3.2.5

Characteristic	Low Energy Counter	High Energy Counter
Window thickness	$8.6 \cdot 10^{-3}$ cms	$1.3 \cdot 10^{-2}$ cms
Window material	Beryllium	Beryllium
Weight of window	6.6 grams	3.87 grams
Detector depth	1.8 cms	1.8 cms
Area of Counter	125 cms^2	135 cms^2
Gas mixture	76.5% A 15% Xe. 8.5% CO_2	76.5% A 15% Xe. 8.5% CO_2
Filling pressure	103.3 cms Hg	106.0 cms Hg
HT Voltage	2120 V	2030 V

Fig. 3.2.6b shows the transmission of beryllium for various photon energies for both detector windows, for X-rays at normal incidence. Similarly, Fig. 3.2.6c shows the appropriate absorption in the gas as a function of photon energy. Clearly, from (11) the efficiency of the detector is dependent on both the depth of gas and window thickness, both of which will vary with the angle of the incident flux according to the relation $t\omega' = t\omega / \cos \theta$ where θ is the angle from the normal, and $t\omega'$ the effective window thickness. Similarly, $tg' = tg / \cos \theta$. Thus the efficiency of the detector is a function of the geometry of the crystal-detector system, as well as of the energy. The computed efficiencies of the detectors as a function of Bragg angle are shown in Fig. 3.2.6d.

A new effective area $A'(\theta_B)$ can now be defined, as the area presented to any incident X-ray beam being the product of the crystal area and detector efficiency. Thus:-

$$A'(\theta_B) = A(\theta_B) \text{ eff } (\theta_B) \quad \text{cm}^2 \quad (12)$$

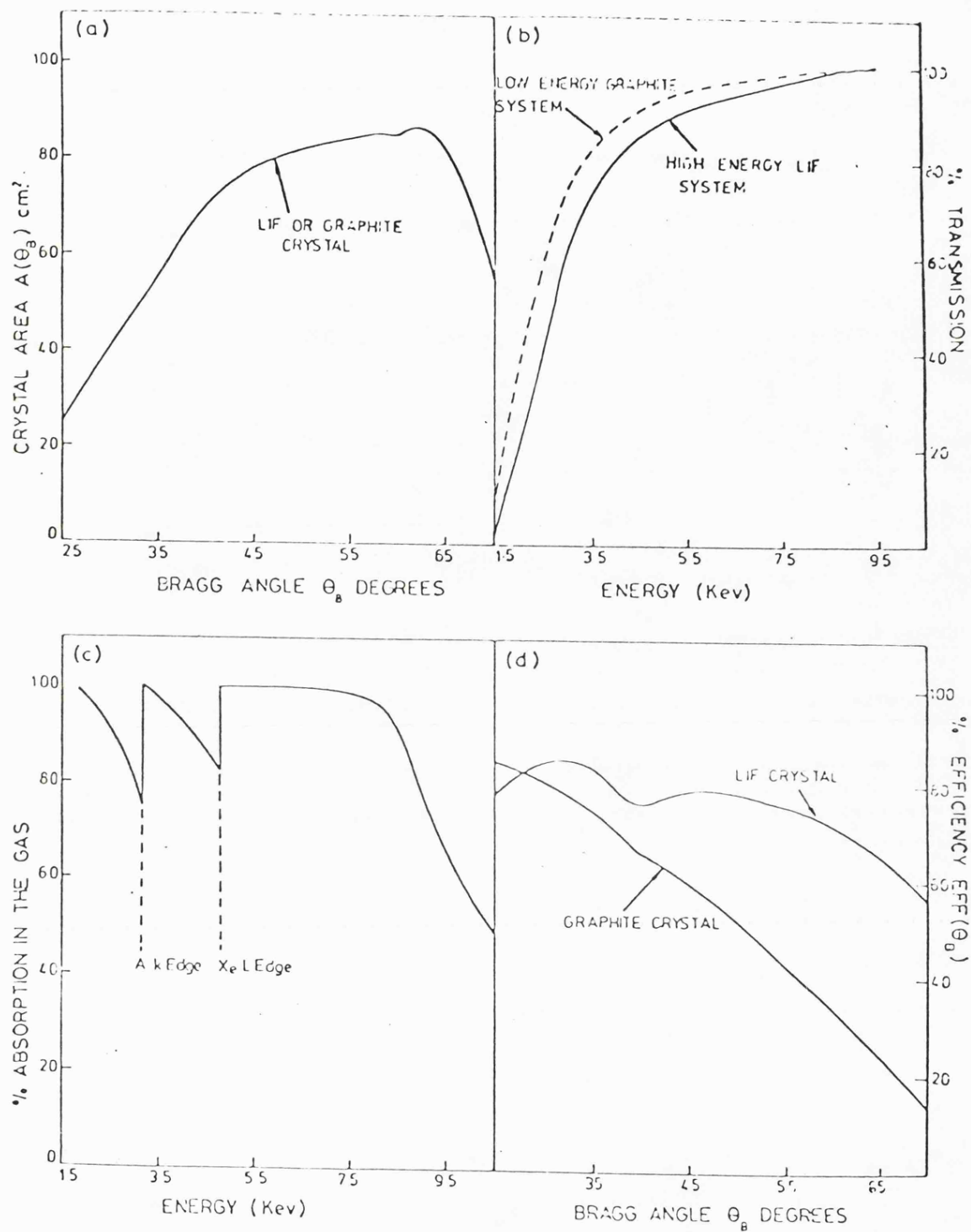


Fig. 3.2.6: (from Peacock 1975)

This function $A'(\theta_B)$, however, shown in Fig. 3.2.7a, does not contain the reflectivity of the crystal.

Because the detectors are also sensitive to background noise effects which reduce the overall instrument sensitivity to polarisation, background rejection systems were employed.

Three sources of background noise have to be dealt with:-

- (i) The diffuse cosmic X-ray background.
- (ii) The cosmic-ray induced background consisting of primary charged particles, and the γ -rays created by them either in the upper atmosphere or in the satellite.
- (iii) E.H.T. breakdown inside the detector, which can be eliminated by careful design.

The diffuse flux can enter the detector either directly or by X-ray diffraction. The former was potentially the much greater of the two and to eliminate this effect plate 'stops', carefully collimated in two planes, were placed in front of the detectors and were attached to the window support frame (see Fig. 3.2.1) to inhibit any flux entering past the honeycomb collimator at a large angle.

Peacock (1975) considered the effect from a diffuse X-ray flux entering the detector by Bragg reflection, and took a background spectrum as

$$\frac{d\epsilon}{dE} = 10.3 E^{-0.35} \text{ keV cm}^{-2} \text{ s}^{-1} \text{ keV}^{-1} \text{ sr}^{-1}$$

Then, for a Bragg angle of $\theta_B = 45^\circ$, this may be substituted into the expression

$$S = A'(\theta_B) R_c(\theta_B) \cot \theta_B 10^{-2} \frac{d\epsilon}{dE} \text{ counts s}^{-1}$$

to determine a count rate of $0.002 \text{ counts s}^{-1}$ expected from the Ariel-V detector for the graphite crystal.

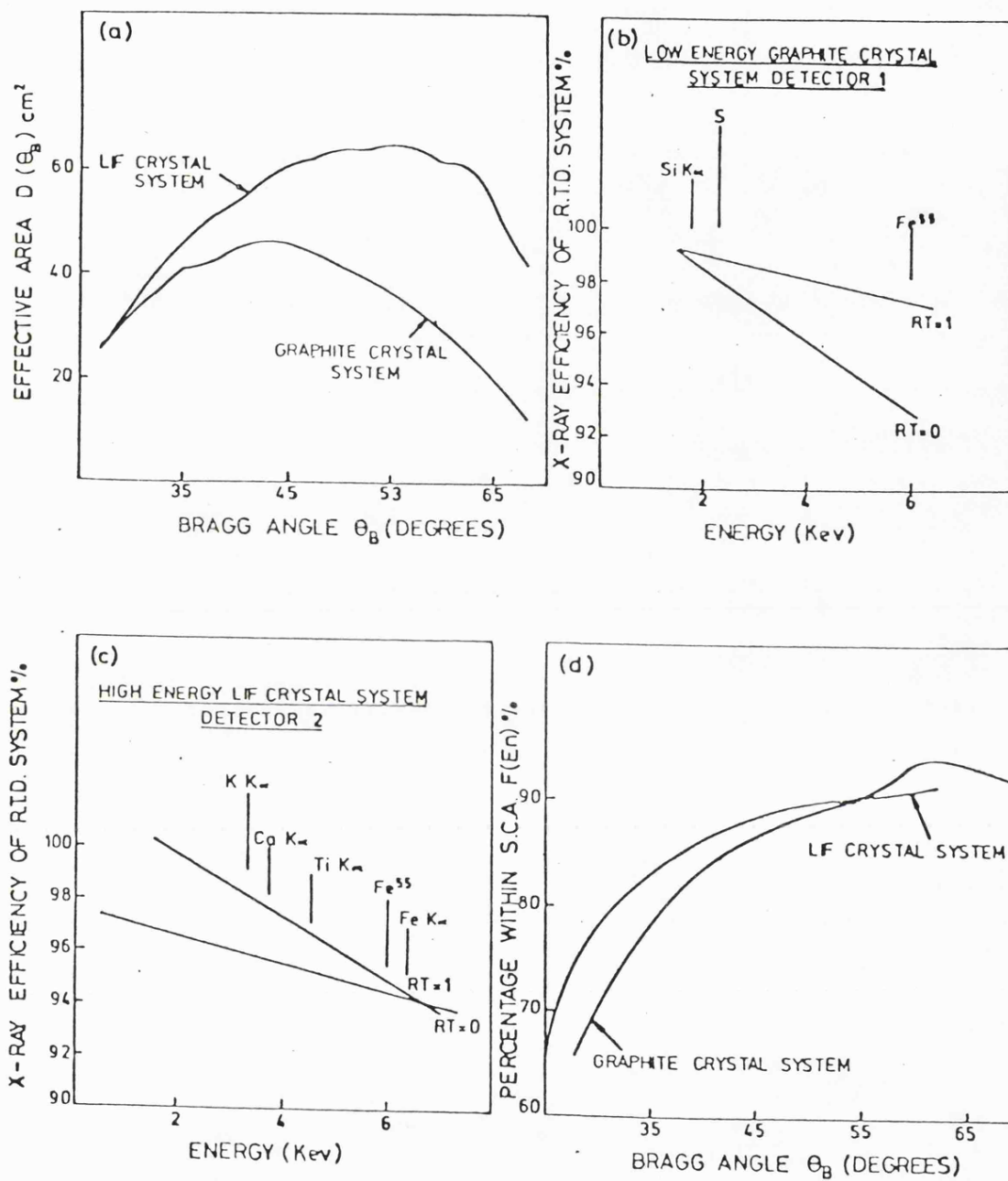


Fig. 3.2.7: (from Peacock 1975)

The flux of primary cosmic rays at the top of the Earth's atmosphere is $\approx 1 \text{ cm}^{-2} \text{ s}^{-1}$, and these particles leave ionisation tracks along the total traversed length of a proportional counter. These long ionisation tracks cause longer rise times for the proportional counter's electronic pulse than expected from an X-ray event, and therefore allows discrimination against counting these events. As this radiation is also highly penetrating, guard detectors placed on 3 sides of each proportional counter can employ anti-coincidence discrimination methods efficiently. Both these techniques were utilised for the exp-D detectors. For penetrating charged particles, anti-coincidence can be $\approx 100\%$ efficient, and rise time discrimination (R.T.D.) about 80% efficient with a loss of about 5-10% in genuine X-ray flux.

Peacock (1975) noted that lower energy secondary radiation which results from cosmic ray interactions in the spacecraft represents a more serious background rejection problem, and this aspect is discussed further in § 5.2.

The Ariel-V instrument was equipped such that the guard counter and R.T.D. could operate in two modes, so that best advantage of discrimination against the encountered background particle environment could be made. The two modes are, (i) $RT = 0$, and (ii) $RT = 1$. For the first mode the R.T.D. efficiency to X-rays is $\approx 95\%$, and the guard counter efficiency to charged particles $\approx 92\%$. That is, the guard will stop 92% of the charged particles but the R.T.D. will stop 5% of the incident X-ray flux. For $RT = 1$ the R.T.D. efficiency is $\approx 97\%$ and the guard efficiency is $\approx 91\%$. Peacock (1975) states that the exact gain in the signal to noise ratio for these different modes will be dependent upon the incident source flux as well as the particle background. The efficiency of the R.T.D. is also a function of energy

of the incoming X-rays and this is shown in Fig. 3.2.7b and c.

The amplified proportional detector pulse is interrogated by upper and lower level pulse height discriminators which confine the accepted events to within specified energy limits. The electronics for this discrimination into a single energy band was known as the "single channel analyser" or S.C.A. The energy band governed by the S.C.A. is moved according to the crystal position, which governs the Bragg angle and hence the energy of the reflected X-rays. At about 2.6 keV the S.C.A. is about 1.2 keV wide for the low energy graphite system. Upper and lower limit boundaries for both crystals at various positions are shown in Fig. 3.2.4, though they will vary throughout the experiment lifetime due to gain variations in the detectors. The S.C.A. boundaries also eliminate detection of higher orders of Bragg reflection $n = 2, 3, \text{etc.}$, given by equation (3).

Before launch of Ariel-V, Peacock (1975) estimated the expected count rates in the experiment-D detectors due to both the diffuse X-ray and cosmic ray background, predicting values of about $0.8 - 0.9 \text{ counts s}^{-1}$ from the graphite system and about 1 count s^{-1} from the LIF system.

The resolution of the proportional counter detectors at energy E_n is given by

$$R_n = \frac{\text{FWHM}(E_n)}{E_n} \quad \text{for a given crystal position } n.$$

The fraction F_n of the photons, with energy E_n , falling within the S.C.A. boundaries can be calculated from

$$F_n = \frac{1}{\sigma \sqrt{2\pi}} \int_{E_{l_n}}^{E_{u_n}} \exp\left(-\frac{(E - E_n)^2}{2\sigma^2}\right) dE \quad (13)$$

where $\sigma = \frac{R E_n}{2.36}$, and E_{1n} and E_{Un} are the upper and lower energy channel boundaries for the S.C.A. when the crystal is at the n -th position such that the peak in the Bragg reflected X-rays occur at energy E_n . The resolution of the detector varies with energy and takes the form (see Peacock 1975)

$$\text{FWHM}(E_n) = 2.36 \sqrt{(E_n K)^2 + \frac{\sigma_c^2 E_n^2}{E_c}} \quad (14)$$

where K is a constant, $\sigma_c \propto E_c^{\frac{1}{2}}$ (see Charles and Cooke, 1968) is the intrinsic counter resolution, and E_c represents the calibration source energy. The variation of F_n with crystal position is shown in Fig. 3.2.7d. In-flight calibration of the detectors is provided by an Fe^{55} source situated at the back of each detector, the resultant count rate distribution being analysed by a 16 channel pulse height analyser on each detector system.

§ 3.2.5 Experiment Modes - and Satellite Handling of Data

Data from this spectrometer/polarimeter experiment was stored in one of the two 4096 word, 8 bit core stores on board the satellite, where the words were grouped into pairs of 16 bits. This experiment had 512 (16 bit) words available for data storage.

Experiment Modes and Submodes

This experiment, in conjunction with the satellite data handling system, was designed to operate in 4 main modes, the mode being selected by two bits in the command word (see § 3.1.6). The mode information was relayed to the data handling system and required a different output from the experiment and a different function from the data handling system. The main modes were as follows:-

- i) Crystal.
- ii) Time Background.

iii) Calibration.

iv) Pulsar.

For each of these modes an interrupt (see § 3.1.3) would normally be generated by the experiment and consequent writing onto the data highway occur for certain conditions, which are as follows:-

- 1) One of the two main proportional counters detects a pulse.
- 2) This pulse is unaccompanied by a guard detector pulse.
- 3) The pulse is unaccompanied by an output from the R.T.D.
- 4) Either (a) the pulse lies between two widely set discriminator levels, or (b) the pulse lies between two closely spaced discriminator levels defined by the S.C.A.

i) Crystal Mode

For this mode interrupts are generated for conditions (1), (2), (3) and (4b). The experiment writes a crystal identity bit, and the spacecraft data handling system writes 4 orbit time bits T1 to T4, and 4 spin-sector bits (from the sector generator) S1 to S4, onto the data highway. Thus counts are distributed into core separated according to time and rotation angle blocks. The 4 orbit time bits give 16 time blocks per orbit, of which the least significant time bit, T4, cycles at 512 sec intervals. Thus, data are integrated for 512 seconds before a new set of core allocations are made. The 4 sector bits divides the full 360° rotation angle of the satellite into 16 azimuthal sections each of $22\frac{1}{2}^{\circ}$ each (i.e. data are collected for $22\frac{1}{2}^{\circ}$ of satellite rotation plane before new core store allocations are allotted). This was the main experiment mode, enabling searches for polarisation and line emission to be made.

ii) Time Background Mode

Interrupts are generated for (1), (2) and (4b). The experiment writes the crystal identity bit, and a bit which indicated whether or not

the R.T.D. has registered. The spacecraft data handling system writes in 7 orbit time bits, making new time blocks every 64 seconds. This mode could be used to study background variations around the orbit and the functioning of the R.T.D.

iii) Calibration Mode

This mode has 2 sub-modes. (Sub-modes require a different function from the experiment but the same function from the data handling system).

Calibration Normal

This mode could be used to check for gain variations in the detectors so that in flight calibration could be made. Interrupts are generated for (1), (2), (3) and (4a) with the experiment writing the crystal identity bit and 4 energy bits onto the data highway. The spacecraft data handling system writes 4 orbit time bits. The Fe⁵⁵ calibration source is switched on and off automatically for alternate orbit time periods, and the resultant count distribution analysed by a 16 channel pulse height analyser for each detector.

Calibration R.T.D.

This mode was designed for R.T.D. studies. Interrupts are generated for (1), (2), (4a) and (3) reversed, i.e. the detector pulse must be accompanied by an R.T.D. pulse. Writing on the data highway is the same as for calibration normal.

iv) Pulsar Mode

This mode also has two sub-modes.

Pulsar Polarisation

This mode was designed either for observation of polarisation from pulsars, or conversely pulsations from polarised sources. Interrupts are generated for (1), (2), (3) and (4b). The spacecraft writes in all 11 bits of information, 4 of pulsar phase, 5 of pulsar time and 2 of

sector information. This experiment mode observes continuously. The output counts are routed into one of 16 time channels in a cyclic manner at the pulsar frequency which is previously specified. Any modulations in the intensity at this frequency will appear as a difference in the count rate accumulated in the various channels. This mode requires the full two 4096 word core stores to be used. Further details of the operation of this mode can be obtained from Peacock (1975).

Pulsar Line

This mode was designed for the study of possible line emission from pulsating sources, and a similar situation exists as for pulsar polarisation mode, except that the experiment only operates over 180° of spacecraft rotation.

§ 3.2.6 Command Register

A 27 bit shift register was used to control this experiment and the function of each bit is given in Table 3.2.8.

Table 3.2.8: Experiment D Command Register

Register Bit Number	Function					
	Bit	24	23	22	Mode	Sub-Mode
24)	Mode	0	0	0	Cal	Normal
23)		0	0	1	Cal	R.T.D.
		0	1	X	Crystal	
22		1	0	1	Time	
		1	1	0	Pulsar	Polarisation
		1	1	1	Pulsar	Line
21	H.T. 1 ON/OFF	'1' = ON				
20	H.T. 2 ON/OFF	'1' = ON				
19	CAL continuous	'1' = CAL, '0' = Normal				
18 to 16)	Crystal 1	Coarse position control				
15 to 13)	(Graphite)	Fine position control				

a) If bits 18 to 13 all '1' or '0' then crystal 1 position unchanged.

12 to 10) Crystal 2 Coarse position control
 9 to 7) (LIF) Fine position control

- b) If bits 7 to 12 all '1' or '0' then crystal 2 position unchanged.
- c) Bits 13 to 18 all '1' and bits 7-12 all '0' = open crystal clamp gas valve.
- d) Bits 13 to 18 all '0' and bits 7-12 all '1' = close crystal clamp gas valve.

6 to 4 S.C.A.2 gain trim
 3 to 1 S.C.A.1 gain trim

25 R.T.D.1 Fast/Slow '1' = slow

26 R.T.D.2 Fast/Slow '1' = slow

27 Background rate flag selector. '1' = Rate flag 1
 (from Exp. C)
 '0' = Rate flag 2
 (from Exp. D)

§ 4 DATA ANALYSIS

		Page No.
§ 4.1	LEICESTER GENERAL DATA HANDLING AND ANALYSIS SYSTEM	65
	1. Introduction	65
	a) Data transmission from the Ground Stations to the U.K. Control Centre	65
	b) Data Handling by the U.K. Control Centre and Transmission to Leicester	65
	2. General Structure	66
	3. Raw Data Bases - and Data Handling System	66
	4. Real Time Analysis - R.T.A.	67
	5. Orbit Slot Analysis - O.S.A.	71
	6. Long Term Analysis - L.T.A.	76
§ 4.2	POLARIMETER DATA ANALYSIS	77
	1. Electromagnetic Radiation and Polarisation	77
	a) Mathematical Introduction	77
	b) The Polarisation Ellipse	79
	c) Phenominological Development of the Stokes Parameters	81
	d) Addition of the Stokes Parameters - and Extention to Partially Polarised Radiation	84
	e) The Degree of Polarisation	87
	f) References Axes - Position Angle of Polarisation	89
	2. Polarisation Properties of the Ariel-V Polarimeter	92
	a) Polarisation Dependence of Bragg Reflection from a crystal.	92
	b) The Modulation Factor: $m = \frac{1-k}{1+k}$	103
	c) Polarisation Interpretation from the Ariel-V Data	105
	d) Determination of the Stokes Parameters	107
	3. Instrument Sensitivity to Polarisation - and Prediction Thereof	111
	a) Introduction	111
	b) Fundamental Statistical Limitations	112
	c) Systematic Errors	139

	Page No.
4. Extraction of Polarisation Parameters from the Ariel-V Data	167
a) Computer Summation of the Ariel-V data (SUNSEC1 program)	167
b) Determination of Modulation Amplitudes and Phases in the Summed Data - and their Standard Deviations	171
c) Determination of the Degree of Linear Polarisation - and its Standard Deviation	176
i) When no spurious modulations exist in the data	176
ii) When spurious modulations exist in the background data	179
d) Determination of the Polarisation Position Angle - and its Standard Deviation	180
e) Computer Program RUNPOL	193

§ 4.1 LEICESTER GENERAL DATA HANDLING AND ANALYSIS SYSTEM

§ 4.1.1 Introduction

§ 4.1.1a Data Transmission from the Ground Stations to the U.K. Control Centre

After reception of an orbits data at the Quito or Ascension ground receiving stations, it was transmitted to the N.A.S.A. Goddard Space Flight Centre (G.S.F.C.). There the data was either held or transmitted directly on, so that arrival at the U.K. control centre could be within about 40 minutes of a ground station pass. The American experiment G data was accessed directly from G.S.F.C.

§ 4.1.1b Data Handling by the U.K. Control Centre and Transmission to Leicester

The U.K. control centre was situated at the Radio and Space Research Station (R.S.R.S.) at Slough, and performed operations with the data relevant to all the other 5 experiment groups concerned.

For about 6 of the 14 or 15 orbits data which the satellite produced each day, immediate processing was performed, for example computing crude satellite attitudes from the spacecraft attitude sensor data. This immediate processing meant that transmission could be made to the experimenter within about 2 hours of initial data transmission from the satellite. This data was termed "quick look", and allowed the experimenter "real time" analysis possibilities. All of each day's 14 or 15 orbits data were processed on a slightly longer timescale, producing slightly more accurate information. This data was termed "Bulk", and was available for transmission the following day.

The U.K. control centre stored all the processed data, creating "master" tapes holding every orbit received and also other tapes which

could be made available to the experimenters.

Transmission of the data to Leicester was performed via the G.P.O. telephone lines, where reception was composed of a modem linked in to a PDP-8/E computer.

§ 4.1.2 General Structure

Because of the large volume of data expected from the satellite from both the Leicester experiments B and D (about 5000 orbits per year), and also the diverse nature of parameters required to be derived from the data, much thought was given to data bases and production of an efficient analysis system. (See Eadie 1976, Silk 1975 and Peacock 1975).

The above requirements naturally led to a computer orientated analysis system utilising data bases suitable for computer access. About 2 years prior to launch were employed developing the data reduction programs, together with continuous post-launch improvements and additions.

Three specific purpose analysis systems were devised, and these are discussed individually, following § 4.1.3.

§ 4.1.3 Raw Data Bases - and Data Handling System

The system by which raw data bases were created was continuously improved according to need, and in the light of experience. Only the essentials of the system are presented.

Data received from the U.K. control centre, via the modem linked to the PDP-8/E computer, was placed immediately onto the computer disk storage. Using this small computer, a first data base (called "MTSAVE") containing every bulk orbits data received, was built up on magnetic tapes by transferring data from the disk. Temporary storage on both disk and magnetic tape of the most recent few months data was also kept as a backup against tape or computer malfunction.

As the PDP-8/E was too small for any major analysis, the data was also written onto magnetic tapes in a format suitable for use with the main university CYBER 72 computer. These ("CDC") tapes were then transferred to the CYBER operations store, creating a second data base there. Backup copies of the CDC tapes were also kept, these in the PDP-8/E "data terminal" room as a measure against loss and spoiling of the original tapes.

§ 4.1.4 Real Time Analysis - R.T.A.

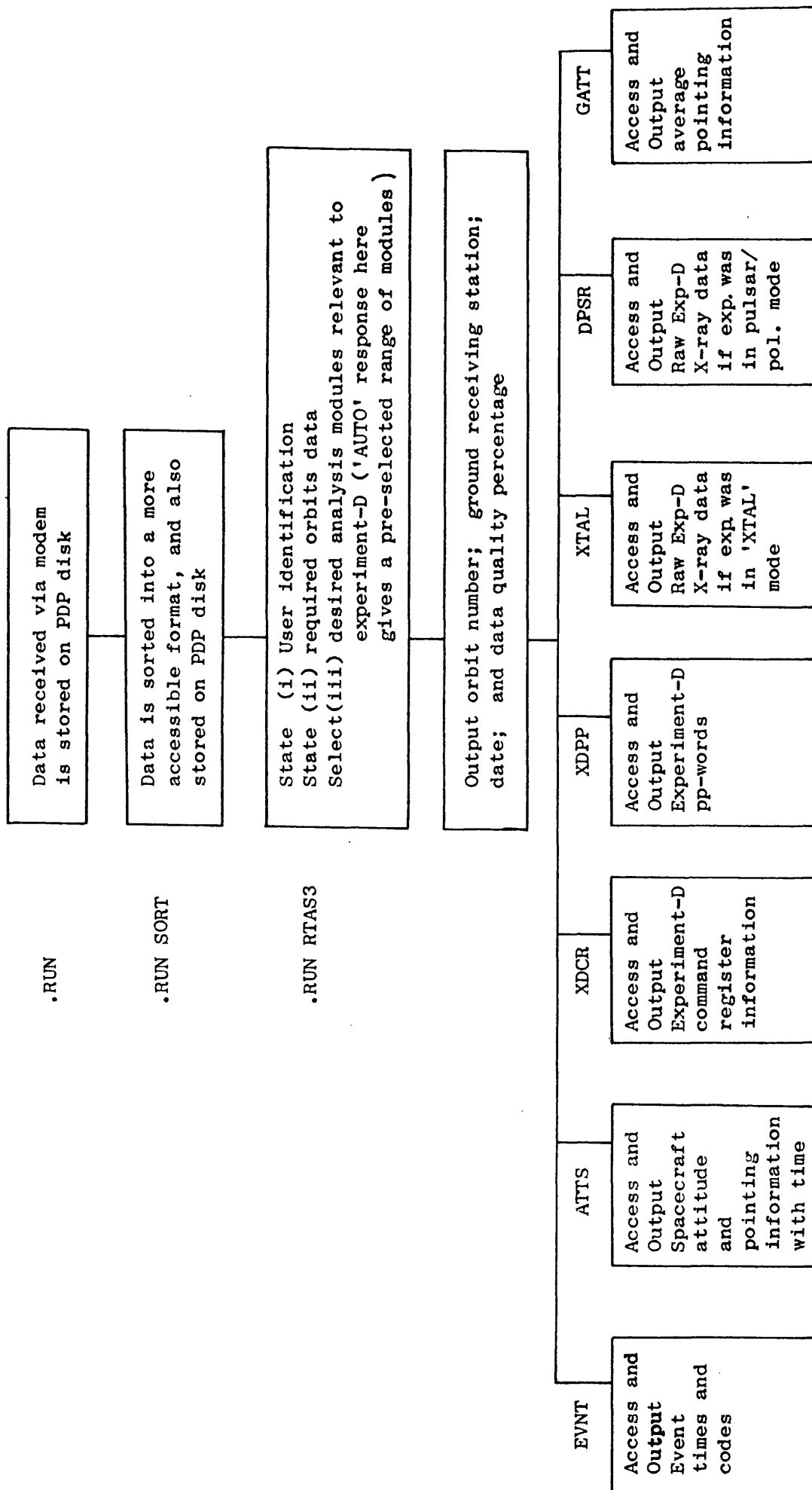
This analysis system was designed to extract preliminary information in 'real time' from an orbits data, and was mainly concerned with the experiment B data where significant scientific information could be obtained from a single orbits data. However, it also served to check for correct experiment functioning, correct experiment mode of operation and also the satellite pointing direction, and therefore was also relevant to experiment D.

Programs for this analysis system were written in PAL-8 assembly language and run on the PDP-8/E, giving line printer and graph plotter output. By using the small PDP-8/E, computer analysis of an orbit's data could be completed within 5 minutes of reception from the U.K. control centre.

Details of this analysis system, shown flow-charted in Fig. 4.1.1, can be obtained from Eadie (1976) and Silk (1975).

R.T.A. was performed daily on up to 6 quick look orbits' data for both experiments B and D. For experiment B alone, R.T.A. was performed on every orbit's data (including Bulk orbits data if not received and analyzed as a quick look pass). This enabled a complete search coverage for transient X-ray sources and any other change in the X-ray sky sensitive to a single orbit integration period. R.T.A.

Fig. 4.1.1a: Experiment-D Real Time Analysis



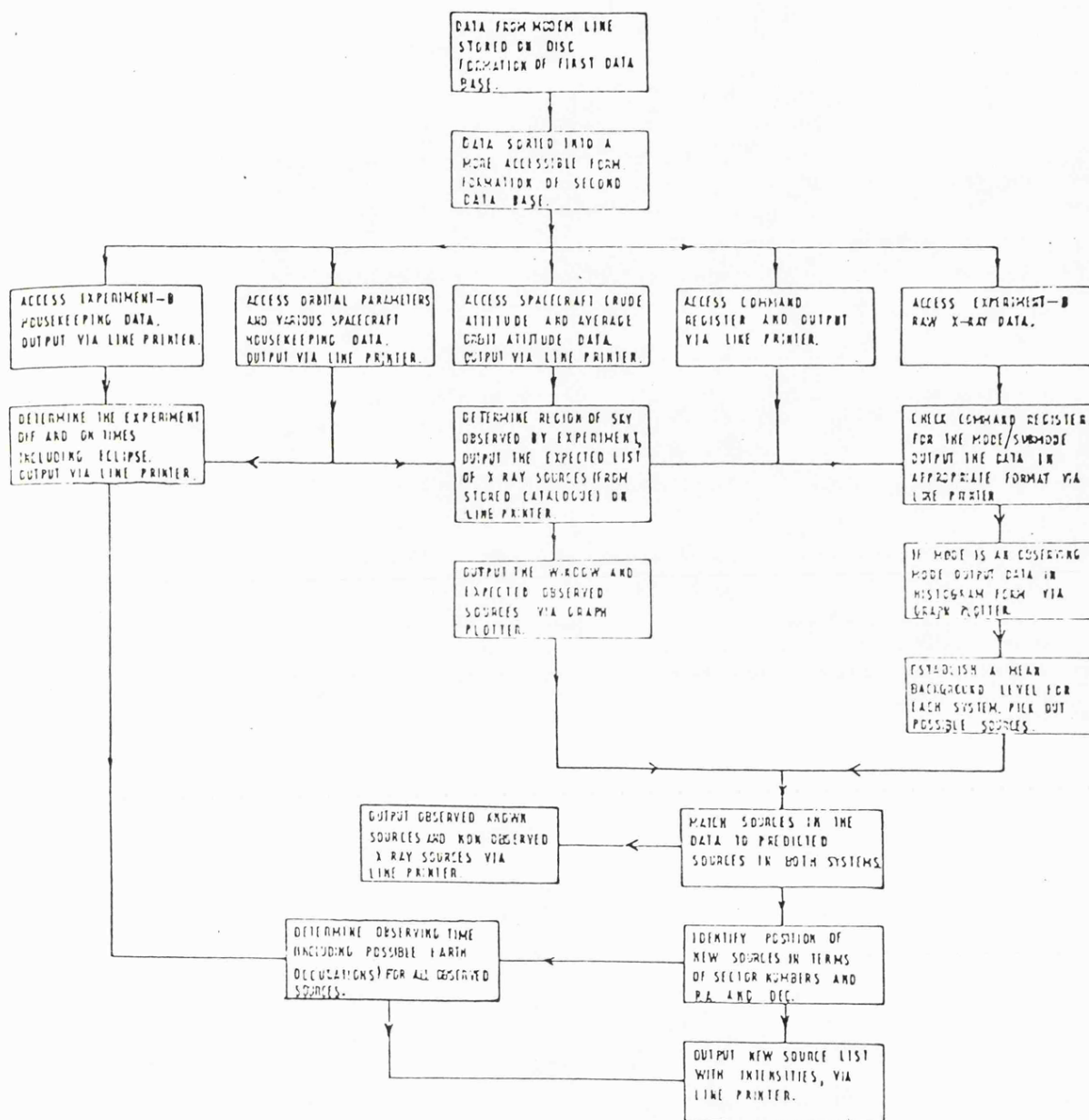


Fig. 4.1.1b: Experiment-B Real Time Analysis Scheme (from Peacock 1975).

was also extended to other than quick look data for experiment D, if requested by an experimenter for a particular observation.

Information relevant to experiment D, output by the R.T.A. System (R.T.A.S.), normally included the following (U.K. control centre data handling documents; M. Ricketts and M. Turner, private communications, 1976):-

- i) Orbit number; identification of ground receiving station; date of data dump and data quality percentage.
- ii) Event times and codes. These give the times for which the experiment power and background monitor rate flags were switched on and off.
- iii) The state of experiment D command register (see § 3.2.6).
- iv) Experiment D performance parameters (experiment-D "pp-words"). These monitor, though in code; the crystal positions; current through the H.T. units; analogue to digital reference voltage (for energy channel boundaries); background monitor count rates and experiment temperature.
- v) Pointing direction information concerning the satellite orientation with respect to the Sun and sky; and spin-period information.
- vi) The raw experiment D data.

An important part of the R.T.A.S. was its design flexibility which allowed either automatic output of a prearranged set of commonly used output modules, or a choice of specific modules. Also, the vast majority of the output was in an easily readable and digestible form, the programs efficiently breaking down and re-ordering the satellite raw coded data.

§ 4.1.5 Orbit Slot Analysis - O.S.A.

This analysis system was designed for use on large numbers of orbits data where the experiment concerned, operated in a single mode and the spacecraft spin-axis was fixed in a single direction. With these conditions it is relatively simple to sum large masses of data to increase the signal to noise ratio.

This analysis was performed mainly from the accumulating CDC data base using the Cyber 72 computer. The programs were written in Fortran.

Access of data for this analysis could be made within about a day of finishing an observation of high analysis priority, and within a few days for most other observations.

In case of an extended breakdown with the PDP-8/E computer O.S.A. Fortran programs, essentially duplicating the R.T.A.S., were also written. For experiment-D the program RAWD was written, and this output the following information for each orbit's data specified:-

- | | | |
|------|---|----------|
| i) | Orbit number | |
| ii) | Experiment-D command register | - DCOMRG |
| iii) | Event times and codes | - EVENT |
| iv) | Experiment-D pp-words | - DPPWDS |
| v) | Orbit average attitude information | - AVGATT |
| vi) | Experiment-D raw data for Crystal mode
operation for both crystal panels | - XTAL |
| vii) | The crystal positions and Bragg angles | - XTLPSN |

(These were only output in code in the R.T.A.S.)

where the subroutine names for each output module are given on the right.

Besides this function of duplicating the R.T.A.S., O.S.A. was designed to serve the main data analysis of both experiment-B and -D data.

The access of data from the computer base was performed using some general subroutines relevant to both experiment-B and -D. These accessed an orbit's data from the Cyber disc (once a block containing the total number of orbits to be analysed had been transferred from the magnetic tape data base), and then assigned that orbit's data to easily manageable, named common blocks (C. Page, 1976, private communication).

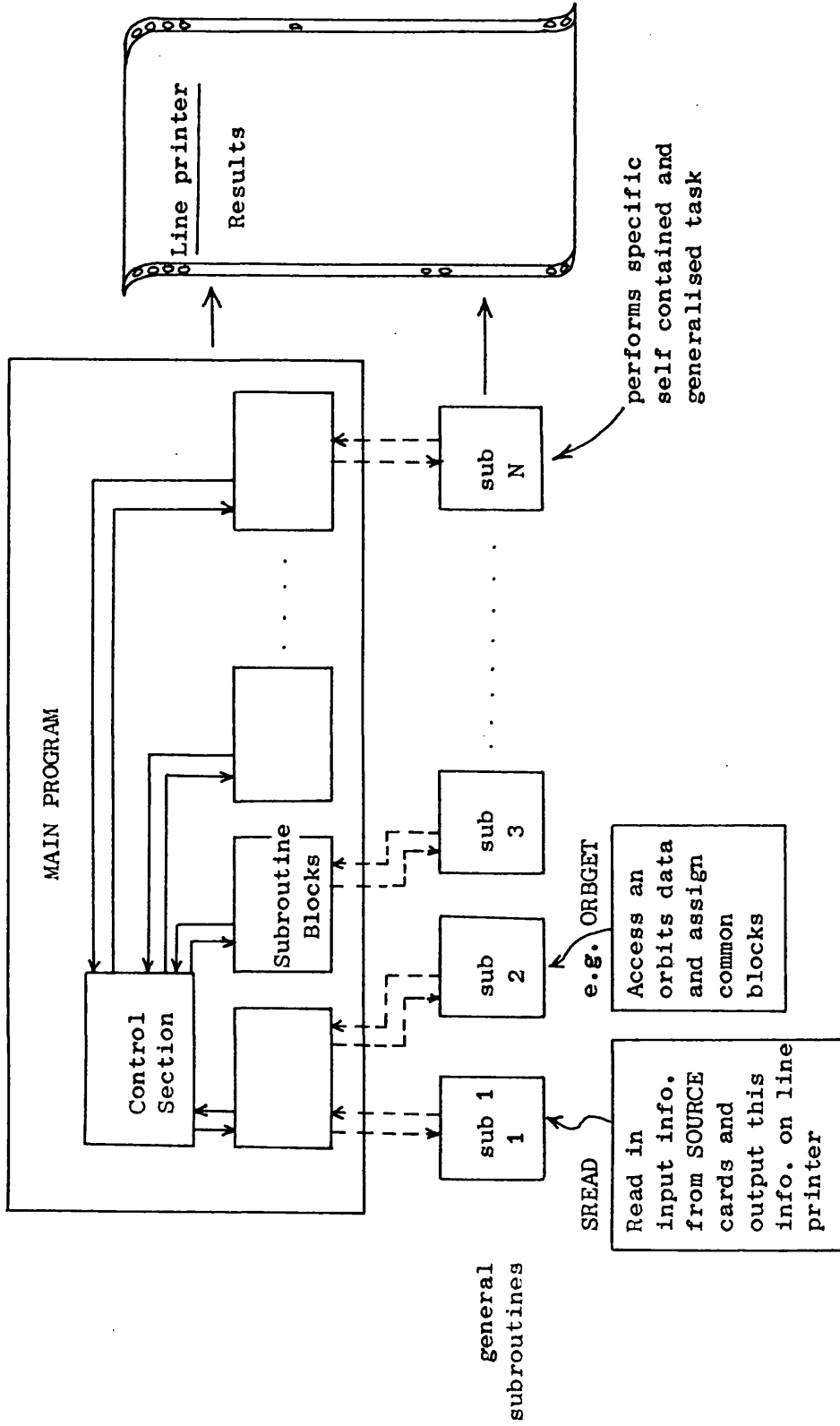
For tasks specific to experiment-D analysis two computer based libraries were built up. One (RAGPL2) contained all the main programs and the other (RAGLIB) general subroutines which performed more or less general tasks common to many different main programs. These libraries were stored on the fast access Cyber disk, within an Update system (CDC Update Reference Manual) which allowed program changes and corrections to be easily made. As a precaution against loss or corruption of these libraries an updated backup on punch cards was also maintained.

A flowchart of the concept of the program structure for the experiment-D analysis is given in Fig. 4.1.2, where, as far as possible, the subroutines were written to be independent modules performing some specific task which might be relevant to many analysis problems. By the addition of such subroutines a coherent analysis structure could be gradually built up.

One of the more widely used subroutines was called SREAD, designed to read in a standardised set of input cards, and also to print out this information. The usefulness of this subroutine arose because of several reasons:-

- (i) The different types of analysis which were performed on a set or orbit's data often required very similar and usually overlapping information.

Fig. 4.1.2: Experiment-D Orbit Slot Analysis Program Structure



- (ii) It was only required to punch these data cards once.
- (iii) An update of data information need only be transferred to this single set of data cards.
- (iv) Fewer data cards would need to be stored within a data card library system.

Supply of this data information was upon a set of cards designated as "Source Cards" which could be read into any experiment-D main program, and provide its information via common blocks within the main program.

These Source Cards contained the following information:-

Cards 1 and 2: These allowed for the provision of a title to appear at the top of the printed output. This usually specified the data set which was being analysed, e.g.

"SCO X-1 1976 OBSERVATION"

		<u>Variable Name</u>	<u>Format</u>
<u>Card 3:</u>	Orbit Start number	LORBIT	I6
	Orbit End number	MORBIT	I6
<u>Card 4:</u>	X-ray source sky position		
	Star R.A. (1950)	STARRA	F9.3
	Star Dec.	STARDC	F9.3
<u>Card 5:</u>	(1) Choice of crystal data to be analysed	IXTAL	I2
	0 = Graphite, 1 = LIF, 2 = Both		
	(ii) Output format option	IOUTF	I2
	0 = full output, 1 = reduced output		
	(iii) Computer (0 = Cyber)	ICOMP	I2
	(1 = Manchester. Initially plans were made to perform analysis on the large Manchester computer)		
	(iv) Minimum fractional observing time on source for a specified time slot.	ALPHA	F5.2

(For some of experiment D crystal mode (see § 3.2.5) the view to the source was obscured by the Earth, and hence an option was introduced so that time slots where not enough time was spent observing the source would be excluded from the analysis.)

	<u>Variable Name</u>	<u>Format</u>
<u>Card 6:</u> Maximum, permissible, spin-axis pointing direction offset from the X-ray source.	RMOFF	F6.2

<u>Cards 7 and 8:</u> Up to 18 orbit numbers. These orbit's data to be excluded from any analysis. This option was introduced to exclude bad orbit's data, which sometimes appeared on the data base. (In general such bad data would be detected by looking at output of RAWD, or otherwise after output from some other of the main programs, had been scanned.	IIIBIT(18)	18I6
---	------------	------

Several other advantageous features of the experiment-D

programs included:-

- 1) Main programs were divided into a block structure, each block performing a well defined task.
- 2) Careful thought was given to providing good documentation within the programs. This makes changes to programs months and years after introduction, and perhaps use for another satellite's data analysis by different personnel, much easier.

Eventually, most program blocks and subroutines were

provided with:-

- i) A heading, stating name and purpose, followed by a short explanation and list of parameters.
 - ii) Helpful comments liberally spread throughout the program.
- 3) Liberal, but very well laid out output was provided, including headings. Where possible the reduced output option was built in as a choice for output. (Usually, full output format allowed either checks for bad data, or gave intermediate program results as a helpful guide to general debugging, checking new modules or effects of different data sets.)

§ 4.1.6 Long Term Analysis - L.T.A.

This analysis system was conceived for situations requiring the combination of various O.S.A. data blocks, where the spin-axis positions or experiment modes associated with the individual data blocks differed.

L.T.A. was considered likely to take place on the order of months subsequent to observations, rather than days, and would require access of relatively old data built up in the data bases.

Individual program systems for L.T.A. only concerned experiment B and are not considered here (see Peacock, 1975).

§ 4.2 POLARIMETER DATA ANALYSIS

§ 4.2.1 Electromagnetic Radiation and Polarisation

The theory of polarisation from the underpinning considerations of the nature of electromagnetic (e.m.) radiation, up to and through the mathematical development of the Stokes parameters which are widely used in the research literature, is briefly outlined. The understanding and mathematical formalism developed is used as a base for the practical determination of polarisation and for considerations of the errors involved.

(Interesting and more complete considerations, both mathematical and giving an extended insight into the physical concept of polarisation, may be obtained from Clarke and Grainger (1971). A more condensed version is given by Feynman et al. (1963).)

§ 4.2.1a Mathematical Introduction

A quasi-monochromatic* electromagnetic disturbance may be represented in terms of the components of the electric vector in orthogonal planes xz, yz as (see Fig. 4.2.1; see also Clarke and Grainger 1971, or Clarke 1974)

$$E_x = E_{x0} \exp \left[i \left(\omega t - \frac{2\pi z}{\lambda} + \delta_x \right) \right] \quad (1)$$

$$E_y = E_{y0} \exp \left[i \left(\omega t - \frac{2\pi z}{\lambda} + \delta_y \right) \right] \quad (2)$$

where E_x , E_y are the values of the electric field in x- and y-directions at the position z and at time t; E_{x0} , E_{y0} are the amplitudes of the x- and y-vibrations and δ_x , δ_y are the phases (advancements) of the x- and

* This term is used since any finite burst of e.m. radiation must consist of an infinite range of frequencies, and therefore monochromatic e.m. radiation cannot exist (see Clarke and Grainger 1971, p. 10).

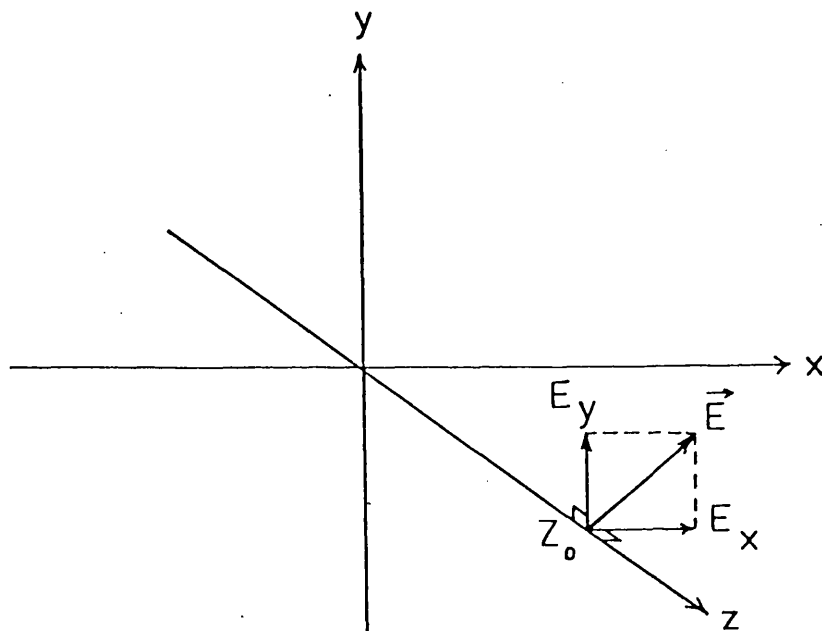


Fig. 4.2.1: Quasi Electromagnetic disturbance travelling in z -direction

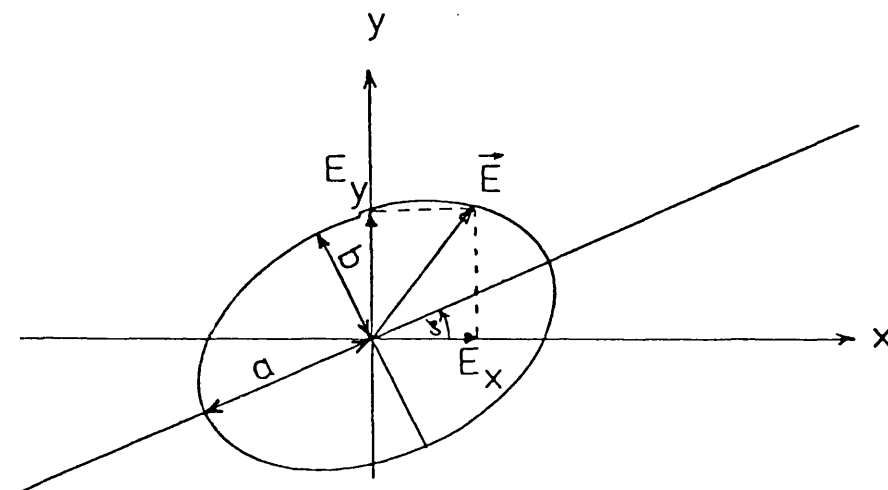


Fig. 4.2.2: The Polarisation Ellipse

y-vibrations at $z = 0$; ω is the angular frequency; λ is the wavelength and i is the square root of -1 . The system x, y, z is usually defined to be a right hand frame.

The polarisation state of this electromagnetic disturbance is dependent upon the path traced out by the tip of the resultant electric vector \underline{E} , as either t increases about some general spatial point $z = z_0$, or along increasing z of the instantaneous profile at $t = t_0$.

If the finite bursts of radiation, which give the resultant electric vector components E_x and E_y , are incoherent such that the phases δ_x, δ_y vary randomly with time or z , then the resultant radiation is said to be unpolarised.

If, however, an observed fixed relation exists between the phases δ_x and δ_y then the radiation is said to exhibit polarisation.

The amount of radiation in a beam which exhibits a phase relation determines the degree of polarisation of the beam. If all the beam intensity exhibits the phase relation then the beam is perfectly polarised. If only a fraction of the beam is involved then the beam is said to be partially polarised.

§ 4.2.1b The Polarisation Ellipse

Consider the real part of equations (1) and (2) at some point z , say $z = 0$. Then (1) reduces to

$$E_x = E_{x0} \cos(\omega t + \delta_x) \quad (3)$$

$$E_y = E_{y0} \cos(\omega t + \delta_y) \quad (4)$$

and by eliminating t from (3) and (4), the path traced out in x - y space by the tip of the electric vector may be obtained, and written as:-

$$\frac{E_x^2}{E_{x0}^2} + \frac{E_y^2}{E_{y0}^2} - \frac{2E_x E_y \cos(\delta_y - \delta_x)}{E_{x0} E_{y0}} = \sin^2(\delta_y - \delta_x) \quad (5)$$

This is the equation of an ellipse. The cross product simply reflects the fact that the reference axes do not coincide with the major and minor axes of the ellipse.

Electromagnetic radiation, where the tip of the electric vector traces out an ellipse, is said to be elliptically polarised. When the ellipse becomes a circle then the radiation is said to be circularly polarised, and when it becomes a line it is said to be linearly or "plane" polarised. If $(\delta_y - \delta_x)$ is constant in time then the shape and orientation of the ellipse, and hence also the type of polarisation, will remain constant in time.

Although the four parameters E_{x0} , E_{y0} , δ_x and δ_y completely describe the ellipse, they are not the most convenient set as they are all related to the coordinate frame. The shape and size of the ellipse may be specified without reference to a system of coordinates. However, the orientation, or "azimuth" of the major axis and the sense of rotation of the tip of the electric vector, known as the "handedness" of the polarisation, must be referred to the coordinate frame.

A convenient set can be derived from the semi-major and semi-minor axes ("a" and "b" respectively), the azimuth ζ of the major axis with respect to a reference direction (the x-axis in this case), and the handedness parameter (see Fig. 4.2.2).

The traditional way of describing the polarisation handedness is to consider the sense of rotation of the electric vector as "viewed" by an observer receiving the radiation. However, more than one convention exists (see Clarke and Grainger 1971).

The shape of the ellipse can be obtained from

$$\eta = b/a \tag{6}$$

where the ellipticity is given by $1 - \eta$; and the intensity of the beam will be given by $I = (a^2 + b^2)$.

Then

$$I = E_{x0}^2 + E_{y0}^2 \quad (7)$$

$$\tan 2\zeta = \frac{2E_{x0} E_{y0} \cos(\delta_y - \delta_x)}{E_{x0}^2 - E_{y0}^2} \quad (8)$$

and

$$\frac{2\eta}{1-\eta^2} = 2 E_{x0} E_{y0} \frac{\sin(\delta_y - \delta_x)}{E_{x0}^2 + E_{y0}^2} \quad (9)$$

§ 4.2.1c Phenominological Development of the Stokes Parameters

Consider a beam of perfectly polarised light characterized by the four parameters E_{x0} , E_{y0} , δ_x and δ_y . After passage through a polariser whose transmission axis* is set at an angle α to the x-axis, the emergent intensity $I(\alpha)$ (assuming no losses) will be given by (see Fig. 4.2.3):-

$$I(\alpha) = E_{x0}^2 \cos^2 \alpha + E_{y0}^2 \sin^2 \alpha + E_{x0} E_{y0} \sin(2\alpha) \cos(\delta_y - \delta_x) \quad (10)$$

which can be re-written as:-

$$I(\alpha) = A_0 + A_1 \cos 2\alpha + A_2 \sin 2\alpha \quad (11)$$

where A_0 , A_1 and A_2 are given by:-

$$A_0 = \frac{1}{2}(E_{x0}^2 + E_{y0}^2) \quad (12)$$

$$A_1 = \frac{1}{2}(E_{x0}^2 - E_{y0}^2) \quad (13)$$

$$A_2 = E_{x0} E_{y0} \cos(\delta_y - \delta_x) \quad (14)$$

* A polariser acts so that only radiation with the electric vector in a single direction will pass through. The orientation of this single direction determines the transmission axis angle.

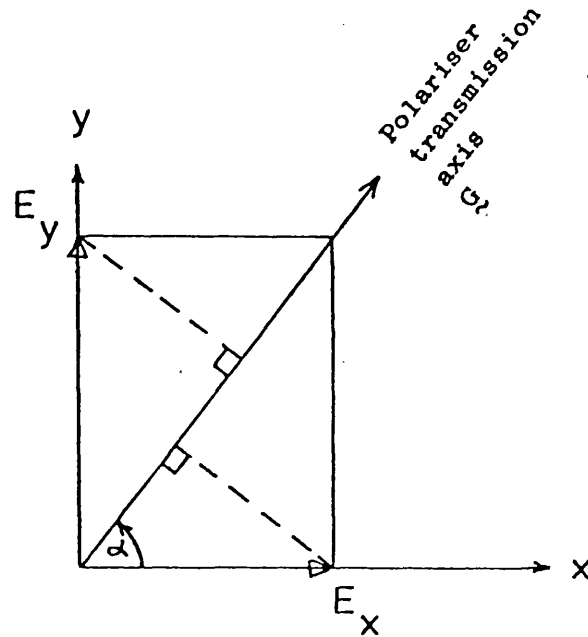


Fig. 4.2.3a: Components of electric vector in transmission axis direction $E_G = E_x \cos \alpha + E_y \sin \alpha$
(Intensity is then $= \langle G^2 \rangle$ (time average))

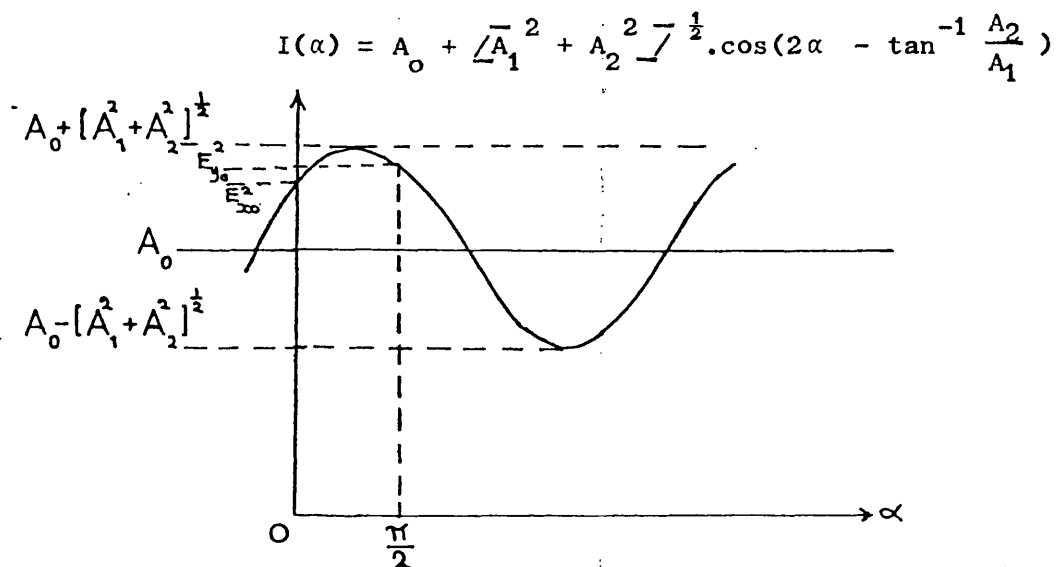


Fig. 4.2.3b: Profile of transmitted intensity of perfect elliptically polarised beam as transmission axis (angle α) is rotated about line of sight to beam (from Clarke and Grainger 1971, p.27).

The coefficients A_1 and A_2 together specify the phase of the oscillatory component.

If intensity measurements were to be made at three different values of α , then A_0 , A_1 and A_2 could clearly be determined and hence also E_{x0} , E_{y0} and $\cos(\delta_y - \delta_x)$. This information would be sufficient to determine the size ellipticity and azimuth of the ellipse but not the sense of rotation of the electric vector. This is a consequence of the fact that 'cosine' is an even function and hence does not indicate the sign of the phase difference ($\delta_y - \delta_x$). The only way to discover which of the orthogonal electric vector components is ahead of the other is to introduce some known change in the relative phase, and observe the effect. Then, for instance, by making a measurement using a retardation phase r of $\frac{\pi}{2}$:-

$$A_{2r} = \pm E_{x0} E_{y0} \sin(\delta_y - \delta_x) \quad (15)$$

and the new values of A_{0r} and A_{1r} will remain the same as those of the measurement without the retarder, i.e. $A_{0r} = A_0$ and $A_{1r} = A_1$. The sign of the right hand side of equation (15) is arbitrary and depends upon which of the 2 orthogonal components is more retarded. For convenience (see Clarke and Grainger 1971) the positive sign will be taken.

The four parameters which now describe the beam are A_0 , A_1 , A_2 and A_{2r} . By convention, since $2A_0$ gives the intensity of the beam, the four parameters usually taken are:-

$$2A_0 \equiv I \equiv I \equiv E_{x0}^2 + E_{y0}^2 \quad (16)$$

$$2A_1 \equiv Q \equiv M \equiv E_{x0}^2 - E_{y0}^2 \quad (17)$$

$$2A_2 \equiv U \equiv C \equiv 2E_{x0} E_{y0} \cos(\delta_y - \delta_x) \quad (18)$$

$$2A_{2r} \equiv V \equiv S \equiv 2E_{x0} E_{y0} \sin(\delta_y - \delta_x) \quad (19)$$

and these are generally known as the 4 Stokes parameters. (I,Q,U,V and I,M,C,S are just different notations commonly used. Here, the I,Q,U,V notation will be adopted.) Note:

$$I^2 = Q^2 + U^2 + V^2 \quad (19a)$$

from the definition of the Stokes parameters, and "I" can therefore be known if Q,U and V are known.

By comparing the definitions of I,Q,U,V with the previous equations (7), (8) and (9), it can be seen that the polarisation or geometrical description of the polarisation ellipse is as follows:-

$$\text{Size (Intensity)} = I \quad (20)$$

$$\text{Azimuth} = \frac{U}{Q} = \tan 2\zeta \quad (21)$$

$$\text{Shape} = \frac{|V|}{I} = \frac{2\eta}{1+\eta^2} \quad (22)$$

$$\text{Handedness} = \text{sign of } V \quad (22a)$$

§ 4.2.1d Addition of the Stokes Parameters - and Extension to Partially Polarised Radiation

Before the Stokes parameters description developed in (c) can be put to practical use, it must first be extended to partially polarised radiation.

In fact, it can be shown that (see Clarke and Grainger 1971) if two perfectly polarised beams, which are incoherent with respect to each other, are passed simultaneously through a polariser then the Stokes parameters for the combined beam are just the sum of the Stokes parameters of the individual beams. i.e.

$$\begin{array}{rcccc}
 \text{Beam 1} & + & \text{Beam 2} & = & \text{Beam 3} \\
 I_1 & & I_2 & & I_3 = I_1 + I_2 \\
 Q_1 & & Q_2 & & Q_3 = Q_1 + Q_2 \\
 U_1 & & U_2 & & U_3 = U_1 + U_2 \\
 V_1 & & V_2 & & V_3 = V_1 + V_2
 \end{array} \quad (23)$$

There is no reason to suppose, however, that the combined beam - even though made up of two perfectly polarised components - will itself be perfectly polarised, and in general it will not be. That is, the combined beam will contain some unpolarised radiation.

It can be seen from (23) that

$$I_3^2 \geq Q_3^2 + U_3^2 + V_3^2 \quad (24)$$

where this inequality arises because of the presence of the unpolarised component.

As has been stated at the end of § 4.2.1a, partially polarised radiation can be considered to behave as an incoherent sum of totally polarised and unpolarised components. The unpolarised radiation in turn can be mathematically considered as two orthogonally, linearly polarised, incoherent beams of equal intensity, each of which can be described by a set of Stokes parameters since they are perfectly polarised. Each of the two linearly polarised beams will have an intensity one half that of the whole, say $\frac{1}{2}I_u$. The Stokes parameters for the beam polarised in the x- and y-directions are:-

$$\left. \begin{aligned} I_x &= E_{x0}^2 + 0 = \frac{1}{2}I_u & I_y &= 0 + E_{y0}^2 = \frac{1}{2}I_u \\ Q_x &= E_{x0}^2 - 0 = \frac{1}{2}I_u & Q_y &= 0 - E_{y0}^2 = -\frac{1}{2}I_u \\ U_x &= 2E_{x0}(0)1 = 0 & U_y &= 2E_{y0}(0)1 = 0 \\ V_x &= 2E_{x0}(0)(0) = 0 & V_y &= 2E_{y0}(0)(0) = 0 \end{aligned} \right\} (25)$$

Since the two beams are incoherent, the Stokes parameters which would be determined for unpolarised radiation are:-

$$\left. \begin{aligned} I &= \frac{1}{2}I_u + \frac{1}{2}I_u = I_u \\ Q &= \frac{1}{2}I_u - \frac{1}{2}I_u = 0 \\ U &= 0 + 0 = 0 \\ V &= 0 + 0 = 0 \end{aligned} \right\} (26)$$

Thus, the combined beam of partially polarised radiation may

now be considered to be made up of two components having the following

Stokes parameters:-

$$\text{Unpolarised Component: } I_u, 0, 0, 0 \quad (27)$$

$$\text{Polarised Component: } I_p, Q_{TOT}, U_{TOT}, V_{TOT} \quad (28)$$

where

$$Q_{TOT}^2 + U_{TOT}^2 + V_{TOT}^2 = I_p^2 \quad (29)$$

$$\text{and } I_u + I_p = I_{TOT} \quad (30)$$

(Thus 5 parameters are required to define a partially polarised beam.)

Furthermore, since both the unpolarised and polarised components are incoherent with respect to each other, then the Stokes parameters for these two beams may be added to give the resultant Stokes parameters for the general case of arbitrarily partially polarised radiation:-

$$\left. \begin{aligned} I &= I_p + I_u \\ Q &= Q_{TOT} \\ U &= U_{TOT} \\ V &= V_{TOT} \end{aligned} \right\} (31)$$

This is important, since it implies that if one can measure the Stokes parameters for an incoherent sum of source and background radiation (as would commonly be the case for practical measurements) and also those of the background radiation alone, then by subtraction, the Stokes parameters and hence the polarisation of the source radiation may be obtained.

$$\text{i.e. } \underline{S}(s) = \underline{S}(s+b) - \underline{S}(b) \quad (32)$$

where $\underline{S}(s) =$ Stokes parameters calculated for the source radiation.

$\underline{S}(s+b) =$ Stokes parameters measured for source and background radiation.

$\underline{S}(b) =$ Stokes parameters measured for background radiation only,

and the $\underline{S}(i)$'s are now conveniently represented in a vector format, as follows:-

$$\underline{S}(i) = \begin{pmatrix} I_i \\ Q_i \\ U_i \\ V_i \end{pmatrix} \quad (32a)$$

§ 4.2.1e The Degree of Polarisation

The degree of polarisation of a partially polarised beam will now be quantified. This is defined as the fraction of the intensity of the beam which is contained in the polarised component, i.e.

$$p \equiv \frac{I_p}{I_u + I_p} = \frac{Q^2 + U^2 + V^2}{I_u + I_p} \quad (33)$$

For the case, however, of partially linearly polarised radiation, another expression for the degree of polarisation has been found convenient, and is frequently used. If the radiation is passed through a polariser, the transmitted intensity will be given by:-

$$I(\alpha) = \frac{1}{2}I_u + I_p \cos^2(\alpha - \zeta) \quad (34)$$

$$= \frac{1}{2}[I_u + I_p] + \frac{1}{2}I_p \cos 2(\alpha - \zeta) \quad (35)$$

where ζ is the azimuth of the polarised component (see Fig. 4.2.4).

(Equation (34) may be obtained similarly to (10), by considering the radiation as two separate components; one completely linearly polarised; and the other completely unpolarised, where the unpolarised component may be split as before.)

From Fig. 4.2.4:-

$$p \equiv \frac{I_p}{I_u + I_p} = \frac{I_{\max} - I_{\min}}{I_{\max} + I_{\min}} \quad (36)$$

Following Gehrel (1974, p.52), the following general definitions

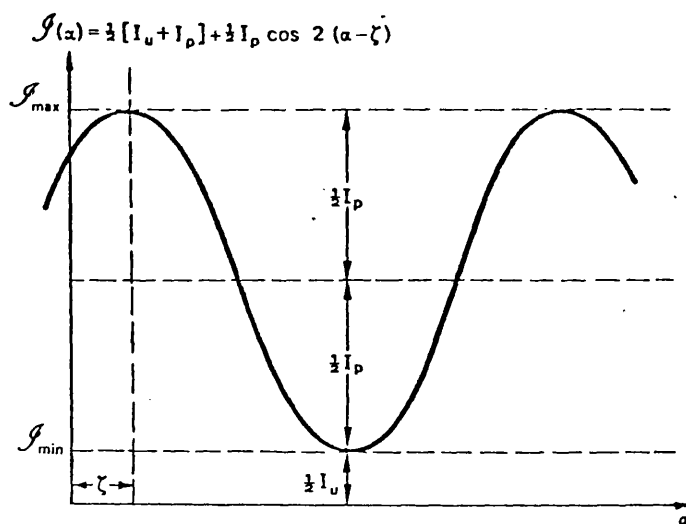


Fig. 4.2.4: Variation of transmitted intensity with polariser orientation, when illuminated with partially linearly polarised radiation (from Clarke and Grainger 1971).

for the degree of both linear polarisation ' p_L ' and circular polarisation ' p_C ' are adopted here.

These definitions are:-

$$p_L \equiv \frac{(Q^2 + U^2)^{\frac{1}{2}}}{I} \quad (37)$$

$$p_C \equiv \frac{V}{I} \quad (38)$$

where it can be seen that a component of linear polarisation, calculated via eqn. (37), will be obtained from elliptically polarised radiation. (Note: As the ellipse associated with elliptically polarised radiation approaches a circle, then the Stokes parameters Q and U calculated via the equations,

$$Q = E_{x0}^2 - E_{y0}^2$$

$$U = 2E_{x0} E_{y0} \cos(\delta_y - \delta_x)$$

will approach zero, as for circularly polarised radiation

$$E_{x0} = E_{y0} \quad \text{and} \quad \delta_y - \delta_x = \frac{\pi}{2} .)$$

The degree of polarisation, together with the shape, azimuth and handedness of the ellipse of the polarised component, gives what is known as the "state of polarisation", and the state of polarisation, together with the absolute intensity, describes the beam of radiation (Clarke and Grainger 1971).

(Note: the degree of polarisation is only a ratio of intensities, and the shape of the polarisation ellipse is only the ratio of the magnitude of the major to minor axis of the ellipse, i.e. no parameter necessary to describe the state of polarisation need contain an absolute intensity.)

§ 4.2.1f Reference Axes - Position Angle of Polarisation

For polarisation observations of a celestial source a convenient set of reference axes are those of declination (equivalent to

x-axis) and right ascension (equivalent to y-axis) with the direction of propagation completing a right-hand frame. Hence, a direction of vibration of the electric vector θ , might be expressed as an angle going from 0° to 180° , increasing in a sense from North through East (see Fig. 4.2.5). This angle θ is called the 'position angle' of the polarisation.

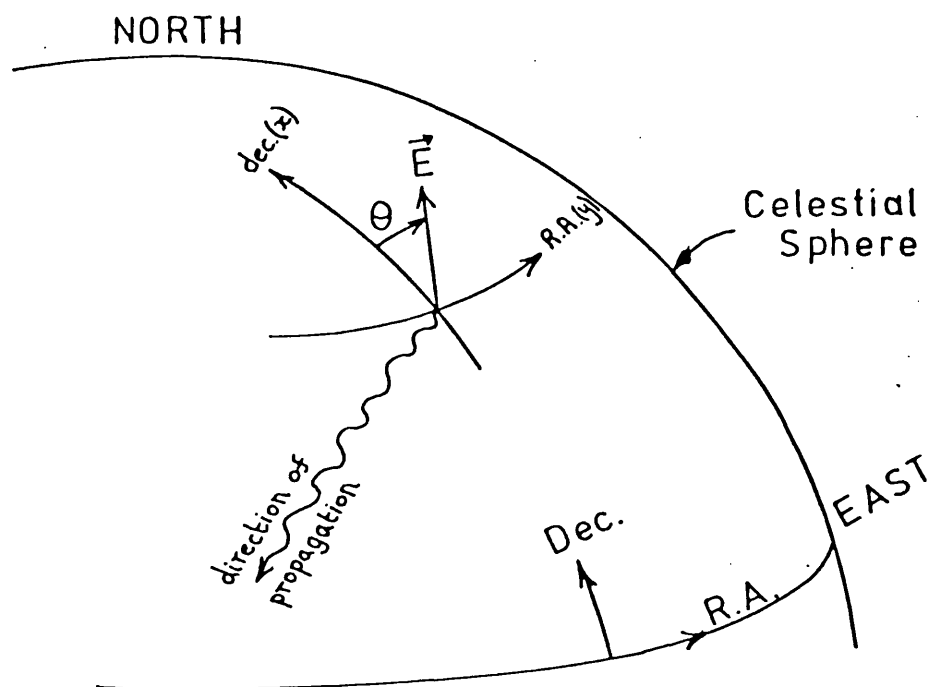


Fig.4.2.5:

Conventional reference axes for specifying the position angle of polarisation, θ .

§ 4.2.2 Polarisation Properties of the Ariel-V Polarimeter

§ 4.2.2a Polarisation Dependence of Bragg Reflection from a
Crystal

(i)	Introduction	93
(ii)	Mathematical Description of an Incident Polarised Beam just before Reflection	95
(iii)	Mathematical Description of the Reflected Beam - and inferring the Degree of Polarisation of the Incident Beam	98
	Case (1) $k = 0$	
	Case (2) $k \neq 0$	

(1) Introduction

In § 3.2 the Bragg reflection formula was given, which determines the wavelength at which constructive interference occurs of the scattered X-rays from a set of scattering centres in a crystal, for a given angle of incidence θ_B (i.e. $n\lambda = 2d \sin \theta_B$). Whereas it is the set of scattering centres which gives rise to the Bragg reflection formula, the polarisation dependence of the scattered intensity is believed to depend on each individual scattering centre.

In simple, classical terms (Compton and Allison 1935), this polarisation effect may be easily seen. If a scattering centre composed of a single electron is considered, where that electron is sinusoidally accelerated by the action of an incoming X-ray traversing it, another X-ray may be re-emitted in a different direction. Consideration of scattering at 90° to the incident X-ray direction is helpful to obtain a simple concept of the polarisation dependence. Fig. 4.2.6 shows an incident X-ray beam propagating horizontally northwards and causing an electron at 'O' to accelerate in a West-East vertical plane. Without loss of generality, the incident beam can be thought of as 2 perpendicular plane polarised components, one with the electric vector vibrating in the vertical direction, and the other in an East-West direction. If there is no plane polarised component (i.e. electric vector) in the vertical direction, then there can be no acceleration of the electron in the vertical direction, and hence there can be no scattered component in the East direction as there is no disturbance of the electric field perpendicular to this direction. However, as for this case a modulated electric vector exists in the West-East direction, then scattering may take place in the vertical direction. By a comparison of intensities received in the vertical and East directions, polarisation of the incident beam may be detected.

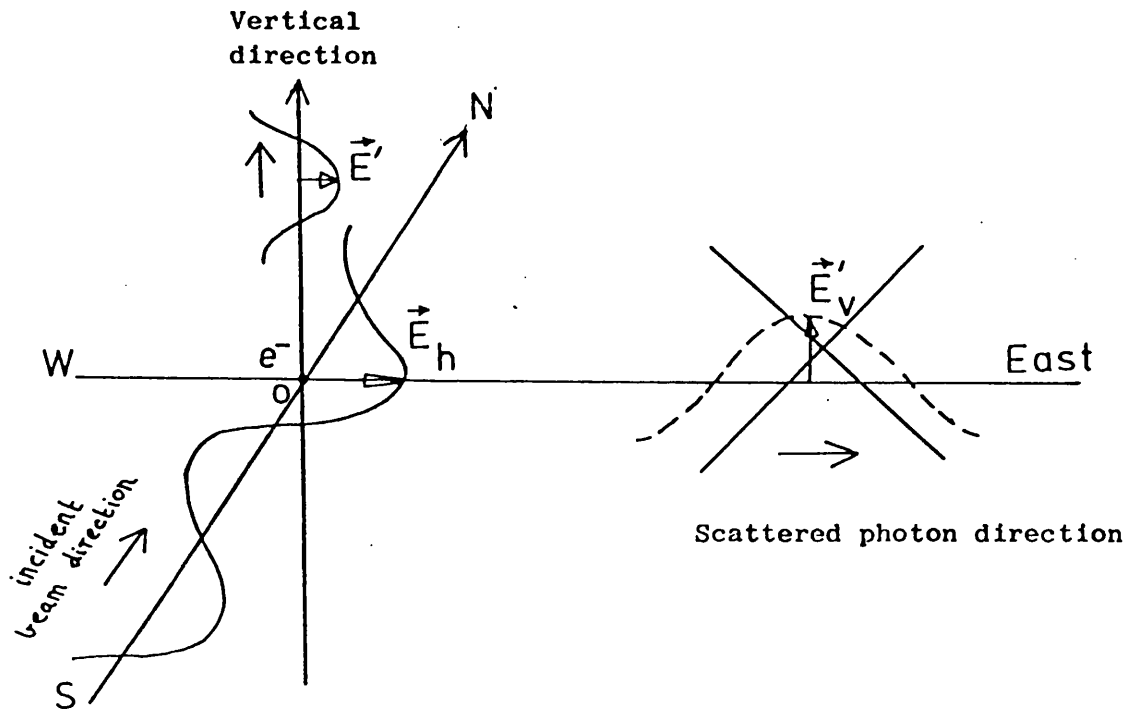


Fig. 4.2.6:

Scattering at 90° to an incident e.m. beam direction.

However, in practice, due to quantum mechanical variation of wavelength on scattering or multiple scattering within a crystal, this simple model is not an exact physical description of the real situation, and a more extensive treatment may be obtained from Compton and Allison (1935).

Also, although the scattered intensities from a polarised beam incident at a Bragg angle θ_B to a crystal face may be theoretically predicted for idealized crystal structures, in practice real crystal structures require calibration.

(ii) Mathematical Description of Incident Polarised Beam just before Reflection

First, the mathematical situation just before reflection at a point 'O' on a crystal (see Fig. 4.2.7) of a polarised beam striking the crystal, is considered. The plane formed by the incident ray, reflected ray and normal to the crystal will be called the 'parallel' plane. The planes perpendicular to this will be called the 'perpendicular' planes.

Let the input beam be arbitrarily polarised, having Stokes parameters I, Q, U, V describing the parameters $E_{x0}, E_{y0}, \delta_x, \delta_y$ and I_u . Let the x-axis be orientated, without loss of generality, coincident with the σ -direction at $t = 0$ so that the σ -axis is rotated at an angle \varnothing from the x-axis at time t (see Fig. 4.2.8). The phase of the polarisation will be orientated at an angle ζ from the x-axis where $\tan 2\zeta = U/Q$.

The intensity components before reflection, in the π - and σ -directions, will now be calculated for a rotation orientation \varnothing of the (π, σ) axes to the (x, y) axes.

For mathematical convenience the incident beam will be

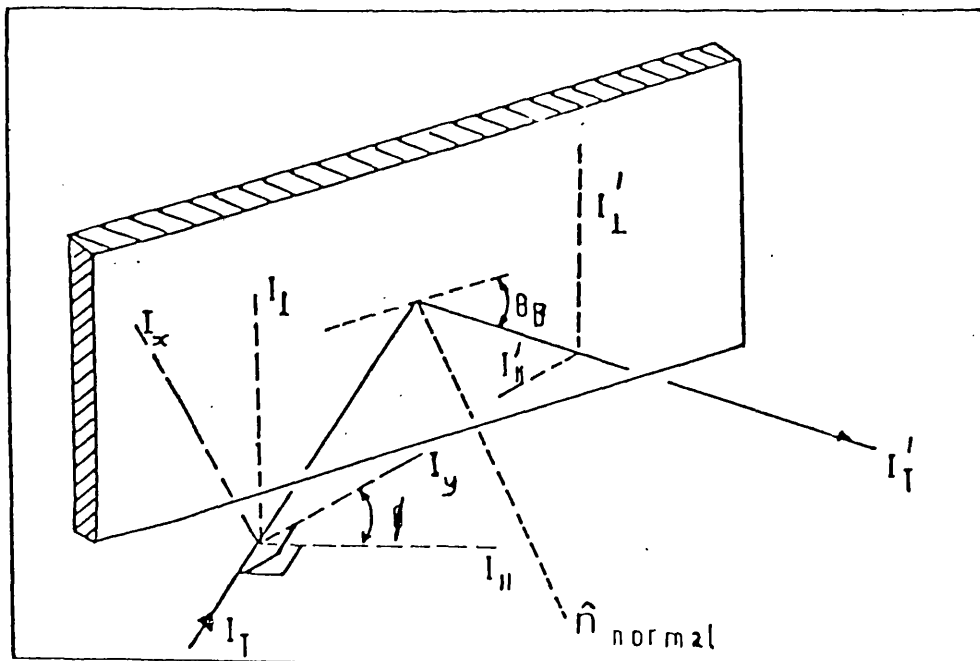


Fig. 4.2.7: Incoming X-ray beam incident on a crystal and reflected by the crystal.

$$(I_{\parallel} \equiv I_{\pi} \text{ and } I_{\perp} \equiv I_{\sigma})$$

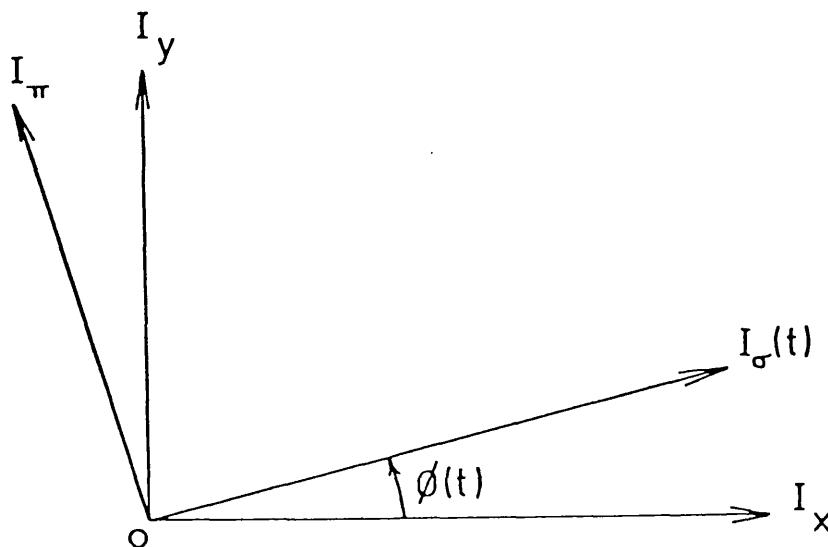


Fig. 4.2.8: Experiment σ - and π -axes; orientation $\phi(t)$ determined from $t = 0$ from the polarisation axes x - and y -.

considered to be made up of a perfectly polarised component and an unpolarised component. The resultant electric vectors of the incoming beam in the π - and σ -directions, for the perfect elliptically polarised component, are then given as follows:-

$$E_{\pi x} = -E_x \sin \phi \quad (\text{i.e. E-vector in } \pi \text{-direction from the x-component})$$

$$E_{\pi y} = E_y \cos \phi$$

$$E_{\sigma x} = E_x \cos \phi$$

$$E_{\sigma y} = E_y \sin \phi$$

where E_x and E_y may be described by

$$E_x = E_{x0} \cos(\omega t + \delta_x)$$

$$E_y = E_{y0} \cos(\omega t + \delta_y)$$

at the point of reflection ($z = 0$, say) (See § 4.2.1)

$$\text{Now } I_{\pi} = I_{\pi x} + I_{\pi y} = 2 \langle (E_{\pi x} + E_{\pi y})^2 \rangle \text{ time average}$$

$$I_{\sigma} = I_{\sigma x} + I_{\sigma y} = 2 \langle (E_{\sigma x} + E_{\sigma y})^2 \rangle \text{ time average}$$

$$\text{So } I_{\pi} = 2 \langle (-E_x \sin \phi + E_y \cos \phi)^2 \rangle$$

(by using same definition for 'I' as in § 4.2.1c)

$$\begin{aligned} \text{giving } I_{\pi} &= E_{x0}^2 \sin^2 \phi - E_{x0} E_{y0} \cos \phi \sin \phi \cos(\delta_y - \delta_x) + E_{y0}^2 \cos^2 \phi \\ &= \frac{(E_{x0}^2 + E_{y0}^2)}{2} - \frac{(E_{x0}^2 - E_{y0}^2)}{2} \cos 2\phi - E_{x0} E_{y0} \cos(\delta_y - \delta_x) \sin 2\phi \end{aligned} \quad (39)$$

and similarly

$$I_{\sigma} = \frac{(E_{x0}^2 + E_{y0}^2)}{2} + \frac{(E_{x0}^2 - E_{y0}^2)}{2} \cos 2\phi + E_{x0} E_{y0} \cos(\delta_y - \delta_x) \sin 2\phi \quad (40)$$

Then, considering the unpolarised component, an additional intensity term of $\frac{1}{2}I_u$ must be added to both I_{π} and I_{σ} (see § 4.2.1e).

Thus, the resultant intensity of the incident beam in the π - and σ -directions before reflection is given as follows:-

$$I_{\pi} = \frac{(I_u + E_{x0}^2 + E_{y0}^2)}{2} - \frac{(E_{x0}^2 - E_{y0}^2)}{2} \cos 2\theta - E_{x0} E_{y0} \cos(\delta_y - \delta_x) \sin 2\theta \quad (41)$$

$$I_{\sigma} = \frac{(I_u + E_{x0}^2 + E_{y0}^2)}{2} + \frac{(E_{x0}^2 - E_{y0}^2)}{2} \cos 2\theta + E_{x0} E_{y0} \cos(\delta_y - \delta_x) \sin 2\theta \quad (42)$$

where (41) and (42) are completely general expressions, representing an arbitrarily polarised incident beam.

The Stokes parameters for this beam are:-

$$I = I_u + E_{x0}^2 + E_{y0}^2$$

$$Q = E_{x0}^2 - E_{y0}^2$$

$$U = 2E_{x0} E_{y0} \cos(\delta_y - \delta_x)$$

where the degree of linear polarisation is given by:-

$$p_L = \frac{(Q^2 + U^2)^{\frac{1}{2}}}{I}$$

so that (41) and (42) can be re-written as:-

$$I_{\pi} = \frac{1}{2} [I - Q \cos 2\theta - U \sin 2\theta] \quad (43)$$

$$I_{\sigma} = \frac{1}{2} [I + Q \cos 2\theta + U \sin 2\theta] \quad (44)$$

iii) Mathematical Description of the Reflected Beam - and Inferring the Degree of Linear Polarisation of the Incident Beam

To determine the polarisation behaviour of the crystal from the reflected intensities, the ratio of the reflection integral value R_c (see § 3.2) for the π -component ($R_{c\pi}$) to that for the σ -component ($R_{c\sigma}$) will be defined, following Evans et al. (1977), as

$$k \equiv \frac{R_{c\pi}}{R_{c\sigma}} \quad (45)$$

For incident radiation of intensity $I(\lambda)$ the reflected power $J(\theta)$ in terms of R_c is given by (see § 3.2.3 equation (8)):-

$$J(\theta) = I(\lambda) \cdot \lambda \cdot \cot \theta_B R_c \quad (\text{energy time}^{-1} \text{ area}^{-1}) \quad (46)$$

where $I(\lambda)$ is expressed in units of $(\text{energy time}^{-1} \text{ area}^{-1} \text{ wavelength}^{-1})$

Thus, after reflection, we can write

$$J_\pi = \lambda \cot \theta I_\pi R_{c\pi} = AkI_\pi \quad (47)$$

$$J_\sigma = \lambda \cot \theta I_\sigma R_{c\sigma} = AI_\sigma \quad (48)$$

$$\text{where } A = \lambda \cot \theta R_{c\sigma} \quad (49)$$

So that the total reflected power is given by:-

$$J = J_\sigma + J_\pi \quad (50)$$

As an example, from Fig. 4.2.7 it can be seen that for $\theta_B = 45^\circ$ the scattering angle will be 90° so that for idealized conditions no reflection should occur for the π -component (i.e. $R_{c\pi} = 0$) whereas maximum reflection would be expected from the σ -component. If the crystal is rotated about the axis of the incident beam then θ would vary from 0 to $2\pi^c$ and a plane polarised component would be alternately received by the crystal as a π - and σ -component. Then, as only the σ -component is reflected, the received power should vary cyclically with rotation angle reaching a maximum twice per revolution. Then, the degree of polarisation of the incident beam is related to the depth of modulation of the received power as the crystal is rotated.

The expression for p_L from the received power modulation will be mathematically derived for the ideal 90° scattering case when $R_{c\pi} = 0$ making $k = 0$, and for realistic cases where $k \neq 0$.

Case (1) $k = 0$

$$\text{If } k = 0 \text{ then } J_\pi = 0$$

$$\text{and } J_\sigma = AI_\sigma$$

so that the total power received is given by the simple expression

$$J = J_\sigma = AI_\sigma$$

$$\begin{aligned}
 \text{i.e. } J &= \frac{A}{2} \left[I + Q \cos 2\vartheta + U \sin 2\vartheta \right] \quad (\text{using (44)}) \\
 &= \frac{A}{2} \left[I + (Q^2 + U^2)^{\frac{1}{2}} \cos(2\vartheta - \tan^{-1} \left(\frac{U}{Q} \right)) \right] \quad (50b)
 \end{aligned}$$

so that as the crystal is rotated $J = J(\vartheta)$ and produces the data modulation shown previously by Fig. 4.2.4.

The degree of linear polarisation will be given by

$$\begin{aligned}
 p_L &\equiv \frac{(Q^2 + U^2)^{\frac{1}{2}}}{I} = \frac{\frac{1}{2}(J_{\max} - J_{\min}) \frac{2}{A}}{\frac{2}{A}(J_{\text{mean}})} \\
 &= \frac{J_{\max} - J_{\min}}{J_{\max} + J_{\min}} \quad (51)
 \end{aligned}$$

So, for the case when $k = 0$ only one component of E-vector (σ -component) is reflected and thus the crystal acts as a simple single polariser (see § 4.2.1e), with the data modulation having the usual sinusoidal form allowing p_L and the phase angle ζ to be calculated in the usual manner.

Case (2) $k \neq 0$

This case arises in two ways.

- (a) When the scattering angle is not 90° . That is $\theta_B \neq 45^\circ$, and
- (b) When $\theta_B = 45^\circ$, but owing to effects which give rise to a non-zero $R_{c\pi}$ component, $k \neq 0$. In fact for all real crystals k is expected to be greater than zero. Reasons for this include multiple scattering; variation in the incident Bragg angle due to imperfect collimation for non-point sources; mosaic crystal orientation spread causing variation in reflected angles; and an incident angle offset from $\theta_B = 45^\circ$ for a point source, due to limited pointing control, for example, as in the Ariel-V pointing system.

For this case, $k \neq 0$,

$$\begin{aligned}
 J &= J_{\sigma} + J_{\pi} \\
 &= A(I_{\sigma} + kI_{\pi}) \\
 &= \frac{A}{2} \left[(I + Q\cos 2\theta + U\sin 2\theta) + k(I - Q\cos 2\theta - U\sin 2\theta) \right] \\
 &= \frac{A}{2} \left[I(1+k) + (1-k)Q\cos 2\theta + (1-k)U\sin 2\theta \right] \\
 &= \frac{A}{2} \left[I(1+k) + (1-k)(Q^2+U^2)^{\frac{1}{2}} \cos \left(2\theta - \tan^{-1} \frac{U}{Q} \right) \right] \quad (51b)
 \end{aligned}$$

So that (letting $\text{Max} = J_{\text{max}}$ and $\text{Min} = J_{\text{min}}$)

$$\begin{aligned}
 \frac{\text{Max} - \text{Min}}{\text{Max} + \text{Min}} &= \frac{2(Q^2+U^2)^{\frac{1}{2}} \frac{A}{2} (1-k)}{\left[\frac{A}{2} I(1+k) + (Q^2+U^2)^{\frac{1}{2}} \frac{A}{2} (1-k) \right] + \left[\frac{A}{2} I(1+k) - (Q^2+U^2)^{\frac{1}{2}} \frac{A}{2} (1-k) \right]} \\
 &= \frac{2(Q^2+U^2)^{\frac{1}{2}} (1-k)}{2I(1+k)} \\
 &= \frac{(1-k)}{(1+k)} P_L
 \end{aligned}$$

$$\text{i.e.} \quad P_L = \frac{(1+k)}{(1-k)} \frac{(\text{Max} - \text{Min})}{(\text{Max} + \text{Min})} \quad (52)$$

Following Evans et al. (1977), the visible modulation in the data will be defined as

$$V \equiv \frac{\text{Max} - \text{Min}}{\text{Max} + \text{Min}} \quad (53)$$

The modulation factor for the polarimeter (see Novick 1974, Weiskopf et al. 1976), becomes defined as

$$m \equiv \frac{1-k}{1+k} \quad (54)$$

thus allowing the expression for the degree of linear polarisation to be written more simply as

$$P_L = \frac{1}{m} V \quad (55)$$

So, from equation (51b), it can be seen that the data modulation

is again of exactly the same form as if produced by a single polariser, save only that the quantitative relation between the depth of modulation and degree of linear polarisation is modified by the introduction of the modulation factor m . It can be seen that this modulation factor arises because of the reflection of the π -component which causes a data modulation at exactly the opposite phase as that for the σ -component. This reduces the relative amplitude of the modulated component and therefore makes the instrument less sensitive to polarisation.

For the idealistic case when $k = 0$, J_{π} disappears. Also, if complete reflection of the J_{σ} component occurs, the instrument will be at its maximum sensitivity and can be said to be a perfect polarimeter. In fact, the almost complete extinction of the J_{π} component at $\Theta_B = 45^\circ$, provided the main reason for operation of the Ariel-V polarimeter at this Bragg angle whenever possible. If spectral line searches were required then operation at Θ_B other than 45° was often necessary (see Peacock 1975) with a subsequent, sometimes serious, reduction in sensitivity to polarisation.

It is, of course, not necessary to rotate a crystal polarimeter about the line of sight to obtain p_L , as this is possible by simply measuring $J(\vartheta)$ at sufficient phase " ϑ_1 " points (3 is the minimum) to determine I , Q and U .

The Ariel-V polarimeter, however, operated by rotation of the polarimeter in the manner described and divided the ' ϑ ' rotation circle into 16 sections (which were called spin-sectors) from which the expected data curve is well over-determined. Then, p_L may be obtained, providing k is known.

§ 4.2.2b The Modulation Factor: $m = \frac{1-k}{1+k}$

(See previous section § 4.2.2a for an introduction to the modulation factor). Although for accurate work k must be obtained by calibrating the instrument to obtain $R_{c\pi}$ and $R_{c\sigma}$, simple theoretical expressions for k have been obtained for two widely diverging cases by Darwin (see Compton and Allison 1935). First, for a perfectly regular lattice in which the atoms are supposed unable to absorb X-rays

$$k = |\cos 2\theta_B| ; \quad (56)$$

and, second, for an "ideally imperfect crystal" which, at least in its surface layers, is supposed to consist of an assembly of very small domains each of which is slightly misaligned (by the order of one to ten milliradians) to its neighbours

$$k = \cos^2 2\theta_B \quad (57)$$

Evans et al. (1977) note that, although real crystals may not behave like either of these models, most of their experimentally determined values of k were within the two extremes and none were observed outside by anything other than an amount consistent with statistical fluctuations. Experimental values for k from Evans et al. (1977), as a function of θ_B , are shown in Fig. 4.2.9 in comparison with the theoretical extremes given by (56) and (57).

We note that for both the theoretical extremes, $k = 0$ at $\theta_B = 45^\circ$ (i.e. when the scattering angle is 90°). (This, as noted before, is when the instrument is most sensitive to polarisation (i.e. $m = 1$ in (55))).

However, in the beginning of the presentation of case (ii) reasons were given why $k > 0$ even at $\theta_B = 45^\circ$ and for reasonably accurate work calibration at $\theta_B = 45^\circ$ should also be carried out. Fortunately, the sensitivity of the Ariel-V instrument was such that

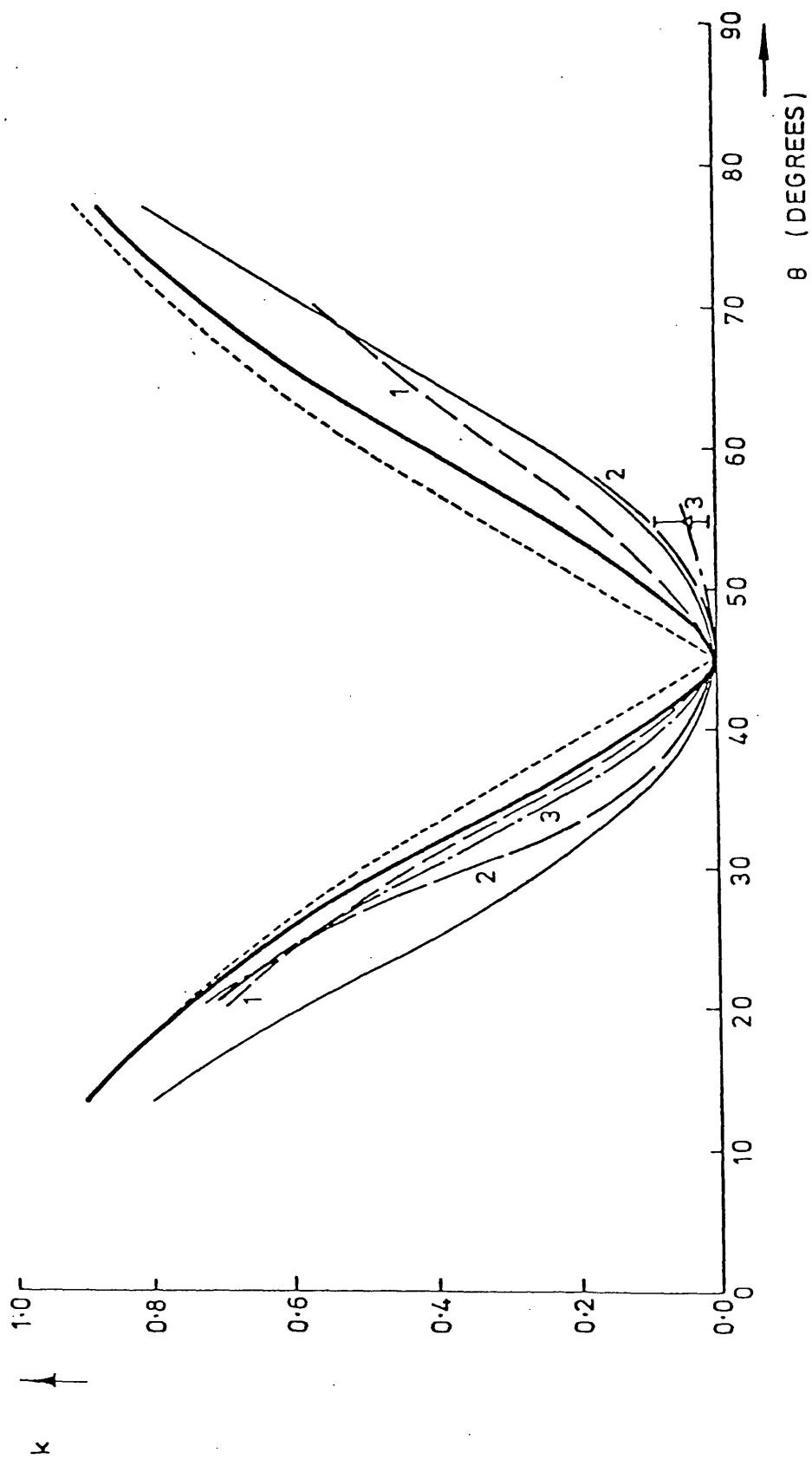


Fig. 4.2.9: Some experimental values of k as a function of θ_B (from Evans et al. 1977). The theoretical models given by $k = |\cos 2\theta_B|$ and $k = \cos^2 2\theta_B$ are also represented, and are the dotted and thin continuous lines respectively.

accurate calibration of the crystals was not required, and estimates of k with suitable error bars were made from k -curves for crystals similarly treated to those actually flown on board Ariel-V.

§ 4.2.2c Polarisation Interpretation from the Ariel-V Data

It has been shown in § 4.2.2a that the intensity (I) versus rotation angle (θ) profile resulting from the Ariel-V polarimeter is identical in shape to that which would be obtained by rotating a single polariser about the line of sight to an incident e.m. radiation beam. This profile has already been illustrated in Figs. 4.2.3 and 4.2.4 where it has been seen that only 3 parameters are required to describe the observed data completely:-

- i) The modulation phase - ζ
- ii) The modulation amplitude - A_p
- iii) The unmodulated amplitude - A_u

We know from § 4.2.1c, since no retarder is employed in the Ariel-V polarimeter, that the handedness of the polarisation cannot be obtained. Thus, only 3 of the 4 further parameters still required to specify the state of polarisation of incident beam $\overline{\zeta}$ (see § 4.2.1d and (e) $\overline{\zeta}$), can hope to be obtained.

The azimuth, or phase angle, of the polarisation ellipse is determined. This is given by the measured modulation phase ζ (see Fig. 4.2.3 for the case of perfect elliptically polarised radiation. The addition of an unpolarised component (§ 4.2.1d) does not affect the magnitude of ζ as it only produces an unmodulated component).

A_p , which is measured, gives, via the modulation factor m , the intensity difference between the major and minor axis components of the polarisation ellipse. (See Fig. 4.2.3, $I(\theta)_{\max}$ occurs when the polariser is aligned with the major axis of the polarisation

ellipse, and $I(\emptyset)_{\min}$ occurs when the polariser is aligned with the minor axis of the ellipse.)

The measured unmodulated amplitude A_u provides ambiguous information, as it may be caused by:-

- a) The shape of the polarisation ellipse (see Fig. 4.2.3), in which case it would be due to the minor axis intensity component of polarisation,
- b) simply an unpolarised component of radiation. (See Fig. 4.2.4).
- or c) the modulation factor m , although this effect can be allowed for if m is known. \checkmark

Thus, for the Ariel-V data, where there is no way of distinguishing between (a) and (b), the shape and size of the polarisation ellipse and also the magnitude of the unpolarised component cannot be known.

Only for the case when the incident radiation is known to be linearly polarised will the unmodulated component A_u be known to be due to the unpolarised component I_u . Then the degree of polarisation, known to be linear, can be obtained via equation (33).

For the general case, where partially elliptically polarised radiation is incident, a modulation will be obtained (as has been discussed previously, both mathematically in part (a) in this section and also conceptually above in considering the measurement of A_p). Then, as before, a value of p_L may be calculated according to equation (36) modified for the Ariel-V polarimeter as (55), giving:-

$$p_L = \frac{1}{m} \frac{I_{\text{major}} - I_{\text{minor}}}{I_{\text{major}} + I_{\text{minor}} + I_u} \quad (58)$$

where I_{major} and I_{minor} are the intensities which would be obtained with a polariser (having $m = 1$) aligned with the major and minor axes of the polarisation ellipse respectively, if only perfect elliptically polarised radiation was present. I_u , then represents the unpolarised

component, as illustrated by Fig. 4.2.4. From equation (58) it can be seen that as the polarisation ellipse approaches a circular shape this degree of linear polarisation measured via equation (36) will decrease, until eventually, no linear component will be obtained from circularly polarised radiation.

It has already been shown in part (a) of this section § 4.2.2 (see equations (51) and (52)), that this calculated degree of linear polarisation is identical to that obtained from the definition expressed by equation (37), i.e.

$$P_L = \frac{(Q^2 + U^2)^{\frac{1}{2}}}{I} = \frac{1}{m} \frac{I_{\max} - I_{\min}}{I_{\max} + I_{\min}}$$

§ 4.2.2d Determination of the Stokes Parameters

Determination of the Stokes parameters from the Ariel-V data is useful because they are standard parameters presented in publications, and also because the Stokes parameters representing the source data can be obtained by subtracting the Stokes parameters of the source + background data from those representing the background data alone. (Though it is possible to simply subtract the mean background plus background modulations from the source + background data, personally it was found easier to determine the errors involved if the subtraction was performed with the data represented in terms of the Stokes parameters.)

From the mathematics of part (a) of this section, the relation between the Stokes parameters representing the incident radiation and the theoretically obtained intensity profile has already been made evident via equation (51b):-

$$\text{i.e. } J(\theta) = \frac{A}{2} \left[I(1+k) + (1-k)(Q^2+U^2)^{\frac{1}{2}} \cos(2\theta - \tan^{-1} \frac{U}{Q}) \right]$$

where $\underline{S} = \begin{bmatrix} I \\ Q \\ U \end{bmatrix} = \begin{bmatrix} I_u + I_p \\ I_{pl} \cos 2\zeta \\ I_{pl} \sin 2\zeta \end{bmatrix}$ (59)

and the right-hand side of (59) has been written so that the Stokes parameters Q , U and I may be conveniently obtained from the observed intensity profile $J(\theta)$ (see Fig. 4.2.10).

From Fig. 4.2.10 2ζ is the phase angle of the polarisation,

so that

$$\tan^{-1} \frac{U}{Q} = 2\zeta$$

$$I_{pl} = (U^2 + Q^2)^{\frac{1}{2}}$$

$$\left[\begin{array}{l} \text{and } I_p^2 = Q^2 + U^2 + V^2 \text{ so that} \\ I_p^2 = I_{pl}^2 + V^2, \text{ making } I_{pl} \leq I_p \end{array} \right]$$

The degree of linear polarisation is given by

$$p_L \equiv \frac{(Q^2 + U^2)^{\frac{1}{2}}}{I} = \frac{I_{pl}}{I} = \frac{1}{m} \frac{A_p}{I} \quad (60)$$

where A_p is the measured modulation amplitude.

$$\left[\begin{array}{l} \text{i.e. } p_L = \left(\frac{1+k}{1-k} \right) \left(\frac{J_{\max} - J_{\min}}{J_{\max} + J_{\min}} \right) = \frac{1}{m} V \end{array} \right. \begin{array}{l} \text{from (52),} \\ \text{(54) and (55)} \end{array} \left. \right]$$

Finally, it must be noted that in using

$$\underline{S}(s) = \underline{S}(s+b) - \underline{S}(b) \quad (60b)$$

$$= \begin{bmatrix} I_{u(s+b)} + I_{p(s+b)} \\ I_{pl(s+b)} \cos 2\zeta_{(s+b)} \\ I_{pl(s+b)} \sin 2\zeta_{(s+b)} \end{bmatrix} - \begin{bmatrix} I_{ub} + I_{pb} \\ I_{pl b} \cos 2\zeta_b \\ I_{pl b} \sin 2\zeta_b \end{bmatrix} \quad (60c)$$

to obtain the Stokes parameters $\underline{S}(s)$, and hence degree of linear polarisation for the incident source radiation, that the $(s+b)$ and (b) intensities in (60c) must be in strict proportion with the relative

observed intensities of the (s+b) and (b) radiation (e.g. an underestimation of I_{ub} , say, will cause more of the I(s+b) intensity in (60c) to be interpreted as being due to the source, and hence

$p_L = \frac{I_p}{I}$ will then also be underestimated).

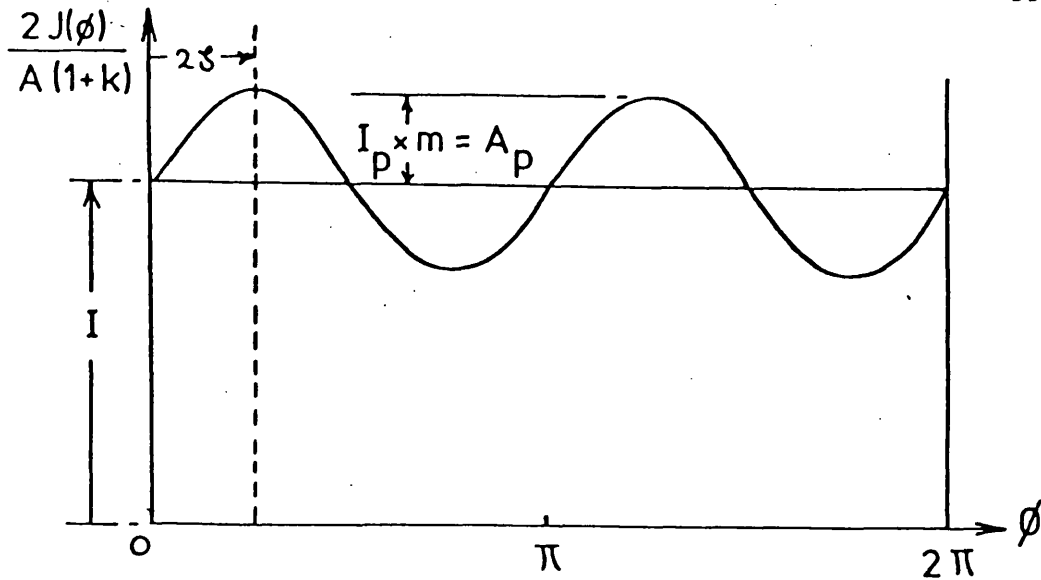


Fig. 4.2.10: Ariel-V polarimeter data profile as a function of rotation angle ϕ , showing the relation to the Stokes parameters representing the incident beam. m is the modulation factor.

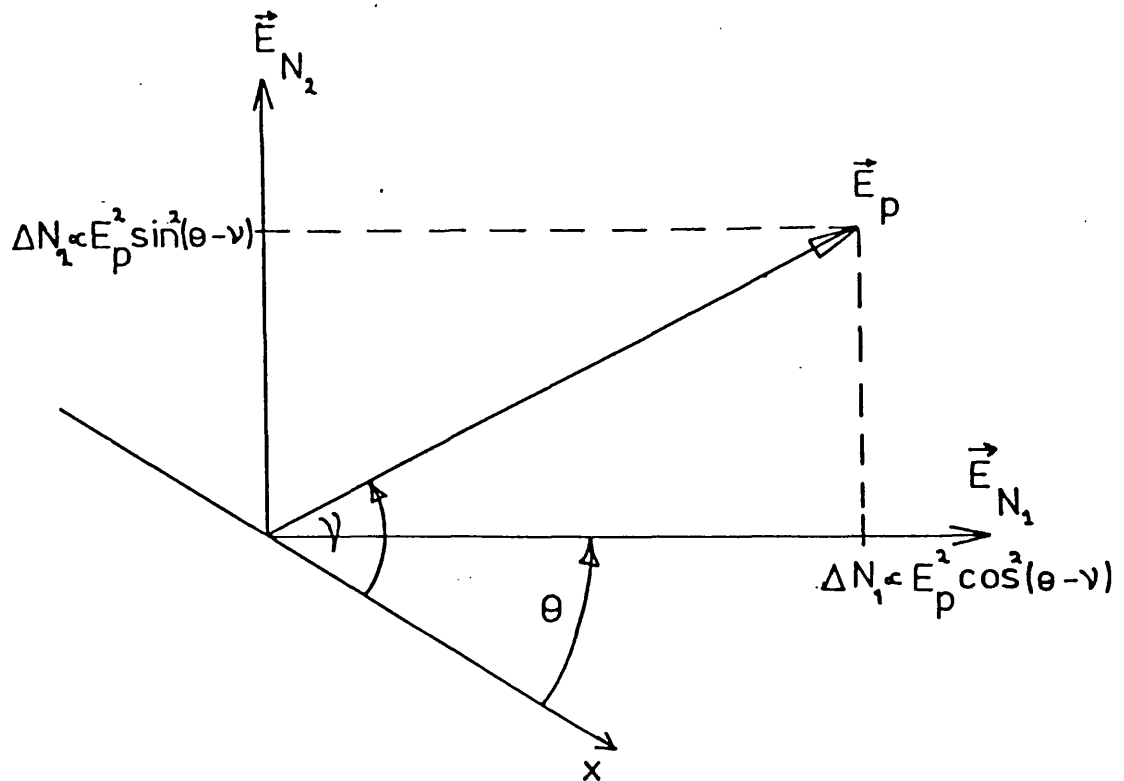


Fig. 4.2.11: Linearly polarised component vector orientated at angle γ to reference x -axis. Intensity measurements taken with a single polariser orientated at directions \vec{E}_{N_1} and \vec{E}_{N_2} . ΔN_1 and ΔN_2 will be the contribution to the total number of photons N_1 and N_2 collected just due to the linearly polarised component.

§ 4.2.3 Instrument Sensitivity to Polarisation - and Prediction Thereof

§ 4.2.3a Introduction

The instrument sensitivity is here defined as the accuracy which may be achieved on a measured parameter in:-

- i) an observation of a specified source
- ii) for a specified duration, and
- iii) under specified observing conditions which should, unless otherwise stated, be realistic.

To determine this sensitivity, the instrument response must be known under the observing conditions, and all statistical and systematic errors must be allowed for.

It is of prime importance that this sensitivity is known as well as possible before operation of the instrument, for if it is not known then the accuracy achieved on any measured parameters subsequent to an observation may be less than the minimum accuracy required for that observation to be useful, or the instrument itself may even be shown to be completely incapable of ever achieving worthwhile results. In practice, a partial prior knowledge of the instrument sensitivity is all that can be obtained as real observations may always contain unknown effects, especially if greater sensitivities than those previously obtained are being attempted, as with the Ariel-V polarimeter. If unknown effects do not occur, then the predicted sensitivity can be very accurate allowing accurate observations to be carefully designed. If unknown effects, or those which were not considered significant do prove significant, then cause analysis of the predicted sensitivity failure will allow future observations (or instruments) to have a predicted sensitivity which includes the new knowledge and which will be valid. Sensitivity calculations also highlight the effects which give rise to the dominant

component of inaccuracy in a result and can thus focus important attention on design aspects for new instruments. The relevance of these statements will become more apparent later, in the observations chapter, where much is learnt concerning limitations on the actual sensitivity of the Ariel-V polarimeter in practice.

The Ariel-V instrument response has been discussed earlier in § 3.2.3 and 4, and § 4.2.2a.

Here, statistical and systematic limitations on sensitivity are discussed.

§ 4.2.3b Fundamental Statistical Limitations

Fundamental statistical limitations on the accuracy which may be achieved by an instrument which analyses a finite number of photons received from a source, are due to random fluctuations which may be expected to occur in that number of received photons. These limitations are further increased by the presence of a background component which is also subject to random fluctuations. The limitations are fundamental in that with a limited number of events, no change in instrument design, except to collect more events, can reduce them. They represent the maximum sensitivity which can be obtained from a data set and can only be realised with a perfect experiment.

Before the flight of the Ariel-V polarimeter these fundamental statistical limitations were the dominant source of error, as shown by the previous results obtained from the short duration rocket flights (see § 2.2.2 for results and references).

The opening up of possible observation times, from a few minutes for rocket flights to durations of the order of a week or more from the Ariel-V satellite, has had the effect of a considerable reduction to these statistical limitations, thus increasing the possible

polarisation sensitivity of observations.

1) Elementary Concepts

Consider a perfect experiment in which a simple polariser is used to measure the received intensity at two orthogonal orientations about a beam which is partially linearly polarised. If the degree of linear polarisation is p , then

$$p \cos 2(\theta - \nu) = \frac{N_1 - N_2}{N_1 + N_2} \quad (\text{see (36)}) \quad (61)$$

where N_1 is the number of photons received (\propto intensity) with the polariser orientated at some angle θ to an x-direction, and N_2 is the number received with the polariser orientation at $\theta + \frac{\pi}{2}$ radians. The linearly polarised component of the incident radiation is orientated at an angle ν from the x-direction (see Fig. 4.2.11).

If the incident beam contains N photons unit time⁻¹ and each polariser measurement takes $\frac{1}{2}$ (unit time) then we would expect $\frac{N}{2}$ photons to be incident for each measurement, where $\frac{N}{2} = I_u + I_p$ (i.e. incident beam composed of unpolarised component plus polarised component). Then, from each measurement, from Fig. 4.2.11, it can be seen that

$$N_1 [\alpha \frac{1}{2} E_u^2 + E_p^2 \cos^2(\theta - \nu)] = \frac{1}{2} I_u + I_p \cos^2(\theta - \nu) \quad (62)$$

$$N_2 [\alpha \frac{1}{2} E_u^2 + E_p^2 \sin^2(\theta - \nu)] = \frac{1}{2} I_u + I_p \sin^2(\theta - \nu) \quad (63)$$

(i.e. a simple polariser passes only half the unpolarised radiation incident upon it).

$$\text{Thus } N_1 + N_2 = I_u + I_p = \frac{N}{2} \quad (64)$$

and it can be seen that for N incident photons only $\frac{N}{2}$ will be eventually recorded.

Letting $P = p \cos 2(\theta - \nu)$ we will consider the standard deviation on a measurement of P .

Then
$$P = \frac{N_1 - N_2}{N_1 + N_2} \quad (\text{from (61)})$$

so
$$\sigma^2(P) = \sigma^2(N_1) \left(\frac{\partial P}{\partial N_1} \right)^2 + \sigma^2(N_2) \left(\frac{\partial P}{\partial N_2} \right)^2$$

from 1st order error theory (see e.g. Bevington 1969), providing N_1 and N_2 are independent quantities so that their fluctuations are incoherent.

Then

$$\sigma^2(P) = \sigma^2(N_1) \left[\frac{1}{N'} - \frac{(N_1 - N_2)}{N'^2} \right]^2 + \sigma^2(N_2) \left[\frac{-1}{N'} - \frac{(N_1 - N_2)}{N'^2} \right]^2$$

where $N' = N_1 + N_2 = \frac{N}{2}$ (65)

so $N'^2 \sigma^2(P) = N_1 [1 - p]^2 + N_2 [1 + p]^2$ (66)

where $\sigma^2(N_1) = N_1$ and $\sigma^2(N_2) = N_2$, assuming validity for use of the Poisson standard deviation for the counting process.

Now, from (62)

$$\begin{aligned} N_1 &= \frac{1}{2} I_u + \frac{1}{2} I_p (1 + \cos 2(\theta - \nu)) \\ &= \frac{1}{2} (I_u + I_p) + \frac{1}{2} I_p \cos 2(\theta - \nu) \\ &= \frac{1}{2} N' (1 + P) \end{aligned} \quad (67)$$

from (64), (33) and (66); and similarly

$$N_2 = \frac{N'}{2} (1 - P) \quad (68)$$

and substituting these expressions (67) and (68) for N_1 and N_2 into (66), the following expression results:-

$$\begin{aligned} N'^2 \sigma^2(P) &= \frac{N'}{2} (1 + P)(1 - P)^2 + \frac{N'}{2} (1 - P)(1 + P)^2 \\ &= \frac{N'}{2} (1 - P^2) [(1 - P) + (1 + P)] \end{aligned}$$

so that $\sigma(P) = \sqrt{\frac{1 - P^2}{N'}} \quad (69)$

i.e. $\sigma(P) = \left[\frac{2(1 - P^2)}{N} \right]^{\frac{1}{2}} \quad (70)$

from (65))

Thus, equation (70) expresses the fundamental statistical limitation on the accuracy of a measurement of P.

It may be noted that if P is small then (70) reduces to

$$\sigma(P) = \left(\frac{2}{N} \right)^{\frac{1}{2}} \quad (71)$$

We will now attempt to develop an expression for the statistical distribution of polarisation values about the mean value. Consider the same experiment where P is given by (61). Then the probability of obtaining a value P to P + dp, (say W(P)dp), is proportional to the probabilities for obtaining N_1 to $N_1 + dN_1$ and N_2 to $N_2 + dN_2$ counts.

$$\text{i.e. } W(P)dP = K g(N_1)dN_1 g(N_2)dN_2 \quad (72)$$

where it is implicitly assumed that N is large enough to provide justification using dN_1 and dN_2 . K is the constant of proportionality.

As N is large it is now assumed that the statistical distributions of the N_1 and N_2 counts can be described by a Gaussian distribution with the Poisson standard deviation (i.e. $\sigma(N_1) = \sqrt{N_1}$ and $\sigma(N_2) = \sqrt{N_2}$ respectively). (72) then becomes:-

$$W(P)dP = \frac{K}{2\pi\sigma_{N_1}\sigma_{N_2}} \exp \left\{ -\frac{(N_1 - N_{10})^2}{2\sigma_{N_1}^2} \right\} \exp \left\{ -\frac{(N_2 - N_{20})^2}{2\sigma_{N_2}^2} \right\} dN_1 dN_2 \quad (73)$$

where N_{10} and N_{20} are the mean recorded values of N_1 and N_2 respectively.

If an observation is made of completely unpolarised radiation,

$$\text{then } N_{10} = N_{20} = \frac{N'}{2}$$

$$\text{and } \sigma_{N_1} = \sigma_{N_2} = \sqrt{\frac{N'}{2}} \equiv \sigma \quad (74)$$

(73) then becomes:-

$$\begin{aligned}
W(P)dP &= \frac{K}{2\pi\sigma^2} \exp\left\{-\frac{1}{2\sigma^2} \left[\left(N_1 - \frac{N'}{2}\right)^2 + \left(N_2 - \frac{N'}{2}\right)^2 \right]\right\} dN_1 dN_2 \\
&= \frac{K}{2\pi\sigma^2} \exp\left\{-\frac{1}{2\sigma^2} \left[\frac{N'^2}{2} - 2N_1 N_2 \right]\right\} dN_1 dN_2 \\
&\text{by using (65)} \\
&= \frac{K}{2\pi\sigma^2} \exp\left\{-\frac{\left(\frac{N'^2}{2} - P^2\right)}{2\sigma^2}\right\} dN_1 dN_2 \quad (74a)
\end{aligned}$$

using (67) and (68) where

$$N_1 = \frac{N'}{2} (1 + P)$$

$$N_2 = \frac{N'}{2} (1 - P)$$

Then, the Jacobian

$$\left| \frac{\partial(N_1, N_2)}{\partial(P, N')} \right| = + \frac{N'}{2}$$

so that (74) becomes:-

$$W(P)dP = \frac{K}{2\pi\sigma^2} \exp\left\{-\frac{\left(\frac{N'^2}{2} - P^2\right)}{2\sigma^2}\right\} \frac{N'}{2} dN' dP \quad (75)$$

where N' , the total number of recorded counts, is treated as approximately constant so that (75) reduces to:-

$$W(P)dP = \frac{k'}{2\pi\sigma^2} \exp\left\{-\frac{\left(\frac{N'^2}{2} - P^2\right)}{2\sigma^2}\right\} dP \quad (76)$$

where k' is the new normalisation constant.

[P is normally given by $(N_1 - N_2)/(N_1 + N_2)$ where its value can range from -1 to $+1$. However, by treating $(N_1 + N_2) = N'$ as a constant, P is then given by $(N_1 - N_2)/N'$ and can take values from $-\infty$ to $+\infty$ instead of the correct range -1 to $+1$. This approximation of N' as a constant will be good when P is small, so that a change in N_1 or N_2 causes a change in P to be dominated by the alteration in the numerator quantity $(N_1 - N_2)$

rather than the denominator quantity ($N_1 + N_2$). i.e. N' can be treated as approximately constant.]

If N' is large, so that the constant term contained in the exponential in (76), $\frac{N'^2}{4\sigma^2} = \frac{N'}{2}$ (from (74)) is also large, then a

good approximation to the integral limits for the normalisation of (76) will be $+\infty$ and $-\infty$ (instead of $+1$ and -1 which are less convenient).

Hence, performing the normalisation to obtain k'

$$\int_{-\infty}^{+\infty} W(P)dP = 2 \int_0^{\infty} W(P)dP = \frac{2k'}{2\pi\sigma^2} \left[\frac{\sqrt{\pi}}{2} \frac{4\sigma}{N'} \right] = 1$$

so that $k' = \sqrt{\pi} N'\sigma$, making

$$W(P)dP = \frac{N'}{2\sqrt{\pi}\sigma} \exp \left\{ -\frac{\left(\frac{N'}{2} P^2\right)}{2\sigma^2} \right\} dP \quad (77)$$

for small $P > 0$.

$$\text{and letting } \sigma'^2 = \frac{2\sigma^2}{N'} \quad (77b)$$

(77) becomes:-

$$W(P)dP = \frac{1}{\sqrt{2\pi\sigma'^2}} \exp \left\{ -\frac{P^2}{2\sigma'^2} \right\} dP \quad (78)$$

i.e. a Gaussian distribution, with mean $P = 0$ and standard deviation σ' .

But $P(\theta) = p \cos 2(\theta - \nu)$ is composed of 2 variables p and ν , and to obtain the degree of polarisation p at least one other measurement of $P(\theta)$ must be made at some angle $\theta_2 \neq \theta_1$.

Then similarly, with a second measurement where, using for convenience the same observing time, N' photons are also expected to be observed, the distribution of P values will be identical, i.e.

$$W(P_2)dP_2 = \frac{1}{\sqrt{2\pi\sigma'^2}} \exp \left\{ -\frac{P_2^2}{2\sigma'^2} \right\} dP_2 \quad (79)$$

and if θ_2 is chosen so that $\theta_2 = \theta_1 + \frac{\pi}{4}$

then $P(\theta_2) \equiv P_2 = p \cos [2(\theta_1 - \nu) + \frac{\pi}{2}] = p \sin 2(\theta_1 - \nu)$

and for completeness (80)

$$P(\theta_1) \equiv P_1 = p \cos 2(\theta_1 - \nu)$$

and $p = (P_1^2 + P_2^2)^{\frac{1}{2}}$ (81)

The probability of detecting a degree of polarisation p from unpolarised radiation is then given by:-

$$f(p)dp = K'' W(P_1)dP_1 W(P_2)dP_2$$

where K'' is the constant of proportionality.

$$= \frac{K''}{\sqrt{2\pi\sigma_1'^2} \sqrt{2\pi\sigma_2'^2}} \exp \left\{ -\frac{P_1^2}{2\sigma_1'^2} - \frac{P_2^2}{2\sigma_2'^2} \right\} dP_1 dP_2$$

and as both experiments took equal times

$$\sigma_1'^2 = \sigma_2'^2 = \sigma_p^2 \text{ say,} \quad (81b)$$

so that

$$\begin{aligned} f(p)dp &= \frac{K''}{2\pi\sigma_p^2} \exp \left\{ -\frac{1}{2\sigma_p^2} (P_1^2 + P_2^2) \right\} dP_1 dP_2 \\ &= \frac{K''}{2\pi\sigma_p^2} \exp \left\{ -\frac{p^2}{2\sigma_p^2} \right\} dP_1 dP_2 \end{aligned} \quad (82)$$

from (80)

and by calculating the Jacobian $J\left(\frac{P_1, P_2}{P, \theta_1}\right)$ via (80),

(82) becomes:-

$$f(p)dp = \frac{K''}{2\pi\sigma_p^2} \exp \left\{ -\frac{p^2}{2\sigma_p^2} \right\} 2pdpd\theta \quad (83)$$

Equation (83) then, represents the probability of detecting a degree of polarisation p at a particular orientation θ from unpolarised data. If

we are interested in detection of p at whatever angle of θ it may arise, then we may integrate (83) over the range $0 < \theta < 2\pi$, giving:-

$$f(p)dp = \frac{2K''}{\sigma_p^2} p \exp\left\{-\frac{p^2}{2\sigma_p^2}\right\} dp \quad (84)$$

Normalisation of (84) (using limits $+\infty$ and zero since $p \geq 0$, from (81)) gives:-

$$f(p)dp = \frac{1}{\sigma_p^2} p \exp\left\{-\frac{p^2}{2\sigma_p^2}\right\} dp \quad (85)$$

i.e.
$$f(p)dp = \frac{N}{2} p \exp\left\{-\frac{Np^2}{4}\right\} dp \quad (86)$$

where σ_p^2 has been substituted by $\frac{2}{N}$ (see (74), (77b), (81b) and (65)), where N is the total number of counts incident for one determination of P , or observed for both measurements of P_1 and P_2 .

$f(p)$ is displayed in Fig. 4.2.12 where it can be seen, even for the unpolarised incident radiation we have considered, that the probability of obtaining a measurement of zero polarisation, is zero. This arises because it has been assumed that N is large enough to make use of dN valid. In practice, with finite N , this probability will be greater than zero. The underlying reason why the probability falls very near to zero as $p \rightarrow 0$ is because of equation (81) which shows that (positive square root always taken) the vast majority of the statistical fluctuations giving rise to P_1 and P_2 will cause a non-zero value of p to be actually measured.

$$\text{As } p = (P_1^2 + P_2^2)^{\frac{1}{2}}$$

then, by first order error propagation theory (e.g. Bevington 1969),

$$\sigma^2(p) = \left[\frac{1}{2} \frac{2P_1}{(P_1^2 + P_2^2)^{\frac{1}{2}}} \right]^2 \sigma^2(P_1) + \left[\frac{1}{2} \frac{2P_2}{(P_1^2 + P_2^2)^{\frac{1}{2}}} \right]^2 \sigma^2(P_2)$$

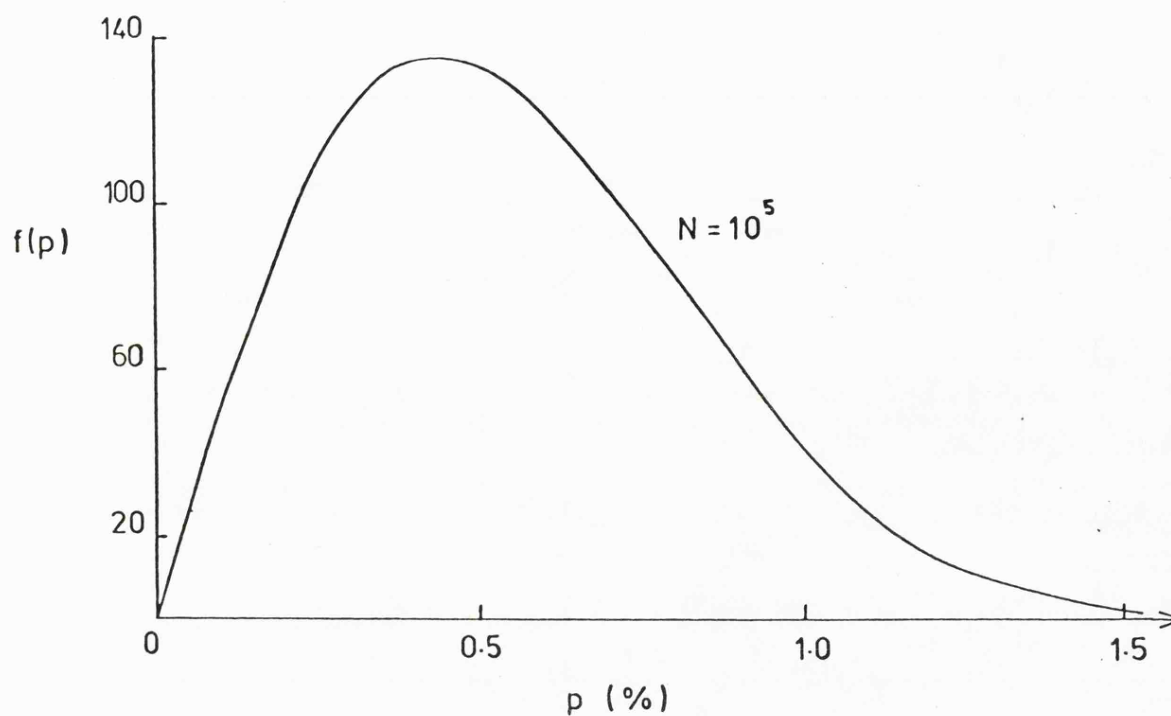


Fig. 4.2.12: Expected statistical distribution of degrees of polarisation p obtained from measurements of an unpolarised source, where N photons are observed for each measurement.

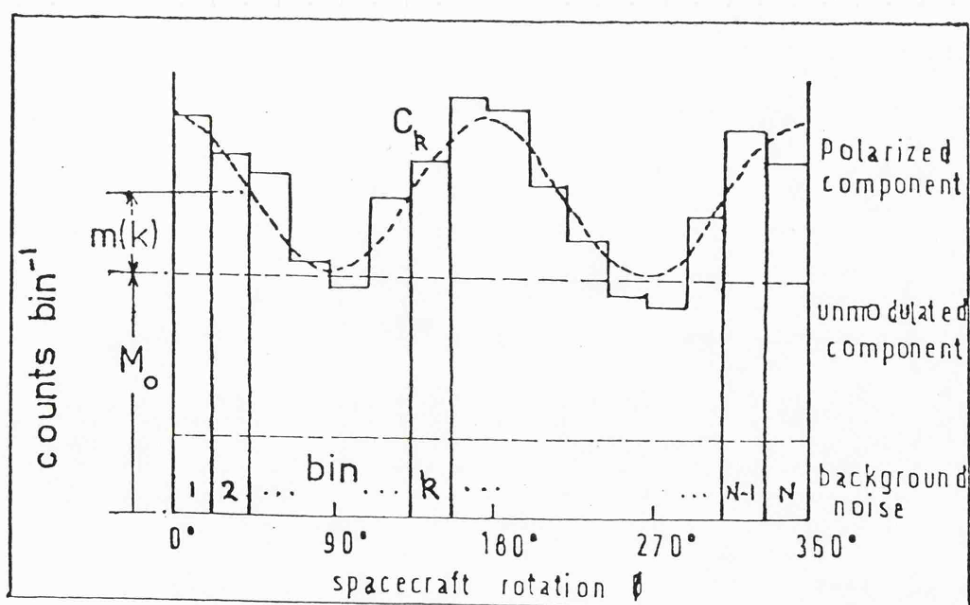


Fig. 4.2.13: Polarisation data divided into N bins according to polariser angle ϕ , the k -th bin contains c_k events.

$$= \frac{P_1^2}{p^2} \sigma^2(P_1) + \frac{P_2^2}{p^2} \sigma^2(P_2)$$

$$\text{i.e. } p^2 \sigma^2(p) = P_1^2 \sigma^2(P_1) + P_2^2 \sigma^2(P_2) \quad (87)$$

and as both measurements are assumed equally accurate

$$\sigma^2(P_1) = \sigma^2(P_2) = \frac{2}{N} \quad (\text{from 71})$$

So, (87) becomes:-

$$p^2 \sigma^2(p) = \frac{2}{N} [P_1^2 + P_2^2] = \frac{2}{N} p^2$$

$$\text{i.e. } \sigma(p) = \left(\frac{2}{N} \right)^{\frac{1}{2}} \quad (88)$$

The expected value of p (given by $\int_0^{\infty} pf(p)dp$) evaluates as

$$E[p] = \sqrt{\frac{\pi}{N}} .$$

Thus, in summary, for a simple experiment involving a single polariser in which 2 sets of orthogonal measurements have been carried out on an incident unpolarised beam, the spread of apparent polarisation degrees obtained has been shown to be described by the distribution

$$f(p)dp = \frac{Np}{2} \exp\left\{ -\frac{Np^2}{4} \right\} dp$$

where the standard deviation about the observed value of p is given by

$$\sigma(p) = \left(\frac{2}{N} \right)^{\frac{1}{2}}, \text{ providing } N \text{ is large and } p \text{ is small.}$$

The sensitivity of this experiment is then given approximately

$$\text{by } 3 \times \sigma(p) = 3 \left(\frac{2}{N} \right)^{\frac{1}{2}} \quad (89)$$

providing no background component exists. That is, in an observation where N photons are observed no measurement p less than $3 \left(\frac{2}{N} \right)^{\frac{1}{2}}$ can be said to indicate a real polarisation of the incident beam at \approx 3-sigma confidence. (A more accurate consideration of the 3-sigma confidence limit follows.)

ii) Sensitivity Estimate of Polarisation Determination from a Rotating Polarimeter - e.g. The Ariel-V Data Collecting System

We will now consider the case where p and ν [$P = p \cos 2(\theta - \nu)$] are determined from data collected in N bins, each $\frac{2\pi}{N}$ radians wide, from a continuous observation employing a uniformly rotating polariser. A noise component, including background counts, will be included at the end of this section. The mathematics are drawn from a short appendix to a paper by Schnopper and Kalata (1969) where their analysis was based on a discussion by F. Floyd (1968 M.I.T. Thesis). However, since Floyd's thesis material is not easily available, the short appendix discussion is augmented here to include some of the intervening argument steps in order that the discussion may be more easily followed.

The raw data is divided into N bins, the k^{th} bin containing C_k events (see Fig. 4.2.13). The total number of X-rays detected is

$$N_T = \sum_{k=1}^N C_k \quad (90)$$

We now Fourier analyze the function $C(k)$, which underlies the recorded data values C_k , assuming that $C(k)$ is continuous and satisfies the Dirichlet conditions in the interval $1 \leq k \leq N$. Then from the Fourier series result that, for a function $\zeta(k)$ satisfying the above conditions,

$$\zeta(k) = \sum_{n=-\infty}^{+\infty} g_n \exp\left\{i \frac{n\pi k}{l}\right\}$$

where

$$g_n = \frac{1}{2l} \int_0^{2l} \zeta(k) \exp\left\{-i \frac{n\pi k}{l}\right\} dk \quad \text{where } 2l = N.$$

The Fourier series for $C(k)$ can then be represented as

$$C(k) = \frac{1}{N} \sum_{j=-N/2}^{+N/2} F_j \omega^*(k, j) \quad (91)$$

where the Fourier coefficients F_j are given by

$$\begin{aligned} F_j &= NH_j = \int_0^N C(k) \exp\left\{ \frac{j2\pi k}{N} \right\} dk \\ &\approx \sum_{k=1}^N C_k \omega(k, j) \end{aligned} \quad (92)$$

$$\text{where } \omega(k, j) = \exp\left\{ i \frac{j2\pi k}{N} \right\} \quad (93)$$

$$\text{and } i = \sqrt{-1}.$$

[In (92) it is assumed that the approximation of the integral to the summation provides an accurate estimation of F_j . We would expect the number of counts observed in the k^{th} bin to be given by the following expression:-

$$C_{k_o} = \frac{1}{(k_b - k_a)} \int_{k_a = k_o - 1}^{k_b = k_o} C(k) dk$$

In (91) the summation range is limited to $j = -\frac{N}{2}$ to $+\frac{N}{2}$ (a range of N) as the data set $\{ C_k \}$ $k = 1, \dots, N$ is completely determined by N F_j frequency coefficients.]

Consider the C_k as distributed randomly with a mean value $M(k)$ which is composed of two parts:-

$$\text{i.e. } M(k) = M_o + m(k) \quad (95)$$

where M_o represents the unmodulated part of the signal composed of contributions from the source and background (see Fig. 4.2.13). $m(k)$ is the modulation due to polarisation. As the C_k represent the number of counts recorded per bin it is assumed that their values follow the

Poisson distribution where the mean and variance are given by

$$E[C(k)] = V[C(k)] = M(k) \quad (96)$$

It is useful to deal separately with the real and imaginary parts of F_j . This can be accomplished by noting that

$$\omega(k, j) = U(k, j) + iV(k, j) \quad (97)$$

where

$$U(k, j) = \cos\left(\frac{2\pi kj}{N}\right) \quad (98)$$

$$V(k, j) = \sin\left(\frac{2\pi kj}{N}\right) \quad (99)$$

so that F_j becomes expressed as, from (92), :-

$$\begin{aligned} F_j &= \sum_{k=1}^N C_k U(k, j) + i \sum_{k=1}^N C_k V(k, j) \\ &= F_{(j)_R} + i F_{(j)_I} = Am_{(j)} e^{-i\phi_j} \end{aligned} \quad (100)$$

where $F_{(j)_R}$ and $F_{(j)_I}$ are the real and imaginary parts of F_j , and $Am_{(j)}$ and ϕ_j are the amplitude and phase of F_j as expressed via the Argand diagram, where:-

$$Am_{(j)} = \left[F_{(j)_k}^2 + F_{(j)_I}^2 \right]^{\frac{1}{2}} \quad (101)$$

and

$$\tan \phi_j = \frac{F_{(j)_I}}{F_{(j)_k}} \quad (102)$$

From the previous analysis of a rotating polariser (§ 4.2.1e, § 4.2.2a and b) we know that the magnitude and phase of the polarisation is related to the amplitude and phase of the second harmonic frequency (see Fig. 4.2.13). Equation (91) analyzes $C(k)$ into its frequency components.

$$C(k) = \frac{1}{N} \sum_{j=-N/2}^{+N/2} F_j \omega^*(k, j)$$

$$= \frac{1}{N} \left[\dots + F_{-n} \omega^*(k, -n) + \dots + F_n \omega^*(k, n) + \dots \right]$$

(a) (b)

and taking the n th harmonic components of $C(k)$ given by the terms (a) and (b), we have

$$C_{|n|}(k) = \frac{1}{N} \left[F_{-n} \exp \left\{ \frac{i2\pi nk}{N} \right\} + F_n \exp \left\{ \frac{-i2\pi nk}{N} \right\} \right]$$

and as $F_{-n} = F_n^* = Am(n) e^{-i\phi_n}$

we obtain

$$\begin{aligned} C_{|n|}(k) &= \frac{Am(n)}{N} \left\{ \exp \left[-i \left(\frac{2\pi nk}{N} - \phi_n \right) \right] + \exp \left[+i \left(\frac{2\pi nk}{N} - \phi_n \right) \right] \right\} \\ &= \frac{2Am(n)}{N} \cos \left(\frac{2\pi nk}{N} - \phi_n \right) \end{aligned} \quad (103)$$

So, when $n = 2$, ϕ_2 represents the phase angle of the polarisation and $\frac{2Am(2)}{N}$ represents the amplitude related to the degree of polarisation.

Thus, the polarisation quantities ϕ_n and $Am(n)$ can be calculated in practice from the raw data C_k by means of Fourier analysis via (91) where the F_j are calculated via (92), and $Am(n)$ and ϕ_n are determined via (101) and (102).

Statistics - Minimum Detectable Polarisation (M.D.P.)

Now that we have Fourier analysed the raw data C_k , and shown how the polarisation degree and phase is obtained, we go on to consider the statistical distribution of the Fourier amplitudes Am . It has been seen already that

$$F_j = \sum_{k=1}^N C_k \exp \left\{ \frac{i2\pi kj}{N} \right\} \quad (104)$$

where the real and imaginary parts are given by

$$F_{(j)_R} = \sum_{k=1}^N C_k \cos \left(\frac{2\pi kj}{N} \right) \quad (105)$$

$$F_{(j)_I} = \sum_{k=1}^N C_k \sin\left(\frac{2\pi kj}{N}\right) \quad (106)$$

and applying the Central limit theorem in statistics. [That is, given a set of n independent random variables x_1, x_2, \dots, x_n each with an arbitrary probability distribution function with finite mean μ_i and second moment σ_i^2 , if the sum

$$y = \sum_{i=1}^n a_i x_i \quad (107)$$

is considered, it is true that

$$\mu(y) = \sum_{i=1}^n \mu_i \quad \text{and} \quad \sigma^2(y) = \sum_{i=1}^n a_i^2 \sigma_i^2 \quad (108)$$

The Central limit theorem then states that as n increases, the distribution of y approaches the normal distribution $\phi(y)$ with mean $\mu(y)$ and variance $\sigma^2(y)$

i.e.

$$\phi(y) = \frac{1}{\sqrt{2\pi} \sigma(y)} \exp\left\{ \frac{-[y - \mu(y)]^2}{2\sigma^2(y)} \right\} \quad (109)$$

it can be seen that the distribution of $F_{(j)_R}$ and $F_{(j)_I}$ will be given by the following:-

$$P[D_j] dD_j = \frac{1}{(2\pi)^{\frac{1}{2}}} \frac{1}{\sigma_{D_j}} \exp\left\{ \frac{-(D_j - \mu_{D_j})^2}{2\sigma_{D_j}^2} \right\} dD_j \quad (110)$$

$$P[E_j] dE_j = \frac{1}{(2\pi)^{\frac{1}{2}}} \frac{1}{\sigma_{E_j}} \exp\left\{ \frac{-(E_j - \mu_{E_j})^2}{2\sigma_{E_j}^2} \right\} dE_j \quad (111)$$

where the subscripting has been simplified by letting

$$F_j = D_j + iE_j = A_{m(j)} e^{-i\phi_j} \quad (112)$$

$$\left[\begin{array}{l} \text{i.e. } F_{(j)_R} = D_j \\ F_{(j)_I} = E_j \end{array} \right]$$

Then, from (108)

$$\mu(D_j) = \sum_{k=1}^N \mu[C_k] \cos\left(\frac{2\pi kj}{N}\right) \quad (113)$$

and

$$\sigma^2(D_j) = \sum_{k=1}^N \sigma^2[C_k] \cos^2\left(\frac{2\pi kj}{N}\right) \quad (114)$$

where similar expressions can be obtained for $\mu(E_j)$ and $\sigma^2(E_j)$.

$\mu[C_k]$ and $\sigma^2[C_k]$ are the mean and standard deviation respectively of the distribution where $C(i)$ is a measured value.

$$\begin{aligned} \mu[D_j] &= \sum_{k=1}^N \mu[C_k] \cos\left(\frac{2\pi kj}{N}\right) \\ &= \sum_{k=1}^N [M_0 + m(k)] \cos\left(\frac{2\pi jk}{N}\right) \text{ using (95)} \\ &= \sum_{k=1}^N M_0 \cos\left(\frac{2\pi jk}{N}\right) \text{ if } \sum_{k=1}^N m(k) \cos\left(\frac{2\pi jk}{N}\right) \\ &\hspace{15em} \text{is small} \end{aligned} \quad (115)$$

(which occurs if the incident radiation is unpolarised or has very little polarisation i.e. $m(k) \ll M_0$.)

$$\begin{aligned} &= M_0 \sum_{k=1}^N \left(\frac{e^{i\theta k} + e^{-i\theta k}}{2} \right) \text{ where } \theta = \frac{2\pi j}{N} \quad (116) \\ &= \frac{M_0}{2} [(e^{i\theta} + e^{i2\theta} + \dots + e^{iN\theta}) + (e^{-i\theta} + e^{-i2\theta} + \dots + e^{-iN\theta})] \\ &= \frac{M_0}{2} \left[e^{i\theta} \left\{ \frac{e^{iN\theta} - 1}{e^{i\theta} - 1} \right\} + e^{-i\theta} \left\{ \frac{e^{-iN\theta} - 1}{e^{-i\theta} - 1} \right\} \right] \end{aligned}$$

by summing the geometric series.

$$\text{i.e. } \underline{\mu[D]} \approx 0 \quad (117)$$

(as $e^{iN\theta} = \cos\left(\frac{2\pi jN}{N}\right) + i \sin \frac{2\pi jN}{N}$ where $j = 0, \pm 1, \pm 2, \dots$

$$= 1$$

making $e^{iN\theta} - 1 = 0$.)

Similarly $\mu [E_j] \approx 0$ (118)

[Note: These means will exactly vanish when all harmonic amplitudes are absent (i.e. $p = 0$). For small values of polarisation (117) and (118) hold approximately true for $m(k) \ll M_o$.]

Now consider the variances $\sigma^2(D_j)$ and $\sigma^2(E_j)$.

$$\begin{aligned} \sigma^2(D_j) &= \sum_{k=1}^N \sigma^2 [C_k] \cos^2 \left(\frac{2\pi jk}{N} \right) \\ &= \sum_{k=1}^N \mu [C_k] \cos^2 (2\pi jk) \quad \text{as for } C_k \text{ Poissonly} \\ &\quad \text{distributed } \sigma^2 [C_k] = \mu [C_k] \\ &= \sum_{k=1}^N [M_o + m(k)] \cos^2 \left(\frac{2\pi jk}{N} \right) \\ &\approx M_o \sum_{k=1}^N \cos^2 \left(\frac{2\pi jk}{N} \right) \quad \text{if, as before} \\ &\quad \sum_{k=1}^N m(k) \cos^2 \left(\frac{2\pi jk}{N} \right) \quad \text{is small} \\ &= M_o \sum_{k=1}^N \left[\frac{e^{+i\theta k} + e^{-i\theta k}}{2} \right]^2 \quad \text{where } \theta = \frac{2\pi j}{N} \\ &= \frac{M_o}{4} \sum_{k=1}^N [e^{i2\theta k} + 2e^{i\theta k} e^{-i\theta k} + e^{-i2\theta k}] \end{aligned}$$

$$\begin{aligned}
&= \frac{M_0}{4} \left[\sum_{k=1}^N e^{i2\theta k} + 2 \sum_{k=1}^N e^{i\theta k} e^{-i\theta k} + \sum_{k=1}^N e^{-i2\theta k} \right] \\
&= \frac{M_0}{4} [0 + 2N + 0] \quad \text{as} \quad \sum_{k=1}^N e^{i\theta k} = 0
\end{aligned}$$

in calculation of $\mu(D_j)$

i.e.

$$\sigma^2(D_j) = \frac{M_0 N}{2} = \sigma^2 \quad \text{say,} \quad (119)$$

$$\text{and similarly } \sigma^2(E_j) = \sigma^2 \quad \text{if } m(k) \ll M_0 \quad (120)$$

$$\text{so that } \underline{\sigma^2(D_j) = \sigma^2(E_j) = \sigma^2} \quad \text{for } m(k) \ll M_0 \quad (121)$$

Now that the means and variances of (110) and (111) have been evaluated, the distribution of the $Am_{(j)}$'s, which are related to the polarisation amplitude, can now be considered.

From (101)

$$Am_{(j)} = [D_j^2 + E_j^2]^{\frac{1}{2}} \quad (122)$$

so that the probability distribution of the $Am_{(j)}$ will be proportional to the distributions for D_j and E_j , i.e.

$$p[Am_{(j)}] dAm_{(j)} = K P(D_j) dD_j P(E_j) dE_j$$

where K is a constant.

$$= \frac{K}{2\pi\sigma^2} \exp\left\{-\frac{(D_j^2 + E_j^2)}{2\sigma^2}\right\} dD_j dE_j \quad (123)$$

[from (110) and (111) with the means and variances substituted in from (117), (118) and (121)].

$$= \frac{K}{2\pi\sigma^2} \exp\left\{-\frac{Am_{(j)}^2}{2\sigma^2}\right\} Am_{(j)} dAm_{(j)} d\theta_j \quad (124)$$

[by use of (122) and that $dD_j dE_j = Am_{(j)} dAm_{(j)} d\theta_j$ by evaluating the

Jacobian $J \left(\begin{matrix} D_j, E_j \\ Am_{(j)}, \theta_j \end{matrix} \right)$

as $D_j = Am_{(j)} \cos \vartheta_j$

and $E_j = Am_{(j)} \sin \vartheta_j$ from the Argand diagram, or from (100).]

Integrating over ϑ_j then gives the probability of obtaining an amplitude irrespective of phase angle

$$\begin{aligned} P[Am_{(j)}] dAm_{(j)} &= \int_0^{2\pi} \frac{K}{2\pi\sigma^2} Am_{(j)} \exp\left\{-\frac{Am_{(j)}^2}{2\sigma^2}\right\} d\vartheta_j dAm_j \\ &= \frac{K Am_{(j)}}{\sigma^2} \exp\left\{-\frac{Am_{(j)}^2}{2\sigma^2}\right\} dAm_{(j)} \end{aligned} \quad (125)$$

The normalisation factor K for this distribution, by setting

$$\int_0^{\infty} P[Am_{(j)}] dAm_{(j)} = 1 \quad \text{where the lower limit is zero as}$$

$Am_{(j)} \geq 0$, is $K = 1$.

The expectation value of $Am_{(j)}$ is given by

$$E[Am_{(j)}] = \int_0^{\infty} Am_{(j)} P[Am_{(j)}] dAm_{(j)} = \sigma \sqrt{\frac{\pi}{2}} \quad (126)$$

The probability of finding $Am > A_0$ is

$$\Pr(Am > A_0) = \int_{A_0}^{\infty} P[Am_{(j)}] dAm_{(j)} = \exp\left(-\frac{A_0^2}{2\sigma^2}\right) \quad (127)$$

Consider now the case where $m(k) = 0$, which is the equivalent to an observation of an unpolarised source.

For a random variable distributed according to Gaussian statistics, a minimum acceptable test for detection of real polarisation is that the result of a measurement exceeds the one expected from chance alone by a factor of 3σ , i.e. the probability of a chance result giving the measured result is only 0.26%.

$$\text{Thus } 0.026 = \exp \left[- \frac{(A_{\min})^2}{2\sigma^2} \right] \quad \text{from (127)} \quad (128)$$

which gives:-

$$A_{\min} \approx 3.45 \sigma = 3.45 \left(\frac{NM}{2} \right)^{\frac{1}{2}} \quad (129)$$

In terms of experimental parameters:-

NM = number of counts recorded, from an unmodulated signal, during a time t , and $M = C_o t$ where $C_o =$ mean counts per bin per unit observing time.

So

$$NM = \left(\frac{I_e}{2} \right) A_e t + I_d A_d t \quad (130)$$

where:- $I_d A_d t$ - is the number of counts due to noise, from background radiation and the counting electronics. I_d and A_d represent, respectively, the effective intensity and area for this noise component.

$\left(\frac{I_e}{2} \right) A_e t$ - is the number of counts recorded due to the unmodulated signal component. I_e represents the effective incident source intensity, and A_e the effective experiment area (see below, $A_e \neq A'$ of § 3.2).

I_e and A_e can also be easily related to more usual parameters.

For an incident unpolarised flux $I(E)$ ($\text{keV keV}^{-1} \text{ area}^{-1} \text{ s}^{-1}$),

the total recorded counts R will be given by the expression

$$R = \frac{I(E_B)}{E_B} E_B R_c \cot \theta_B A_e t \quad (130b)$$

where E_B is the peak energy for Bragg reflection. Here A_e is defined as the 'effective area' and includes all factors except that due to the reflectivity of the crystal (the reflectivity factor is taken into account by the term $R_c E_B \cot \theta_B$); and A_e is given by

$$A_e = T(\Delta) A' E_B F_{Rn} \quad (130c)$$

where E_R represents the efficiency of the rise-time discriminator and guard detector system, and the other terms are defined in § 3.2.

(Fig. 4.2.14 shows conceptually the effects on the intensity of an input flux $I(E)$ as it encounters sequentially each part of the Ariel-V polarimeter, to eventually depositing R counts to the output storage.)

To define an effective incident flux of photons (photons area⁻¹ s⁻¹) from the source spectral distribution I (keV keV⁻¹ area⁻¹ s⁻¹), the following expression may be used (see Schnopper and Kalata 1969):-

$$I_e = \left[\frac{I(E_B)}{E_B} \right] \Delta E \quad (130d)$$

where ΔE controls the magnitude of this relation, and represents a measure of the range of energies about the peak energy E_B for which Bragg reflection occurs. (ΔE is equivalent to the range of energy which would be required if the crystal reflectivity was 100% efficient for the range E centred about E_B and zero elsewhere.)

Then, for an idealised polarimeter where:-

- (1) No absorption occurs in the $R_{c\sigma}$ reflection process,
- (2) The modulation factor $m = 1$ (i.e. none of the $R_{c\pi}$ component is reflected), and
- (3) where we are considering the incident radiation to be unpolarised -

we would expect exactly half of the effective incident flux to be reflected, i.e. $\left(\frac{I_e}{2} \right)$.

(Since the $R_{c\pi}$ component is not reflected at any instant, and orthogonal intensity components of the incident flux are equal, then exactly half the incident beam intensity will not be reflected. The no-absorption condition (1) ensures that the other half of the incident intensity component is completely reflected.)

Then, equating this idealised expression $\frac{I_e}{2} A_e t$ for the

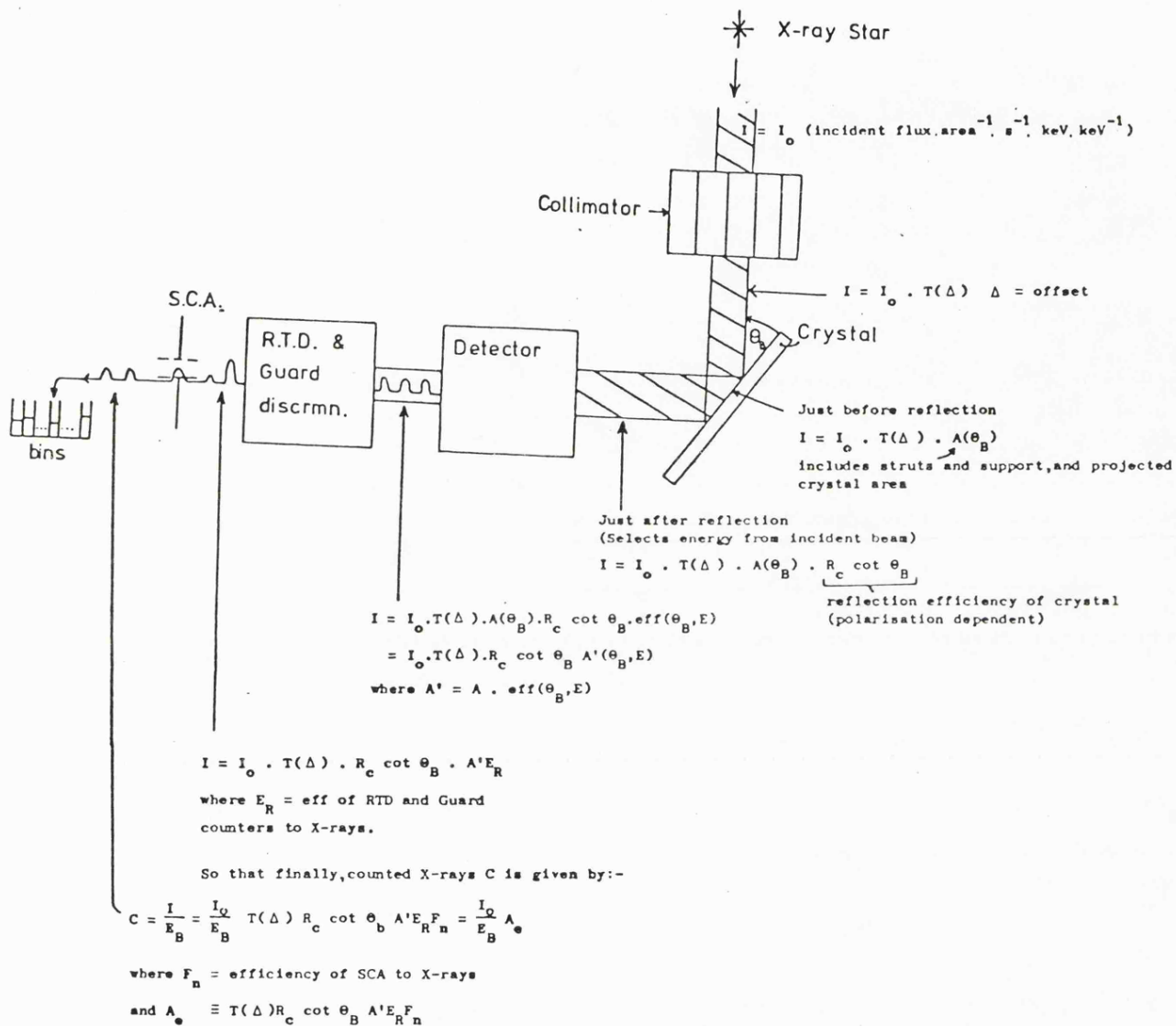


Fig. 4.2.14: Exp-D sensitivity to an incident X-ray beam of intensity I.

reflected intensity with R , the total recorded number of photons obtained from experimental characteristics of the real polarimeter, a realistic value for I_e may be obtained.

$$\text{i.e.} \quad \left(\frac{I_e}{2}\right) A_e t = \left(\frac{I(E_B)}{E_B} \epsilon_B R_c \cot \theta_B\right) A_e t \quad (130e)$$

so that I_e is given by:-

$$\begin{aligned} I_e &= \left[\frac{I(E_B)}{E_B}\right] \epsilon_B 2R_c \cot \theta_B & (130f) \\ &= \left[\frac{I(E_B)}{E_B}\right] \Delta E \quad \text{from (130d)} \end{aligned}$$

and hence ΔE is given by:-

$$\Delta E = 2R \epsilon_B \cot \theta_B \quad (130g)$$

From [(103) et. seq.] the amplitude of the polarisation harmonic is $\frac{2A_{\min}}{N}$, and in terms of experimental parameters this must equal $\frac{1}{N} \left(p_{\min} \frac{I_e}{2} A_e t \right)$ which represents $\frac{1}{N}$ x (the number of counts due to the polarisation modulated portion of the input signal) [since $p = I_p/I$ then $I_p = pI \approx p \frac{I_e}{2} A_e t$ if $I_p \ll I$].

Therefore

$$2A_{\min} = p_{\min} \frac{I_e}{2} A_e t \quad (131)$$

and substituting this equation and (130) into (129) gives:-

$$p_{\min} \frac{I_e}{2} A_e t = 3.45 \sqrt{2} \left[\frac{I_e}{2} A_e t + I_d A_d t \right]^{\frac{1}{2}}$$

so that

$$p_{\min} \approx 6.9 \frac{[I_e A_e t + 2I_d A_d t]^{\frac{1}{2}}}{I_e A_e t} \quad (132)$$

In terms of new parameters defined by:-

$$S_o t = \frac{I_e}{2} A_e t \quad \text{where } S_o \text{ is the experiment count rate due to the source, and}$$

$$B_o t = I_d A_d t \quad \text{where } B_o \text{ is the count rate due to noise (which for the Ariel-V polarimeter was believed mainly due to particle background (see § 3.2.4)),}$$

(132) reduces to:-

$$\begin{aligned} P_{\min} &= 6.9 \frac{[2S_o t + 2B_o t]^{\frac{1}{2}}}{2S_o t} \\ &= 3.45 \frac{[2(S_o + B_o)t]^{\frac{1}{2}}}{S_o t} \end{aligned} \quad (133)$$

p_{\min} , then, represents the minimum detectable polarisation from an observation where the received source count rate is S_o , background count rate is B_o and the observation time is t .

p_{\min} will only represent the sensitivity of an observation if systematic errors are not present and the modulation factor m for the polarimeter is unity.

However as $p = \frac{1}{m} V$ from (55)

then p_{\min} can be redefined to include the modulation factor, as:-

$$\text{M.D.P.}(3-\sigma) \equiv p_{\min} \equiv \frac{1}{m} 3.45 \frac{[2(S_o + B_o)t]^{\frac{1}{2}}}{S_o t} \quad (134)$$

So that only systematic errors are now excluded, and M.D.P.(3- σ) is defined as the Minimum Detectable Polarisation. [We note that (134) differs slightly from the expression usually quoted by Novick (1974, 1975) where 3.45 is replaced by 3. This may arise because of a slight difference in argument whereby Novick is lead to the equivalent of 3σ in (129) instead of 3.45σ].

It is interesting to note that if the background component is

small [as it may be if the detector is small making A_d small, which would apply to proposed focusing polarimeters (see Schnopper and Kalata 1969, Novick 1974, 1975) and one at present in flight (Weisskopf et al. 1976)] that the expression for p_{\min} becomes:-

$$\begin{aligned}
 p_{\min} &= \frac{3.45}{m} \frac{[2(S_o)t]^{\frac{1}{2}}}{S_o t} \\
 &= \frac{3.45}{m} \sqrt{\frac{2}{S_o t}} \quad (135)
 \end{aligned}$$

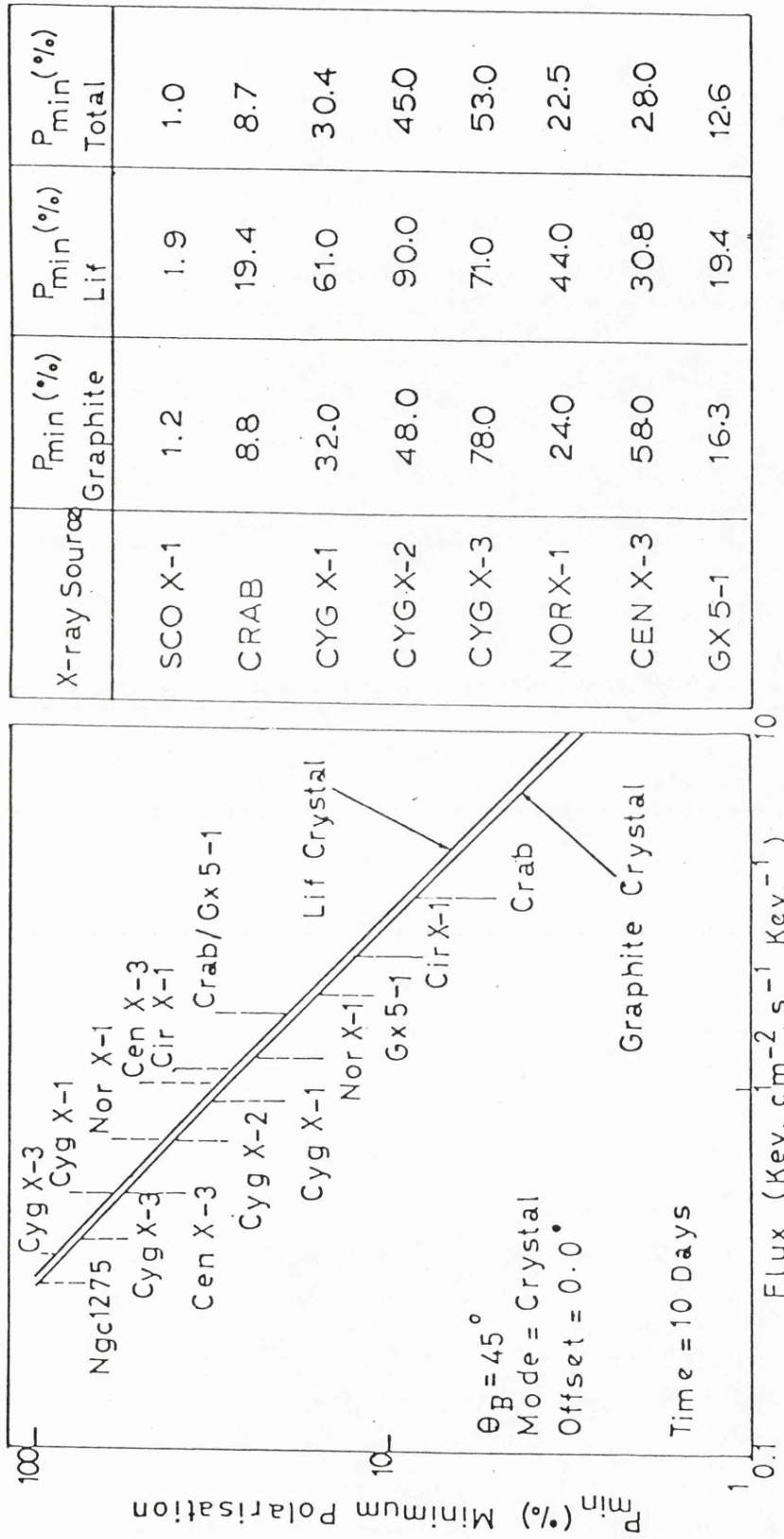
which gives a reduced p_{\min} and consequently higher sensitivity. As will be seen from the results obtained with the Ariel-V polarimeter, where for all but the brightest X-ray sources $B_o \gg S_o$ (e.g. $B_o \approx 100S_o$ for a 100 Uhuru Unit source), this shows that the reduction of such extremely, relatively high background levels is very desirable. The manner proposed, involving focusing instruments, appears to be a useful solution to this problem.

For the Ariel-V polarimeter, Minimum Detectable Polarisation calculations based on the foregoing mathematics were made by Peacock (1975) using his background estimates, and the results of these are presented in Fig. 4.2.15 for several of the stronger X-ray sources. The chosen Bragg angle was the optimum at $\theta_B = 45^\circ$. The amount of observing time was taken as $t \approx 5 \times 10^5$ s which is equivalent to ≈ 5.8 days continuous observation or ≈ 10 days practical observing time. Continuous observation would not be possible since the experiments would be switched off for the night section of ≈ 37 mins of the orbit period of ≈ 97 mins, and further small losses would occur when data collection would be inhibited because of high background levels (see § 3), notably due to the South Atlantic Anomaly.

From this Fig. 4.2.15 it can be seen that, for example, the instrument will have a predicted 3-sigma sensitivity to linear polarisation

of the Crab Nebula X-ray flux of 8.7% from a 10 day observation period (if systematic sources of error are not significant). This predicted sensitivity is approximately an improvement by a factor of two over the previous best Crab Nebula polarisation measurement (Novick et al. 1972) which gave an equivalent $\approx 15\%$ sensitivity. For Sco X-1 the previous best statistical sensitivity to polarisation was 12% reported by Kestenbaum et al. (1971), and for the Ariel-V polarimeter this may be improved by a factor of 10, to 1% at 3-sigma confidence, again for a 10 day observation.

Also, obviously, with the Ariel-V satellite the observation time can be increased so as to further reduce p_{\min} ($p_{\min} \propto t^{-\frac{1}{2}}$).



X-ray Source	P_{min} (%) Graphite	P_{min} (%) Lif	P_{min} (%) Total
SCO X-1	1.2	1.9	1.0
CRAB	8.8	19.4	8.7
CYG X-1	32.0	61.0	30.4
CYG X-2	48.0	90.0	45.0
CYG X-3	78.0	71.0	53.0
NORX-1	24.0	44.0	22.5
CEN X-3	58.0	30.8	28.0
GX5-1	16.3	19.4	12.6

Fig. 4.2.15: Peacock's (1975) Minimum Detectable Polarisation calculations of the 3- σ sensitivity of the Ariel-V polarimeter.

§ 4.2.3c Systematic Errors

Systematic sources of error were generally of secondary importance in the calculation of previous results from the short duration rocket flights. This was because of the, as then, still very large counting, statistical limitations. However, the significant reduction in statistical limitations shown by the calculations for the Ariel-V polarimeter has greatly increased the need for control and estimation of systematic sources of error.

It is important to be able to check for, or to know of the theoretical presence of systematic errors, as they may be mistaken for properties of the observed source. Also, if systematic errors are important it is as well to know before operation as, for the case of the Ariel-V polarimeter, operation of the instrument can sometimes be optimised to reduce them. Finally, discovery and then understanding of systematic errors can be used to eliminate or reduce them in future instrument design.

Three main groups of systematic errors were considered:-

- i) X-ray sources offset from the experiment pointing direction.
- ii) Time variations in the X-ray source continuum intensity.
- iii) Background radiation effects.

1) X-ray sources offset from the experiment pointing direction

Systematic effects arising from this method are usually due to the X-ray source itself which is being studied, unless other sources are in the field of view (f.o.v.) of the polarimeter.

However, elimination of the effects of other sources in the instrument f.o.v., especially required for sky regions where X-ray sources are dense, can be achieved by design of a suitably narrow f.o.v.

An offset of the X-ray source being studied, from the experiment pointing direction, can occur for several reasons:-

- 1) Limited pointing control of the satellite spin-axis will allow the X-ray source to 'drift' to various offset positions as time progresses. For the Ariel-V satellite, correction of the spin-axis drift once every two days, say, gave a maximum offset drift of $\approx 0.7^\circ$ with a mean offset drift of $\approx 0.3^\circ$.
- 2) A permanent offset effect will be caused by fixed misalignments of a) the polarimeter axis to a geometric axis within the satellite, b) the geometric axis to the satellite spin-axis, and c) misalignment of the collimator. Peacock (1975) considered these offsets for the Ariel-V polarimeter, and gave respectively 1', 10' and 4' as upper limits to the misalignments.
- 3) For employment of the Ariel-V instrument as a spectrometer an offset of a degree or so is a required parameter in order that the Bragg reflection energy, and hence source continuum, is scanned in search of line emission.

Systematic data modulations can arise from these offset angles, also in several ways:-

- 1) Variation of the collimator transmission function.

- 2) Variation of projected crystal area, and asymmetric experiment support structure.
- 3) Detector effects.
- 4) Variation of the modulation factor - m.
- 5) Variation of X-ray source continuum with energy - and the effect of line emission.
- 6) Crystal reflectivity effects - variation of $E_B R_c \cot \theta_B$.
- 1) Variation of the Collimator Transmission Function

This situation is illustrated in Fig. 4.2.16a (Peacock 1975)

where θ represents the combined misalignment between the experiment and spin-axis in degrees, and Δ is the offset between the spin-axis and X-ray source. The depth of modulation produced by the transmission effect can then be defined as follows:-

$$\begin{aligned} \% \text{ mod} &\equiv 100 \left[\frac{\text{Trans Max} - \text{Trans Min}}{\text{Trans Max} + \text{Trans Min}} \right] \\ &= 100 \left[\frac{T(\Delta - \theta) - T(\Delta + \theta)}{T(\Delta - \theta) + T(\Delta + \theta)} \right] \end{aligned} \quad (136)$$

where the transmission function is given by

$$T(\beta^\circ) = 0.81 \left(1 - \frac{\beta^\circ}{7.5^\circ} \right)$$

for the Ariel-V polarimeter (see § 3.2.2).

This % mod is shown as a function of spin-axis offset angle from the X-ray source for several misalignment angles θ in Fig. 4.2.16b. From this figure it can be seen that significant modulations from about 1 to 4% may be expected even when the spin-axis offset may be less than 1° . However, from Fig. 4.2.16a, it can be seen that this modulation will be mainly at the frequency of rotation of the satellite and not at twice the rotation frequency at which the polarisation modulation occurs. The majority of this modulation can therefore be easily eliminated, for

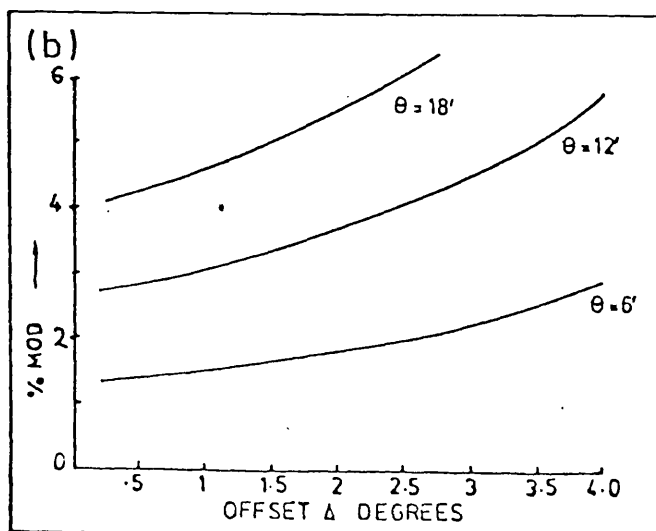
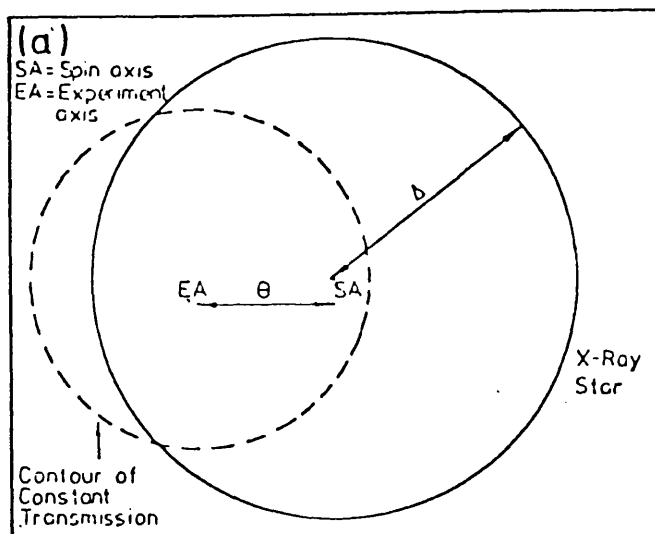


Fig. 4.2.16: Modulation effect of a misalignment between the Ariel-V polarimeter collimator and an X-ray source.

example by Fourier analysis of the data.

Also, since the collimator was constructed out of fabricated honeycomb, of which each element is a hexagon which is not totally regular (they are longer in one direction due to the production technique) the contours of transmission are not therefore perfect circles. Whilst a single element of an elongated honeycomb cell would be expected to produce a data modulation at twice the satellite rotation frequency, the experiment D collimator construction occurred so that the elongated cells were mounted in two orientations (at 90° to each other), and in this manner a modulation at four times the satellite rotation frequency would be expected to occur. Peacock (1975) estimated this fourth harmonic modulation to be less than 1% or a 2° offset. It is expected that any residue of modulation at twice the satellite rotation frequency from this effect would be smaller than this fourth harmonic modulation.

Finally, it is noted that collimator misalignment would be expected to have more importance when a narrow f.o.v. is desired. (For the Ariel-V polarimeter, the fixed and pointing misalignments were estimated to be $< 4'$ and $\approx 20'$ respectively, which are relatively small compared with a f.o.v. of 7.5° F.W.H.M.).

2) Variation of Projected Crystal Area, and Asymmetric Experiment Support Structure

X-rays, having been transmitted by the collimator, then have to traverse the internal experiment structure and be reflected off the crystal face before being detected.

The effective geometric area of the plane, Ariel-V, crystal panel face to the incident X-ray beam is given by $A(\theta_B) = A_0 \sin \theta_B$ (see § 3.2.3 equation (10)) where θ_B is the Bragg angle. For an offset source this angle θ_B varies periodically at the satellite rotation

frequency (see Fig. 4.2.17) and hence $A(\theta_B)$ and also the recorded count rate varies at this same frequency. Thus, determination of polarisation which occurs at twice the above frequency, is unaffected by this variation which is estimated to be approximately 2% modulation for a 1° offset (for θ_B nominally (i.e. at no offset) set at 45°).

However, the experiment support structure including struts and detector window supports, by interposing itself between incoming X-rays from an offset source and the detectors, at various satellite rotation angles, can possibly produce data modulations at any frequency. The amplitude of modulations produced in this way can be determined by laboratory calibration of the experiment before flight. For the Ariel-V polarimeter a computer program was developed to simulate the effects of the experiment boundary and support structure, projected crystal area and the detector window stops, for the complete mounted experiment (Ricketts, M.J. 1976, private communication). Frequency analysis of results from this program, for $\theta_B = 45^\circ$ and an offset of 2° , gave no significant modulation at twice the rotation frequency. Limitations on the number of incident X-rays which were handled by the program meant that a 3-sigma upper limit to the statistical sensitivity of the result was $< 0.9\%$ modulation.

3) Detector Effects

The efficiency of the Ariel-V detectors as a function of Bragg angle θ_B was discussed in § 3.2.4 and graphically displayed in Fig. 3.2.6d. However, the geometrical situation for an offset source causing the angle of incidence for incoming X-rays to be changed to θ_B' , and hence also altering the angle of incidence at the detector window, is not the same as repositioning the crystal to observe a source at an angle of incidence θ_B' . Hence there is no simple way in which Fig. 3.2.6d can be used to accurately predict modulations in the Ariel-V polarimeter from this effect. Here again, pre-flight calibration or

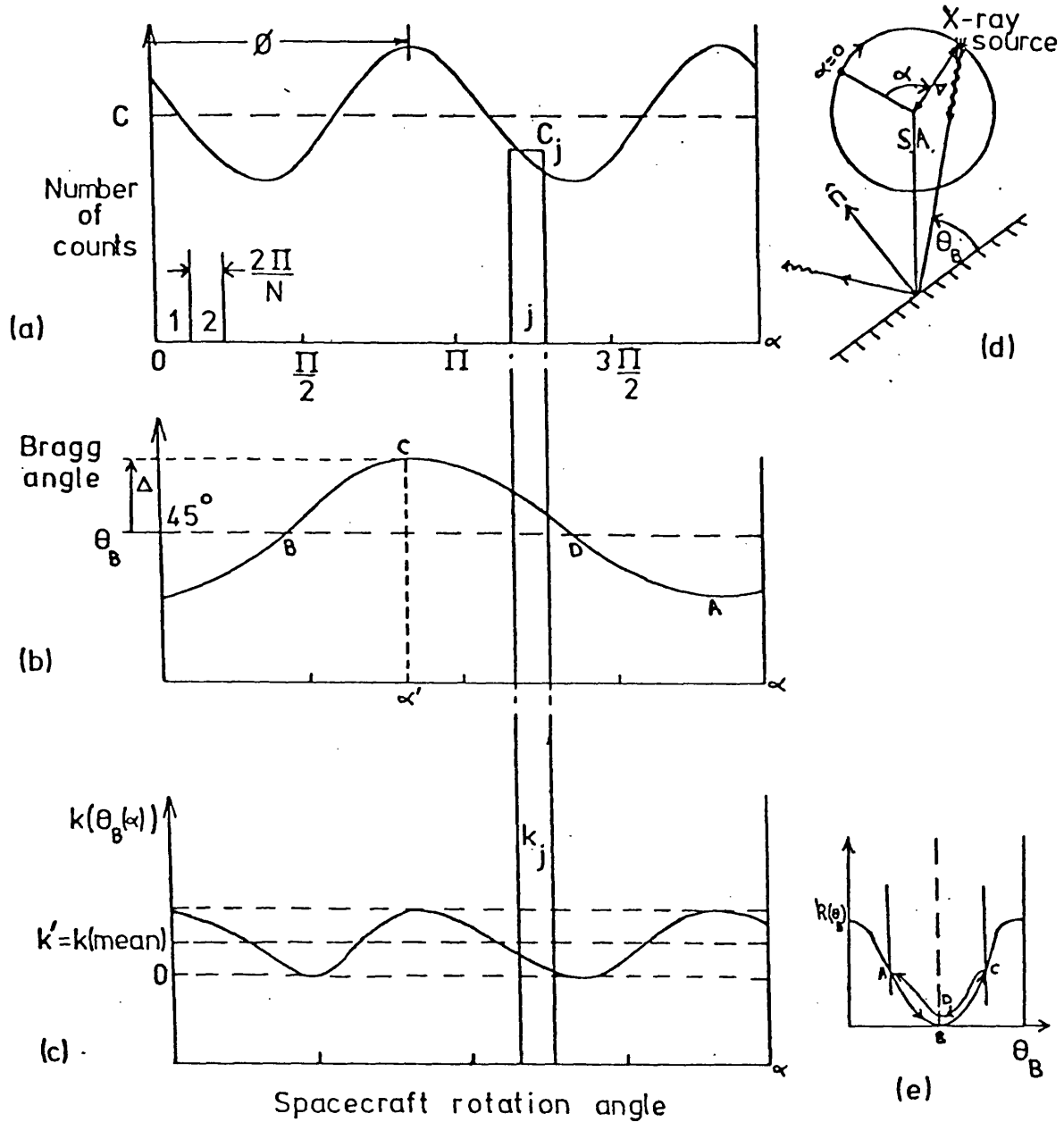


Fig. 4.2.17: Variation of Bragg angle θ_B and modulation factor m with rotation angle of spacecraft when source is offset from spacecraft spin-axis by an angle Δ . Bragg angle assumed nominally set to 45° for a non-offset source.

computer simulation of the instrument is desirable. A simple appraisal of Fig. 3.2.6d indicates that the detector efficiency changes by only about 3% for a 2° offset at $\theta_B = 45^\circ$ and that this change would primarily cause a modulation at only the satellite rotation frequency. Thus, it would be expected, as a first order estimate only (for the real situation which is not governed exactly by Fig. 3.2.6d), that modulations produced at the polarisation frequency would be less than $\approx 3\%$ when the offset is $\lesssim 2^\circ$.

Also, as a first order approximation (from Fig. 3.2.7d), it is expected that the instrument resolution should be approximately similarly stable.

For completeness (Novick 1974), note that for focusing polarimeters it will be important that the detector efficiency over the entrance window should be constant, as for an offset source the focal spot for the converging X-ray beam will move around the entrance window as the satellite rotates. It will be also required that the focal spot is small enough so that no part of the source image, even for an offset source, will miss the entrance window. Also, two-fold symmetry with window support structure, or anode wires perpendicular to the X-ray beam, could cause a spurious data modulation at the polarisation frequency.

4) Variation of the Modulation Factor m

A source offset from the experiment axis will cause the Bragg reflection angle θ_B , to the incident X-rays, to vary at the rotation frequency of the satellite. This in turn will cause the modulation factor m , which is dependent upon θ_B (see § 4.2.2a and b) to vary. Then, as m determines the depth of modulation due to the polarised component of the incident radiation (via $p = \frac{1}{m} V$ § 4.2.2a), this

expected modulation depth will vary continuously as the satellite rotates thus producing a systematic modulation in the data.

Let the incident X-ray flux produce a mean detected count rate S_o counts s^{-1} bin $^{-1}$ where the satellite rotation plane is divided into N bins, and the degree of ^{linear} polarisation is p , and let the observation time per bin be t .

For an observation with a polarimeter where $m = 1$, the data will be spread throughout the bins such that the mean number of counts per bin C_{mean} , is given by $C_{\text{mean}} = S_o t$, and as a function of satellite rotation angle α , $C(\alpha)$ will be given by

$$C(\alpha) = S_o t + p S_o t \cos(2\alpha - \varnothing) \quad (137)$$

where \varnothing is the phase angle of the polarisation and $S_o = \frac{I(\lambda)}{2} \lambda \cot \Theta_B R_{c\sigma}$ where $I(\lambda) = I_u(\lambda) + I_p(\lambda)$ (see equations (50b) and (49)).

For a polarimeter observation where $m < 1$, (137) becomes, (from 51b):-

$$C(\alpha) = S_o t [(1+k) + (1-k) p \cos(2\alpha - \varnothing)] \quad (138)$$

as

$$m = \frac{1-k}{1+k} \quad \text{from (54) and}$$

$$k = k(\Theta_B) \quad (\text{see 4.2.2a and b}).$$

Ideally, when Θ_B is constant, p can be obtained from the observed data function $C(\alpha)$ as $k(\Theta_B)$ is known and constant. However, when an X-ray source is offset from the spacecraft spin-axis, Θ_B does not remain constant but varies with spacecraft rotation angle α as shown in Fig. 4.2.17. In this case it is not so easy to relate p and \varnothing to the observed data function $C(\alpha)$ as k has also become a function of α . [i.e. $\Theta_B = \Theta_B(\alpha)$].

For N bins there will be N data points, so that

$$\begin{aligned}
C(\alpha_1, \theta_{B1}) &= C_1 = S_o t [(1+k_1) + (1-k_1)p \cos(2\alpha_1 - \emptyset)] \\
C(\alpha_2, \theta_{B2}) &= C_2 = S_o t [(1+k_2) + (1-k_2)p \cos(2\alpha_2 - \emptyset)] \quad (139) \\
&\vdots \\
C(\alpha_N, \theta_{BN}) &= C_N = S_o t [(1+k_N) + (1-k_N)p \cos(2\alpha_N - \emptyset)]
\end{aligned}$$

i.e. N equations to solve for the three unknowns S_o , p and \emptyset .

The set of equations (139), however, represents the counts received in each bin when the spin-axis is at a single position. For another orbit the spin axis may have drifted to a new position, so that data collected in the new position will be described by the new N equations:-

$$\begin{aligned}
C_{12} &= S_o t_2 [(1+k_{12}) + (1-k_{12})p \cos(2\alpha_1 - \emptyset)] \\
&\vdots \\
C_{N2} &= S_o t_2 [(1+k_{N2}) + (1-k_{N2})p \cos(2\alpha_N - \emptyset)] \quad (139a)
\end{aligned}$$

For this new orbit it is possible that both the magnitude and phase of the offset has changed. A pure change in phase would be caused by the spin-axis drifting circularly around the source at constant offset, this causing the phase α' at which the max Bragg angle θ_B occurs, to be positioned at a different value of rotation angle α .

We first consider changes only in the phase α' of the offset. Then, summing such data from z orbits, say, the counts falling into the jth bin will be given by the following expression:-

$$\begin{aligned}
C_j &= S_o t_1 (1+k_{j1}) + S_o t_1 (1-k_{j1})p \cos(2\alpha_j - \emptyset) + \\
&\quad S_o t_2 (1+k_{j2}) + S_o t_2 (1-k_{j2})p \cos(2\alpha_j - \emptyset) + \\
&\quad \dots + S_o t_z (1+k_{jz}) + S_o t_z (1-k_{jz})p \cos(2\alpha_j - \emptyset) \quad (140)
\end{aligned}$$

where the t_i are the observing times for the ith orbit.

Therefore, grouping terms

$$C_j = S_o [\{ t_1(1+k_{j1}) + t_2(1+k_{j2}) + \dots + t_z(1+k_{jz}) \} + \{ t_1(1-k_{j1}) + t_2(1-k_{j2}) + \dots + t_z(1-k_{jz}) \} p \cos(2\alpha_j - \emptyset)] \quad (141)$$

and defining

$$E_j \equiv \sum_{i=1}^z t_i(1+k_{ji}) \quad (142)$$

$$F_j \equiv \sum_{i=1}^z t_i(1-k_{ji}) \quad , \quad (143)$$

(141) can be written more compactly as

$$C_j = S_o [E_j + F_j p \cos(2\alpha_j - \emptyset)] \quad (144)$$

Now, if the observing times are also approximately equal

(142) and (143) become:-

$$\begin{aligned} E_j &\approx t \sum_{i=1}^z (1+k_{ji}) \\ &= t [z + (k_{j1} + k_{j2} + \dots + k_{jz})] \\ &= tz [1 + k_j''] \end{aligned} \quad (145)$$

where

$$k_j'' = \frac{1}{z} \sum_{i=1}^z k_{ji} \quad (146)$$

and k_j'' represents a mean value of k_j , caused by k_j taking on different values for each orbit due to the spin-axis drifting around the source at constant offset.

Then, similarly,

$$F_j \approx [tz \ 1 - k_j''] \quad (147a)$$

Furthermore, if a large number of orbits z are involved and the spin-axis phase drifts are random, then we would expect

$$k_j'' \approx \frac{1}{2\pi} \int_0^{2\pi} k(\alpha) d\alpha = k' \quad \text{for all } j. \quad (147b)$$

where $k(\alpha)$ represents the variation of k as a function of rotation angle for any single orbit 1 to z where the offset magnitude remains unchanged. This is the function shown in Fig. 4.2.17c.

Then, from (144), the following may be written

$$C_j \approx S_o t z [(1+k') + (1-k') p \cos(2\alpha_j - \phi)] \quad (148)$$

so that

$$C(\alpha) \approx S_o t z [(1+k') + (1-k') p \cos(2\alpha - \phi)] \quad (149)$$

where p can then be obtained from the $C(\alpha)$ function as before, from

$$p = \left(\frac{1-k'}{1+k'} \right) v$$

and where

$$m = \left(\frac{1-k'}{1+k'} \right)$$

is now the modified modulation factor calculated from the value k' illustrated in Fig. 4.2.17c, which is simply seen to be the mean of the maximum and minimum values obtained by $k(\theta_B)$ with the offset source.

Thus, if θ_B was nominally set to 45° it can be seen that, for an offset source, the value of k to be used to calculate the effective modulation factor will be increased above the set value $k(45^\circ)$ because of the symmetrical shape of the $k(\theta_B)$ function (Fig. 4.2.17e) about $\theta_B = 45^\circ$. However, if θ_B is nominally set away from 45° , so that the offset source does not cause k to range through 45° , then it can be seen that the nominal value of k will be approximately correct.

We shall now attempt to calculate the effects on m when the magnitude of the spin-axis offset varies.

If there are "r" sets of data similar to (148) involving different spin-axis offsets, then by summing these, the number of counts obtained in the j-th bin will be approximately given by:-

$$\begin{aligned}
 C_j \approx & S_o t Z_1 [(1+k_1') + (1-k_1') p \cos(2\alpha_j - \emptyset)] + \\
 & + S_o t Z_2 [(1+k_2') + (1-k_2') p \cos(2\alpha_j - \emptyset)] + \\
 & + \dots + S_o t Z_r [(1+k_r') + (1-k_r') p \cos(2\alpha_j - \emptyset)] \quad (150)
 \end{aligned}$$

(Equation (150) is approximate since it has been assumed that the transmission function remains constant with offset. In practice, since the transmission to X-rays decreases with increasing offset, this will cause a bias to those k values obtained from data collected with lower offset magnitudes. Therefore the calculations presented here represent an approximation which will gradually lose accuracy for offset ranges which cause larger changes in the transmission function.)

(150) reduces to

$$\begin{aligned}
 C_j = & S_o t [\{ Z_1(1+k_1') + Z_2(1+k_2') + \dots + Z_r(1+k_r') \} + \\
 & \{ Z_1(1-k_1') + Z_2(1-k_2') + \dots + Z_r(1-k_r') \} p \cos(2\alpha_j - \emptyset)] \quad (151)
 \end{aligned}$$

Then, by letting

$$G = \sum_{i=1}^r Z_i (1+k_i') = \left(\sum_{i=1}^r Z_i \right) \left[\frac{1 + \sum_{i=1}^r Z_i k_i'}{\sum_{i=1}^r Z_i} \right] \quad (152)$$

and

$$H = \sum_{i=1}^r Z_i (1 - k_i') = \left(\sum_{i=1}^r Z_i \right) \left[\frac{1 - \sum_{i=1}^r Z_i k_i'}{\sum_{i=1}^r Z_i} \right] \quad (153)$$

(151) becomes:-

$$C_j = S_o t [G + H p \cos(2 \alpha_j - \phi)] \quad (154)$$

$$= S_o t B [(1+K) + (1-K) p \cos(2 \alpha_j - \phi)] \quad (155)$$

where

$$B = \sum_{i=1}^r Z_i \quad \text{and} \quad K = \frac{\sum_{i=1}^r Z_i k_i'}{B} \quad (156)$$

and since K is not a function of j, (155) can easily be generalized to

$$C(\alpha) = S_o t B [(1+K) + (1-K) p \cos(2 \alpha - \phi)] \quad (157)$$

Then, from this equation:-

$$V = \frac{C_{\max} - C_{\min}}{C_{\max} + C_{\min}} = \frac{(1-K)}{(1+K)} p$$

i.e. $p = \frac{1}{M} V$

where $M = \frac{1-K}{1+K}$ (158a)

and the further modified K is evaluated from (156) which represents the weighted mean of all the k_i' values, the Z_i being the respective observing times.

For the very simple case when $Z_1 = Z_2 = \dots = Z_r = Z$

(156) becomes

$$K = \sum_{i=1}^r \frac{Z k_i'}{rZ}$$

$$= \frac{(k_1' + k_2' + \dots + k_r')}{r} \quad (158b)$$

so that K is just the average value of all the k' values (i.e. of the modified k values). A qualitative picture of how this affects the value of M is illustrated in Fig. 4.2.18.

Here again, the same argument applies as for the phase variations only. K will be approximately equal to the nominal value of k set for a non-offset source if the range of θ_B does not include 45° , but may be increased significantly if nominal $\theta_B = 45^\circ$ or the range of θ_B includes 45° , thus producing a systematic reduction in the modulation factor m . The magnitude of this systematic reduction Δm in m , given by $\Delta m = m - M$ depends on the nominal value of θ_B and the distribution of the magnitudes of the offset angles used.

Results of calculations on the approximate effects on m for various single offset values are given in Table 4.2.19.

As $p = \frac{1}{m} V$, then the effect of a systematic error in m of $x\%$ will have a direct $\approx x\%$ effect on the calculated degree of polarisation. For example, an observation using $\theta_B = 45^\circ$ with a source offset of 3° (which may be desired by other Ariel-V experiments) would systematically cause p to be underestimated by 1 to 9.5% if the above correction to m was not made.

The reduction correction to m above is seen to be smallest (i.e. $\approx 1\%$) and the instrument sensitivity highest (which occurs for largest value of m), when the crystal behaviour is governed by the $k = \cos^2 2\theta_B$ model. Fortunately, the instrument efficiency also is greatest when k is governed by this model (see § 3.2.3 and § 4.2.2). Furthermore, it is expected that the Ariel-V crystals will tend more to follow this favourable $k = \cos^2 2\theta_B$ model for which the corrections to m are smallest, because of the way the crystals were prepared (Evans, 1976, private communication).

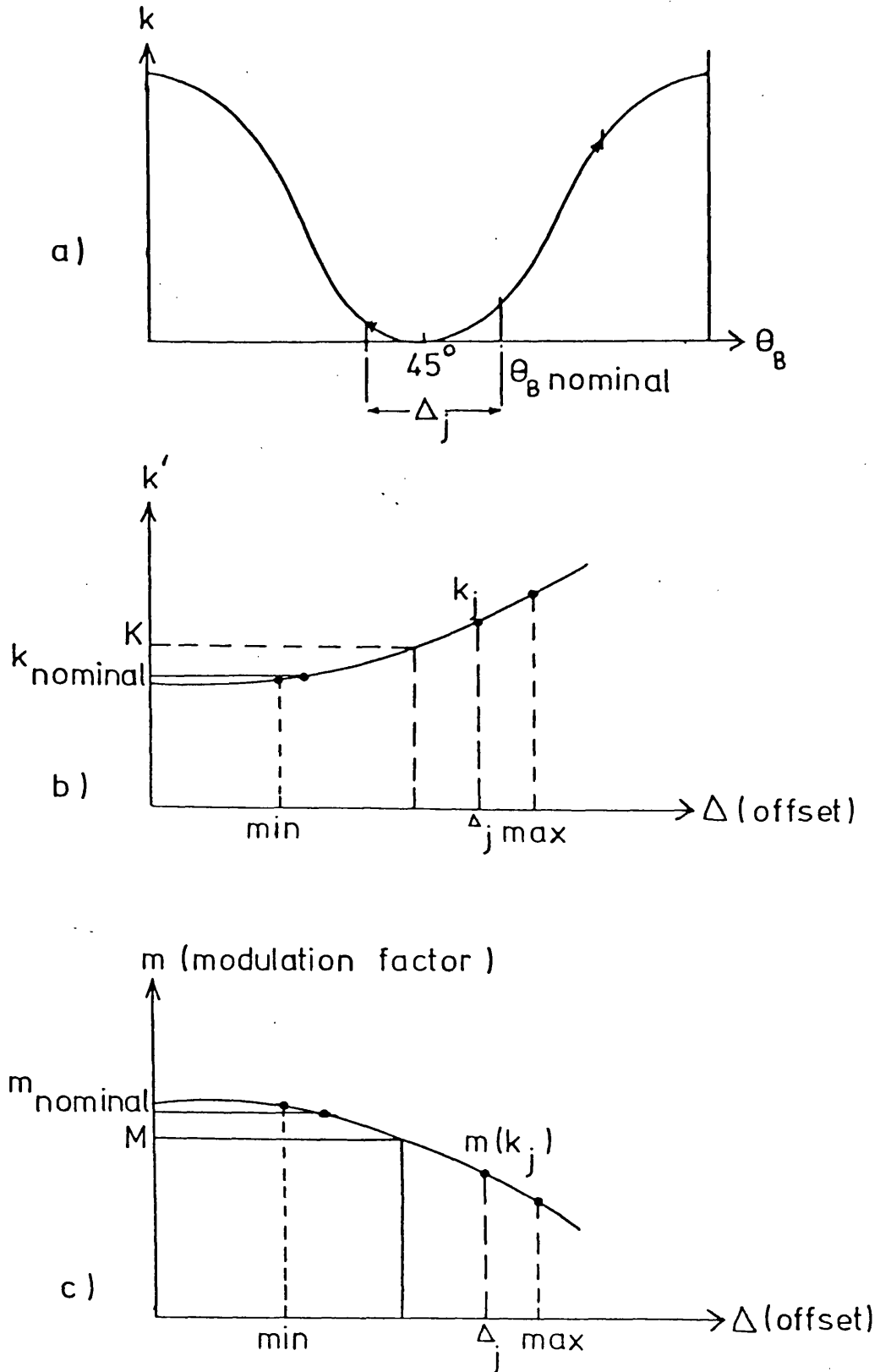


Fig. 4.2.18: Bragg angle set to $\theta_{B(\text{nominal})}$. Effects on the resultant k' and M values due to source being positioned at various offsets from the experiment pointing direction. Requires a minimum offset $\Delta_o = |\theta_{B(\text{nom})} - 45^\circ|$ before k' and M can alter greatly from their nominal values.

Table 4.2.19

Effects of an offset source on the calculated value of the modulation factor m when the nominal Bragg angle has been set to 45° ($k_{\text{nominal}} = 1$)

Source Offset Angle Δ°	Minimum Modulation Factor, $m_{(\text{min})}$		Reduced Modulation Factor, M			
	(a) $k = \cos 2\theta_B $ model	(b) $k = \cos^2 2\theta_B$ model	(a) $k = \cos 2\theta_B $ model	(b) $k = \cos^2 2\theta_B$ model	Δm (%) reduction (a) (b)	
.1 $^\circ$.993	1.000	.997	1.000	.4	.0
.3 $^\circ$.979	1.000	.990	1.000	1.0	.0
.6 $^\circ$.959	.999	.980	1.000	2.0	.0
1.0 $^\circ$.933	.998	.966	.999	3.4	.1
2.0 $^\circ$.870	.990	.935	.995	6.5	.5
3.0 $^\circ$.811	.980	.905	.989	9.5	1.1
5.0 $^\circ$.704	.942	.852	.971	14.8	2.9

For Ariel-V, on-source observations (i.e. nominal zero offset), the pointing axis drift usually amounted to an average offset magnitude of $\approx 0.3^\circ$. The corresponding modulation factor correction for this offset can range from 0 to 1%, which would be negligible for all sources except possibly Sco X-1 where a 10 day observation was predicted to produce a 3-sigma Minimum detectable Polarisation (M.D.P.) sensitivity of $\approx 1\%$.

It is also to be noted that, if offset magnitudes and phases are not distributed randomly (evenly), then the calculated solutions for the reduction in modulation factor are only approximate. The minimum attainable values of m with any given magnitude of offset are shown in Table 4.2.19, and these values represent the worst case solutions where

the distribution of various offsets is taken at the maximum offset magnitude at a single phase. The percentage depression of the modulation factor for these worst cases is twice the depression required to obtain the corrected mean M values listed in Table 4.2.19. An approximate estimate of the 1-sigma error on M from this non random distribution effect can be taken as $\frac{1}{3}$ of the difference between the mean and extreme values of M . (Of course other and larger errors on M may arise from lack of knowledge of the dependence of k with Bragg angle θ_B , if no calibration or poor calibration has been carried out.) A value for $\sigma(M)$ may also be estimated in this way for cases where nominal $\theta_B \neq 45^\circ$.

In summary, Table 4.2.19 indicates that modulation factor corrections would normally only be significant for observations where large offsets of several degrees are employed, or where very accurate polarisation measurements are possible (unless the insensitive $k = |\cos 2\theta_B|$ model is a valid approximation).

Again, for design requirements, it is fortunate that the highest instrument efficiency and sensitivity is governed by the $k = \cos^2 2\theta_B$ model for which the above correction effects to m are smallest.

5) Variation of X-ray Source Continuum with Energy - and the Effect of Line Emission

Fig. 4.2.17 already shows how the Bragg angle varies as the satellite rotates for an offset source. The peak efficiency of detected X-rays is given by the Bragg reflection function $n\lambda = 2d \sin \theta_B$, so that the peak detected energy is given by:-

$$E_B = \left(\frac{ch n}{d} \right) \frac{1}{\sin \theta_B} \quad (\text{see } \S 3.2.3)$$

Thus it can be seen (from Fig. 4.2.20a) for a source continuum spectrum which is monotonically decreasing about the Bragg energy E_B , that the

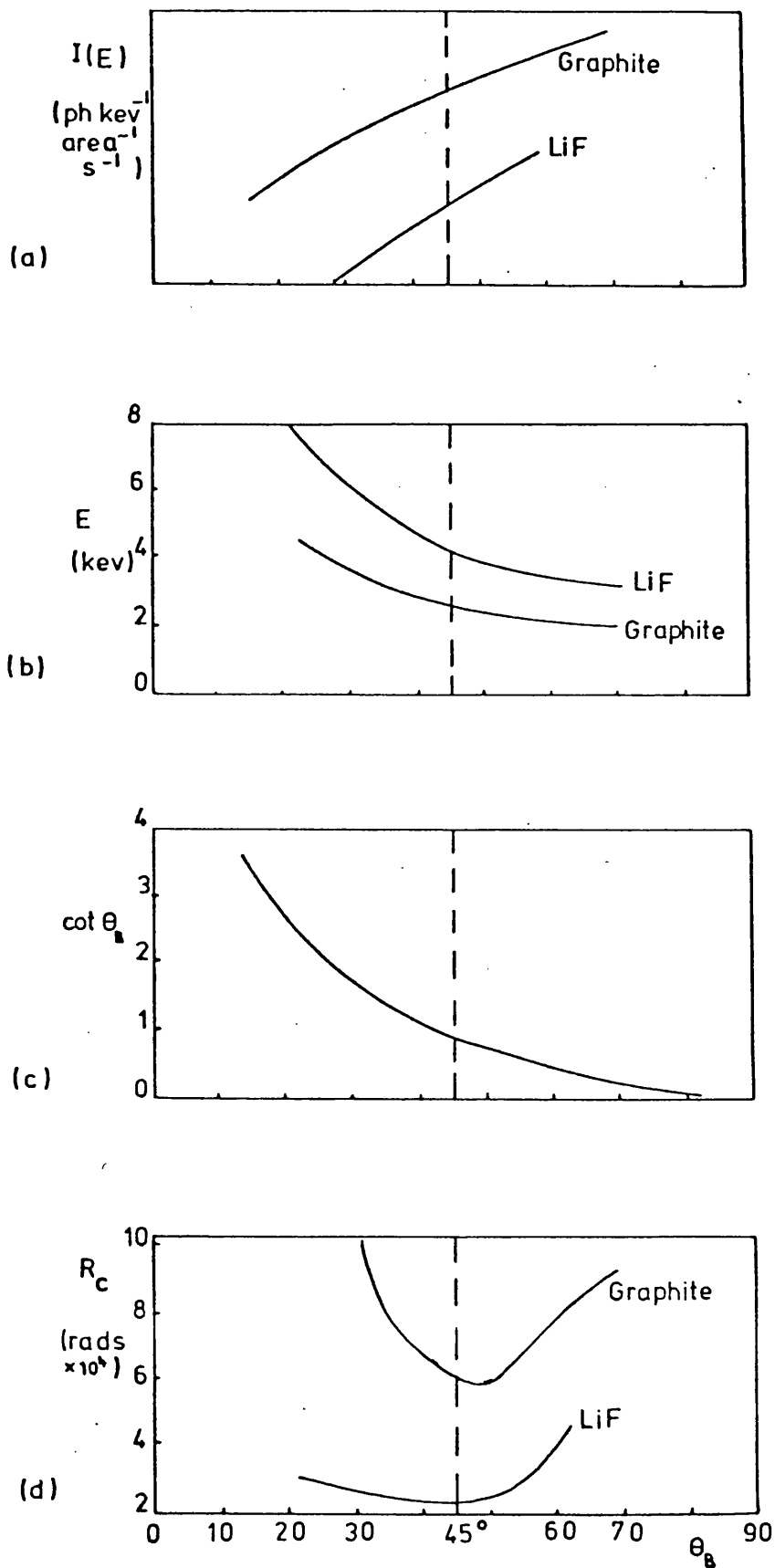


Fig. 4.2.20: Variation of source continuum intensity and crystal reflectivity terms, with Bragg angle.

number of counts recorded as E is scanned will be modulated almost only at the satellite rotation frequency. Therefore this effect should not be important, as it is not expected to produce any significant modulation at the polarisation frequency of twice the satellite rotation rate.

However, if some line emission exists superimposed upon the continuum then this would produce two peaks in the data for each satellite rotation, precisely at the phases expected for a sinusoidal modulation due to polarisation. Fortunately for most X-ray sources, evidence of line emission has proven rather elusive. Also the shape of the count variation with rotation angle, not being expected to be sinusoidal, will have a correspondingly smaller sinusoidal component at the polarisation frequency. Finally, variation of the phase and magnitude of the offset of the source from the spin-axis will cause any line emission peak to be spread over various rotation angle bins, thus tending to cancel any modulation from this effect. (For line emission analysis each separate orbit's data is rotation angle phase shifted to allow for this effect, so that any line emission will always be summed into the same bins (Peacock 1975).)

Ideally, to eliminate any significant effect from line emission, polarisation observations should be performed with offsets carefully chosen by symmetry so as to completely cancel this effect, or be performed in a broad energy band, or in spectral regions where there is a known absence of line emission at a significant level with respect to the required polarisation sensitivity.

6) Crystal Reflectivity Effects - variation of $R_c \cot \theta_B$

As shown by equation (130b) the number of photons, N, Bragg reflected by a crystal set at an angle θ_B to a continuum of intensity I (ph keV⁻¹ area⁻¹ s⁻¹) is given by

$$N = I(E_B) E_B R_c \cot \theta_B \quad (\text{ph area}^{-1} \text{ s}^{-1})$$

The variation of the source spectrum $I(E)$ with E has been considered above in (5). The other terms E_B , R_c and $\cot \theta_B$ will also vary as θ_B , and hence the peak energy E_B for Bragg reflection, is scanned as the satellite spins about an offset source. The variation of each of these terms with Bragg angle is shown in Fig. 4.2.20b, c and d.

From Fig. 4.2.20b and c, it can be seen that both E_B and $\cot \theta_B$ monotonically decrease with increasing θ_B . Then, analogously as in the above discussion of the variation of $I(E)$, almost all of any such modulation produced would only be expected at the spin-frequency of the satellite. The phases for these spin frequency modulations, arising from individual variations of E_B and $\cot \theta_B$, would also be expected to be the same, therefore combining both individual modulations into an enhanced 1-st harmonic modulation.

From Fig. 4.2.20d, however, depicting the calibration curves for variation of integrated reflectivity, R_c , for both the graphite and LiF crystals, it can be easily seen for the graphite crystal that a scan range of θ_B which included the minimum would be expected to produce a spurious modulation at the polarisation frequency. Thus, variation of R_c for such a scan range of Bragg angles, holds some importance. Fortunately, for operation of the Ariel-V polarimeter at the optimum Bragg angle of 45° , an offset greater than 3° would be required before any spurious modulation at the polarisation frequency would be expected. Maximum, spurious, polarisation modulation would occur for θ_B nominally set at $\approx 48^\circ$, and for this case an offset of 3° would be expected to produce a spurious polarisation modulation of about 2.5%.

As an example, for the graphite crystal set to the optimum Bragg angle of 45° , with a 3° offset, the R_c calibration curve shows that

only a significant 1-st harmonic modulation would be expected to be produced. This modulation would be expected to be $\approx 4\%$ and at the same phase as for 1-st harmonic modulations estimated at $\approx 6\%$ and $\approx 10\%$ for variation of E_B and $\cot \theta_B$ respectively. For this example, the combined modulation effects would therefore only be expected to occur significantly at the 1-st harmonic frequency, and this modulation would be expected to be quite large at $\approx 20\%$.

ii) Time Variations in the X-ray Source Continuum Intensity

If variations in the X-ray source continuum flux occur with a periodic component at twice the satellite rotation rate, then this will produce modulations in the data which may mistakenly be interpreted as being due to polarisation.

Also, if the X-ray continuum flux is subject to aperiodic fluctuations (such as flare phenomena), then it also is possible that a data modulation component will arise at the polarisation frequency. This effect may be important if the observation timescale is comparable with the fluctuation timescales. If, however, the observation time is relatively long compared with the fluctuation timescale then some compensation by an averaging of effects can be expected to occur.

These effects must be considered separately for each individual source, since they depend upon the time behaviour of the X-ray flux from the individual source under observation.

Fortunately, there exists a simple, polarimeter, construction design which effectively eliminates spurious effects due to time fluctuations in the source intensity. This is important as, for many sources where fluctuations occur, practical observations may have durations of approximately the timescale of the possible fluctuations or not be long enough to produce any convincing elimination of effects by the averaging procedure. All that this construction design involves is the use of two separate polarimeters simultaneously, each orientated differently so that a complete component of polarisation is theoretically measured at every instant of time whatever the source intensity at that time (see Clarke and Grainger 1971, p. 137 ff, and Novick 1974, 1975, Weisskopf et al. 1976). For example, if these two polarimeters are fixed such that they have a permanent rotation angle phase difference of $\frac{\pi}{2}^c$ to each other, then the outputs from the two simultaneous signals can be

written as:-

$$I_1(\alpha, t) = I(t) \frac{G_1}{2} \{ 1 + p_L \cos 2(\alpha - \zeta) \} \quad (159)$$

$$I_2(\alpha, t) = I(t) \frac{G_2}{2} \{ 1 - p_L \cos 2(\alpha - \zeta) \} \quad (160)$$

where $I(t)$ represents the source intensity; G_1 and G_2 are the gains of the two detectors, which will in general not be equal; and ζ represents the phase of the polarisation (see equations (50b) and (49)). Then, the recorded data for an observation over the interval $t = 0$ to $t = T$ will be given by:-

$$\begin{aligned} C_1(\alpha) &= \int_0^T I(\alpha, t) dt \\ &= \frac{G_1}{2} \{ 1 + p_L \cos 2(\alpha - \zeta) \} \int_0^T I(t) dt \end{aligned} \quad (161)$$

$$\text{and } C_2(\alpha) = \frac{G_2}{2} \{ 1 - p_L \cos 2(\alpha - \zeta) \} \int_0^T I(t) dt \quad (162)$$

Then, putting $P = p_L \cos 2(\alpha - \zeta)$, we obtain

$$P(\alpha) = \frac{C_1(\alpha) - h C_2(\alpha)}{C_1(\alpha) + h C_2(\alpha)} \quad (163a)$$

where we have let

$$h = \frac{G_1 \int_0^T I(t) dt}{G_2 \int_0^T I(t) dt} \quad (163b)$$

and where it can be seen that the integrals in (163b) cancel, even though we do not know $I(t)$, as the time limits for the integration are identical. Therefore, it can be seen that (163a) is independent of any fluctuations in the source intensity $I(t)$. Then, by making measurements at other values of α at different times, the degree of linear polarisation

p_L and phase angle ζ can be obtained from (163a) free from the effects of such fluctuations.

If, however, a polarimeter similar to the Ariel-V instrument is employed, where measurements can only be made at a single orientation α at any instant, then the integrals in (161) and (162) become respectively

$$\int_0^T I(t) dt \quad \text{and} \quad \int_{T'}^{T'+T} I(t) dt.$$

Then, in this case, these integrals

do not cancel in (163b) since any fluctuation in $I(t)$ at $t = t_0$, say, can occur in only one of the integrals. For sources which can vary markedly in intensity for such time spans T , the spurious effects could be very large if (163b) was assumed true.

[Only for sources which are reasonably constant in time can the cancellation of the integrals in (163b) be taken as a good approximation when the time limits to the integrals are different. Also, if $I(t)$ varies with time, but in a known way, then h can be calculated by direct evaluation of each integral.]

iii) Background Radiation Effects

The effect that a systematic background data modulation can have, in terms of producing a spurious polarisation measurement, depends on the relative strength of background to signal detection. For the Ariel-V instrument, an observation on the Crab Nebula for instance (see § 5) (an ≈ 1000 Uhuru Unit source), produced a signal to background ratio ($R = S_0/B_0$) of only 0.1, so that a background modulation of as little as 1% is equivalent to the production of a 10% spurious polarisation measurement if not allowed for. Clearly then, elimination of background modulations in the Ariel-V data held much importance.

Causes of background induced data modulations include time variations in the background level; anisotropies in either the background radiation itself, or in its interaction with the spacecraft and detector system; and any polarisation of the diffuse X-ray background.

For the Ariel-V system the diffuse X-ray component of the total background level was found to be very small (a crude measurement gave $2 \pm 2\%$, see § 5.3.2) and therefore relatively unimportant. For future instrument design, where the rest of the background component may be considerably reduced by use of a focusing polarimeter (see § 4.2.3b), the diffuse component may take on more importance. However, the diffuse component also may be reduced, by narrowing the polarimeter f.o.v. Furthermore, the existence and any degree of polarisation of this diffuse component may be determined and thus allowed for, by observing sky regions close to the target source.

Previous X-ray polarimetry flights to Ariel-V, where background levels were similarly dominated by cosmic ray induced effects, had discovered no modulation effects (Angel et al. 1969, Wolff et al. 1970, and Novick et al. 1972), thus indicating at worst, that only a small degree of modulation should be expected with the Ariel-V polarimeter

observations. No anisotropy had been discovered in the background radiation, and effects of the East-West anomaly and albedo gamma rays (resulting from interaction primary cosmic rays in the Earth's atmosphere) had been considered.

However, early results from the Ariel-V polarimeter (see § 5.2 and Peacock 1975) show that background modulations as high as about 2 to 6% were present at the polarisation frequency, and because of this background systematic effects became the dominant limitation on the achievable, polarisation, sensitivity with the Ariel-V instrument.

A cause of these Ariel-V background modulations was consistent with albedo neutrons from the Earth's atmosphere interacting with the satellite mass (see § 5.2 or Griffiths et al. 1976a for further details).

For the Ariel-V observations, the best way found for partially eliminating the effects of the complicated background modulations was to make observations of these modulations on either side of the target source before and after the source observation. Then, an estimate of the background modulations existing at the time and spin-axis position of the source observation could be made by interpolation, thus allowing subtraction of these modulations from the source data. In this way a theoretical knowledge of the cause of the background modulations was not required - an observational knowledge only, of the modulations stability with time and pointing-axis position, was sufficient.

Whether background modulations prove such a serious problem in the future will depend primarily upon the extent to which the general background level can be reduced. Already, for the focusing polarimeter launched by the Columbia group during 1975, the background level has been reduced to an extent that the signal to background ratio for an observation, say, on the Crab Nebula will be of the order $R = S_0/B_0$ (Crab) ≈ 10 (from Weisskopf et al. 1976, extrapolating from GX5-1

and Cen X-3 data) which is a factor of $\approx 10^2$ better than for the Ariel-V polarimeter. Then a 1% modulation in the background is equivalent to only a 0.1% spurious polarisation modulation. If, for example, a further increase in R by a factor of 10 can be made by increasing the area or improving the focusing quality of such an instrument, then a similar freedom from background induced, spurious, polarisation modulations will exist for observations of sources 10 times weaker than the Crab Nebula. Thus, if progress can be made in this way, future polarisation observations of practically any weak source by a Bragg crystal focusing instrument should not be troubled by background modulations as existed with the Ariel-V polarimeter.

In addition to these above, main causes of systematic errors, a further, very minor effect was considered. For the Ariel-V satellite a Sun-sensor was employed to determine the absolute rotation angle of the satellite, and for long duration observations movement of the Sun in the sky by about 7° in R.A. and up to a similar amount in Declination, for an observation of a week, would cause the phase of any detected polarisation to be spread by about this amount. This in itself (see § 4.2.3d, where other smaller contributing effects are also listed) will cause a consequent lowering in the detected amplitude due to polarisation. Fortunately, though, the effect was calculated to be quite small amounting to a reduction of $< .3\%$ modulation for a one week observation.

§ 4.2.4 Extraction of Polarisation Parameters from the Ariel-V Data

In order to extract the degree of linear polarisation and its position angle from the Ariel-V data, first the computer raw data base was accessed for the selected group of orbits data required. Then these data were summed for each individual time slot within an orbit's data set (16 time slots of 512s each were provided by the main polarisation 'crystal' mode, see § 3.2.5) and for all the orbits concerned. According to this summation, sets of total counts received as a function of satellite rotation angle were obtained (crystal mode divides the rotation plane into 16 bins, or spin-sectors, of $22\frac{1}{2}^{\circ}$ each). Then, Fourier analysis of these sets of spin-sector data determined all the modulation amplitudes and phases, where the modulation at twice the satellite rotation frequency is related to the degree of linear polarisation and its position angle. So that the fractional data component due to the background could be obtained, the total observing times on both background and source were calculated and summed. Likewise the mean spin-axis offset from the source was computed so that, together with the nominally set Bragg angle θ_B , an estimation of the modulation factor could be made (see § 4.2.2b and § 4.2.3c). Then, after elimination or subtraction of estimated modulations due to the background - the degree of linear polarisation and its position angle could be obtained.

Finally, standard deviations on each of the determined parameters, notably the modulation amplitudes and phases, were obtained - in order that final standard deviations could be determined for the degree of linear polarisation and its position angle.

§ 4.2.4a Computer Summation of the Ariel-V data - (SUNSEC1 PROGRAM)

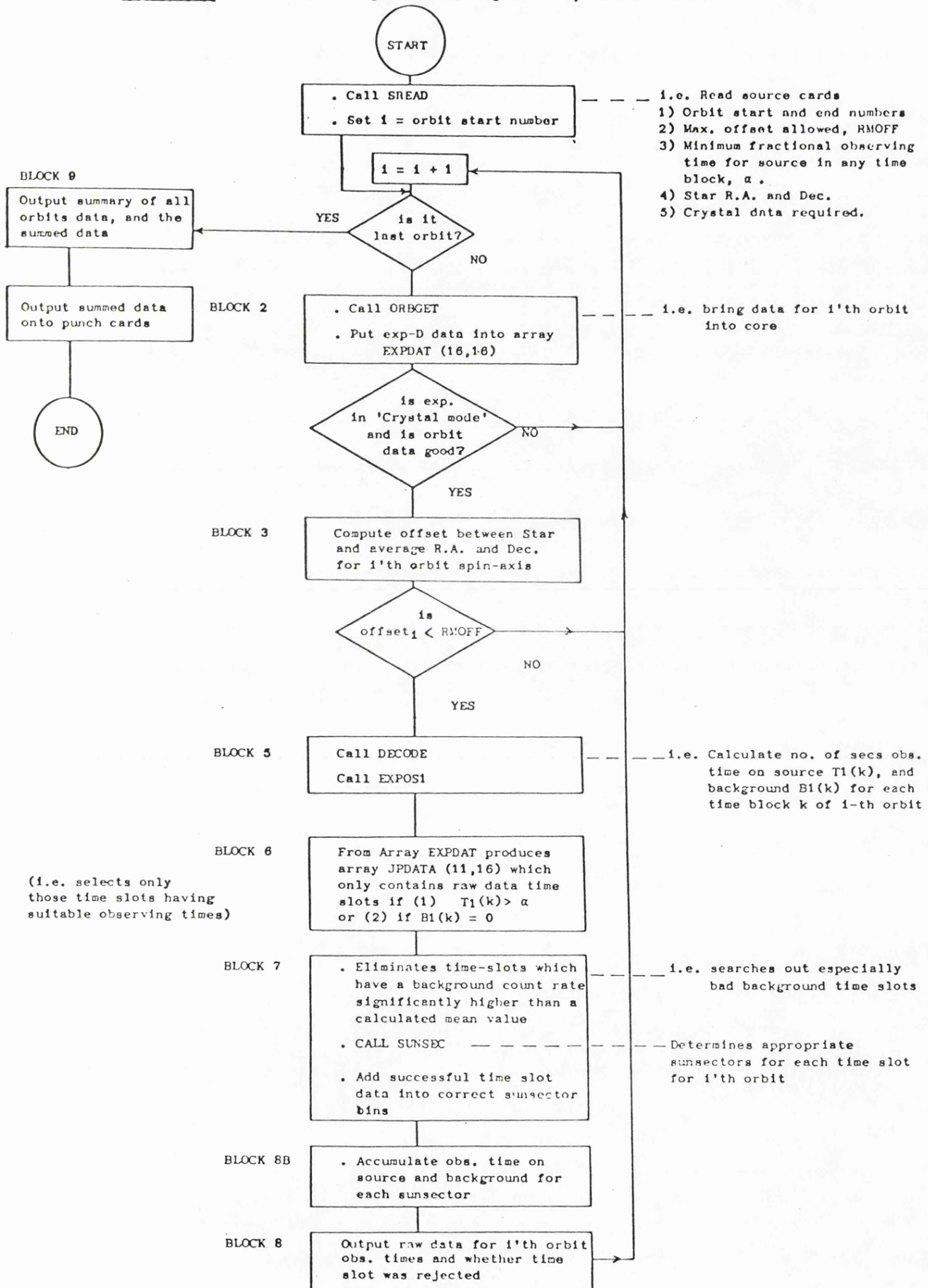
A flowchart of the computer program "SUNSEC1", written to

provide automatic access and summation of the Ariel-V data for a specific polarisation observation (observing slot, see § 4.1.5), is given in Fig. 4.2.21.

Initially, only one set of 16 numbers representing the spin-sector bins (counts per satellite rotation angle) were produced. However, subsequent to the discovery of the background modulation amplitude and phase variations around the orbit, the program was modified to sum the data into sections according to where in the satellite orbit the data was collected. These orbit regions were called "sun-sectors" from the manner in which they were defined (Ricketts, 1976, private communication)(see Fig. 4.2.22). Eleven sun-sector regions were used, of 20° width each, covering the sunlit portion of the orbit during which the experiment was switched on. (This gave approximately the same integration time, i.e. time resolution, as for each of the 512s time slots.) Division of the data in this way was also convenient since that portion of the orbit for which the Earth occulted the f.o.v. to the X-ray source always occurred in the same sun-sectors, thus constraining the background data (and hence source data also) to a definite set of sun-sectors. As well as allowing a study of background count rates and also modulation amplitude and phase variations around the orbit from this data division, an additional bonus occurred in that the approximate count rate due to the source could be obtained from the mean count rate profile with sun-sector.

The final sets of summed data were also output on punch cards. This allowed i) an easy form of input to the next program of whose task was to determine the modulation amplitudes and phases; ii) prevented typing errors by hand punching data from the printed output; and iii) allowed a file of summed data for the various polarisation observations to be created. This file meant that the frequently updated and improved

Fig. 4.2.21: Flowchart of Program for summing Ariel-V polarimeter data.



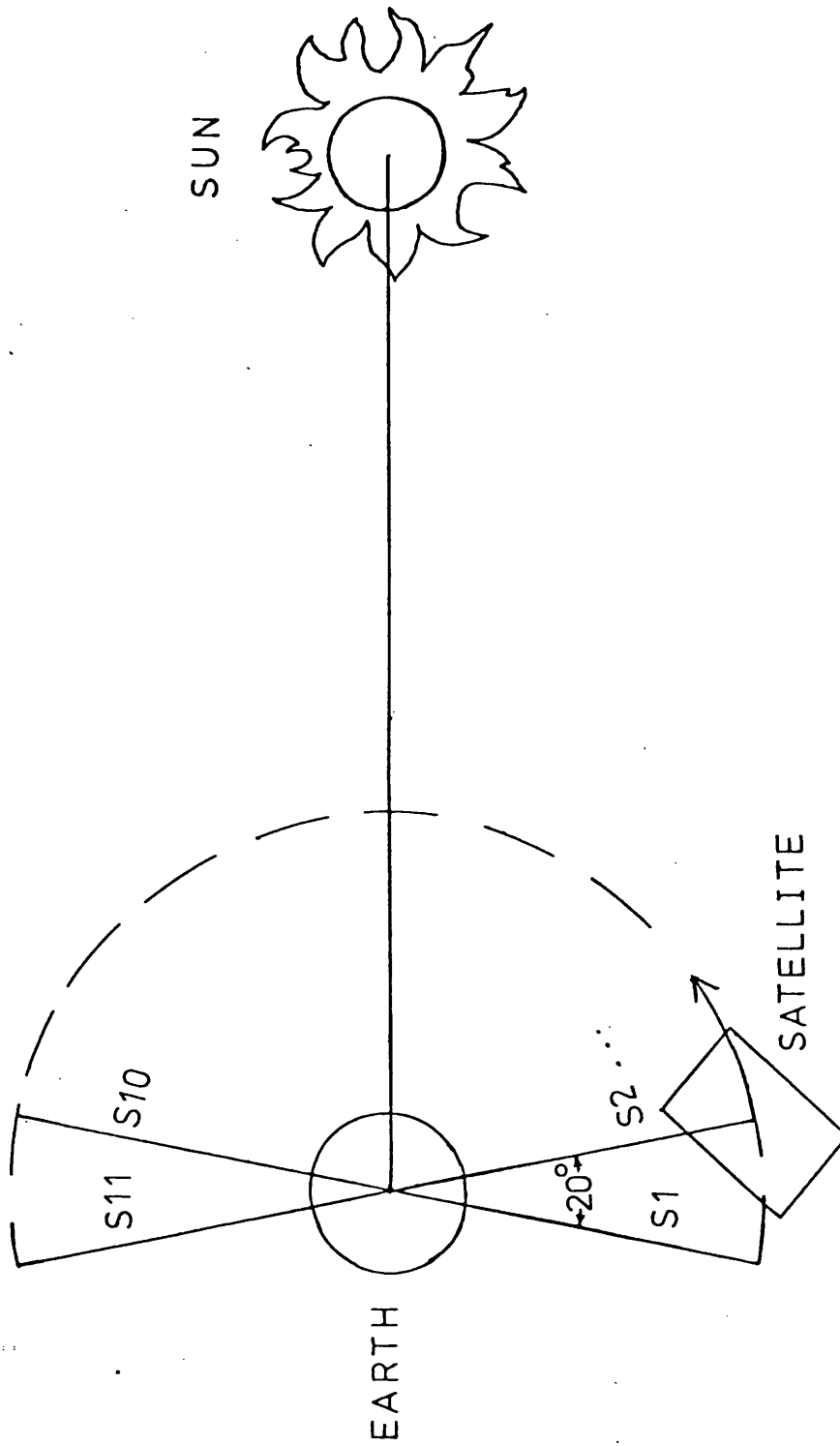


Fig. 4.2.22: Division of satellite Orbit into "sun-sectors" S1 to S11.

versions of the frequency analysis program could be run again on any desired data set without having to perform the computer, very time-consuming, job of re-summing from the raw data.

§ 4.2.4b Determination of Modulation Amplitudes and Phases in the Summed Data - and their Standard Deviations

Because of the various modulations expected at different frequencies in the data (see § 4.2.3c), Peacock (1975) wrote a computer program employing the Fourier analysis method outlined by Schnopper and Kalata (1969) (and given here in § 4.2.3b), to extract all these harmonics. He successfully pre-flight tested this program by re-analysis of Novick et al.'s (1972) data obtained from an observation of the Crab Nebula.

Standard deviations on the determined modulation amplitudes and phases were obtained as follows:-

Consider the data distributed into N spin-sector bins, the k -th bin containing $A(k)$ events. ($N = 16$ for Ariel-V crystal mode). (See § 4.2.3b and Fig. 4.2.13). It is assumed that the true function which underlies the N data points can be represented by the Fourier function $f(k)$, such that

$$f(k) = A_0 + \sum_{n=1}^q (A_n \cos \theta_n + B_n \sin \theta_n) \quad (164)$$

where the A_0 , A_n 's and B_n 's are constants,

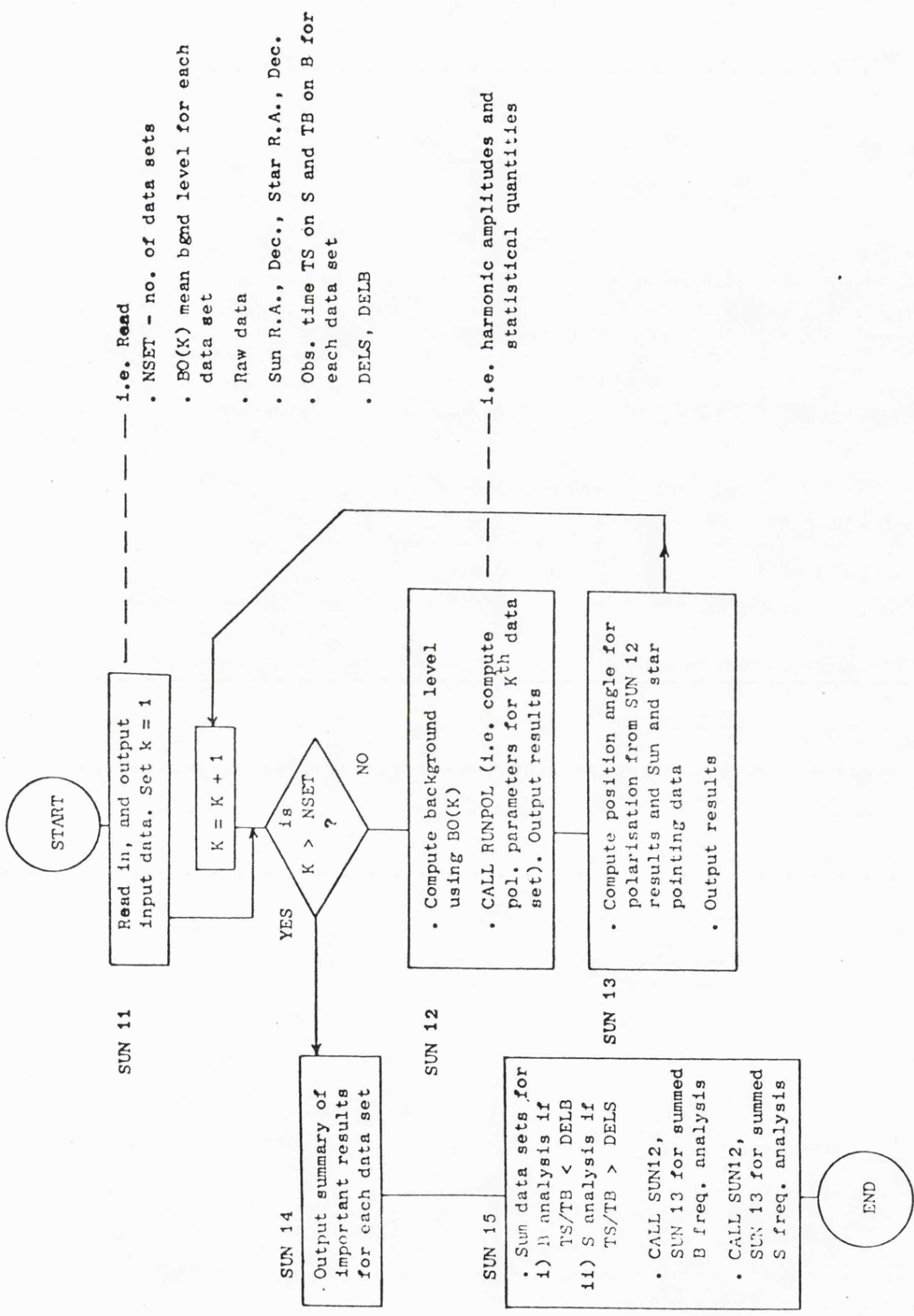
$$\theta_n = \left(\frac{2\pi n}{N} \right) k \quad (165)$$

and $q = \frac{N}{2}$ for N even.

Then, let the observed data set be given by

$$A(k) = f(k) + U_k \quad k = 1, \dots, N \quad (166)$$

Fig. 4.2.23: Flowchart of Program "RUNPOL" used to compute polarisation parameters from data summed as a function of rotation angle.



where U_k represents the statistical variation in counts received in the k -th bin, such that the following expected values are produced:-

$$\epsilon(U_k) = 0 \quad (167)$$

$$\epsilon(U_k^2) = \sigma^2 \quad (168)$$

$$\epsilon(U_k U_l) = 0 \quad \text{when } k \neq l \quad (169)$$

(l an integer also)

where σ^2 represents the expected variance of the observed data set to the assumed true function $f(k)$. That $\epsilon(U_k U_l) = 0$, represents the independence of the errors U_k for all k .

Then, by using the method of least squares it can be shown, (see Anderson 1971), that the best value estimates for the A's and B's of (164) to the observed data $A(k)$ will be given by the following expressions:-

$$A_0 = \frac{1}{N} \sum_{k=1}^N A(k) \quad (170a)$$

$$A_n = \frac{2}{N} \sum_{k=1}^N A(k) \cos\left(\frac{2\pi n k}{N}\right) \quad (170b)$$

$$B_n = \frac{2}{N} \sum_{k=1}^N A(k) \sin\left(\frac{2\pi n k}{N}\right) \quad (170c)$$

(and it may be noted that these expressions are equivalent to those which would be obtained by Fourier analysis of the observed data points $A(k)$, c.f. § 4.2.3b(ii)).

Then, by using 1st order propagation of error theory on (170a), (170b) and (170c), it can be shown that the variances on these determined parameters will be given by

$$\sigma^2(A_0) = \frac{\sigma^2}{N} \quad (171a)$$

$$\sigma^2(A_n) = \sigma^2(B_n) = \frac{2\sigma^2}{N} \quad (171b)$$

where an unbiased estimate of σ^2 is given by s^2 , where

$$s^2 = \frac{1}{T-(2q+1)} \sum_{k=1}^N [A(k) - f(k)]^2 \quad (172)$$

Consider just one frequency component of $f(k)$, f_n say, so that

$$f_n = A_n \cos \theta_n + B_n \sin \theta_n = C_n \cos (\theta_n - \phi_n) \quad (173)$$

where C_n , then, represents the desired amplitude of the modulated

frequency component, and ϕ_n the phase. Therefore, from (173) by

expanding $\cos(\theta_n - \phi_n)$, the C_n and ϕ_n are given in terms of A_n and B_n

by the expressions:-

$$C_n^2 = A_n^2 + B_n^2 \quad (174)$$

$$\phi_n = \tan^{-1} \left(\frac{B_n}{A_n} \right) \quad (175)$$

$$\text{since } B_n = C_n \sin \phi_n \quad (176)$$

$$\text{and } A_n = C_n \cos \phi_n \quad (177)$$

Then, using 1-st order error propagation theory (see Bevington 1969), as A_n and B_n are independent parameters,

$$\begin{aligned} \sigma^2(C_n) &= \sigma^2(A_n) \left(\frac{\partial C_n}{\partial A_n} \right)^2 + \sigma^2(B_n) \left(\frac{\partial C_n}{\partial B_n} \right)^2 \\ &= \sigma^2(A_n) \frac{A_n^2}{C_n^2} + \sigma^2(B_n) \frac{B_n^2}{C_n^2} \quad \text{by using (174)} \\ &= \frac{2\sigma^2}{N} \frac{(A_n^2 + B_n^2)}{C_n^2} \quad \text{from (171)} \\ &= \frac{2\sigma^2}{N} \quad \text{[from (174)]} \quad (178) \end{aligned}$$

Thus, the standard deviation on the determined modulation amplitude can be calculated according to

$$\sigma^2(C_n) \approx \frac{2s^2}{N} \quad (179)$$

Similarly, again using 1-st order propagation of errors,

$$\sigma^2(\phi_n) = \sigma^2\left(\frac{B_n}{A_n}\right) \left[\frac{\partial \phi_n}{\partial \left(\frac{B_n}{A_n}\right)} \right]^2 \quad (180)$$

Now, $\frac{d \tan \phi}{d \phi} = \frac{1}{\cos^2 \phi}$, so that $\frac{d \phi}{d \tan \phi} = \cos^2 \phi$

So, $\frac{\partial \phi_n}{\partial \left(\frac{B_n}{A_n}\right)} = \frac{\partial \phi_n}{\partial \tan \phi_n} = \cos^2 \phi_n$ (181)

(Using (176) and (177))

and also, by letting $\frac{B_n}{A_n} = \alpha_n$:-

$$\sigma^2(\alpha_n) = \sigma^2(A_n) \left(\frac{\partial \alpha_n}{\partial A_n} \right)^2 + \sigma^2(B_n) \left(\frac{\partial \alpha_n}{\partial B_n} \right)^2$$

so that

$$\frac{\sigma^2(\alpha_n)}{\alpha_n^2} = \frac{\sigma^2(A_n)}{A_n^2} + \frac{\sigma^2(B_n)}{B_n^2}$$

i.e. $\sigma^2(\alpha_n) = \left(\frac{2\sigma^2}{N} \right) \frac{B_n^2}{A_n^2} \left[\frac{1}{A_n^2} + \frac{1}{B_n^2} \right]$ using (171)

$$= \left(\frac{2\sigma^2}{N} \right) \frac{1}{C_n^2 \cos^4 \phi_n} \quad [\text{from (174) and (177)}] \quad (182)$$

Then, substituting (181) and (182) back into (180) we obtain:-

$$\begin{aligned} \sigma^2(\phi_n) &= \left[\frac{2\sigma^2}{N} \frac{1}{C_n^2 \cos^4 \phi_n} \right] \left[\cos^2 \phi_n \right]^2 \\ &= \frac{2\sigma^2}{NC_n^2} \end{aligned}$$

so that $\sigma(\phi_n)$ is given by the simple expression:-

$$\sigma(\vartheta_n) = \frac{\sigma(C_n)}{C_n} \quad \text{radians} \quad (183)$$

[from (178)]

(However, we note that in terms of dimensions of satellite rotation angle, (183) must be modified to become

$$\sigma(\vartheta_n) = \frac{\sigma(C_n)}{C_n} \left(\frac{1}{n} \right) \quad (183b)$$

as for the n-th harmonic, n full cycles occur for each complete satellite rotation.)

Thus, in summary, the standard deviations for the observed data modulation amplitudes and phases were calculated according to the expressions (179) and (183)

i.e.

$$\sigma^2(C_n) = \frac{2s^2}{N}$$

$$\sigma^2(\vartheta_n) = \frac{\sigma^2(C_n)}{C_n^2}$$

where s^2 was calculated according to (172).

§ 4.2.4c Determination of the Degree of Linear Polarisation - and its Standard Deviation

(i) When no spurious modulations exist in the data

For this case it is an easy matter to extract the degree of linear polarisation. It can be calculated from the following expression, applied direct to the raw summed data (see § 4.2.2a):-

$$P_L = \frac{1}{m} \frac{A_p}{(M - B)} \quad (184)$$

where m is the modulation factor; A_p is the modulation amplitude at twice the satellite rotation frequency, calculated in the previous section (§ 4.2.4b); M is the mean count level recorded in the data per spin-sector; and B is the mean background level.

Once these right-hand side parameters are known and their individual standard deviations, it is also relatively easy to calculate the standard deviation on the degree of linear polarisation p_L .

Re-writing (184) as

$$p_L = \frac{1}{m} V, \quad \text{or} \quad \frac{1}{m} p_{Lo} \quad (185)$$

where p_{Lo} is the degree of linear polarisation obtained when the modulation factor is unity. It is easy to show, using 1-st order propagation of errors, that the standard deviation on V will be given by:-

$$\sigma^2(V) = \frac{p_o^2}{A_p} [\sigma^2(A_p) + p_o^2 (\sigma^2(B) + \sigma^2(M))] \quad (186)$$

where $\sigma^2(A_p)$ has been calculated in the previous section.

The mean recorded count level M is given by:

$$M = \frac{N_T}{N} \quad \text{where } N_T = \text{total number of counts recorded,}$$

and N is the number of spin-sectors. Then

$$\sigma^2(M) = \sigma^2(N_T) \left(\frac{\partial M}{\partial N_T} \right)^2 = \frac{N_T}{N^2}, \quad \text{as it is assumed that the}$$

distribution of counts is Poissonian.

The mean background level B is given by:-

$$B = \frac{B_o}{N} \times T_b \quad (\text{counts spin-sector}^{-1}) \quad (187)$$

where B_o is the mean background count rate (counts s^{-1}) and T_b is the observing time (s) on the background during the polarisation observation.

$$\text{Therefore } \sigma^2(B) = \sigma^2\left(\frac{B_o}{N}\right) T_b^2 + \sigma^2(T_b) \left(\frac{B_o}{N}\right)^2 \quad (188)$$

The accuracy of measuring the observing time with the Ariel-V polarimeter was such that the observing times sent with the raw data were accurate to

$\pm 8s$ for each time slot measurement of up to 512s integration time.

[Approximately 5 (between ≈ 1 and 10) useful time slots, where the source was visible, were obtained per orbit.] Thus, T_b was composed of multiple observing time measurements per observation. Then, $\sigma^2(T_b)$ is given by:-

$$\sigma^2(T_b) = \sigma^2(T_1) + \sigma^2(T_2) + \dots + \sigma^2(T_j)$$

where T_i is the i -th measurement of observing time, and in all j measurements were made. (Usually, the observing time error measured in this way gave only a minor contribution to the total error on p_L .)

B_o , the mean background count rate, was determined from observations of the background only. However, determination of B_o and its error depended upon the way in which the background measurements, without the source in the instrument f.o.v. and possibly at a different time, were related to the background estimated to exist during the source observation. For the Ariel-V observations more than one method of determination of B_o was used (they included both extrapolation and interpolation methods), and these are discussed for the individual source observations listed in § 5.

Knowledge of the above parameters and errors then, enable V and $\sigma^2(V)$ to be calculated. The degree of linear polarisation and its standard deviation can then be obtained via (185) and the following equation derived from (185):-

$$\sigma^2(p_L) = p_L^2 \left[\frac{\sigma^2(m)}{m^2} + \frac{\sigma^2(V)}{V^2} \right] \quad (189)$$

The determination of the modulation factor m and its error was, in general, related to the discussion on systematic errors in § 4.3.3c as well as to the calibration of crystals similar to those flown on Ariel-V. Specific examples of the determination of m are given in § 5.

(ii) When spurious modulations exist in the background data

When a modulation at twice the satellite rotation frequency exists in the background data, it can be seen that this would introduce a spurious element into the value of p_L obtained via (184), where only the mean background level B is allowed for.

A general method for the elimination of such an effect has been mentioned previously in § 4.2.1d and 2d. This method simply involves determination of 'Stokes parameters' for the source + background [$\underline{S}(s+b)$] data and subtracting 'Stokes parameters' estimated for the background contribution [$\underline{S}(b)$] alone. Expressing this analogously to (32):-

$$\underline{S}'(s) = \underline{S}'(s+b) - \underline{S}'(b) \quad (190)$$

i.e.

$$\begin{bmatrix} I_s \\ I'_{p1s} \cos 2\zeta_s \\ I'_{p1s} \sin 2\zeta_s \end{bmatrix} = \begin{bmatrix} I_{(s+b)} \\ I'_{p1(s+b)} \cos 2\zeta_{(s+b)} \\ I'_{p1(s+b)} \sin 2\zeta_{(s+b)} \end{bmatrix} - \begin{bmatrix} I_b \\ I'_{p1b} \cos 2\zeta_b \\ I'_{p1b} \sin 2\zeta_b \end{bmatrix} \quad (191)$$

[see (59)]

where, in (190), the \underline{S}' s refer to what could be termed 'modified Stokes parameters' in that they assume the modulation factor is unity [i.e. $I'_{p1} = A_p$; cf (60) where $I_{p1} = A_p/m$]. Then, the true value of p_L is easily obtained from

$$p_L = \frac{1}{m} \frac{I'_{p1s}}{I_s} \quad [\text{cf (60)}] \quad (192)$$

(Note: an equivalent method would have been to use the correct Stokes parameters determined by $I_{p1} = A_p/m$, though this has the disadvantage that the modulation factor is introduced early into the calculations. If the value of m is initially unknown, or subject to change, then the

method adopted above allows all computations short of p_L to be completed independent of m .)

Determination of the errors on p_L and ζ are obtained simply by application of first order propagation of errors to the relations (192) and (191).

The modified Stokes parameters $\underline{S}'(s+b)$ for the source + background observation were obtained from Fourier analysis of the $(s+b)$ summed data, where the relations between the Fourier determined and Stokes parameters are given by (51b) and (59 et seq.). Then application of first order error theory through these relations (51b), (59 et seq.), allowed errors on the Stokes parameters to be determined from those on the Fourier determined parameters.

The background modified Stokes parameters $\underline{S}'(b)$ were also determined via these (51b), (59 et seq.) equations, which relate specifically the estimated mean, modulation amplitude and phase at twice the satellite rotation frequency to the associated Stokes parameters. However, as the method of estimating these background parameters was not standard, they are discussed individually, for particular Ariel-V observations, in § 5.

§ 4.2.4d Determination of the Polarisation Position Angle - and its standard deviation

Reference axes for the polarisation position angle are defined in § 4.2.1f. The mathematics for conversion of the polarisation phase angle to that of position angle for the Ariel-V satellite, were developed by R. Griffiths (private communication, 1976).

Let \emptyset (radians of satellite rotation angle, see (183b)) be the phase angle from the sector start to I_{\max} in the Ariel-V summed data due to polarisation only (see Fig. 4.2.24). (Assume that any

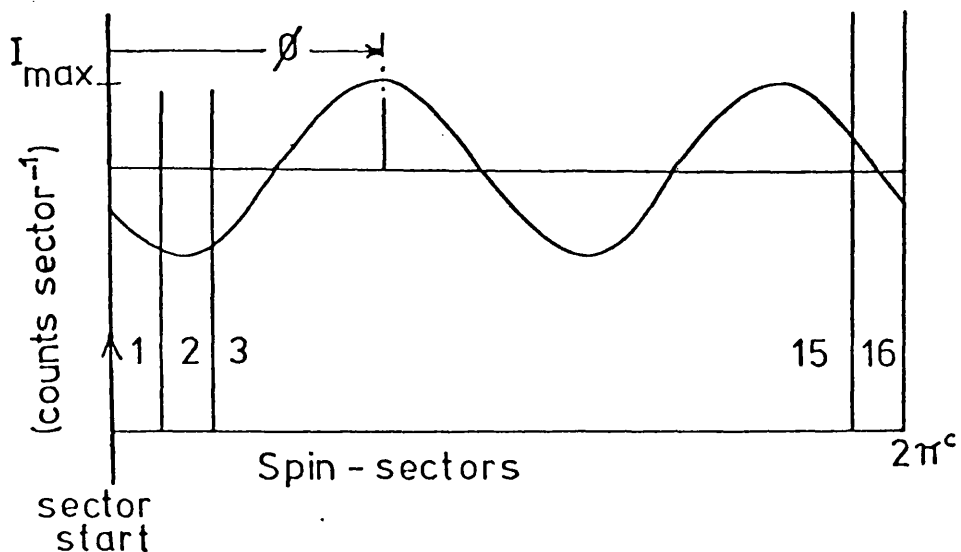


Fig. 4.2.24: Phase angle ϕ of polarisation from sector start orientation.

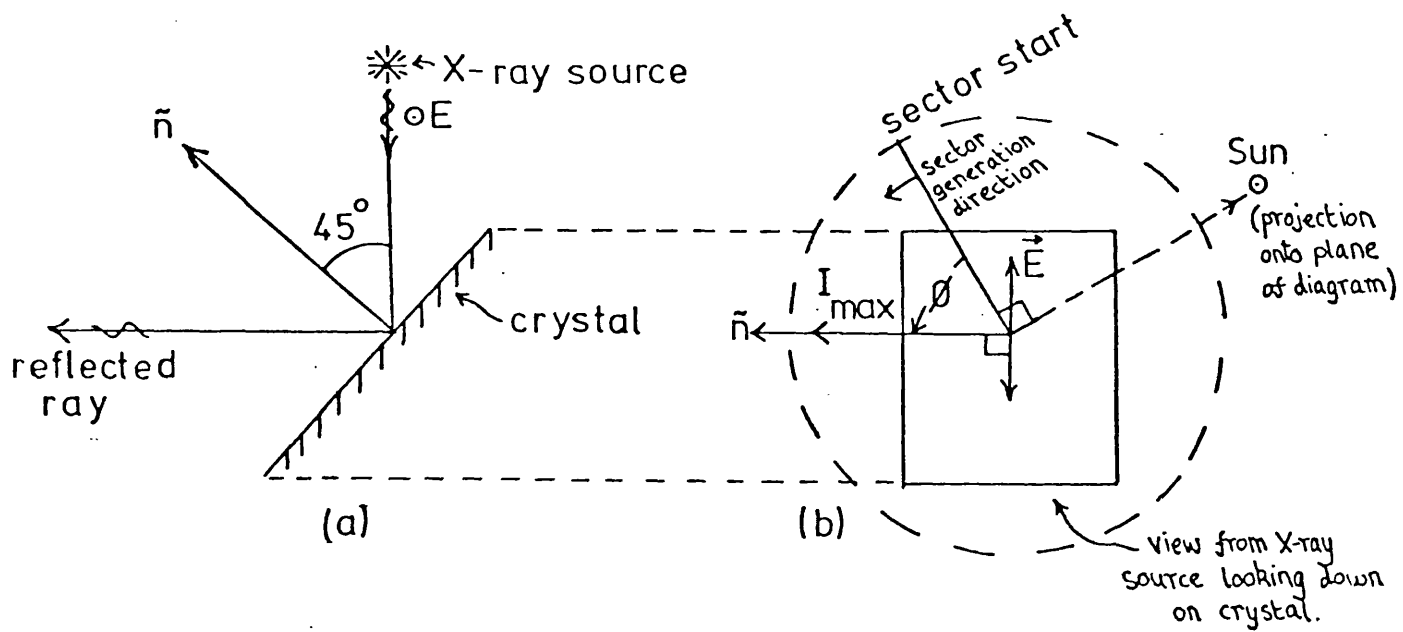


Fig. 4.2.25: Relative I_{max} , solar, crystal, electric vector and sector start orientations.

background modulations have been subtracted out.)

From the properties of Bragg reflection from a crystal (§ 4.2.2a) we know that I_{\max} occurs when the direction of vibration of \underline{E} is perpendicular to the reflected ray (see Fig. 4.2.25a). Then it can be seen from the projected view b of Fig. 4.2.25, that this angle of vibration of \underline{E} is then 90° to the projected normal (\underline{n}) to the crystal.

Fig. 4.2.26 shows the spacecraft rotation orientation when the sun-sensor SS1 detects the Sun. The pulse from SS1 then triggers the sector generator to begin generating a new set of 16 spin-sectors for the polarimeter experiment (see § 3.1). It can also be seen from Fig. 4.2.26 that the orientation of Experiment-D within the satellite, at sector zero, is such that the crystal normal direction (\underline{n}) is perpendicular to the Sun acquisition direction.

Then, considering position angles on the celestial sphere, it can be seen that (from the projection of Fig. 4.2.25b) the following relation holds true:-

$$\text{PnA (pol)} = \text{PnA (Sun)} - \emptyset \quad (193)$$

where $\text{PnA (pol)} =$ position angle of polarisation,

and $\text{PnA (Sun)} =$ position angle of the Sun.

That is, the position angle of polarisation is equal to the position angle of the Sun, minus \emptyset (the position angle of the Sun relative to \underline{E}). (See Fig. 4.2.27).

\emptyset is obtained either directly from the Fourier analysis of the polarimeter data or via the determination of the Stokes parameters.

The only further requirement is to obtain the position angle of the Sun which can be calculated from the spacecraft data by considering the sky diagram of Fig. 4.2.28.

By using the spherical trigonometry relation

$$\cos a = \cos b \cos c + \sin b \sin c \cos A \quad (194)$$

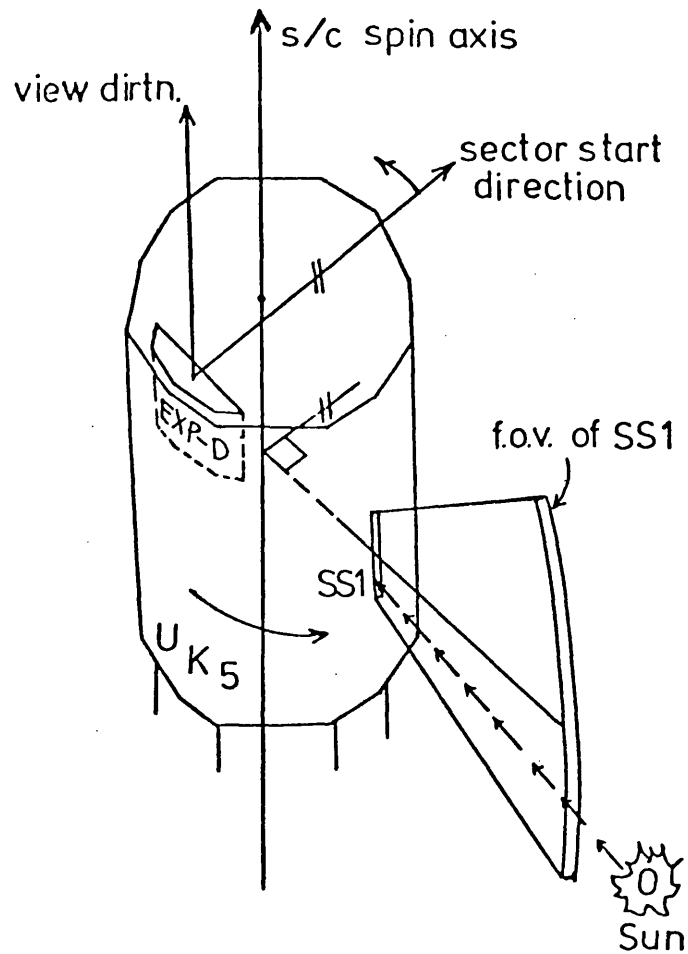


Fig. 4.2.26: Relation of sector start orientation to Sun direction. SS1 is the satellite sun-sensor.

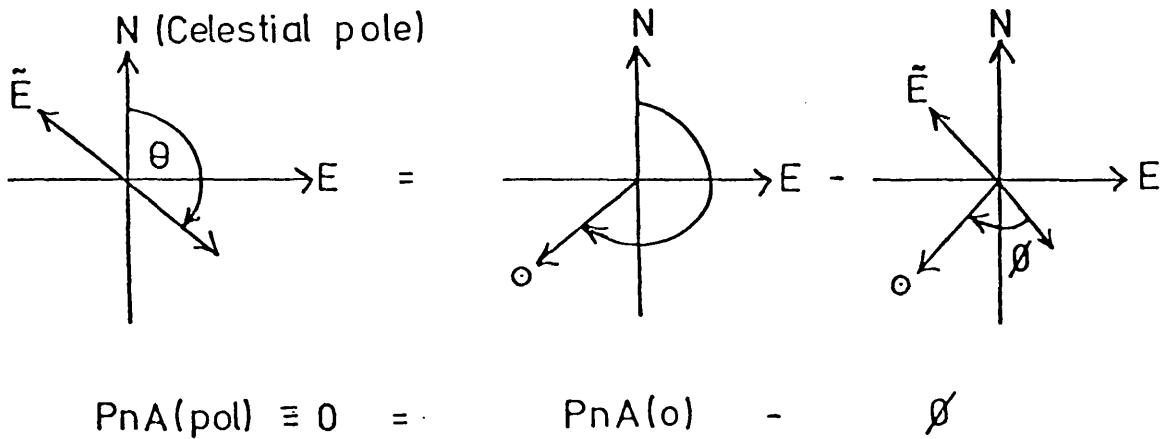


Fig. 4.2.27: Relationship between celestial sphere position angles and phase angle of polarisation.

$PnA(pol)$ = position angle of polarisation

$Pn(\theta)$ = position angle of sun

ϕ = polarisation phase angle.

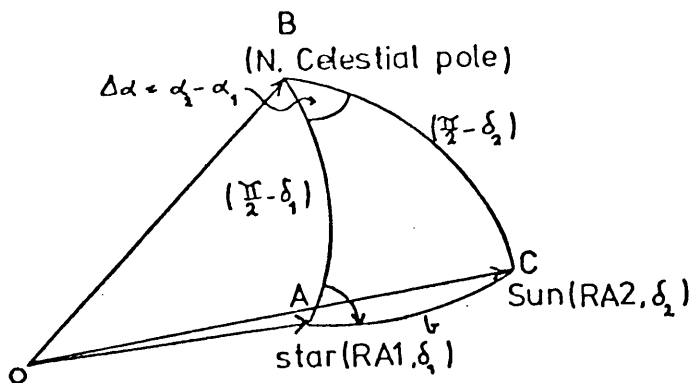


Fig. 4.2.28: Spherical Geometry of North celestial pole, X-ray star (~ spacecraft spin-axis) and the Sun. "A" is the position angle of the Sun from the spacecraft pointing direction.

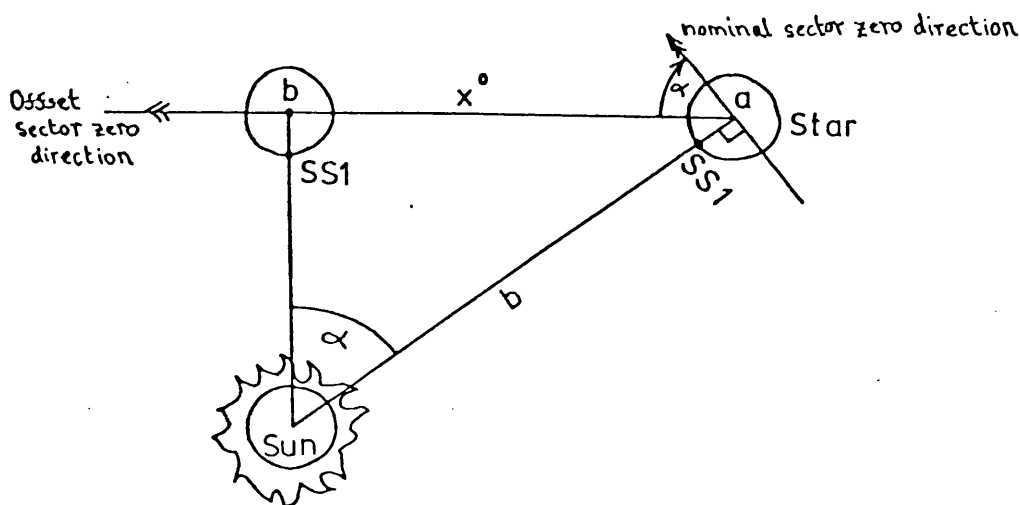


Fig. 4.2.29: Change in angular orientation α of sector start when the satellite is not pointed at the star at 'a' but offset by x° at position 'b'. SS1 is the satellite sun-sensor.

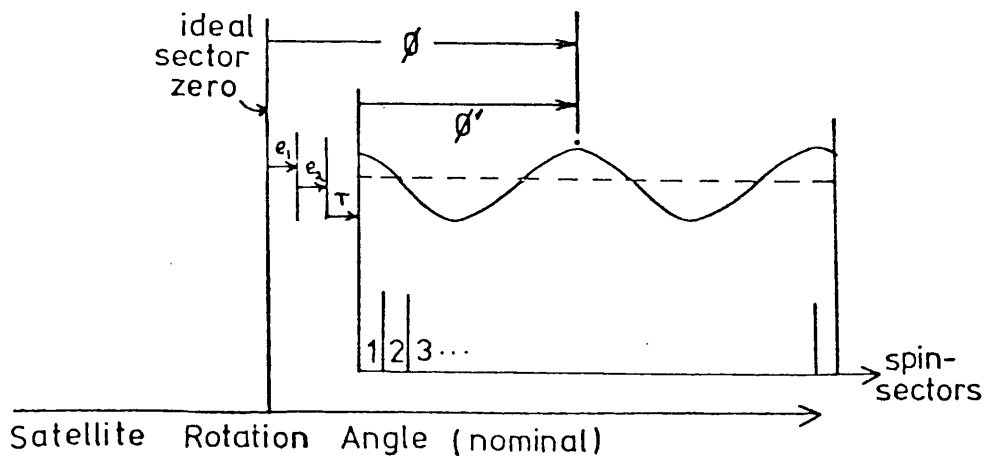


Fig. 4.2.30: Schematic illustration showing relation of errors on the measured polarisation phase angle ϕ' , to the true value ϕ .

we can obtain the following relations:-

$$\begin{aligned}\cos b &= \cos\left(\frac{\pi}{2} - \delta_1\right) \cos\left(\frac{\pi}{2} - \delta_2\right) + \sin\left(\frac{\pi}{2} - \delta_1\right) \sin\left(\frac{\pi}{2} - \delta_2\right) \cos \Delta\alpha \\ &= \sin \delta_1 \sin \delta_2 + \cos \delta_1 \cos \delta_2 \cos \Delta\alpha\end{aligned}\quad (195)$$

and

$$\cos\left(\frac{\pi}{2} - \delta_2\right) = \sin \delta_2 = \sin \delta_1 \cos b + \sin b \cos \delta_1 \cos A \quad (196)$$

where some of the parameters represent the following coordinates

<u>Coords</u>	<u>R.A.</u>	<u>Dec.</u>
North Celestial Pole	(,	$\pi/2$)
Sun	(α_2 ,	δ_2)
Spacecraft spin-axis pointing direction	(α_1 ,	δ_1)

$$\text{and where } \Delta\alpha \equiv \alpha_2 - \alpha_1 \quad (197)$$

'A' \equiv PnA (Sun), represents the position angle of the Sun from the pointing direction of the satellite spin-axis; and the other parameters are given in the Fig. 4.2.28. So, from (196)

$$\cos A = \frac{\sin \delta_2 - \sin \delta_1 \cos b}{\sin b \cos \delta_1} \quad (198)$$

Then, as the sky position coordinates of both the Sun and spin-axis pointing direction are given with the spacecraft raw data, the position angle "A" of the Sun can be calculated from (198), where b can be determined from (195).

These relations, (193) to (198), for the production of the polarisation position angle were written into a computer program, and some care was taken to allow for several factors:-

- (i) Correct position angle results, but outside the desired range $(0, 180^\circ)$.

It can be seen that use of (193) could produce PnA (pol) results

which are (a) $> 180^\circ$ or (b) $< 0^\circ$ depending on the geometry outlined by Fig. 4.2.27. For those cases (a) and (b) it is easily seen that subtraction or addition of 180° respectively will convert an otherwise correct result to the desired range.

- (ii) Discontinuities in the R.A. system of measurement, i.e. (0° to 360° to 0°).

In the calculation of the angular distance b between the Sun and the celestial X-ray source, the term " $\cos(\alpha_2 - \alpha_1)$ " in (195) is involved. However, this term is unaffected by the discontinuities in R.A.'s around the celestial sphere as $\cos(\Delta\alpha \pm 360^\circ) = \cos(\Delta\alpha)$.

- (iii) The returned magnitudes in the calculation of the angular distance b .

This is calculated from (195) where

$$b = \text{acos}(\cos b)$$

and the returned values are from the "acos" function which are usually limited to a range of π^c . For the university Cyber '72 Fortran system the returned range was $[0, \pi]$, which effectively meant that only magnitude, but not direction, along the great circle route joining the Sun and spin-axis pointing positions, could be differentiated. That is, West and East could not be differentiated by use of the 'acos' function alone. This, in turn, would mean that the position angle of the Sun might be, erroneously, measured North via West instead of East. Recourse to the actual geometrical positions of the Sun and pointing axis on the sky supplied the necessary information to solve this problem. In fact, consideration of the two determining cases of whether $\Delta\alpha = \alpha_2 - \alpha_1$ (i) was \geq or $<$ 0 and (ii) $>$ or $\leq 180^\circ$ was found sufficient. (For example, if $\Delta\alpha \geq 0$ and also $> 180^\circ$, then α_2 would be East of α_1 by $> 180^\circ$, and b , returned as the shortest angular distance from α_2 to α_1 , would imply that the position angle of polarisation was being measure North via

West instead of East. The correct position angle would then be given by 2π minus the calculated one.)

Determination of the error on the position angle of Polarisation

The position angle is calculated from (193) and therefore the variance on this determination will, to 1-st order, be given by:-

$$\sigma^2 [\text{PnA(Pol)}] = \sigma^2 [\text{PnA(Sun)}] + \sigma^2 [\varnothing] \quad (199)$$

The determination of the variance on the phase angle \varnothing has already been discussed in the previous sections 4.2.4b and (c), and for the Ariel-V data this was the dominant term. For example (see § 5), a 50 orbit summation of data would give $\sigma^2 [\varnothing] \approx 25^\circ$ whilst $\sigma^2 [\text{PnA(Sun)}]$ would amount to $\lesssim 1^\circ$.

It shall now be shown that random and systematic errors can arise in the calculation of the polarisation angle which act to complicate the simple expression (199).

In particular, it will be shown that errors other than $\sigma^2(\varnothing)$ can become significant if:-

- (i) The satellite is pointed at an offset from the source, although this error can be eliminated as it is systematic. (Perhaps special consideration would be required for observation of an extended source, where each part of the source would be at a unique and different offset from the experiment pointing direction.)
- (ii) The declination of the source is high, say $> 80^\circ$.
- (iii) The angular separation between the source and Sun is small.
 - a) Errors associated with the measurement of \varnothing - the phase angle of I_{max} from the start-sector direction.

Until now it has been assumed that the start-sector direction is

a perfect 90° from the direction to the Sun. However, this start-sector is determined from the acquisition time of the Sun by the sun-sensor SS1 and random errors will occur for this acquisition time. Also, when the satellite is offset from the source, this will generally produce a different Sun-acquisition time and cause, as before, the rotation angle of the satellite to be different for the start-sector direction. For example (see Fig. 4.2.29), if the satellite is offset by, say, x° from its nominal pointing direction, then the maximum error in orientation of the sector-start direction ' α ' will be given by $\sin \alpha = x/b$ ($\alpha \approx x/b$, if x/b is small).

If we let \emptyset be the true phase angle and \emptyset' be the measured phase angle (for example from Fourier analysis of a single orbit's data), then the following relation can be seen to exist between \emptyset and \emptyset' (see Fig. 4.2.30):-

$$\emptyset = \emptyset' + e_1 + e_2 + r \quad (200)$$

where

e_1 = error due to the satellite pointing direction being offset from the X-ray source position.

e_2 = error due to "jitter" on the start sector position.

r = small systematic error for the fixed misalignments of
(i) internal experiment axis to spin-axis of satellite
and (ii) Sun-sensor.

But now, \emptyset was, in actuality, obtained from data summed from several orbits, in which case for a z-orbit sum we obtained, as a good approximation:-

$$\begin{aligned} \emptyset &\approx \emptyset' + \frac{(e_{11} + e_{12} + \dots + e_{1z})}{z} + \frac{(e_{21} + e_{22} + \dots + e_{2z})}{z} + r \\ &= \emptyset' + e_1' + e_2' + r \end{aligned} \quad (201)$$

where ϑ' is now the resultant measured phase angle (from, for example, Fourier analysis of the summed data); e_2' is the mean of the jitter error, for which the expectation value is zero; and e_1' is the mean of the satellite offset errors where

(i) e_1' will have an expectation value of almost zero if the satellite pointing direction was nominally on the source but has drifted slowly, and with a degree of randomness, around the source direction.

(ii) e_1' will have a positive expectation value if a definite satellite offset was purposely set for the observation.

(See § 4.2.3c for reasons for this.)

So, for an observation with no intentional offset

$$\sigma^2(\vartheta) \approx \sigma^2(\vartheta') + \frac{\sigma^2(e_1)}{z} + \frac{\sigma^2(e_2)}{z} + \sigma^2(r) \quad (202)$$

where r is included, for convenience, as a statistical error on the true value of ϑ , i.e. $r_{\text{mean}} = 0$ but has variance $\sigma^2(r) > 0$); $\sigma^2(e_2)$ assumes an approximate constant jitter error for each orbit, which for the Ariel-V satellite has been estimated as 0.09° (see Peacock 1975); and $\sigma^2(e_1)$ represents the mean offset error which is estimated to be $\approx 0.1^\circ$ per orbit for Ariel-V observations (see § 4.2.3c).

Therefore a good approximation to (202) for the Ariel-V observations, where no definite spin-axis offset from the source is specified and $\sigma^2(\vartheta') \approx 25^\circ$ for $m \approx 50$, is given by:-

$$\sigma^2(\vartheta) \approx \sigma^2(\vartheta') \quad (203)$$

as the other error terms are relatively insignificant.

If, however, the satellite pointing direction was designed to have a definite non-zero offset from the source, then the effect of this must be allowed for by its inclusion in the term e_1 , where this can be achieved by letting $e_1 = e_{1a} + e_{1b}$ where e_{1a} is the portion allowing for

drift errors such that the expectation value $\epsilon(e_{1a}) \approx 0$ and e_{1b} is due to the definite offset where $\epsilon(e_{1b}) \neq 0$. This effect can then be included into (203) as an additional term of approximately $\leq \frac{x}{b}$ (see above), giving:-

$$\sigma(\varnothing) \approx \sigma(\varnothing)' + \frac{x}{b} \quad (\text{radians of satellite rotation angle}) \quad (204)$$

(Only if $\frac{x}{b}$ becomes appreciable compared with $\sigma(\varnothing)'$ will recourse to a more accurate calculation of e_{1b} become appropriate, using the geometry of Fig. 4.2.29, to reduce this component.)

b) Errors associated with the measurement of the Sun position angle - PnA(Sun).

The position angle of the Sun is calculated from equations (198) and (195) wherefrom the following points may be observed.

(i) the position of the source star is usually known accurately (e.g. to better than $0.01^\circ \approx 36''$) and we would normally not expect any large error to arise from this positional uncertainty. However, it can be seen from (198) that the cosine of the position angle of the Sun is proportional to $1/\cos \delta_1$, and is therefore sensitive to the declination of the source star. (A calculation using the 1-st order propagation of errors on (198) shows that a declination of 84° would give approximately 10 times the standard deviation on $\cos [\text{PnA(Sun)}]$ than that of a zero declination source). Some calculated values for the variance $\sigma^2 [\text{PnA(Sun)}]$ are given later for various source star declinations.

(ii) The position of the Sun is also known accurately. However, for long observations spread over several days, the Sun position will move in the sky, and the use of an average R.A. and Dec. for the Sun can introduce larger errors than its simple positional error at any one time. For example, during an observation interval of a week the Sun can move

$\approx 7^\circ$ in R.A. and about as much in declination. For Ariel-V observations, a rough estimate of the error on the average determined Sun position for an observation of ≈ 50 orbits is $\approx \pm 2$ orbits, which corresponds to $\pm 0.14^\circ$.

(iii) It can also be seen from (198) that the cosine of the position angle of the Sun is also proportional to $1/\sin b$ and is therefore sensitive to the angular separation between the source and Sun. Fortunately, with the Ariel-V satellite this effect was unimportant, as power constraints for the satellite prevented pointing directions closer than 45° to the Sun (see § 3.1).

Some approximate calculations appropriate to Ariel-V observations were made, using first order propagation of errors theory on (195) and (198), where the following positional errors were assumed

$$\text{Star: } \sigma(\delta_1) = \sigma(\alpha_1) = 0.01^\circ$$

$$\text{Sun: } \sigma(\delta_2) = \sigma(\alpha_2) = 0.14^\circ$$

and where b was taken at the minimum separation distance allowed for the Ariel-V satellite of 45° . The results of these calculations, for sources of various declinations, are presented in Table 4.2.30, where it can be seen that the obtained standard deviations are small compared to the dominant term due to $\sigma(\emptyset)$. [Also, by using the correct value of b for an observation the tabulated errors can be reduced further. For example, an observation of the Crab Nebula (where $\delta_1 \approx 20^\circ$) with b larger than the minimum and, say, $\approx 50.5^\circ$, reduces $\sigma[\text{PnA}(\text{Sun})]$ from 0.7 (predicted approximately by Table 4.2.30) to 0.4.]

Table 4.2.30

Approximate values for the standard deviation on a measurement of the Sun position angle PnA(Sun) with the Ariel-V satellite.

(Assume number of orbits analyzed ≈ 50 , $b = 45^\circ$, $\sigma(\delta_1) = \sigma(\alpha_1) = 0.01^\circ$, $\sigma(\delta_2) = \sigma(\alpha_2) = 0.14^\circ$).

δ_1 Star Dec.	cos(Star Dec)	σ [PnA(Sun)] (degrees)
80	.173	3.6
70	.342	1.8
60	.500	1.3
50	.643	1.0
40	.766	0.8
30	.866	0.7
20	.940	0.7
10	.985	0.6
0	1.000	0.6

§ 4.2.4e Computer Program RUNPOL

This computer program performed the main tasks of the polarisation analysis, and was designed to take as input the results from the computer summation of the raw data via the SUNSEC1 program. RUNPOL incorporated the Fourier analysis program module written by Peacock (1975) plus several more modules which together, and finally, produced almost all the parameters previously discussed in this section plus many useful statistical results. A flowchart of RUNPOL is given in Fig. 4.2.23. RUNPOL'S output parameters included:-

- i) Count rates for each data set, plus their standard deviations. (Usually count rates around the orbit if sun-sector data sets are input.)
- ii) The modulation amplitudes and phases, plus their standard deviations (as discussed in b).
- iii) Degrees of polarisation and position angles, plus their standard deviations; where this output assumed that
 - a) no background or other 2nd harmonic, spurious modulations were present in the data (i.e. only for those cases discussed in § 4.2.4c(i)),
 - and b) that the modulation factor m was unity. (This condition is relatively unimportant, since for cases where $m < 1$, the true value of p_L can be obtained via the simple relation (185).

This output required the background count rate to be input for the data set. For the Ariel-V data where condition (a) did not hold, the method described in § 4.2.4c(ii) was used to obtain the degree of polarisation and its position angle.

- iv) Statistical quantities, such as:-
- a) The expected modulation amplitude simply due to statistical fluctuations in the data, and the probability of only statistical fluctuations causing the observed modulation.
 - b) Chi-square fit values of the modulation at the satellite rotation frequency, and also at that frequency plus the modulation at twice that frequency. (This provided an estimate of the likelihood of any significant modulations existing in the data at higher frequencies.)
- and
- c) Minimum Detectable Polarisation values (which give the best polarisation sensitivity obtainable from the data with that particular input background count rate). [See § 4.2.3b for the evaluation of these statistical parameters.]

The input data for RUNPOL include the Source Cards and 'n' sets of counts/satellite rotation angle, where for each data set the observing time on the source and background must be supplied. Supply of background count rates for each data set was made optional. If 'n' was set to 11 then RUNPOL accepted the output data set from the SUNSEC1 program.

RUNPOL automatically produced the above output parameters for each single data set, and finally separately summed all the data sets containing 'only' background counts (those containing not more than a specified percentage of time on the source) and similarly for those source data sets (containing not less than another predetermined percentage of time on the source) and then analysed these summed (background) and (source + background) data sets as if they were simply two further data sets. Analysis of these two summed data sets, therefore, produced the maximum statistical sensitivity obtainable from the data.

(Usually, if the input data was from the SUNSEC1 program, the results from the single data sets were used to study background variations around the orbit, and the summed data, because of the reduction in the statistical errors, was used to extract the polarisation parameters, whether by the method described in § 4.2.4c(i) or (ii)).

§ 5	<u>OBSERVATIONS AND RESULTS</u>	
§ 5.1	OBSERVING PROGRAM	197
§ 5.2	PRELIMINARY OBSERVATIONS	199
	1) Modulations in the Background Data	199
	2) Estimation of Background Contribution	207
	3) Source to Background Count Rate Ratio, and Polarisation Sensitivity	208
§ 5.3	1975 SCO X-1 POLARISATION SEARCH	209
	1) Description of the Observation	210
	2) Data Analysis and Results	210
	3) Conclusions and Discussion	227
§ 5.4	CRAB NEBULA POLARISATION OBSERVATION	229
	1) Description of the Observation	229
	2) Data Analysis and Results	230
	3) Discussion and Conclusions	243
§ 5.5	A0620-00 (MON X-1) POLARISATION SEARCH	247
	1) Observation Plans	247
	2) Description of Observation	248
	3) Data Analysis, Results and Conclusions	250
§ 5.6	1976 SCO X-1 POLARISATION SEARCH	253
	1) Description of Observation	253
	2) Data Analysis and Results	254
	a) 'Source + Background' Parameters	254
	b) Background Count Rate Estimate	257
	c) Background and Other Spurious Modulation Estimates	259
	d) Calculation of the Polarisation Parameters for the Source Sco X-1	264
	3) Interpretation of Result	266
	4) Discussion and Conclusions	267

§ 5.1 OBSERVING PROGRAM

Since six experiments were carried aboard the Ariel-V satellite, most having their own separate observing requirements (e.g. sources for observation, desired spin-axis offsets, dates and durations of observation), a system for sharing the available observing time was adopted.

The satellite itself also provided further observing constraints (see Peacock 1975). These included:-

- i) An estimated satellite lifetime of about 1 to 2 years.
- ii) Fuel limitations; restricting spin-axis manoeuvres to approximately 6000 degrees.
- iii) Power constraints (see § 3.1), which prevented pointing the satellite spin-axis to within 45° of the Sun or anti-Sun direction. This meant that circular regions of the sky could not be observed, and that these would move periodically around the sky once a year following the apparent motion of the Sun.
- iv) The satellite spin-axis could also not be pointed to within 5° of the Moon.
- v) The power constraints also limited the observing program in an additional way, since the experiments were only powered in the sunlit portion of the satellite's orbit. During part of the orbit the area of sky in the spin-direction may be occulted by the Earth (depending on the spin-axis declination), although if this part of the orbit occurred when the spacecraft was in eclipse no observing time would be lost. However, in general, any given direction from the satellite had associated with it a 'visibility' factor defined as the percentage of the sunlit time which was not occulted by the Earth, and this varied from \approx 30 to 100%. (Thus, the maximum observing time gained per orbit

would be when the visibility was 100%.)

These satellite observing constraints and visibility factors were computed for each individual X-ray source by the U.K. control centre at Slough, and outputs provided to the experimenters. Then, by reference to these outputs, an observation proposal could be checked for viability and merit within the framework of the above observing constraints. Suitable observations could then be forwarded to the periodically held (\approx monthly) 'observing program' meetings (which consisted of representatives of all the concerned experiments and of the Slough Ariel-V control centre), where they might then be adopted into the satellite observing program.

Fortunately, the experiment-D observing priorities before launch consisted of only a limited number of strong sources (see § 4.2.3b) which appeared likely candidates for either line emission or polarisation studies, and although the required observations were relatively long, (\approx 10 days), no serious difficulties were encountered with the observing program for these few sources.

§ 5.2 PRELIMINARY OBSERVATIONS

Analysis of data from about the first 6 months' observations with the Ariel-V polarimeter provided information on the instrument performance, discovered spurious unexpected modulations in the data, and provided some guidelines for better, future, observing use of the instrument.

Information for this section is derived partially from Peacock's (1975) thesis, where a data example from an observation of Cygnus X-3 between 1st to 6th November 1974 is reproduced in Figs. 5.2.1 and 2. The graphite crystal was set to a Bragg angle of 45° , the LiF crystal to 28° , and 67 orbits data were included in the analysis. Further information was provided by Martin Ricketts (private communication, 1976) who analyzed a lot of the early and later data, especially with regard to background variations (see also Griffiths et al., 1976a), and from some data analyzed by myself presented in Figs. 5.2.3, 4 and 5.

Some of the main features revealed by this early data (and also evident in the later data presented further on) included the following:-

§ 5.2.1 Modulations in background data

(1) The total count rate in the detectors was observed to vary around the orbit (even after removal of noisy data arising from nearby the South Atlantic Anomaly).

This modulation is shown in Peacock's Cyg X-3 data illustrated in Fig. 5.2.1b, where the orbit blocks are $22\frac{1}{2}^\circ$ wide and centred about the sub-solar point. The Earth occulted the view to Cyg X-3 for just over 4 of the orbit blocks. However, the large increase in observed count rate in the LiF data was not attributed to Cyg X-3, since the increase in count rate was spread over 90° of the orbit and was not a sharp transition such as would be expected from occultation of a point source. Furthermore, the increase in the LiF count rate was a factor of over 30 more than would

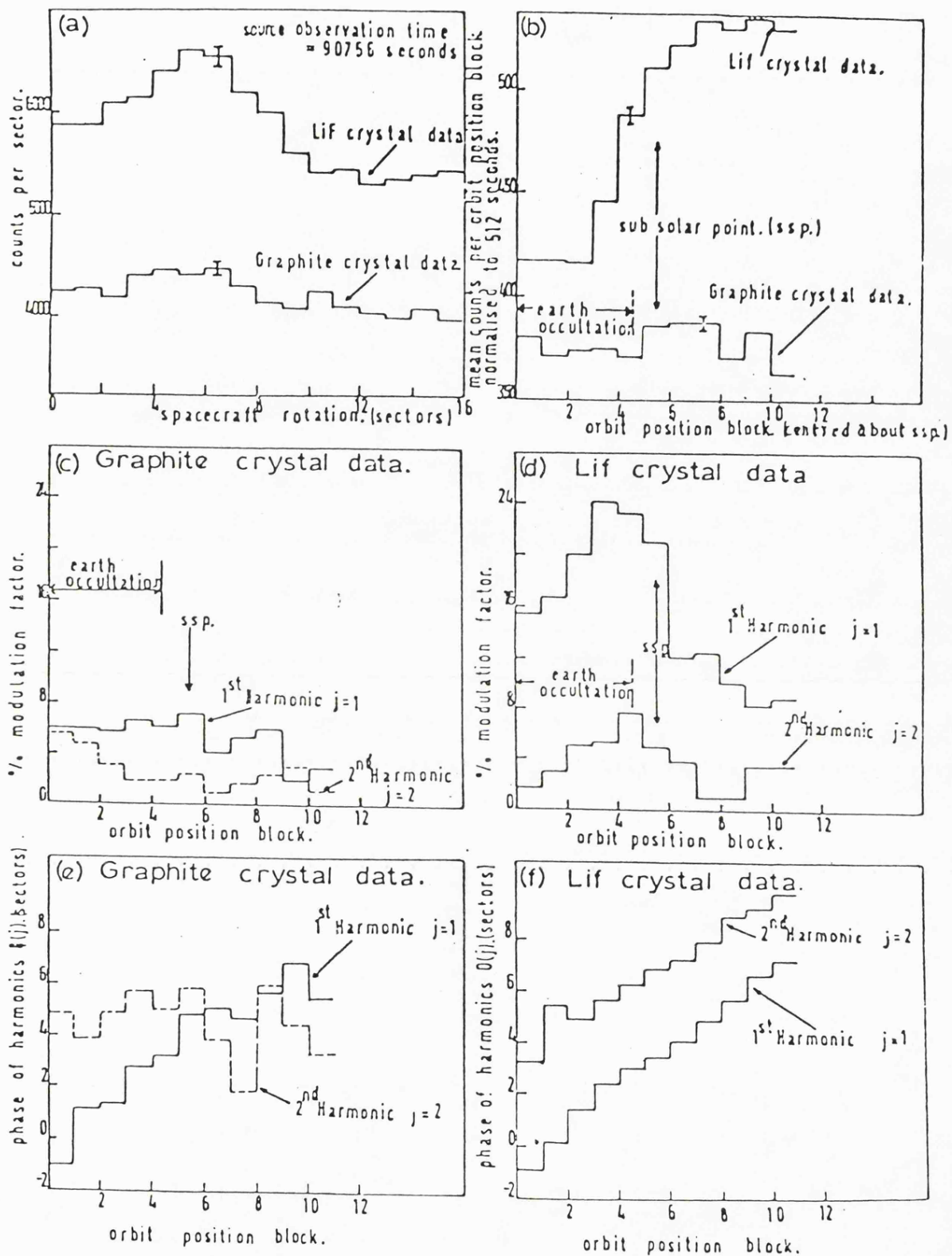


Fig. 5.2.1: Cyg X-3 data Modulation Analysis (from Peacock 1975).

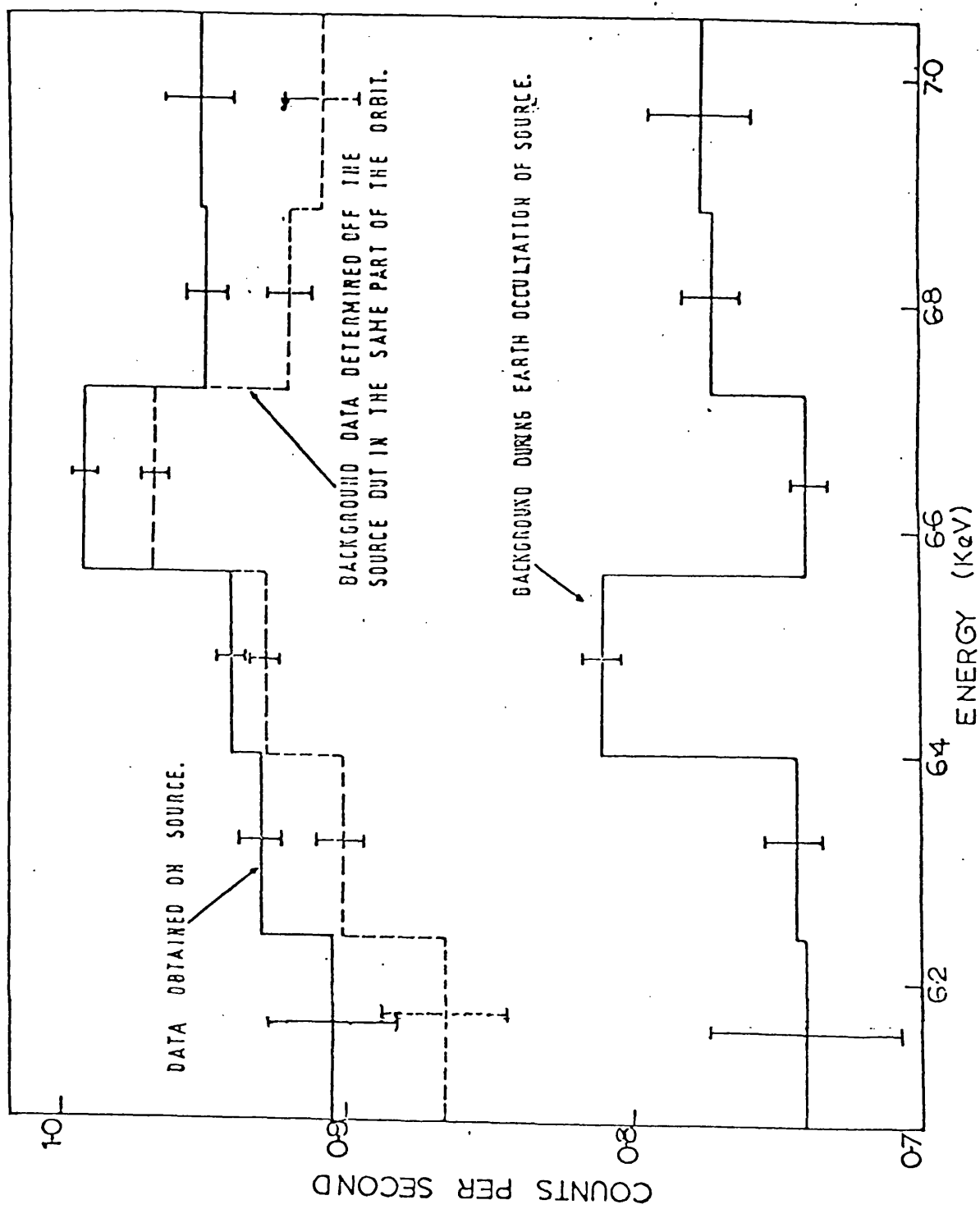


Fig. 5.2.2: Cyg X-3 data: LiF Crystal Spectrometer Analysis (from Peacock 1975).

be expected due to Cyg X-3 in its high state. Peacock therefore concluded that this variation in count rate around the orbit must be attributed to the background and not Cyg X-3.

This viewpoint of the background count rate varying around the orbit was enhanced by an analysis of graphite crystal data obtained from 1974 November 21st to 23rd, consisting of a summation of 12 orbits data (orbit numbers 566-580), whilst the spin-axis was pointed to within about 3° of the North Galactic Pole (Spin-axis R.A. (1950) ≈ 194.3 , Declination ≈ 26.3). The graphite crystal was set to a Bragg angle of $\approx 45^\circ$, and the experiment was in 'Time' mode (see § 3.2.5) especially designed for such background studies - the orbit data being collected into separate 64s time blocks. Fig. 5.2.3 shows the resulting, sinusoidally appearing modulation. (This data was summed approximately in Earth longitude blocks, rather than by the Sun direction, and hence the position of the South Atlantic Anomaly is shown by the gap in the data.

The results of analysis of additional, purely background data, obtained from both the graphite and LiF crystal systems during 1974 December 7th to 11th, whilst the experiment axis was pointing to R.A. (1950) $\approx 168^\circ$ and Declination $\approx -14^\circ$ (henceforth called the 'B-position'), is presented in Fig. 5.2.4. For both this graphite and LiF data, Bragg angles set at 44.6° and $\approx 45^\circ$ respectively, the modulation is small but noticeable, somewhat similar to the Cyg X-3 graphite data. The experiment for this B-position observation was in the normal 'CRYSTAL' mode which divided the data into 512s time blocks. Summation of the data into orbit blocks was performed via the standard sun-sector division method (see § 4.2.4) giving 20° wide blocks, and 40 orbits 808 to 867 were analyzed.

Data obtained from the graphite crystal whilst the experiment axis was pointing at a mean offset of 3.7° from the source GX5-1, and presented in Fig. 5.2.5, also shows similar slight modulation behaviour.

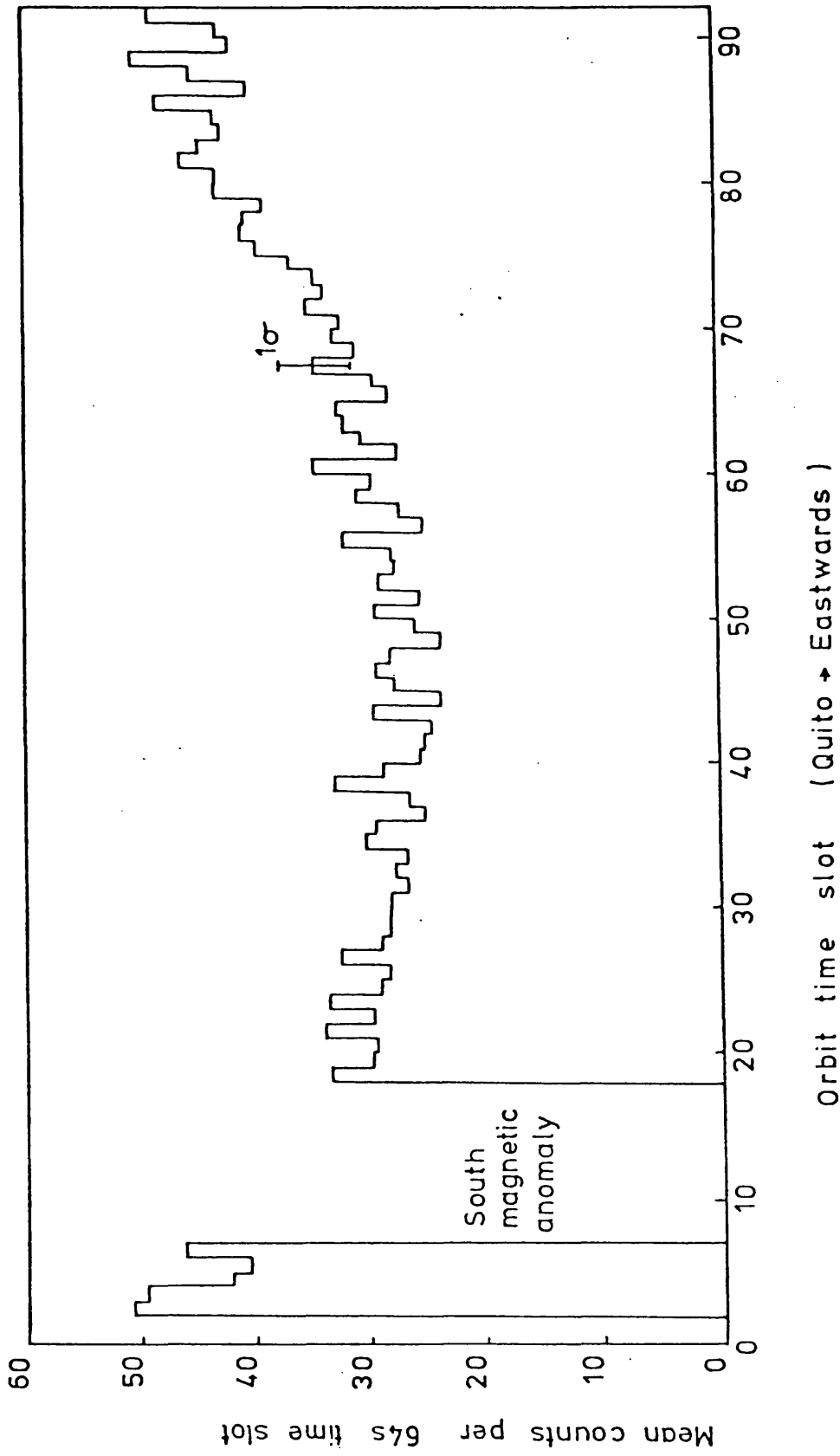


FIG. 5.2.3: Ariel-V Polarimeter background Counting Profile whilst Pointed at the North Galactic Pole. (Observation 1974 Nov. 21 to 23).

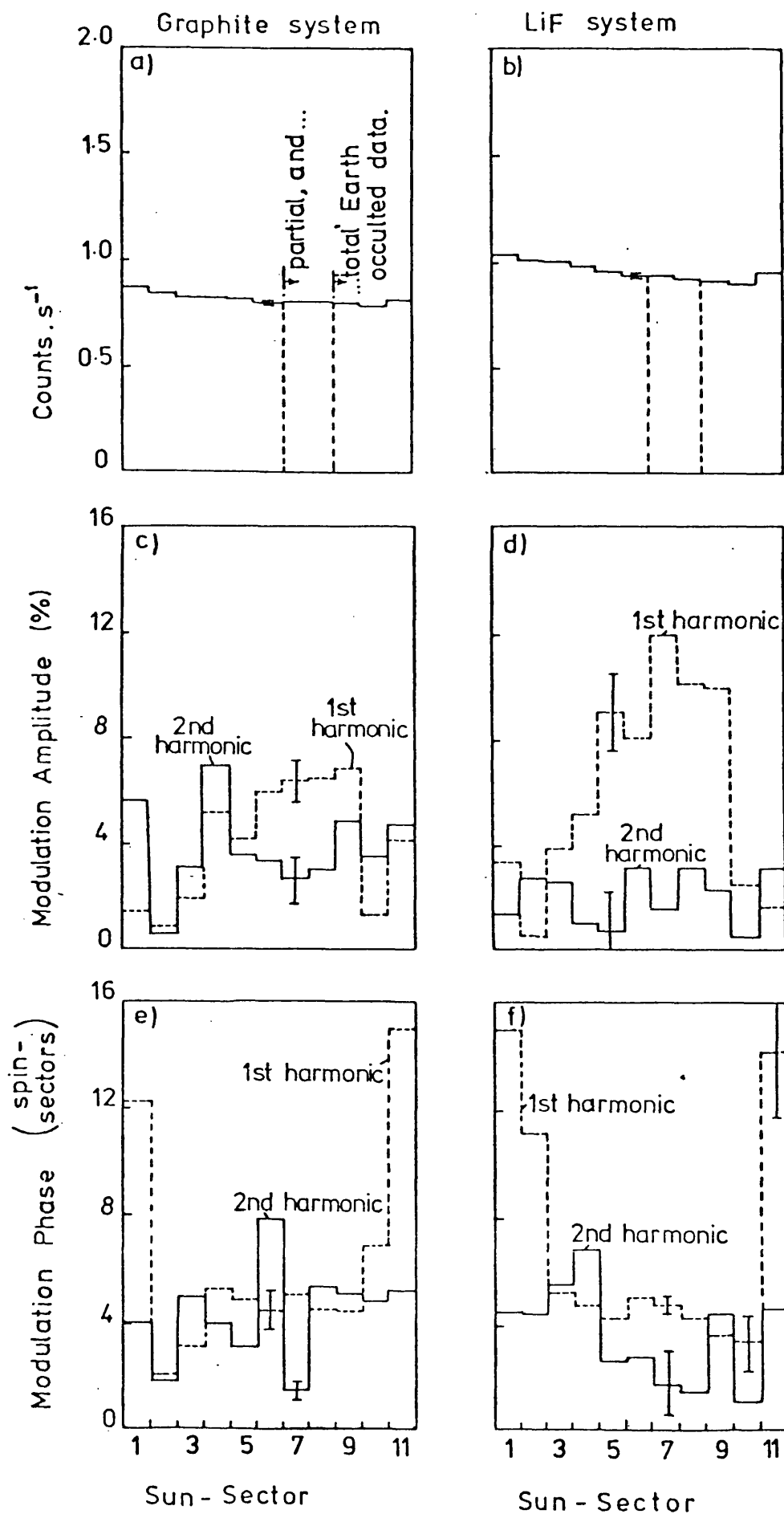


Fig. 5.2.4: Ariel-V Polarimeter background data whilst pointed at B-Position (R.A. \sim 168° , Dec. \sim -14° . Observation 1974 Dec. 7 to 11. Some typical $1-\sigma$ error bars given.)

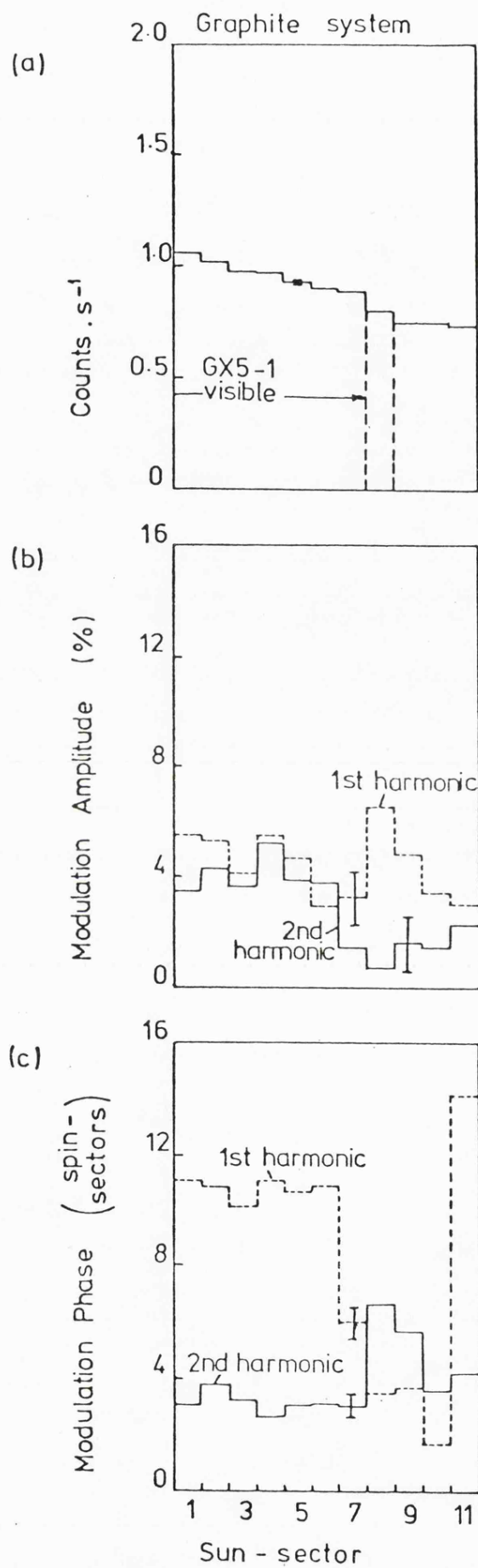


Fig. 5.2.5: Ariel-V Polarimeter data from an observation of GX5-1 from 1975 Feb. 24 to March 1. (Estimated 1- σ error bars given.)

This observation was from 1975 February 24th to March 1st, the pointing axis was R.A. (1950) $\approx 269.5^\circ$ and Declination $\approx -25^\circ$, θ_B was 44.6° , and 69 orbits from 2000 to 2081 were analyzed.

(ii) The detector background count rates were also observed to vary with the rotation angle of the satellite.

This variation was especially important since a modulation in the background at twice the satellite rotation frequency could be mistaken as due to source polarisation (see § 4.2.3c).

Peacock's Cyg X-3 data shows strong variations at the rotation frequency (1-st harmonic) and at twice that frequency (2-nd harmonic). The 2-nd harmonic modulation was observed to be weaker than the 1-st, and the modulations also observed to be weaker in the graphite data. For the graphite data these rotation modulations were typically 6% and 2% for 1-st and 2-nd harmonic modulations respectively. For the LiF data the 1-st harmonic modulations ranged from (8 to 24)% and the 2-nd harmonic modulations from (2 to 8)% (see Figs. 5.2.1c and d). These modulations also had phases which appeared to vary linearly with the satellite position around the orbit (see Fig. 5.2.1e and f).

These variations in degree of rotation modulation and phase around the orbit could also be seen in the B-position background data depicted in Figs. 5.2.4c, d, e and f, and in the GX5-1 data shown in Figs. 5.2.5b and c.

(iii) It was also noted (Peacock 1975, Griffiths et al., 1976a), that the background modulations appeared to be a definite function of the spin-axis declination.

A successful and reasonable model which could account, at least in part, for the above background modulations was developed (see Griffiths

et al., 1978a). This was based on the fact that the polarimeter was located asymmetrically with respect to the centre of mass of the spacecraft. Then, albedo neutrons travelling radially outwards from the Earth's atmosphere, and interacting with the satellite mass, would form a directional source of gamma-rays within the vehicle with respect to the polarimeter location. These gamma rays would then be detected by the experiment as primarily a modulation at the spin-frequency of the satellite. Modulations around the orbit could also be generated in this way, and the modulation differences which were found to be a function of the spin-axis declination. (Ricketts applied this model to much of the early data with a fair amount of success using only simple assumptions. It was noted, though, that provision of more realistic parameters such as non-radial neutron directions, a more accurate satellite mass distribution and asymmetric sensitivity parameters of the particle detectors and rejection systems, could possibly account for much more of the observed effects with greater accuracy.)

§ 5.2.2 Estimation of Background Contribution

Although the variation in background count rate around the orbit in Peacock's Cyg X-3 LiF data was shown to be large (see § 5.2.1), giving a grossly overestimated signal count rate by using a comparison between the occulted background data and un-occulted 'signal + background' data, it would be seen that by taking the background from the same part of the orbit, but from a different spin-axis position off the source, the signal estimate from Cyg X-3 was greatly improved (see Fig. 5.2.2). However, the calculated change in count rate through the occultation region for the Cyg X-3 graphite data (for which the background count rate variation with sun-sector was observed to be much less than that for the LiF data) did not show the same discrepancy, and was consistent with that predicted due

to Cyg X-3 in its high intensity state (Peacock 1975).

§ 5.2.3 Source to Background Count Rate Ratio, and Polarisation

Sensitivity

The low signal to background count rate evident in the above Cyg X-3 graphite data (Fig. 5.2.1b), combined with the limited duration of the observation (≈ 5 days), resulted in a calculated minimum degree of polarisation which could be detected from the data of about 100% at 3-sigma confidence (Peacock 1975), (i.e. the calculated M.D.P. ($3-\sigma$) value was 100%). This emphasised the need for greater signal to background ratios or/and the necessity for the longer predicted observing times (see § 4.2.3b).

Further information concerning the polarisation sensitivity of the Ariel-V instrument follows.

§ 5.3 1975 SCO X-1 POLARISATION SEARCH

This observation was carried out during the early part of the observing program before many of the preliminary results were known. It was planned to provide a polarisation result on Sco X-1 much more sensitive than the two previous (rocket) observations had managed to achieve (see § 2.2.2), and also to provide information concerning the best way to use the instrument as a polarimeter.

The Sco X-1 data was considered most appropriate to analyse first for polarisation, because Sco X-1 was by far the strongest X-ray source then observed, and would therefore have produced the highest signal to background ratio. This was considered important for a polarisation search, since it was already known that problems had been encountered by other members of the X-ray group because of the weak signals combined with spurious modulations in the background data, where both of these factors were made worse because of uncertainty in determination of the mean background level. The high signal to background ratio for the Sco X-1 data also gave advantages to its use for an initial checkout on the computer analysis programs. This was because the change in count level, as Sco X-1 came into the instrument f.o.v. out of Earth occultation, was large enough so that it could be seen by eye in the raw data. Then, by use of the 'full output format' option in the computer programs (see § 4.1.5), the output observation durations assigned to the background (which was 'experiment on-time') and signal (duration that experiment was on but Sco X-1 not occulted by the Earth) could easily be checked against the raw data. In the same way it could also be easily checked that the data was being allocated to the correct orbit (sun-sector) blocks, as the sun-sector region for which Sco X-1 was visible, or occulted by the Earth, always occurred in the same general sun-sector region.

§ 5.3.1 Description of the Observation

Sco X-1 was observed from 1975 March 1st to 4th, and 40 orbits data, from orbit numbers 2085 to 2133, were included in the analysis. The graphite crystal was set to a Bragg angle of 44.6° making it sensitive to a narrow band of X-ray energies ($\approx \pm 0.01$ keV) centred on 2.6 keV, and the LiF crystal was set to 27.9° making this crystal panel sensitive at 6.6 keV. The mean satellite spin-rate was 0.15 rev s^{-1} .

A sky map, showing the movement of the spin-axis positions previous to, during, and subsequent to the observation on Sco X-1, as well as locating the positions of all the nearby known X-ray sources, is shown in Fig. 5.3.1. During the observation on Sco X-1 the spin-axis was offset from Sco X-1 by an average of 3.1° . (This rather large offset was set by other experiments (Griffiths et al. 1976a).) The maximum recorded offset was 3.6° and the minimum 2.5° . This mean spin-axis offset of 3.1° caused a scan in Bragg angle equivalent to an energy scan, with the graphite crystal, from about 2.4 to 2.8 keV for the observed X-rays.

The X-ray intensity of Sco X-1 during this observation was monitored by the Ariel-V modulation collimator experiment (Experiment A) and, averaged over single orbit intervals during the 4 day observation, was observed to vary by approximately a factor of 3 (Skinner 1976).

§ 5.3.2 Data Analysis and Results

Only the graphite crystal data was used for a polarisation search since its set Bragg angle θ_B of $\approx 45^\circ$ meant that its modulation factor m would be almost unity, thus making this data much more sensitive to polarisation (see § 4.2.2b) than the LiF data for which θ_B was set to 27.9° making $m \approx 0.5$.

This graphite data was summed as a function of orbit position, and the count rates obtained for each sun-sector are displayed in Fig.

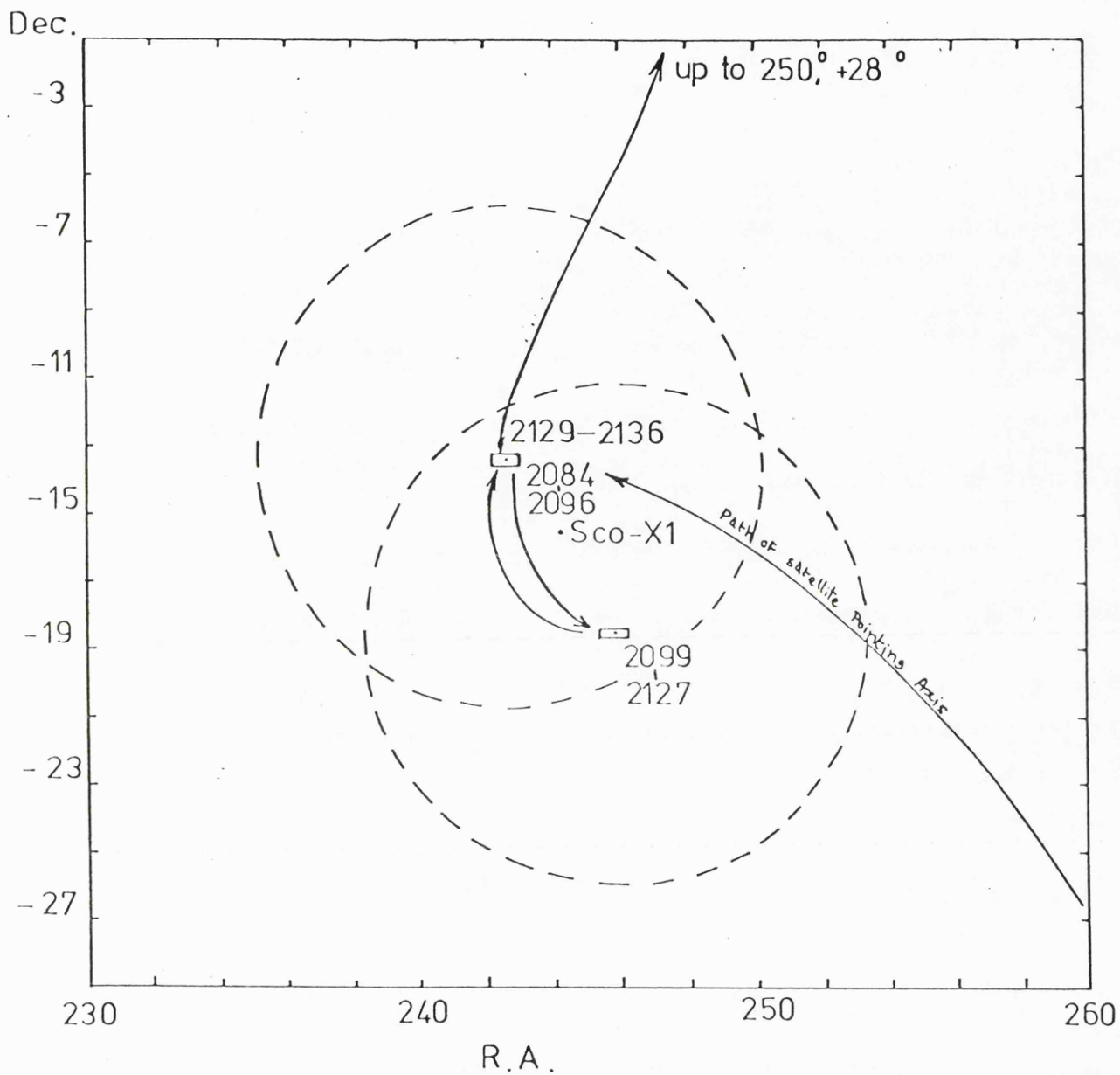


Fig. 5.3.1: Sco X-1 Sky Grid; 1975 Observation.
 (The dashed circles enclose that area of sky about the spin-axis pointing direction for which the theoretical collimator transmission function $T(\Delta)$ is greater than zero.)

5.3.2b. In the sun-sector region S8 to S11, where Sco X-1 was completely eclipsed by the Earth, a mean background count rate of $B'_o = 0.8124 \pm 0.0043$ counts s^{-1} was measured. The count rate due to X-rays from Sco X-1 is represented only approximately by the increase in count rate from the (S8 to S11) region to the (S1 to S5) region, where Sco X-1 was then in full view of the instrument f.o.v., since it was already known from the preliminary results that the background count rate varied with sun-sector.

The intermediate count rates recorded in S6 and S7 arose from time block data containing the occultation transition, so that only a fraction of the observing time was spent on Sco X-1. These intermediate count rates were spread over more than one sun-sector due mainly to 'digitisation' error in assigning data collected according to time blocks to a specific sun-sector.

The graphite data from S1 to S7, for which Sco X-1 was observed for an appreciable fraction of the total observing time, was summed as a function of satellite rotation angle and is shown in Fig. 5.3.2a.

Polarisation of the X-rays from Sco X-1 should then be evident in this summed data as a sinusoidal modulation at the 2-nd harmonic frequency.

The background level is given by $B = \frac{B'_o T_b}{16}$ (counts spin-sector $^{-1}$)

where the total observing time recorded on the background was calculated as $T_b = 74,862 \pm 50$ s.

To obtain an improved background estimate B_o , which would supersede B'_o , for this (S1 to \approx S7) region, an empirical analysis of the background count rate variation with sun-sector was undertaken.

Examination of count rates obtained from S1 to S5, revealed a small increase in a direction away from the (S8 - S11) region where B'_o had been measured. However, this increase could be due to either background variations, or perhaps intensity variations of the X-ray flux

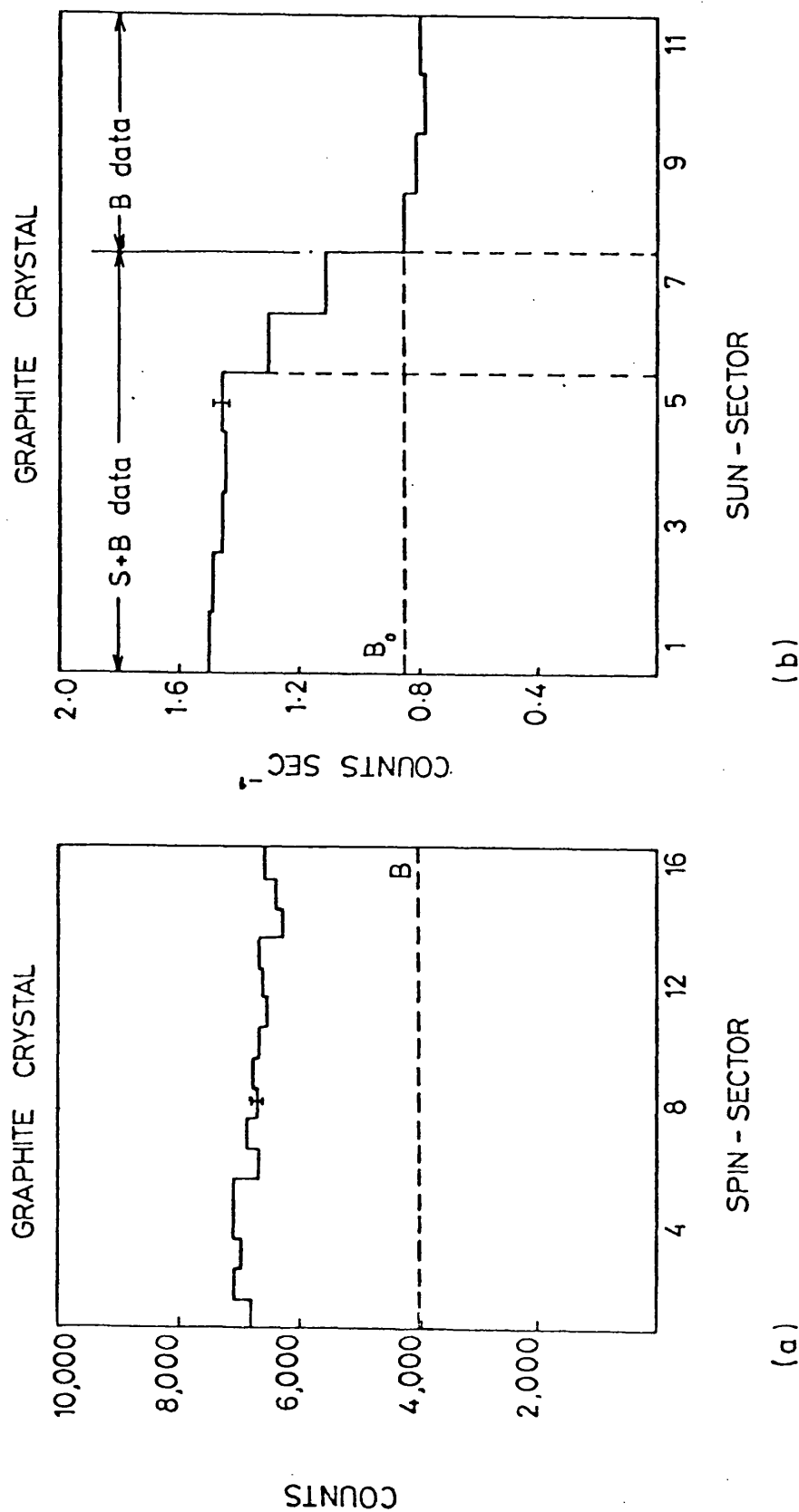


Fig. 5.3.2: Ariel-V polarimeter data obtained from an observation of ScO X-1 from 1975 March 1 to 4. (The dashed lines indicate the estimated background contribution.)

from Sco X-1. A similar count rate increase, though, was also found from analysis of the GX5-1 data and the purely background B-position data previously mentioned, therefore strongly indicating the increase to be due to a background variation. [The B-position and GX5-1 data were selected because, (i) the declinations of these two sources are similar to that of Sco X-1 and therefore the background characteristics were more likely to follow those of Sco X-1 (see § 5.2.1 (iii)), and (ii) because the graphite crystal positions were identical with that used for this Sco X-1 observation, which meant that the same geometrical configuration of the instrument would be presented to background radiation.] Then, allowance for this small gradual increase in count rate from sun-sector S7 to S1, interpreted as being due to the background, raised the estimated background count rate B_0 for this region to 0.8419 ± 0.0105 counts s^{-1} .

A further background component, which could also be allowed for, was the small expected count rate component due to the diffuse X-ray flux (see § 3.2.4). This background component would be expected to occur only in the same data (S1 to \approx S7) for which Sco X-1 was observed, since the polarimeter f.o.v. to the sky would be unobscured by the Earth for this region. Also, a further difference in count rate for the two regions (S1 to \approx S7) and (S8 - S11) is similarly possible, due to any other anisotropy in background environment which could arise from the experiment pointing towards or away from the Earth for these two regions. These diffuse X-ray flux and possible anisotropy effects were estimated from an examination of the B-position data, which, from a simple comparison of count rates from the completely un-occulted S5 region and occulted (S9 - S11) regions, revealed a minor increase ΔB_0 estimated at 0.016 ± 0.016 counts s^{-1} for the region where the f.o.v. was not occulted. (This small value ΔB_0 was also consistent with that predicted from the diffuse X-ray background (see § 3.2.4), although the relatively large error on ΔB_0 did

not make this a sensitive comparison).

Then, addition of this small component of background ΔB_0 to the previous estimate, gave a final value of B_0 as 0.8579 ± 0.0191 counts s^{-1} .

From this background information and determined mean value of counts spin-sector⁻¹, obtained from Fourier analysis of the data on Sco X-1 summed as a function of satellite rotation angle (see Table 5.3.3), the sensitivity of the observation was calculated as a 3-sigma Minimum Detectable Polarisation (M.D.P.) of 3.7% (assuming the modulation factor $m \approx 1$ for $\theta_B \approx 45^\circ$. See § 4.2.2b). This meant that, under ideal conditions where no spurious modulations occur in the data, a degree of polarisation as low as $\approx 3.7\%$ could have been detectable from Sco X-1 at the 3-sigma confidence level.

The measured modulation at the 2-nd harmonic polarisation frequency, with the mean background subtracted out, was $M_{obs} = 4.78 \pm 1.45\%$, and included any spurious modulation effects such as previously experienced from the preliminary observations. The χ^2 -value of 20.3 with 11 degrees of freedom, which resulted from fitting a mean, a 1-st harmonic and the 2-nd polarisation harmonic to the data, was rather high for the errors from this fit to be assumed to have a Gaussian distribution. This suggested that some spurious modulations also existed in this Sco X-1 data, (although a low χ^2 -value could not have excluded spurious modulations at either the 1-st or 2-nd harmonic frequency). Then the actual degree of polarisation of Sco X-1 could only be inferred from the measured 2-nd harmonic modulation, when the spurious modulations had been estimated and allowed for.

To estimate the spurious modulations, their sources of origin were divided into 2 main groups; (i) the background environment and (ii) point, or localised sources of unpolarised X-rays (see § 4.2.3c).

Table 5.3.3: Results of Fourier and statistical analysis of the Sco X-1, graphite crystal, summed data, from the observation of 1975, March 1 to 4.

χ^2	M	AOBS	M.D.P.	M_{obs}	$\sigma(M_{\text{obs}})^*$
11 d.o.f.	Counts spin-sector ⁻¹	Counts	(3- σ)% (Assuming $m \approx 1$)	%	%
20.3	6715.6 \pm 20.3	129.4	3.7	4.17	1.45

* Calculated using a regression method on the observed data.

i) Spurious modulations from the background environment

Since no purely background data was available from this observation for the sun-sector S1 to S7 region where Sco X-1 was observed, then background modulations for this region were approximately inferred from data taken outside this region and from other observations. From the preliminary results previously discussed, it had already been observed that the background modulation amplitudes and phases varied with sun-sector. Therefore, the background modulation of $2.34 \pm 1.51\%$ (at the 2-nd harmonic frequency) obtained from the combined (S8 to S11) data from this Sco X-1 observation, might be nothing more than a very crude estimate for the region where Sco X-1 was observed. For this reason background modulations from other observations were also determined, and these are given in Table 5.3.4. (The modulations given in this table, except where stated, were determined by averaging the modulations determined from Fourier analysis of the single sun-sector data blocks, and the errors given were calculated from the simple distribution of the individual modulations about the average value. Background data from a later observation of A0620-00 (Mon X-1) from 1975 August 25 to 29th of orbits 4771 to 4826 is also included, although this source has a declination of -0.3° which is greater by about 14° than the other observations. The set Bragg angles for this A0620-00 observation included both $\theta_B = 49.6^\circ$ and 44.6° so that it was never more than 5° greater than that used during the Sco X-1 observation.) Examination of the 2-nd harmonic modulations given in Table 5.3.4 for the (S8 to S11) region, for all the sources involved, show that they were all consistent with a constant value, within the standard deviations given. Similarly, the two background modulations obtained for the (S1 to S6) region, for which Sco X-1 was mainly observed, are also consistent with a single modulation value. In addition the average modulation $4.04 \pm 1.06\%$ of the two (S1 to S6) values were consistent with

Table 5.3.4: 2nd harmonic modulations with satellite rotation angle, obtained from the graphite crystal panel for several Ariel-V polarimeter observations.

Dates of Observation	X-ray Source	B data only (% Modulation) (S8 to S11)	(S+B) data (% Modulation) (S1 - S6)
1975 March 1-4	* Sco X-1	2.34 ± 0.87	-
1974 Dec. 7-11	B-Position	3.98 ± 0.83	((B data only) (3.80 ± 2.07
1975 Feb. 23-28	GX5-1	1.84 ± 0.98	(So/Bo weak .08) (4.28 ± 0.52
1975 Aug. 25-29	** Mon X-1 (A0620-00)	{(S10 and S11 only) (2.84 ± 0.75	-
	Mean Values	2.75 ± 0.84	$4.04 \pm 1.06^{**}$

* Modulations obtained from averaging values obtained from Fourier analysis of combined sun-sector data units, (S8 data summed with S9 data) and (S10 data summed with S11 data).

** Standard deviations obtained using propagation of errors (see Bevington 1969), i.e. from mean modulation $M = (M_1 + M_2)/2$,

$$\sigma^2(M) = \frac{\sigma^2(M_1) + \sigma^2(M_2)}{4}$$

the average value $2.75 \pm 0.84\%$ of the (S8 to S11) values, their standard deviations being separated by little more than one standard deviation.

The modulation phases for both the graphite and LiF data of this Sco X-1 observation are shown in Fig. 5.3.5, and those for the B-position background observation in Fig. 5.2.4. However, the complexity of interpreting these variations with sun-sector prevented any similar estimation as with the degree of the modulations.

ii) Spurious modulations from point, or localised, sources of unpolarised X-rays

For this Sco X-1 observation, no source of X-rays other than Sco X-1 was in the f.o.v. of the polarimeter. (See the sky grid, Fig. 5.3.1, where dashed circles mark the boundary of the polarimeter f.o.v. when the pointing axis is at the centre of the circle. All known X-ray sources were included in the grid.)

Any spurious modulations at the 2-nd harmonic polarisation frequency due to pulsations of the X-rays from Sco X-1 would be expected to be less than 1% since Friedman et al. (1969) had placed this upper limit for periods ranging from 0.07 to 4's, which included half the spin-period of the Ariel-V satellite.

Since the polarimeter pointing direction was offset from Sco X-1 by an average of 3.1° for this observation, then spurious modulations due to this offset could arise from the unpolarised continuum flux from Sco X-1 (see § 4.2.3c).

The sky grid (Fig. 5.3.1) reveals essentially two spin-axis positions, one on either side of Sco X-1, from which all the data from Sco X-1 was obtained. Each position was offset by about 3° from Sco X-1 and approximately half the data was collected at each position. Summation as a function of satellite rotation angle of the Sco X-1 source (S1 to ~ S7) data for each spin-axis position is shown in Figs. 5.3.6a and b, where

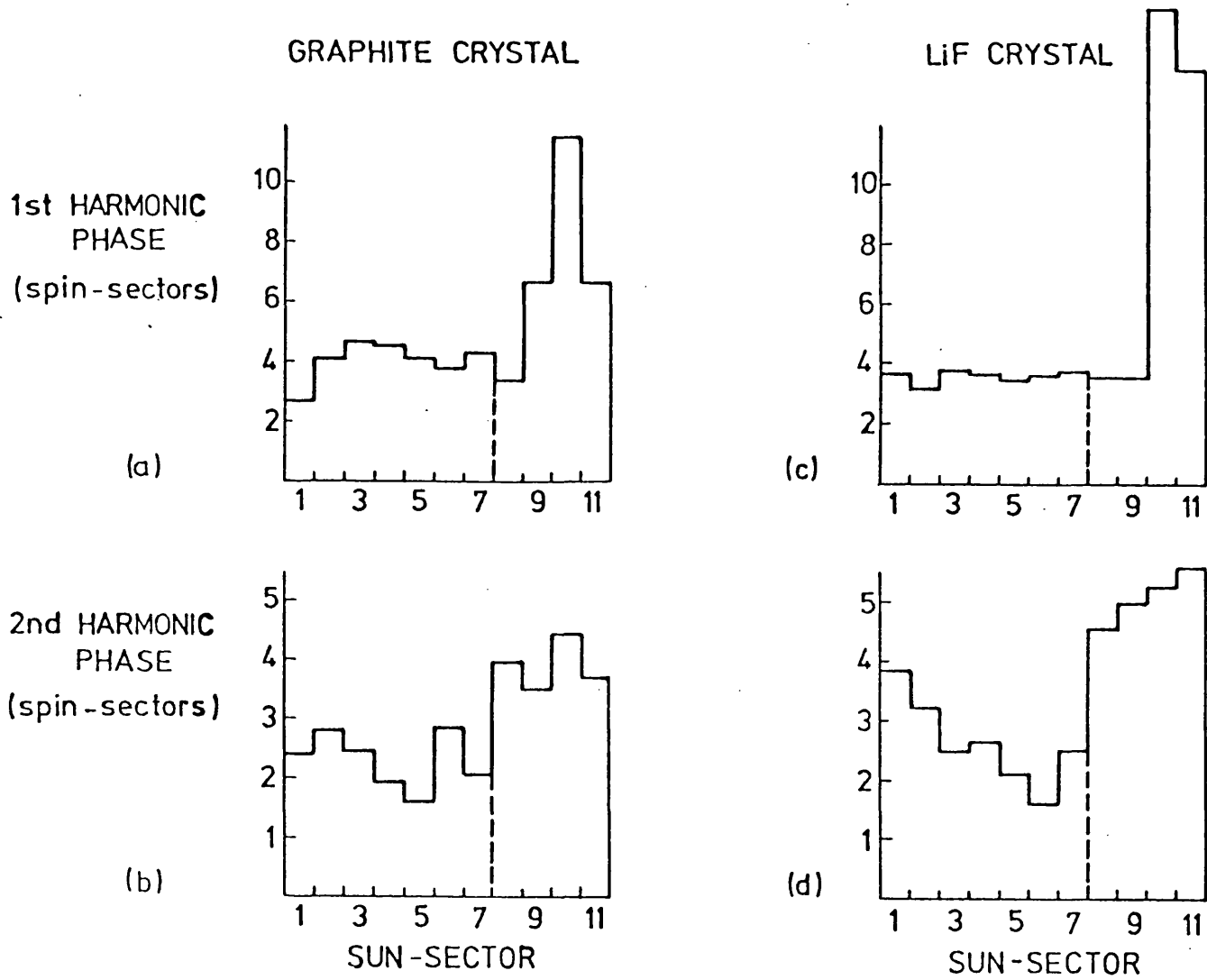


Fig. 5.3.5: Sco X-1 1975 March 1 to 4 observation; modulation phase variations with sun-sector.

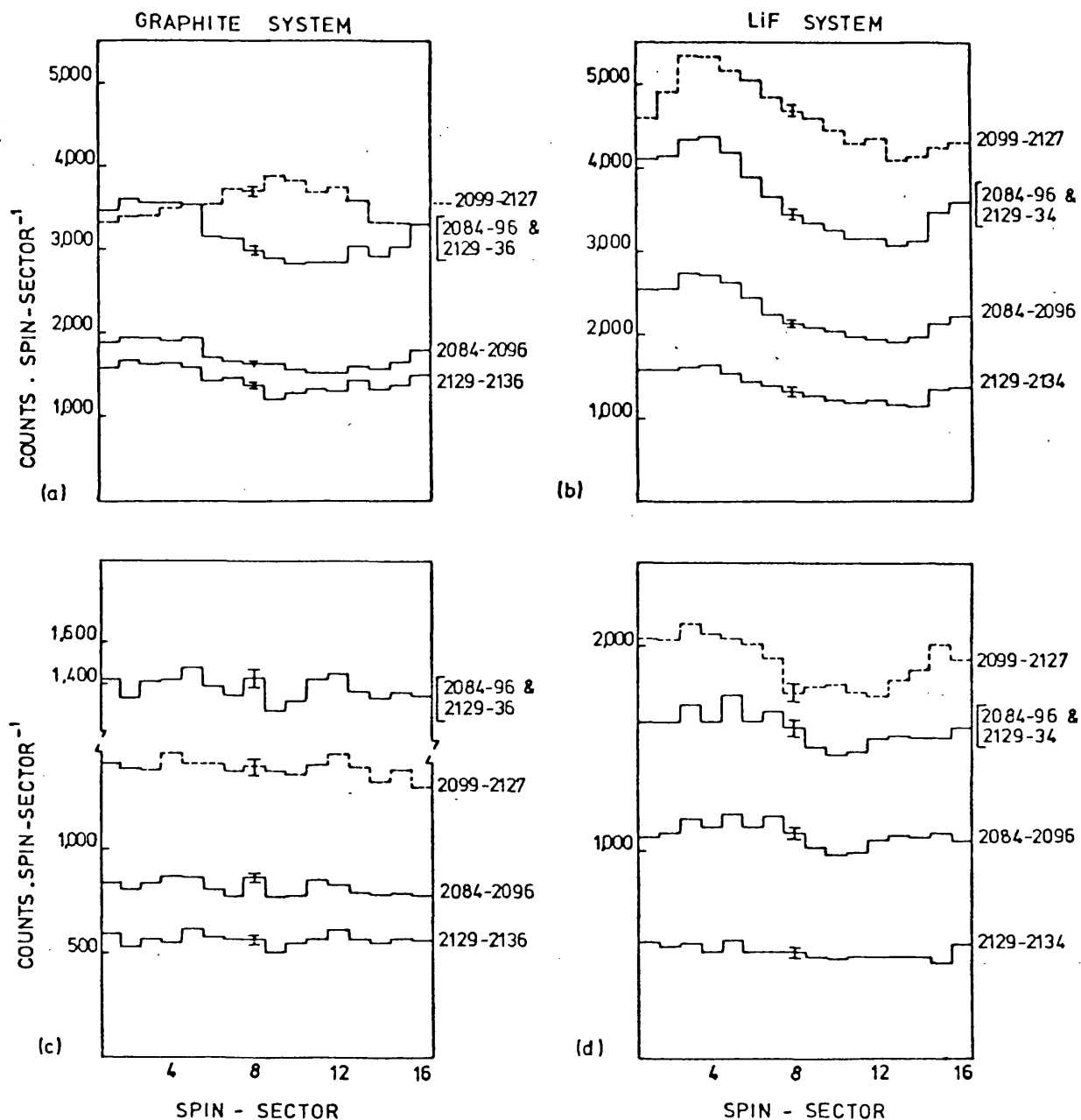


Fig. 5.3.8: Sco X-1 1975 March 1 to 4 observation; data taken from ≈ 30 offset positions on either side of Sco X-1. (See Fig. 5.3.1 to relate orbit numbers to spin-axis pointing positions. (a) and (b) are composed of sun-sector S1 to \approx S7 data, and (c) and (d) composed of sun-sector S6 to S11 data.)

analysis of this data showed a distinct change in phase of $\approx 180^\circ$ for the 1-st harmonic modulation from data taken at opposite offset positions. This phase change is expected from modulations due to variation in the instrument effective area and crystal reflectivity function $E_B R_c \cot \theta_B$ as the satellite rotates with the spin-axis offset from the source; and to spectral variation of the continuum flux as θ_B is scanned (see § 4.2.3c(i)). The observed 1-st harmonic modulation degrees in the source + background data of 8% and 12%, for orbit numbers (2099 to 2127) and (2084 - 2096 and 2129 - 2136) respectively, were in reasonable agreement with the theoretically predicted modulation of $\approx 6.3\%$ due to the above instrument and spectral effects. The predicted modulation from each individual effect for the source data alone, and the total predicted modulation, are shown in Table 5.3.7 for the case of a 3° offset. The phase angles for these observed 1-st harmonic modulations also agreed with those predicted theoretically. (Furthermore, the predicted mean count rate from the Sco X-1, also shown in Table 5.3.7, of $0.7 \text{ counts s}^{-1}$ was in reasonable accord with the observed value of $0.6 \text{ counts s}^{-1}$.)

Concerning a predicted, spurious, 2-nd harmonic modulation due to instrumental or spectral effects, the mean Bragg angle for this Sco X-1 observation of 44.6° together with an offset of 3° , meant that no significant modulation would be expected due to variation of crystal reflectivity parameters ($E_B R_c \cot \theta_B$), detector resolution, or the source spectrum. A small, spurious, 2-nd harmonic modulation estimated at $0.7 \pm 0.4\%$ would, however, be expected due to variation of the detector efficiency, and a similar effect of about 1% or perhaps less could be possible arising from variation of the collimator transmission (see § 4.2.3c). Frequency analysis of Ricketts (1976, private communication) computer simulation of the mechanics of the Ariel-V instrument (which included only effects such as variation of projected crystal area, experiment boundary and support

Table 5.3.7: Predicted count rate and instrument modulations from the graphite crystal at the satellite rotation frequency, from observation of Sco X-1 30 offset from the satellite spin-axis, and θ_B nominally set to 44.6°.

$$\text{Received flux } \frac{dN}{dt} = T(\Delta) I(E_B) E_B R_c \cot \theta_B F_n \quad (\text{ph s}^{-1})$$

where $I(E)$ (ph keV⁻¹ cm⁻² s⁻¹) is the incident source spectrum and the other terms are defined in § 3.2.

Bragg Angle θ_B	A_e cm ²	$I(E_B)^*$	E_B keV	R_c radians	$\cot \theta_B$	F_n	Predicted $\frac{dN}{dt}$ (ph s ⁻¹)	Observed (ph s ⁻¹)
min 41.6°	45	23.1	2.75	6.3×10^{-4}	1.11	0.84	0.82	
nominal 44.6°	46	25.0	2.60	5.7×10^{-4}	1.00	0.86	0.71	0.62
max 47.6°	43	27.2	2.45	5.8×10^{-4}	0.87	0.87	0.61	
1st Harmonic Modulation %	+2.8	-8.2%	+5.8%	+4.2%	+12%	-1.9%	+15%	+22%***

Notes

The value of $T(\Delta)$ was taken as $T(3^\circ) = 0.49$ from § 3.2 equation

* The Sco X-1 spectrum was obtained from Gould (1967). Then $I(E) \propto 1/E \exp(-E/kT)$ and kT was taken as 6 keV from Griffiths et al. (1976a) in agreement with that determined from the Ariel-V M.S.S.L. proportional counter experiment by White (see Griffiths et al. 1976a).

** Positive and negative signs indicate phase of the modulation (i.e. 180° phase difference between '+' and '-').

*** Modulation of source data given by $\left[(\text{Obs. Mod.}) \times \frac{(S+B)}{S} \right]$ and $\left(\frac{S+B}{S} \right)$ for the 1975 Sco X-1 observation was ≈ 2.4 .

structure, and the window stops), gave 1-st and 2-nd harmonic modulations of $4.6 \pm 0.2\%$ and $< 0.9\%$ at 3-sigma confidence respectively (see also § 4.2.3). In addition, analysis of the $\approx 3^\circ$ offset Mon X-1 observation, previously mentioned (see § 5.3.2(i)), gave a 2-nd, polarisation, harmonic modulation of $2.4 \pm 0.8\%$, just consistent with no modulation at all of the sun-sector data where Mon X-1 was observed (see Fig. 5.3.8). This Mon X-1 modulation could possibly, however, contain a significant modulation component due to background (even though S_0/B_0 is high, see Fig. 5.3.8) estimated at $1.3 \pm 0.3\%$; and perhaps some small contribution from polarisation of the X-rays from Mon X-1, which had been shown to be $< 2\%$ at 3-sigma confidence (Griffiths et al. 1976b). However, the observed 2-nd harmonic modulation from Mon X-1 did not disagree with either the instrumental, spectral, or frequency analysis predictions of the simulated experiment.

In summary, for the spurious modulations relevant to this Sco X-1 observation, a modulation in the background data of $M_b = 4\%$ and a $M_s = 1\%$ modulation of the unpolarised continuum flux from Sco X-1 would seem reasonable estimates in view of the uncertainties. Also, because of the unknown nature of the phases of these modulations for the Sco X-1 (S1 to \approx S7) data, the maximum polarisation modulation that these spurious modulations could have on the (S1 to \approx S7) background subtracted data, will be given by:-

$$M_{\text{spur(max)}} = \frac{SM_s + BM_b}{S} = M_s + \frac{B}{S} M_b \quad (1)$$

where B was given previously, and $S = M - B = 2701.5 \pm 91.7$ counts spin-sector⁻¹ was the calculated data contribution due only to X-rays from Sco X-1. M was the total mean counts observed per spin-sector⁻¹ and is given in Table 5.3.3.

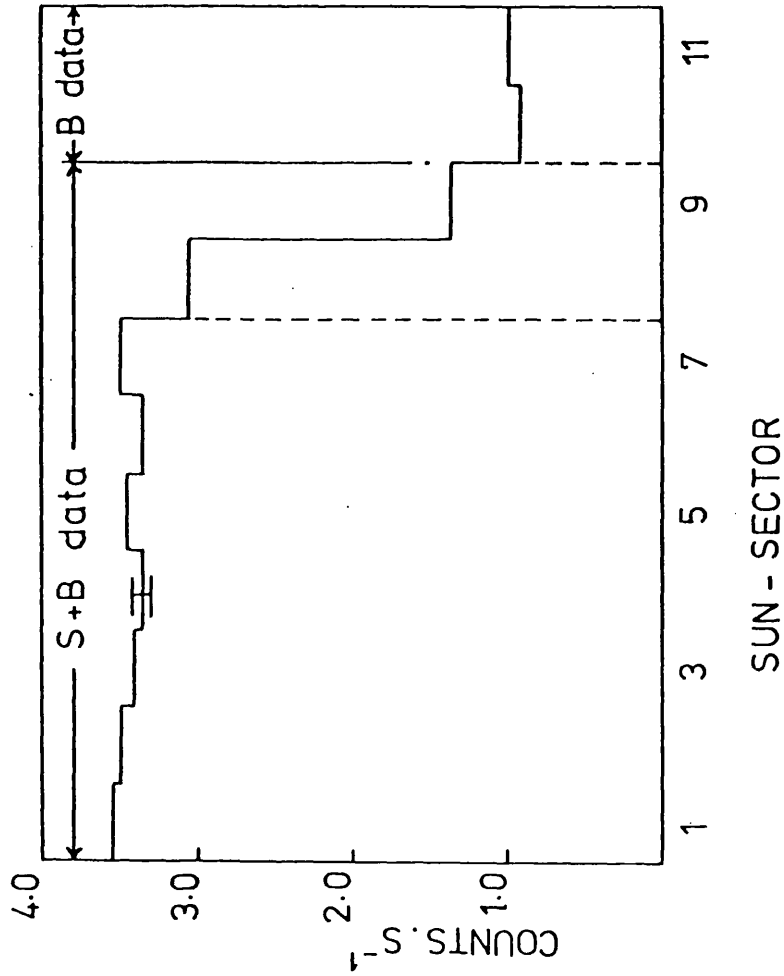
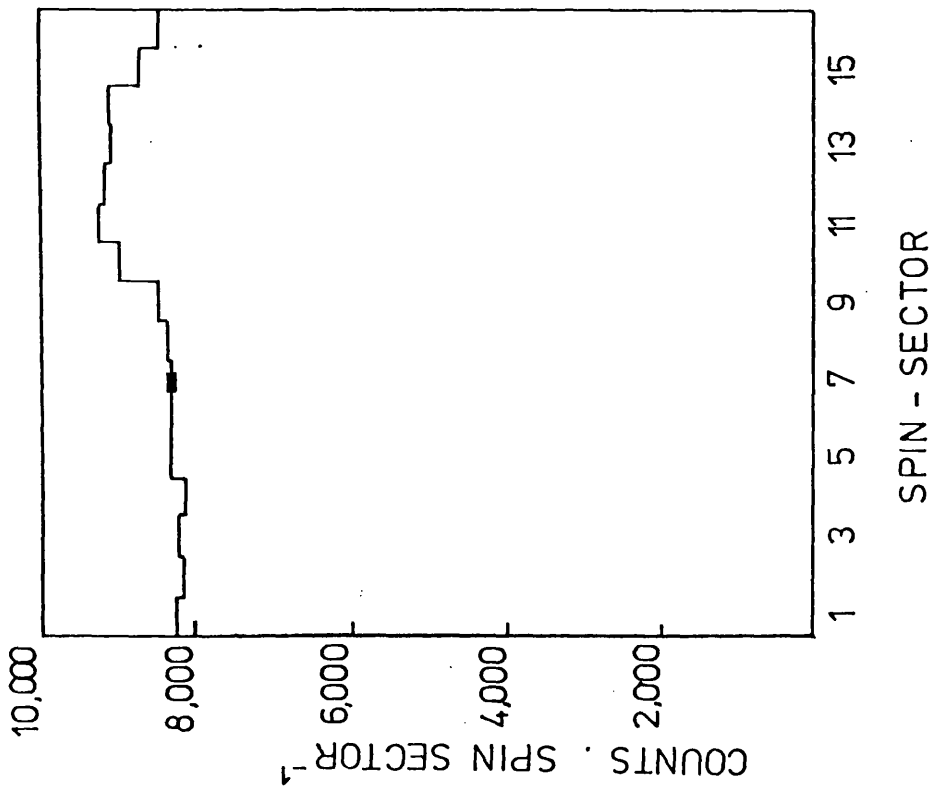


Fig. 5.3.8: Ariel-V polarimeter data obtained from an observation of Iion X-1 from 1975 Aug. 25 to 29. (Estimated 1- σ error bars are shown).

Then, using the above modulation estimates and parameters in (1), a value for the maximum modulation effect in the Sco X-1 source data $M_{\text{spur(max)}}$ of 6.9% was obtained.

Thus, (for the moment ignoring the statistical uncertainty on the measured value of M_{obs}) polarisation modulations in the Sco X-1 source data could lie within the general range:-

$$M_{\text{pol}} = M_{\text{obs}} \pm M_{\text{spur(max)}} \quad (2)$$

i.e. $-2.2 \leq M_{\text{pol}} \leq 11.7\%$, where it can be seen that the range of values M_{pol} includes zero modulation, consistent with Sco X-1 being an unpolarised X-ray source.

An upper limit to the polarisation modulation, which includes the statistical uncertainty on the measured value of M_{obs} and is dependent upon the spurious modulation amplitude estimate, was calculated from

$$M_{\text{pol(U.L.)}} = M_{\text{obs}} + 3\sigma(M_{\text{obs}}) + M_{\text{spur}} \quad (3)$$

$$= 9.13 + M_{\text{spur}} \quad (4)$$

which, for $M_{\text{spur(max)}} = 6.9\%$ gave an upper limit of 16.1% at approximately 3-sigma confidence for the statistical fluctuations.

To translate these polarisation modulations of the X-rays from Sco X-1 to degrees of polarisation, the modulation factor m for the observation was estimated. Allowing for the scan in Bragg angles for this 3.1° offset observation (see § 4.2.3c), a value for k (remember that $m = 1-k/1+k$ (see § 4.2.2b)) was taken from an upper limit estimate of its highest expected value (which occurs at $\theta_B = (44.6 - 3.1^\circ)$), using results taken from crystals similarly prepared to those actually flown on Ariel-V (Evans, K.D. 1976, private communication). This gave a lower limit estimate for m of 0.905, suitable for use in producing an upper limit to the polarisation of X-rays from Sco X-1. Then, since the degree of polarisation is given by

$$p_L = \frac{1}{m} M_{pol}, \quad [\text{from } \S 4.2.2 \text{ equation (55)}] \quad (5)$$

insertion of the previously calculated $M_{pol(U.L.)}$ modulation of 16.1% gave an \approx 3-sigma upper limit to the degree of linear polarisation from Sco X-1 of 17.8%, for 2.6 keV X-rays.

§ 5.3.3 Conclusions and Discussion

From a background estimate of $0.8579 \text{ count s}^{-1}$, an observed 2-nd harmonic modulation of the X-rays from Sco X-1 of $4.78 \pm 1.45 \%$, and an estimated maximum effect due to spurious modulations in this data of 6.9%, a 3-sigma upper limit to the degree of polarisation of 2.6 keV X-rays from Sco X-1 of 17.8% was produced.

This result agreed with the two previous results reported by Angel et al. (1969) and Kestenbaum et al. (1971), both consistent with Sco X-1 as an unpolarised X-ray source.

The upper limit value of 17.8% was also slightly lower than the 20% value given by Angel et al., to the degree of linear polarisation in any direction, though by not enough to significantly constrain existing theories concerning the nature of the X-ray emission from Sco X-1. (These are discussed at the end of § 5.6, which contains a description of the 1976 Sco X-1 observation). However, this upper limit was not as sensitive as that given by Kestenbaum et al. of 12.9% for just the North-South component of polarisation.

From the point of view of this observation being a preliminary observation also, much was learnt.

(i) It could be seen that lack of knowledge of the background modulation amplitudes, though notably the phases, led to a serious reduction in polarisation sensitivity which could have been achieved by this observation. Allowing for $m = 0.905$, the M.D.P. calculated of 4.1% gave the achievable polarisation sensitivity, had the background

modulations been known and subtracted from the data. It was realised that such background information could possibly be obtained from purely background observations using pointing axis positions near to the target source and at time intervals close to the source observation. This choice of background position and time of observation would act to minimise the already known background modulation variations with declination, and also other possible variations with space or time. Such background observations could also provide more accurate and reliable estimates of the background count rate.

(ii) Secondly, it was realised that with future use of zero offset observations, the collimator transmission to X-rays from a source would be much greater (see § 3.2) thereby increasing the S_o/B_o ratio by about a factor of 1.7 over this $\approx 3^\circ$ offset observation. This increase in S_o/B_o ratio would reduce the M.D.P. value for an observation of the same duration, and, perhaps much more importantly, act so as to not too considerably magnify uncertainties in background modulations into uncertainties in polarisation measurement (e.g. as in the $\frac{B}{S} M_b$ term in (i)). In addition, zero offset observations would increase confidence in the $1\% A_g$ spurious modulation estimate, since most modulations from an unpolarised continuum flux are expected to disappear at zero offset.

(iii) Finally, the reasonable agreement between the predicted and observed, large, 1-st harmonic modulations, both in amplitude and phase, and between the expected and observed count rate from Sco X-1, provided good evidence that the instrument was operating as planned.

§ 5.4 CRAB NEBULA POLARISATION OBSERVATION

This observation was also a preliminary observation, without separate background estimates, and therefore necessitated a similar, limited, analysis procedure as that adopted for the previously discussed Sco X-1 observation. Although the Crab Nebula is considered a strong source of X-rays (≈ 1000 Uhuru Units), the data from this observation would have a much smaller signal to background ratio (S_0/B_0 of ≈ 0.1) than that obtained from the Sco X-1 ($\approx 10,000$ Uhuru Units) observation where S_0/B_0 was ≈ 0.7 . This smaller signal to background ratio would then magnify the background spurious modulation effect to an even greater extent than in the Sco X-1 data, thus making detection of polarisation from the Crab Nebula a much more difficult task.

An important reason, however, for attempting to analyse the data from this particular source was that it was the only source for which a definite non-zero degree of X-ray polarisation had been previously obtained. Novick et al. (1972) had measured a degree of linear X-ray polarisation of $15.4 \pm 5.2\%$ consistent with the optical polarisation when averaged over the X-ray emitting region of the Nebula. Thus, a possible detection of the same value from this Ariel-V observation, as well as confirming the previous polarisation result, would simultaneously provide strong evidence that experiment-D was functioning correctly as a polarimeter. That is, the Crab Nebula could also possibly serve as a calibration source.

§ 5.4.1 Description of the Observation

The Crab Nebula was observed from 19th to 28th April 1975, from which 117 orbits' data from orbit numbers 2828 to 2962 were analysed. The graphite crystal was set to a Bragg angle of 44.6° and the LiF crystal to 45.07° . The mean pointing direction offset from the Crab Nebula was 0.3° . The maximum offset was 0.5° . A sky map showing the

movement of the spin-axis position before, during, and subsequent to this Crab Nebula observation, as well as locating the positions of all the nearby known X-ray sources is given in Fig. 5.4.1.

§ 5.4.2 Data Analysis and Results

Count rates obtained from both the graphite and LiF data, summed as a function of orbit position, are shown for each sun-sector in Figs. 5.4.2a and b. The line of sight to the Crab Nebula was mostly ($\approx 98\%$ of the observing time) blocked by the Earth for the orbit region sun-sectors S1 and S2 and these therefore collected almost purely background data. For sun-sectors S4 to S11 the Crab Nebula was visible for practically all (99.6%) of the observing time, producing a somewhat higher count rate which would be expected from an additional count rate component due to X-rays from the Nebula. Since this observed increase was strongest for the graphite crystal data, again, only this crystal data was concentrated upon in an effort to obtain a polarisation result. Sun-sector S3 contained the occultation transition and produced the expected intermediate count rates.

Similarly, as for the 1975 Sco X-1 observation, where again no separate background observations were performed, an attempt was made to obtain an improved background count rate estimate for the S4 to S11 region, in order to supersede 0.7983 ± 0.0037 counts s^{-1} obtained from the sun-sector S1 to S2 region for the graphite data. To obtain this background count rate improvement, further graphite data was analysed from two observations on the background which took place several months after this Crab Nebula observation. For convenience only, the spin-axis pointing positions for these two observations were labelled pos. 12 and pos. 20 and are plotted on the sky grid Fig. 5.4.1. Both these background spin-axis positions were chosen at approximately the same declination as

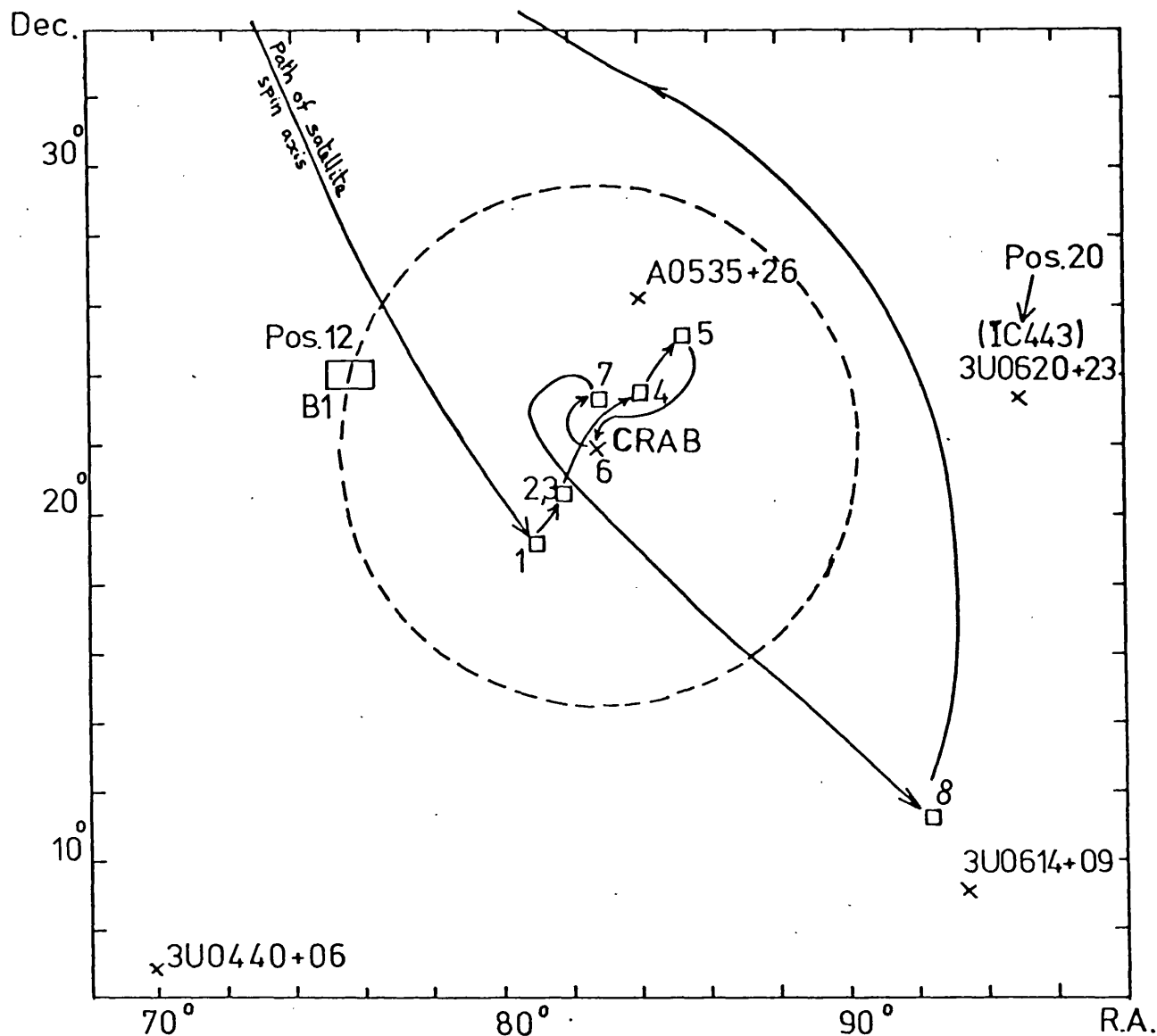


Fig. 5.4.1: Crab Nebula sky grid.

(The pointing positions adopted by the satellite are indicated in general by the \square symbol, and have for convenience been numbered. 3U0620+23 is listed as only a 5 Uhuru unit source in the 3U catalogue (Giacconi et al. 1974). The dashed circle encloses the theoretical area of the sky for which the collimator transmission function $T(\Delta)$ is > 0 when the Ariel-V polarimeter is pointed at the centre of that circle. The position 12 and 20 pointing axis positions represent a portion of a later series of observations. 117 orbits data from pointing position 6 were analysed for polarisation).

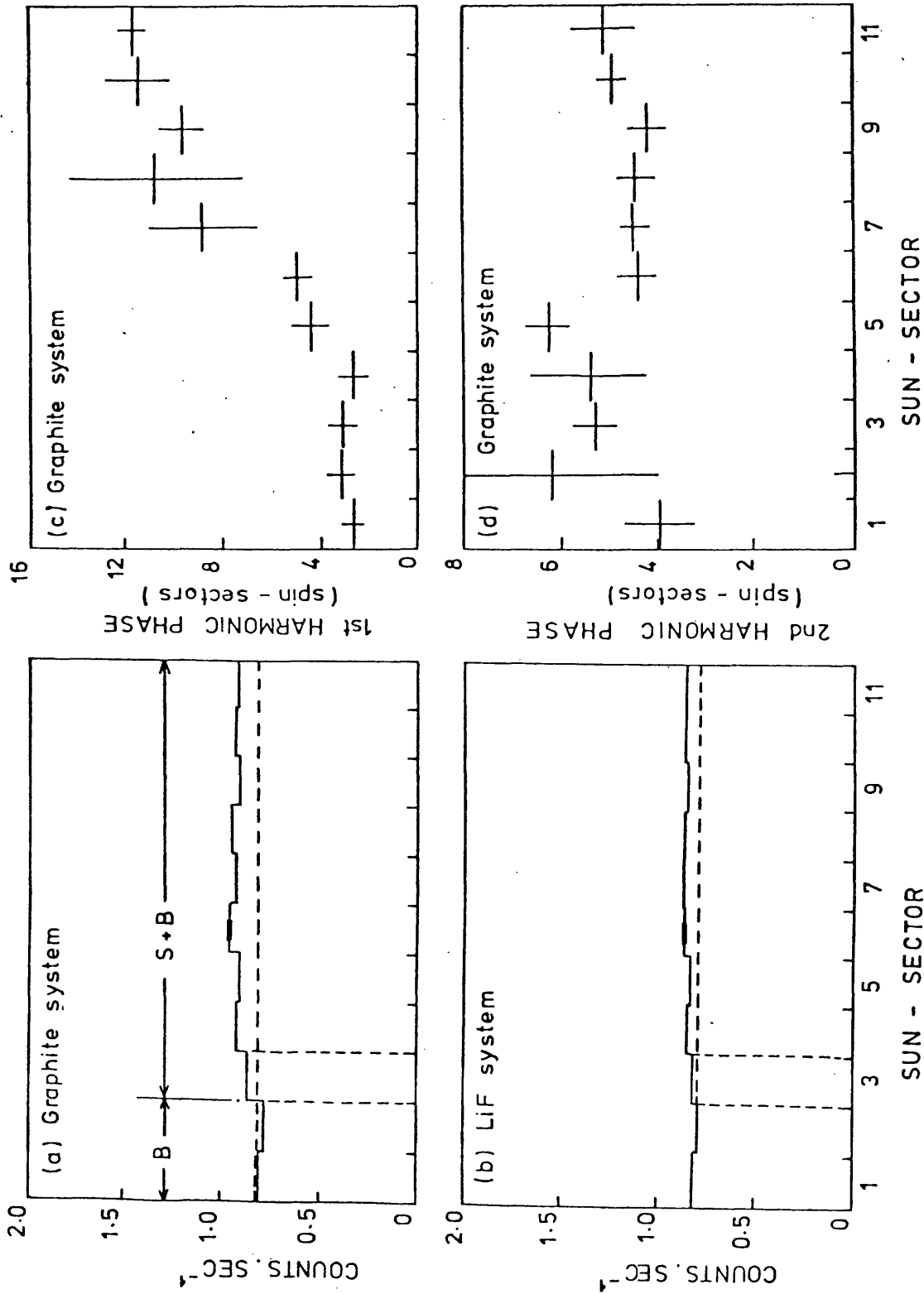


Fig. 5.4.2: Ariel-V polarimeter data from an observation of the Crab Nebula from 1975 April 19 to 28. (1- σ error bars shown).

the Crab Nebula, therefore minimising the differences in background characteristics which were discovered to depend upon declination (see § 5.2.1). Also, the set Bragg angles were identical to those set for this Crab Nebula observation. Mean spin-axis offsets of approximately 7° and 11° from the Crab Nebula were obtained from these pos. 12 and pos. 20 observations respectively. (Although 7° offset was not sufficient to completely prevent X-rays from the Crab Nebula being detected by the instrument, it could be simply estimated that only a minor contribution upon the background count rate of about $0.7\% B_0$ would be produced. See § 3.2.2 for the collimator transmission function.)

From the pos. 12 observation a total of 44 orbits' graphite data, from orbit numbers 4973 to 5025, collected from 8th to 11th September 1975, were analysed. Similarly, 48 orbits' graphite data, from orbit numbers 5179 to 5237, collected from 21st to 25th September 1975, were analysed from the pos. 20 observation. The count rate variation with sun-sector for these two observations are displayed in Figs. 5.4.3a and 5.4.4a, where it can be seen that the occulted and un-occulted orbit regions occur in different sun-sector regions than for the Crab Nebula observation. (The long time lapse between the observations allowed the Sun to move a considerable angular distance in R.A.). Fortunately there were strong indications from all the observations previously described plus also the 1976 Sco X-1 observation yet to be discussed in § 5.6 (where θ_B for the graphite crystal panel for all these observations was set to $\approx 45^\circ$), that the background count rate appeared to be correlated with the occulted and un-occulted orbit regions rather than with fixed sun-sector divisions; the background count rate always showing a small increased value for the un-occulted data. Then, because of this indication, mean background count rates were calculated for the occulted and un-occulted regions for both these pos. 12 and pos. 20 observations,

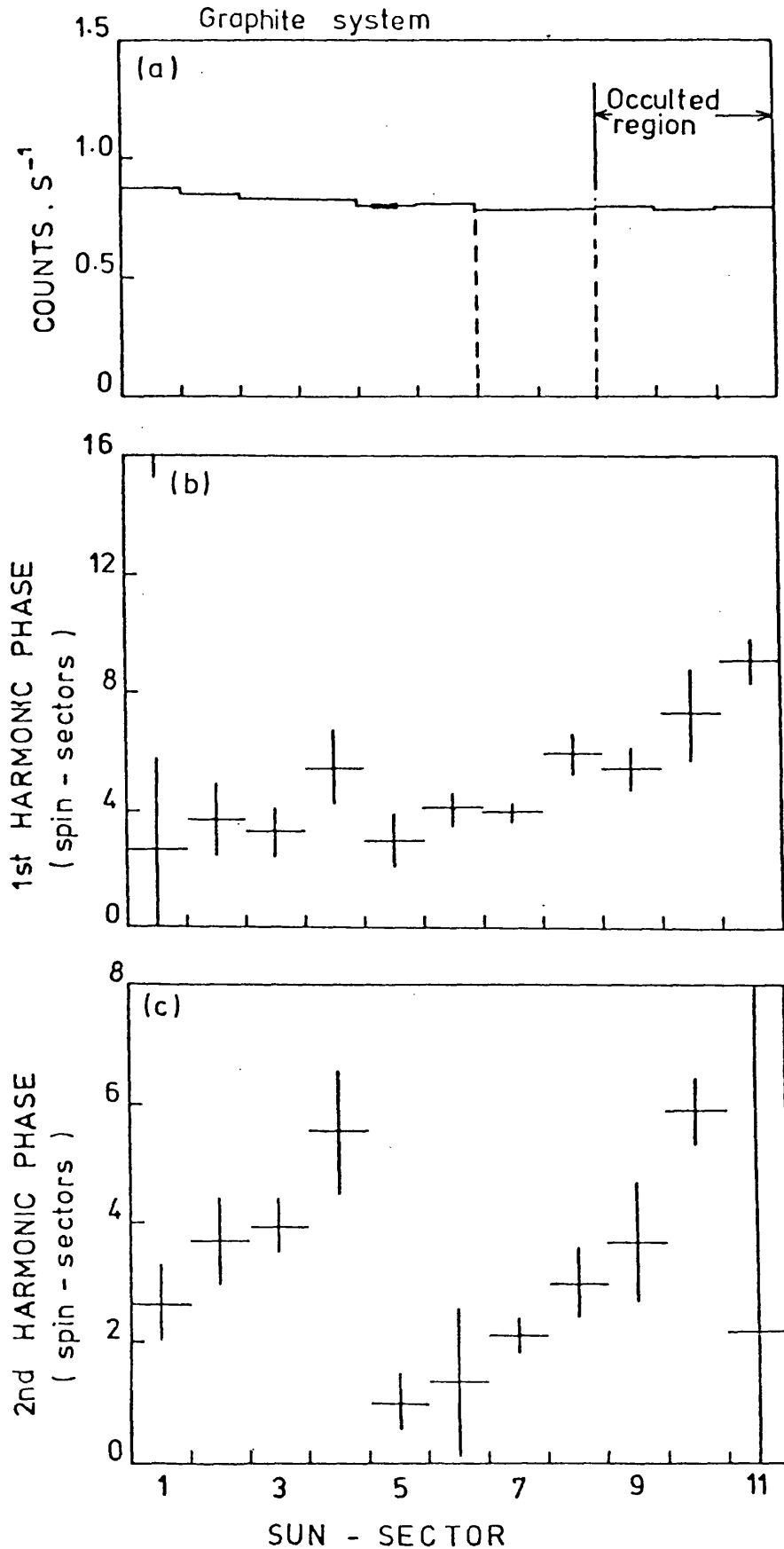


Fig. 5.4.3: Ariel-V polarimeter data from an observation of the background near the Crab Nebula from 1975 Sept. 8 to 11. This observation position was called 'position 12'. (1- σ error bars are shown.)

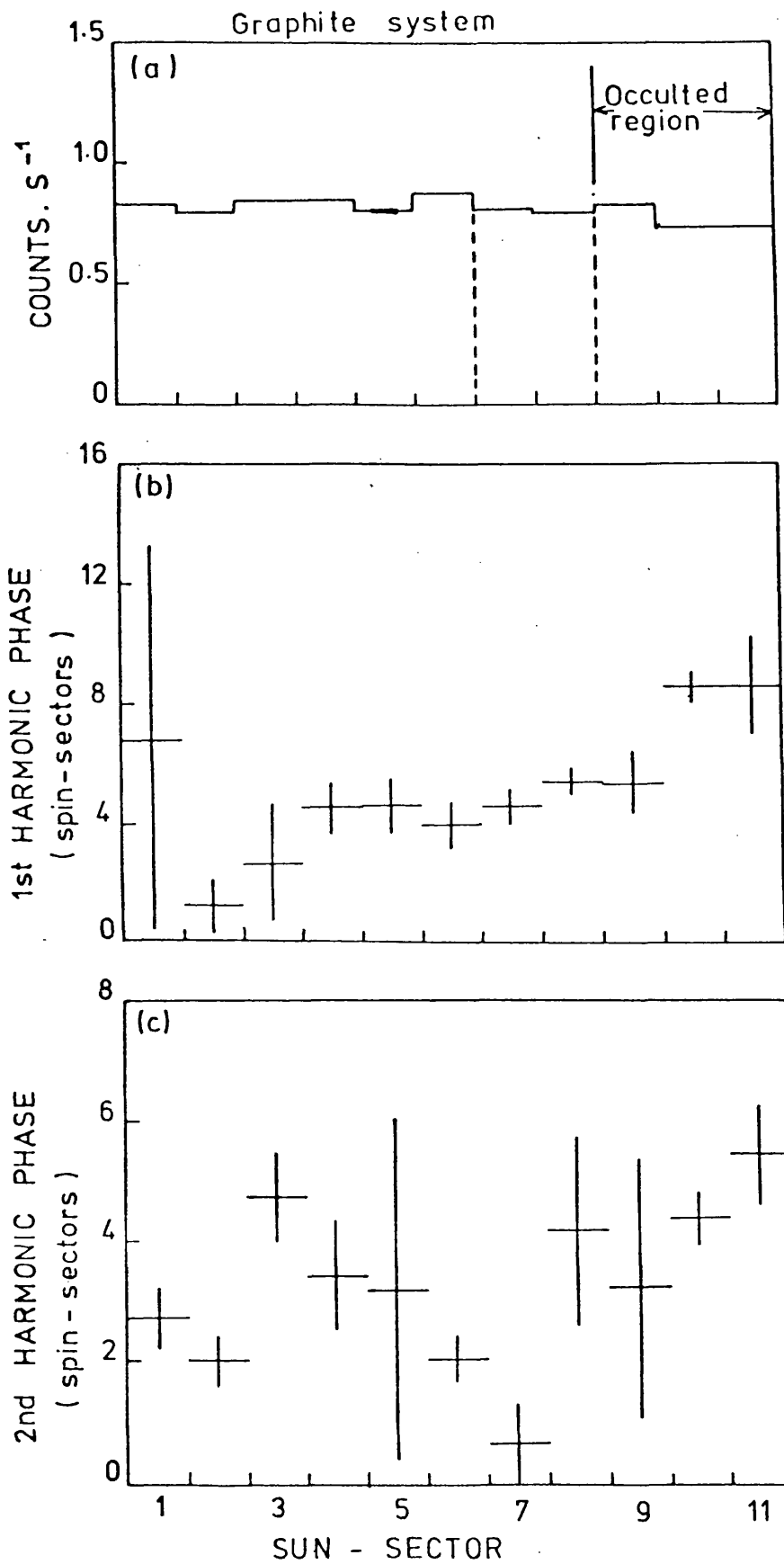


Fig. 5.4.4: Ariel-V polarimeter data from an observation of the background near the Crab Nebula from 1975 Sept. 21 to 25. The observation position was called 'position 20'. ($1-\sigma$ error bars are shown.)

and these values are displayed in Table 5.4.5 where they are compared with the analogous occulted and un-occulted count rates obtained from the Crab Nebula observation. This table, from the occulted background data, shows the stability of the background count rate over the time interval between the observations, where it may be taken as constant to within the statistical limits of the data. Also, a consistent increase in background count rate, ΔB_o , is shown from the occulted to the un-occulted data for the two background positions. The mean value for this increase was calculated as $\Delta B_o = 0.0590 \pm 0.0323 \text{ counts s}^{-1}$. Then, addition of ΔB_o to B_o shown for the (S1 to S2) region for the Crab Nebula observation, produced a final, modified, background count rate estimate for the (S4 to S11) region, where the Crab Nebula was observed, of $B_o = 0.8573 \pm 0.0325 \text{ counts s}^{-1}$, consistent with all the analysed data.

The graphite data from the S3 to S11 region, for which the Crab Nebula was observed for 99% or more of the total observing time in any 512s time slot (see § 3.2.5 for 'Crystal' mode division of data), was summed as a function of satellite rotation angle and is displayed in Fig. 5.4.6. The mean background level calculated from $B = \frac{B_o T_b}{16}$, where the observing time T_b on the background was $289\,350 \pm 87 \text{ s}$ (about 80 hours), was calculated as $B = 15\,504 \pm 588 \text{ counts spin-sector}^{-1}$ and is shown as an horizontal dashed line in Fig. 5.4.6. The error bar shown on this dashed line is one standard deviation $\sigma(B)$, and almost totally arises from the standard deviation $\sigma(B_o)$ estimated at 3.8% of B_o . The estimated count level due to X-rays from the Crab Nebula is given by $S = M - B = 1151 \pm 588 \text{ counts spin-sector}$, where M , the mean count level recorded, was $16\,654.7 \text{ counts spin-sector}^{-1}$. The signal to background ratio $S/B = 7.4\% = S_o/B_o$ (as the observing time on the source equalled the observing time on the background).

Table 5.4.5: Mean Background Count Rates Concerning the Crab Nebula Observation.

Observation (and orbit numbers)	Mean Background Count Rate (counts s ⁻¹)	
	Occulted Orbit Region	Un-occulted Orbit Region
Crab Nebula (2828 - 2962)	(S1 to S2) 0.7983 ± 0.0037	(S4 to S11) [0.9228 ± 0.0164] *
Pos. 12 (4973 - 5025)	(S8 to S11) 0.7843 ± 0.0103	(S1 to S6) 0.8345 ± 0.0266
Pos. 20 (5179 - 5237)	(S8 to S11) 0.7682 ± 0.0461	(S1 to S6) 0.8359 ± 0.0349

* not a background count rate - includes contribution from Crab Nebula
(Errors given are 1 standard deviation)

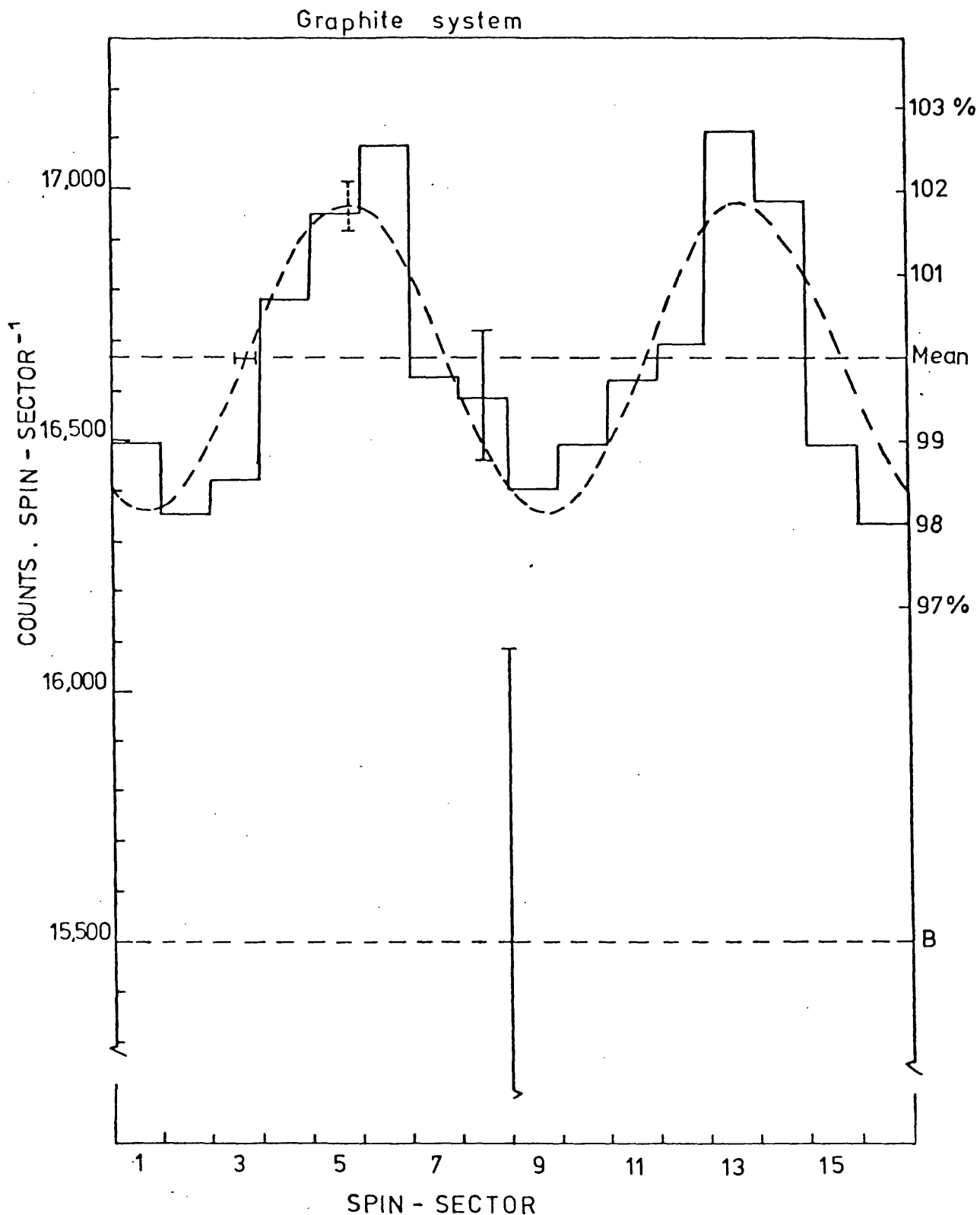


Fig. 5.4.6: Ariel-V polarimeter data from an observation of the Crab Nebula from 1975 April 19 to 28. Data is shown summed as a function of satellite rotation angle (spin-sector) and the estimated background level is shown by the dashed straight line marked B. The sinusoidal dashed line represents only the 2-nd harmonic component in the data. ($1-\sigma$ error bars are shown for both the summed data, and the estimated curve and background values).

Using this estimated background B and its associated error $\sigma(B)$, Fourier and statistical analysis were performed on this Crab Nebula data summed as a function of satellite rotation angle, and the results of this analysis are shown in Table 5.4.7.

Table 5.4.7: Results of Fourier and Statistical Analysis of the Crab Nebula, graphite crystal, summed data from the Observation of 1975 19th - 28th April.

χ^2	M	A_2^{**}	M.D.P.	M_2	$\sigma(M_2)^*$
11 d.o.f.	Counts	Counts	(assuming	%	%
	spin-sector ⁻¹	spin-sector ⁻¹	$m = 1$)%		
12.10	16,654.8	308.27	13.7	26.8 ±	14.3

* Calculated from use of a regression method on the observed data (see Anderson 1971)

** Amplitude of 2-nd Harmonic modulation.

The Minimum Detectable Polarisation ($3-\sigma$, assuming the modulation factor $m = 1$) was calculated as 13.7%, sufficiently small to be able to extract a polarisation measurement of comparable accuracy to that obtained by Novick et al., providing an accurate knowledge of the background and spurious modulations could be obtained. The modulation M_2 of the source data S at the polarisation, 2-nd harmonic, frequency resulted in an amplitude $A_2/S = 26.8 \pm 14.3\%$ at a phase of 4.76 ± 0.2 spin-sectors, and includes any spurious modulations, whether originating from the background or source continuum data. This modulation was consistent with both zero polarisation and the $\approx 15\%$ modulation expected from polarisation of X-rays from the Crab Nebula.* In general, this result was also consistent

* Since $p_L = \frac{1}{m} M_2$ (see § 4.2.2a) where, since the mean offset was 0.3° , m would be almost unity. (For very similar observing conditions m was estimated at 0.97 for the Sco X-1 1976 observation.)

with modulations, or approximately degrees of polarisation of X-rays from the Crab Nebula, between 0 and 69.7%, this ignoring possible spurious modulations which could further extend this range. [It is, however, interesting to note that of the large 14.3% error on this measured modulation, only about 4.2% was due to statistical counting limitations, the majority being directly caused by just the uncertainty in the background level.]

The measured phase angle had a small associated error since it does not depend upon the mean background level, though spurious modulations not yet allowed for could be crucial in interpreting this as due solely to polarisation of Crab Nebula X-rays. From the measured mean position of the Sun for the Crab Nebula observation of R.A. (1950) = 30.7° , Declination = 12.5° , the position angle of the Sun was determined as 268.2° . Then, from use of this Sun position angle, the measured 2-nd harmonic phase angle was calculated to correspond to a position angle of North $161.1 \pm 4.5^\circ$ East, remarkably, though perhaps coincidentally, similar to the polarisation position angle of $156 \pm 10^\circ$ already determined by Novick et al. (1972) for X-rays from the Crab Nebula.

Concerning the existence of possible spurious modulations in the data for this observation, Fig. 5.4.6 shows clearly, only, a significant 2-nd harmonic modulation as would be expected due to polarisation of X-rays from the Crab Nebula. A 1-st harmonic modulation of only $0.41 \pm 0.28\%$ of M was observed, consistent with just statistical fluctuations from unmodulated data. Also, from a fit of a mean and a 1-st harmonic to the data a χ^2 value of 57.26 (13 degrees of freedom (d.o.f.)) was obtained, strongly indicating the presence of significant modulations in the data at higher harmonics. However, from addition of the 2-nd harmonic to the fit, the χ^2 value was reduced to 12.10 (11 d.o.f.) this indicating the unlikelihood of any significant modulations in the data at harmonics

higher than the 2-nd. This indication was confirmed from results of modulations obtained from the Fourier harmonics up to 8, where only the 4-th harmonic produced a modulation that was almost significant at the 3-sigma level, producing a 0.7% modulation. A significant 4-th harmonic modulation though, would not be unexpected because of a likely asymmetry in the honeycomb collimator (see § 4.2.3c). However, a significant spurious modulation at the 2-nd harmonic frequency has not been excluded, and to determine the existence of any such modulation a search for systematic variations of 2-nd harmonic phases and amplitudes with sun-sector, was mounted.

For the Crab Nebula graphite data, amplitude variations with sun-sector for both 1-st and 2-nd harmonic modulations are displayed in Figs. 5.4.8a and b, and the analogous phase variations are displayed in Figs. 5.4.2c and d.

An apparently systematic monotonic increase in 1-st harmonic phase with sun-sector is displayed, plus also an apparent systematic variation in the corresponding amplitude, even though there was no indication of any systematic 1-st harmonic modulation in the summed (S4 to S11) data. Clearly, data collected in separate orbit blocks can exhibit spurious modulations which do not necessarily show up in data summed over several orbit blocks.

The 2-nd harmonic phases in the (S4 to S11) region show an almost constant value, as expected from detection of polarisation. The background (S1, S2, and background dominated S3) 2-nd harmonic phases supported this viewpoint by showing no such signs of constancy, indicating more the usual detection of background spurious effects. Also, similar plots of 1-st and 2-nd harmonic phases obtained from both the background pos. 12 and pos. 20 observations, shown in Figs. 5.4.3b and c, and Figs. 5.4.4b and c, indicate a deep (and apparently sinusoidal) variation of the

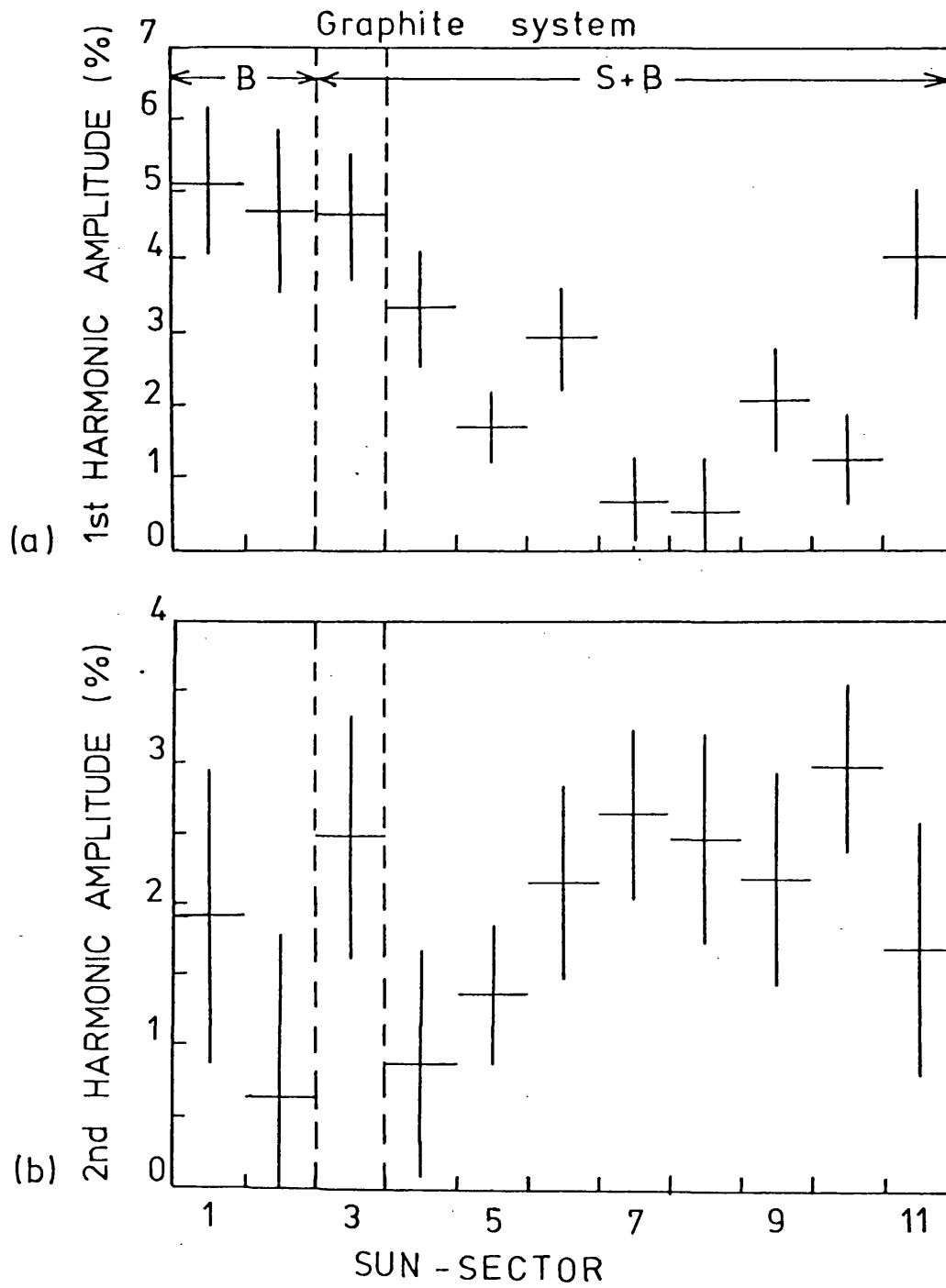


Fig. 5.4.8: Amplitude modulation variation with sun-sector for an Ariel-V polarimeter observation from 1975 April 19 to 28 on the Crab Nebula.

2-nd harmonic phase with sun-sector, over all the sun-sectors. Comparison of the pos. 12 and pos. 20 1-st harmonic phase profile with sun-sector, however, follows closely that of the Crab Nebula observation, therefore adding weight to the existing belief that the anomalous constancy of the 2-nd harmonic phase in the S4 to S11 region for the Crab Nebula observation, is indeed caused by detection of polarisation.

Conversely, the 2-nd harmonic (S4 to S11) amplitudes for the Crab Nebula observation indicate a systematic variation with sun-sector, consistent with a significant, and perhaps large, 2-nd harmonic spurious modulation for this sun-sector region where detection of polarisation is indicated.

However, without a usefully accurate knowledge of the 2-nd harmonic, spurious modulation which existed at the time of this Crab Nebula observation, no direct subtraction of such a spurious modulation from the observed 2-nd harmonic modulation could be made. Furthermore, since such a spurious modulation component might be large, no simple amplitude estimate, irrespective of phase, could be usefully employed, as in the 1975 Sco X-1 observation. Consequently, no degree of polarisation and position angle were extracted from the observed 2-nd harmonic amplitude and phase for this Crab Nebula observation.

§ 5.4.3 Discussion and Conclusions

The potential sensitivity of this Crab Nebula observation was clearly displayed by the calculated Minimum Detectable Polarisation ($3-\sigma$) value of 13.7% showing it to be comparable with Novick et al.'s (1972) determined accuracy of $\pm 15.6\%$ also at $3-\sigma$ confidence.

Comparison of the Ariel-V summed data given in Fig. 5.4.6 with that obtained by Novick et al., plotted here in Fig. 5.4.9, shows that the Ariel-V data displays a more 'obvious' 2-nd harmonic modulation (i.e.

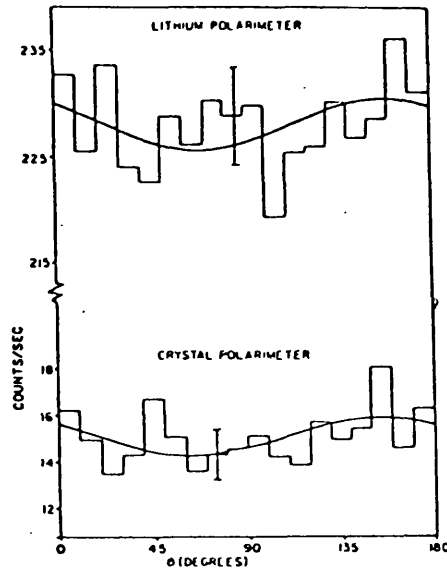


Fig. 5.4.9: Data taken from Novick et al. (1972) from a rocket flight X-ray polarimetric observation of the Crab Nebula. Depicts variation of counts with position angle θ modulo 180° . The solid lines are best fits to a function periodic at twice the rotation frequency of the rocket.

appears statistically superior to Novick et al.'s). The 2-nd harmonic phase of the Ariel-V data also produces a position angle consistent with that obtained by Novick et al. for polarisation of the Crab Nebula (although perhaps coincidentally, because of the possible presence of spurious modulations).

However, although the Ariel-V data appeared statistically superior to Novick et al.'s, we have seen that no polarisation result was obtained from this particular observation for two reasons:-

(i) The determination of the background count rate B_0 was of insufficient accuracy, enough to produce by itself 13.6% of the 14.3% error on the determined 2-nd harmonic amplitude. (Statistical counting error alone was not predominant and on its own would give only an $\approx 4.2\%$ error.)

However, an error on the mean background determination would only become significant for observations similar to this one which have a low signal to background S_0/B_0 ratio. Then, S , calculated from $M - B$, would be small such that the error on S , propagated from that on B , would become large compared with S . This large error on S would then propagate directly onto any determined fractional modulation of S .

(ii) The lack of knowledge of spurious modulation amplitudes and phases.

This prevented interpretation of the measured modulation amplitudes and phases, already having large associated errors, into a degree of polarisation and a position angle.

However, it seemed likely that from utilisation of separate background observations, similar to those proposed in the conclusion to the 1975 Sco X-1 observation, that such limitations caused by (i) and (ii) could be considerably reduced. Then, a future Ariel-V polarisation

observation of the Crab Nebula could possibly produce a definite result, perhaps of comparable accuracy to that obtained by Novick et al.

Finally, although no definite polarisation result was obtained from this observation, it must be noted that all the data modulations obtained were consistent with detection of the expected degree of polarisation from the Crab Nebula and at the correct position angle, thus giving every indication that the instrument was functioning correctly as a polarimeter (and that the computer analysis procedures were also correct). Thus, in this indicative sense, this Crab Nebula observation also successfully served as a calibration observation.

§ 5.5 A0620-00 (MON X-1) POLARISATION SEARCH

During 1975 August 3-rd a new X-ray source subsequently named A0620-00 was observed, having characteristics of an X-ray Nova, and was reported a few days later by Elvis et al. (1975a) when its intensity had approached that of the Crab Nebula. This source subsequently brightened to be by far the strongest non-solar X-ray source in the sky, outshining Sco X-1 in the 2-6 keV range by a factor of 3 or 4 (Elvis et al. 1975b).

The high X-ray intensity of this source meant that it would be an "ideal" object for study by the Ariel-V polarimeter, and observation plans were made without delay. Also, the additional knowledge obtained from the then, nearly completed, analysis of the 1975 Sco X-1 observation could be usefully employed in the planning of this observation.

§ 5.5.1 Observation Plans

In order to obtain an accurate determination of the polarisation of Mon X-1, the required amount of observation time would need to be estimated. For this purpose, a comparison with the Minimum Detectable Polarisation calculated for the 1975 Sco X-1 observation under the actual Ariel-V observation conditions was used, together with the assumption that the intensity of Mon X-1 would be approximately 3 times that recorded from the Sco X-1 observation (see § 4.2.3b for dependency of MDP on source strength and observing time). This meant that in an observing time of only 2 days a degree of polarisation as small as 2.3% would be able to be theoretically detectable from Mon X-1 with 3-sigma confidence. Similarly, from a 4 day observation this Minimum Detectable Polarisation would be reduced to 1.6%.

In order to reduce possible effects of spurious modulations, and therefore to be able to obtain as near the theoretical polarisation sensitivity as possible, it was realised that any satellite pointing

direction offset from Mon X-1 should be as small as possible, preferably zero. Then S_{\circ}/B_{\circ} would be at a maximum and effects of background spurious modulations would not be magnified so much as for the case of the 1975 Sco X-1 observation.

Operation of the instrument at a Bragg angle of 45° , combined with zero offset, would also optimise the modulation factor.

Finally, it was also advised that separate, purely background, observations might be profitably integrated into the observing program, thereby allowing subtraction of observed background modulations from the 'source + background' data.

§ 5.5.2 Description of Observation

The above suggested observing parameters and program, after subsequent interaction with other Ariel-V observation priorities, and detection by the graphite system (Griffiths et al. 1976b) of a pre-observation weakening of the Mon X-1 X-ray flux, were incorporated into two separated ≈ 4 day observation intervals, but only on the source Mon X-1. The occulted data was to be used to measure the mean background level. Also, since the S_{\circ}/B_{\circ} ratio obtained from Mon X-1 would still be $\approx 2\frac{1}{2}$ times greater than that from the 1975 Sco X-1 observation, this would allow a polarisation analysis considerably less influenced by spurious background modulations, even without the desired, separate background observations.

In detail, see Table 5.5.1, the Ariel-V spin-axis was pointed at A0620-00 with nominal 0° offset (i.e. as precisely as the attitude control system would allow) from 1975 September 28th to October 1st and from October 12th to 15th, with the crystals set near the optimum 45° Bragg angle for polarisation measurements.

A sky grid showing the location of Mon X-1 and surrounding

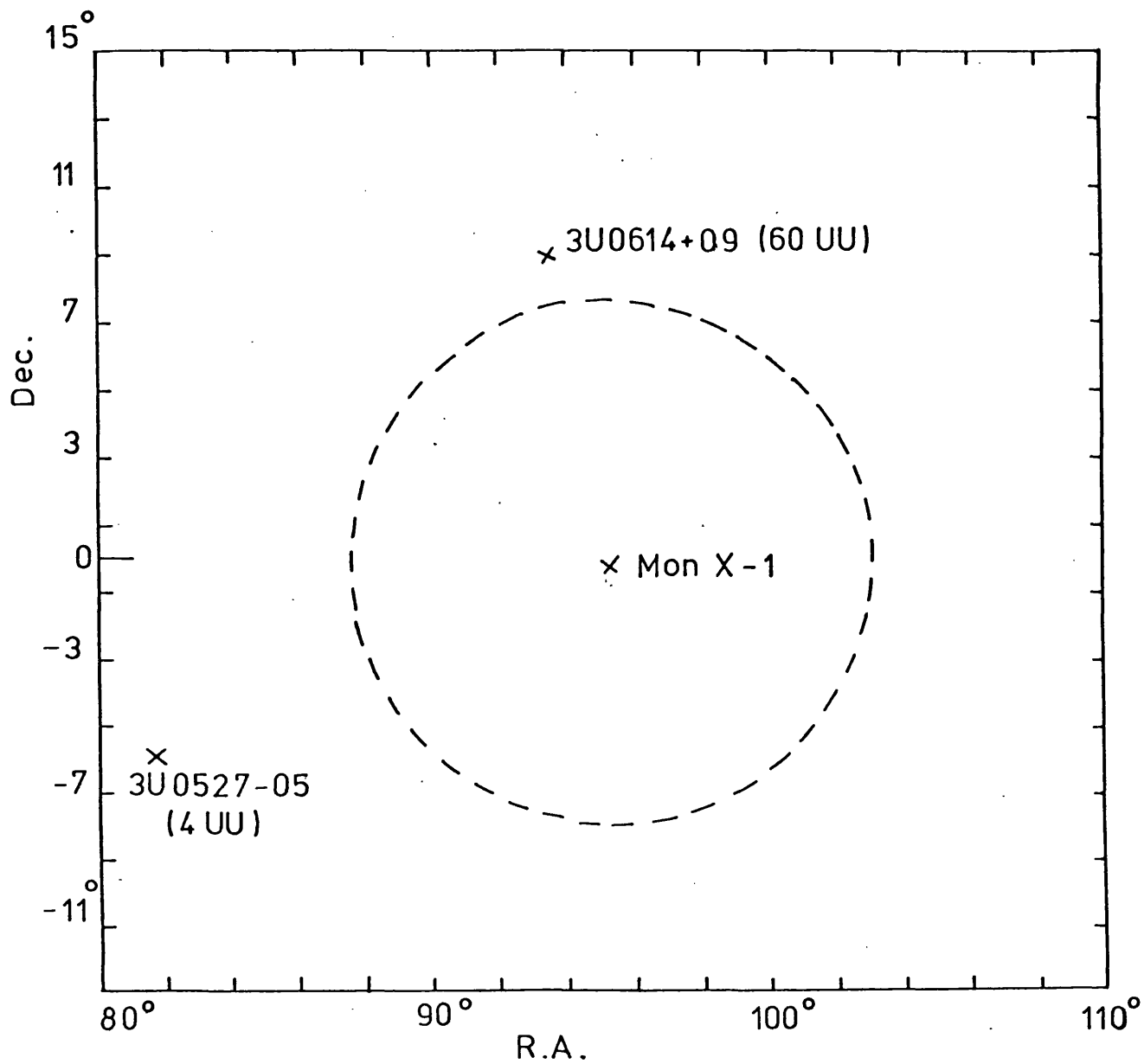


Fig. 5.5.2: Mon X-1 sky grid, depicting nearby X-ray sources and their Uhuru intensity in UU (Uhuru Units). The dashed polarimeter transmission circle is centred on Mon X-1 (see Fig. 5.4.1 for its significance).

sources is given in Fig. 5.5.2.

Table 5.5.1: A0620-00 Observation Parameters

Orbit Numbers	No. of orbits analysed	Nominal pointing direction		Mean source offset	Nominal Bragg angles	
		R.A.	Dec.		graphite	LiF
5287-5341	46	95°	-0.0°	0.4°	44.6°	45.1°
5498-5556	42	95°	-0.0°	0.6°	44.6°	45.1°

§ 5.5.3 Data Analysis, Results and Conclusions

The data analysis and interpretation of results for this observation was performed by other members of the Leicester X-ray astronomy group, and reported by Griffiths et al. (1976b). For this reason, only a brief summary will be presented here.

Essentially, the data analysis was analogous to that described for the two previous, 1975 Sco X-1 and Crab Nebula, observations. The 'source + background' and purely background data were separated by ("sun-sector") division of the orbit according to whether the source was fully visible or completely Earth occulted in any 512 s time integration block. The results of Fourier frequency analysis performed on this separated data, summed as a function of satellite rotation angle, are shown in Table 5.5.3a. From these frequency analysis results, especially concerning the graphite data, it was noted that a much reduced modulation was obtained from the 'source + background' data than from the background data alone. This reduced modulation was consistent, at least in part, with the addition of an unpolarised X-ray flux from Mon X-1. The upper limit to polarisation was then taken simply as the observed 2-nd harmonic amplitude from the 'source + background' data, assuming that this amplitude was completely due to the source alone, plus the Minimum Detectable

Table 5.5.3: Results of analysis of Ariel-V polarimeter data obtained from an observation of Mon X-1 (from Griffiths et al., 1976b).

(a) Summary of Fourier frequency analysis results

Crystal	Observation	Exposure (s)	Counting rate (s^{-1})	Amplitude of 1st satellite spin frequency (%)	2nd harmonic of satellite spin frequency Amplitude (%)	Phase (rad)
Graphite	Source + background	1.3×10^5	2.21	1.44 ± 0.37	0.40 ± 0.37	1.97
	Background	1.1×10^5	0.78	1.67 ± 0.69	2.54 ± 0.69	0.95
LiF	Source + background	1.3×10^5	0.84	3.10 ± 0.60	1.53 ± 0.60	1.28
	Background	1.1×10^5	0.70	2.40 ± 0.73	1.37 ± 0.73	2.66

(b) Polarisation interpretation of the frequency analysis results

Crystal	MDP (%)	Measured polarisation (Obs. Amp. $\times \sqrt{S+B}/S$)%	3σ upper limit on source polarisation (%)
Graphite	1.4	0.6	2.0
LiF	8.9	9.2	18.1

Polarisation (M.D.P.) calculated from the observed data. These calculated values are given in Table 5.5.3b. The 3-sigma upper limits to the degree of linear polarisation of X-rays from Mon X-1, obtained in this way, were 2% at 2.6 keV from the graphite crystal panel, and 18% at 4.6 keV from the LiF crystal panel.

The graphite polarisation upper limit was interpreted in terms of a model consisting of thermal X-rays emitted from an accretion disk having an electron scattering opacity $\tau_{es} \approx 20$, consistent with other observations on Mon X-1. For an assumed thin accretion disk where $\tau_{es} \gg 1$ the 3- σ upper limit to polarisation of 2% implied that the inclination of the disk "i" to the sky must be $< 57^\circ$.^{*} If the accretion disk is not thin, then for a direction of view, i, between 60° and 120° , the polarisation perpendicular to the major axis will be less than 2% for $\tau_{es} \approx 20$ if $c/a \gtrsim \frac{1}{3}$, where c and a are the semi-minor and semi-major axes of the disk (i.e. the emitting plasma is an oblate spheroid). It was noted that other factors which could possibly modify the expected polarisation from an optically-thick disk were summarised by Rees (1975).

Dolan (1975) had observed small degrees of linear, optical, polarisation from Mon X-1 of only 1.6 to 1.7%, consistent with an interstellar origin in magnitude, position angle and wavelength dependence. Then, from Angel's (1969) comment that linear polarisation should also be observed at optical wavelengths if the emission mechanism is common, because the classical Thomson scattering cross-section is independent of wavelength, it was noted that Dolan's results could possibly place even tighter constraints on accretion disk emission from Mon X-1.

* A more detailed outline of interpretation of a polarisation upper limit in terms of an accretion disk model is given with the following report of the 1976 Sco X-1 observation.

§ 5.6 1976 SCO X-1 POLARISATION SEARCH

From utilisation of all the knowledge learned from the preliminary observations and from the previous 1975 observation on Sco X-1, it could be seen that a second observation, properly planned, could be expected to produce a much more sensitive polarisation measurement.

§ 5.6.1 Description of Observation

The graphite crystal panel was set to a Bragg angle of 44.6° , the optimum setting allowed by the Ariel-V polarimeter for polarisation studies.

The LiF crystal panel was set to a Bragg angle of 27.2° in order to conduct an Fe XXV spectral line search, and as an indicator of modulation amplitude and phase behaviour from the background radiation relevant to the polarisation measurement (since, at $\theta_B \approx 27^\circ$ the LiF modulation factor would be approximately half that for the graphite crystal, and also a signal count rate of ≈ 4 times less than from the graphite crystal would be expected (see Griffiths et al. 1976a)).

Data were collected from Sco X-1 for ≈ 10 days from 1976 March 31st to April 10th (U.T. 91.7 to 101.5). In order to obtain the maximum count rate from Sco X-1, the satellite spin-axis was pointed as close to Sco X-1 as the attitude control system would allow. This resulted in a mean spin-axis offset from Sco X-1 of 0.4° . The maximum offset allowed for data to be included for analysis was set at 0.7° . This maximum offset caused a scan in Bragg angle of $\pm 0.7^\circ$ and is equivalent to an energy scan of about ± 0.03 keV about the mean reflected energy for X-rays of 2.63 keV for the graphite crystal.

To provide data for an accurate estimation of the background count rate and modulations, two separate, purely background observations of ≈ 3 days each were performed, one before and the other subsequent to

the polarisation observation on Sco X-1.

The first background observation was from 1976 March 28th to 31st (U.T. 88.3 to 91.3) and the final background observation was from 1976 April 10th to 14th (U.T. 101.5 to 105.3). Since the preliminary observations (see § 5.2) had shown only a slow variation in background modulations with declination, these background spin-axis positions were chosen within 2° of declination of each other at [R.A. (1950) $\approx 234.2^\circ$, Dec. $\approx -15.6^\circ$] and [R.A. (1950) $\approx 251.6^\circ$, Dec. $\approx -13.9^\circ$] for the first and final background observations respectively.

These spin-axis pointing positions for both the source and background observations are shown on the sky grid Fig. 5.6.1.

§ 5.6.2 Data Analysis and Results

The modulation factor is dependent upon the Bragg angle (see § 4.2.2b and), and for the source observation where θ_B was set to 44.6° and Sco X-1 was at an average spin-axis offset of 0.4° , this was estimated to be 0.973 ± 0.013 in agreement with experimental results carried out on crystals similar to those flown on Ariel-V (Evans 1976, private communication).

a) 'Source + Background' Parameters

Only counts from Sco X-1 X-rays collected in the sun-sector (S1 to S4) orbit region, where the polarimeter f.o.v. to Sco X-1 was completely unobscured for all the observation time, were included in the polarisation analysis.

This (S1 to S4) 'source + background' data from the source observation, summed as a function of satellite rotation angle from which polarisation of Sco X-1 X-rays should be evident as a 2-nd harmonic modulation, are displayed in Fig. 5.6.2. From frequency analysis of this data the mean counts per spin-sector was determined as $13\,379.3 \pm 14.5$,

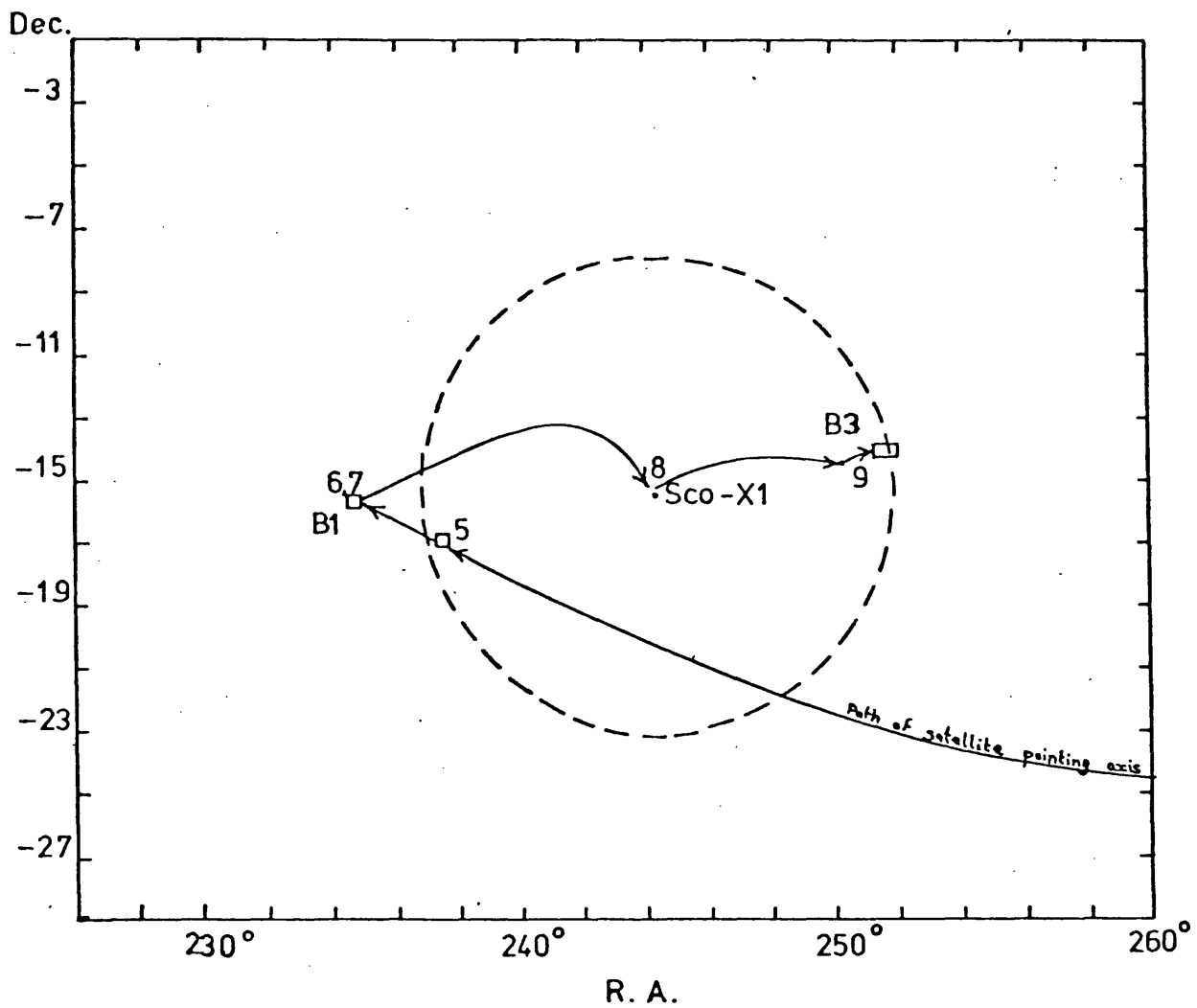


Fig. 5.6.1: Sco X-1 sky grid; 1976 observation. (See Fig. 5.4.1 for significance of the dashed circle and numerals indicating the satellite pointing positions).

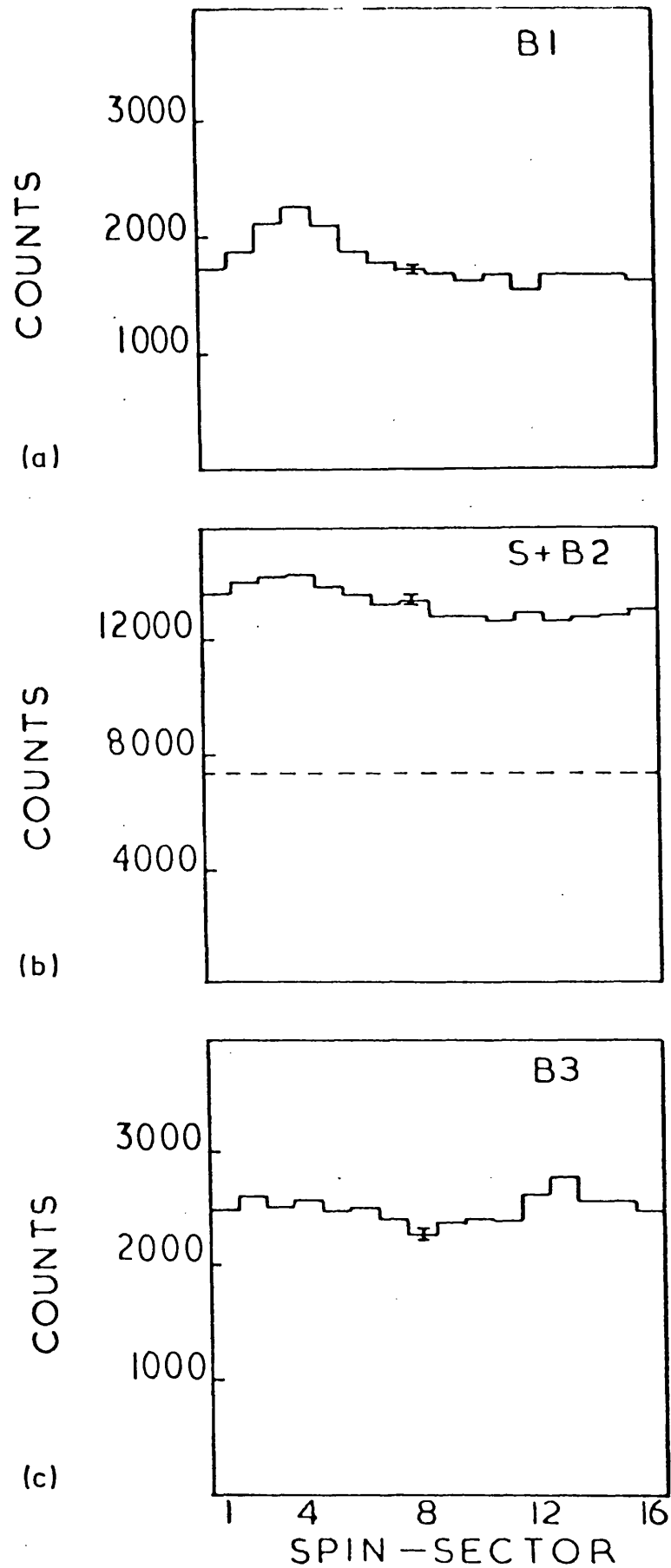


Fig. 5.6.2: Variation of summed data with spacecraft rotation angle for the 1976 Sco X-1 observation with the Ariel-V polarimeter. (Only data from that part of the satellite orbit, sun-sectors S1 to S4, for which the view to Sco X-1 is unobscured by the Earth was included in the summation). The summed data from the first background observation (B1) are depicted in (a), the source plus 2nd background data (S+B2) in (b), and the third background observation (B3) data in (c).

and the 2-nd harmonic modulation amplitude as $1.64 \pm 0.34\%$ at a phase angle of 1.08 ± 0.11 radians.

The observation time on the background for this source observation was $T_B = 120\,864 \pm 56$ S.

The count rates for each sun-sector for the two background observations, and the observation on Sco X-1, are displayed in Fig. 5.6.3. The increase in count rate of ≈ 0.9 counts s^{-1} from the (S6 to S11) to the (S1 to S4) region, almost only due to X-rays from Sco X-1, shows an approximate gain factor of 1.5 in signal count rate compared with the 0.6 counts s^{-1} obtained from the 1975 Sco X-1 observation.

b) Background Count Rate Estimate

The provision of the two separate background observations allowed the background count rate applicable to the source observation, for the (S1 to S4) region where Sco X-1 was visible, to be simply taken as the mean of the count rates from the same orbit region from these two background observations. The background count rate estimated in this way for the (S1 to S4) source observation was $B_o = 0.9785 \pm 0.0139$ counts s^{-1} .

All the mean count rates obtained from the occulted (S6 to S11) data, and unocculted (S1 to S4) data, for the source and both background observations, are displayed in Table 5.6.4. A check that the general background level did not vary significantly during these observations was provided by the count rates obtained from the (S6 to S11) data, where it can be seen from Table 5.6.4 that they remained constant to within a standard deviation.

From use of B_o and T_B the estimated background contribution

$B = \frac{B_o T_B}{16}$ (counts spin-sector⁻¹) to the 'source + background' observation (S1 - S4) data, is shown by the dashed line in Fig. 5.6.2b.

GRAPHITE CRYSTAL

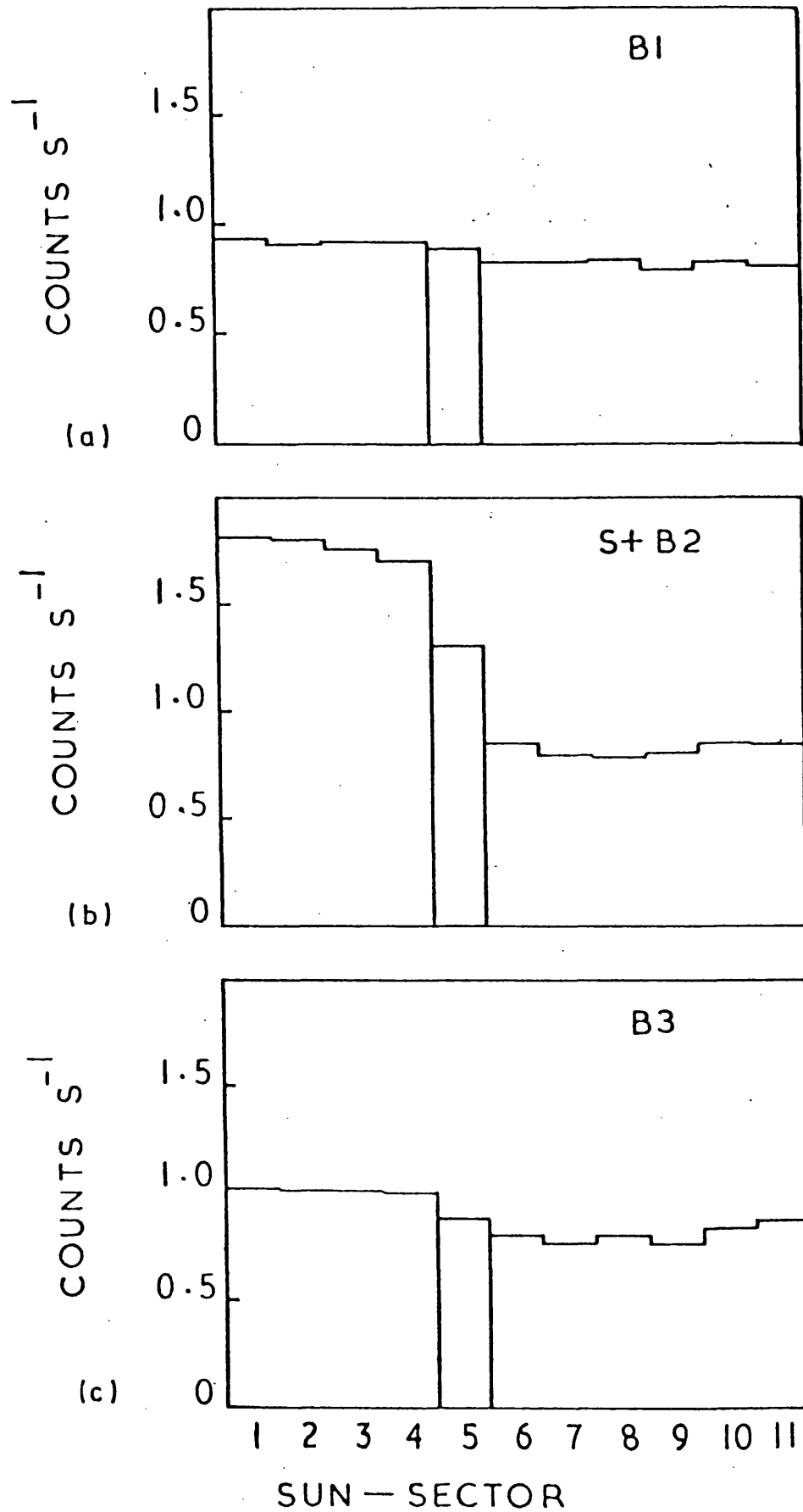


Fig. 5.6.3: Variation of count rates with orbit position for the Ariel-V polarimeter B1, S + B2, and B3 pointing positions associated with the 1976 Sco X-1 observation.

Table 5.6.4: Mean Count Rates, obtained from the graphite crystal assembly for the 1976 Sco X-1 Observation.

Observation	(S1 to S4) region (counts s ⁻¹)	(S6 to S11) region (counts s ⁻¹)
B1	0.9235 ± 0.0117	0.8303 ± 0.0147
S + B2	1.7741 ± 0.0470	0.8324 ± 0.0305
B3	1.0486 ± 0.0249	0.8206 ± 0.0429

Also, from use of B_0 , together with the modulation factor and the 'source + background' parameters, the Minimum Detectable Polarisation was calculated as $\approx 1\%$ for 3- sigma confidence.

c) Background and Other Spurious Modulation Estimates

Estimation of background modulation amplitudes A_B and phases ϕ_B , which existed at the time of the source observation, was made by careful study of those modulations which existed in the purely background observations before and after the source observation, and interpolation between these measured values.

Modulations at the satellite rotation frequency, which do not affect measurement of polarisation, are clearly visible in Figs. 5.6.2a and b. These measured 1-st harmonic modulations, obtained from the first background observation (B1), the 'source + background' observation (S + B2), and the final background observation (B3), were $12.9 \pm 1.6\%$, $5.3 \pm 0.4\%$ and $3.9 \pm 1.1\%$ respectively.

Modulations of the background data at twice the satellite rotation frequency, which can produce spurious polarisation measurements if not allowed for, were observed to be at a reduced level compared with the 1-st harmonic modulations. These 2-nd harmonic modulation amplitudes, plotted in chronological order of the observations B1 through the source

observation to B3, are shown in Figs. 5.6.5a to d. The source observation was divided into three approximately equal sections Sa, Sb and Sc, also in chronological order, to enable a clearer indication of any time variations of these 2-nd harmonic amplitudes. The time variation of the analogous 2-nd harmonic phases, are shown in Figs. 5.6.6a to d. Data from the LiF crystal panel was included to provide an independent indication of background modulations, and also because of its relative insensitivity to polarisation (discussed earlier in § 5.6.1). [This insensitivity together with the mean background count rate measured for the LiF data of $\approx 0.57 \text{ counts s}^{-1}$, was such that polarisation of X-rays from Sco X-1 would be expected to produce a modulation some ≈ 4.5 times less in the LiF than the graphite data, and therefore allowed this LiF crystal panel to provide, during the 'source + background' observation, a more sensitive measurement of background modulation variations.]

An interpolation procedure was adopted to obtain the background modulation amplitudes and phases which existed during the source observation. To aid in this endeavour, polynomials were fitted to follow the background graphite, and all the LiF, modulation time variations. These polynomial fits are shown as dashed lines, in Fig. 5.6.5a and Figs. 5.6.6a and d, each with a 1-sigma error bar representing the accuracy of the fit.

Concerning the graphite, background, modulation amplitudes, an exponential like decay was observed. This may have been related to a major solar flare (Solar-Geophy. Data 1976) which occurred at the beginning of the first background B1 observation, since this correlated with abnormal, extremely high background levels from both the experiment B and D detectors. (The first few orbits' data of the B1 observation were excluded from the data summation because of these high background levels.) The higher energy LiF modulation amplitudes appeared to remain much more constant.

SCO X-1 OBSERVATION, APRIL 1976

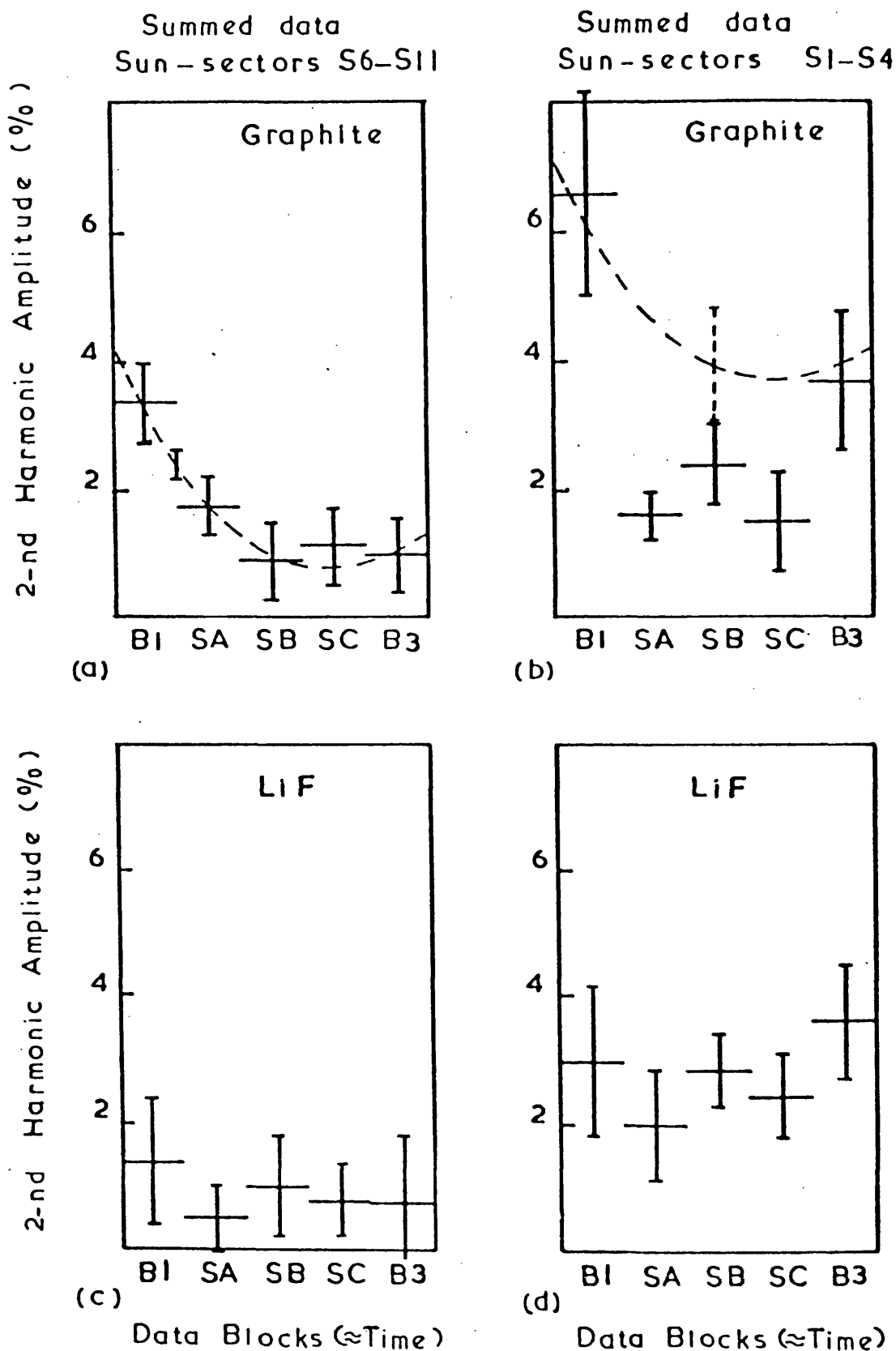


Fig. 5.6.5: 2nd harmonic amplitude modulations plotted in chronological order of observation. (Dashed lines indicate best fit 2nd-order polynomials to the data. Error bars are one sigma standard deviations).

SCO X-1 OBSERVATION, APRIL 1976

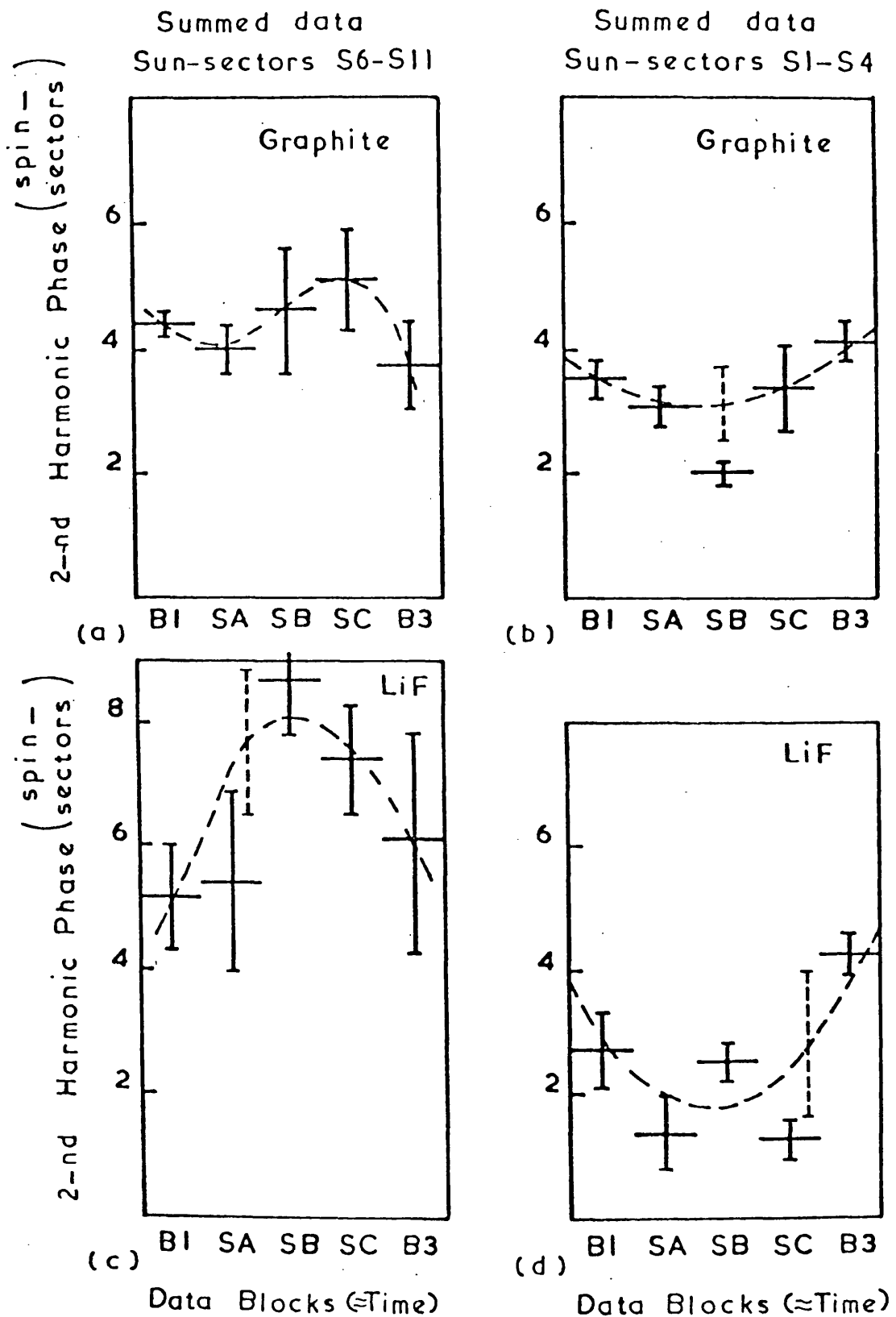


Fig. 5.6.6: 2nd harmonic phase variations plotted in chronological order of observation. (Dashed lines indicate best fit polynomials to the data: 3rd order polynomial to (a), and 2nd order to (b), (c) and (d). Error bars are one sigma standard deviations).

Then, as the two background modulation amplitudes for the (S1 - S4) graphite data also appeared to be appropriate samples of the (S6 - S11) decay curve, it was decided to use this decay curve to obtain a value of the background modulation which existed during the source observation (S1 - S4) data. This decay curve was fitted to the (S1 - S4) graphite B1 and B3 points by minimisation of the χ^2 value for the fit. The error for the fit was determined by variation of the modulation amplitude until the minimum χ^2 value increased by 1 (see Bevington 1969). This fit, and the 1-sigma error, is shown by the dashed curved in Fig. 5.6.5b. Then, the background modulation which existed at the time of the source observation was taken as the mean of the background modulations predicted by this fitted curve at the times of the SA, SB and SC observation blocks. This gave an interpolated background modulation for the (S1 - S4) 'source + background' data as $4.12 \pm 0.90\%$, consistent with the available evidence.

Variations in the 2-nd harmonic background phases were treated in a similar manner to the amplitudes. However, the phase variation trends appeared to correlate with orbit position rather than the crystal as for the case of the amplitude modulations. Following the empirical trends, the polynomial fit to the LiF (S1 - S4) data, reduced in phase variation extent by an amount consistent with the reduced variations exhibited by the graphite data, was fitted to the graphite (S1 - S4) B1 and B3 phase points. From this fit, shown in Fig. 5.6.6b, in an analogous manner as for amplitude variations, the interpolated background phase representative of the source observation was obtained as $\phi_B = 1.03 \pm 0.23$ radians.

Spurious data modulations can also arise from a point, or localised, source of X-rays offset from the satellite spin-axis. However, during the source observation, only Sco X-1 was visible at a mean offset

of 0.4° , where very little 2-nd harmonic modulation would be expected from such an offset. A crude estimation, from variation of calibration curves for the Ariel-V polarimeter, of about $\lesssim 0.4\%$ was obtained. A spurious 2-nd harmonic modulation due to periodic intensity variations of Sco X-1 X-rays would be $\leq 1\%$ (see 1975 Sco X-1 observation).

d) Calculation of the Polarisation Parameters for the Source Sco X-1

The polarisation properties of the source data were determined by subtraction of the above interpolated values for the spurious background modulation amplitude and phase representative of the 'source + background' data, via the method of modified Stokes parameters discussed in § 4.2.4c(ii).

The modified Stokes parameters representing the source data, obtained in this way, were given by

$$\underline{S}'(s) = \begin{pmatrix} I_s' \\ Q_s' \\ U_s' \end{pmatrix} = \begin{pmatrix} 11\ 974.64 \pm 217.78 \\ 274.97 \pm 204.95 \\ 45.93 \pm 260.62 \end{pmatrix}$$

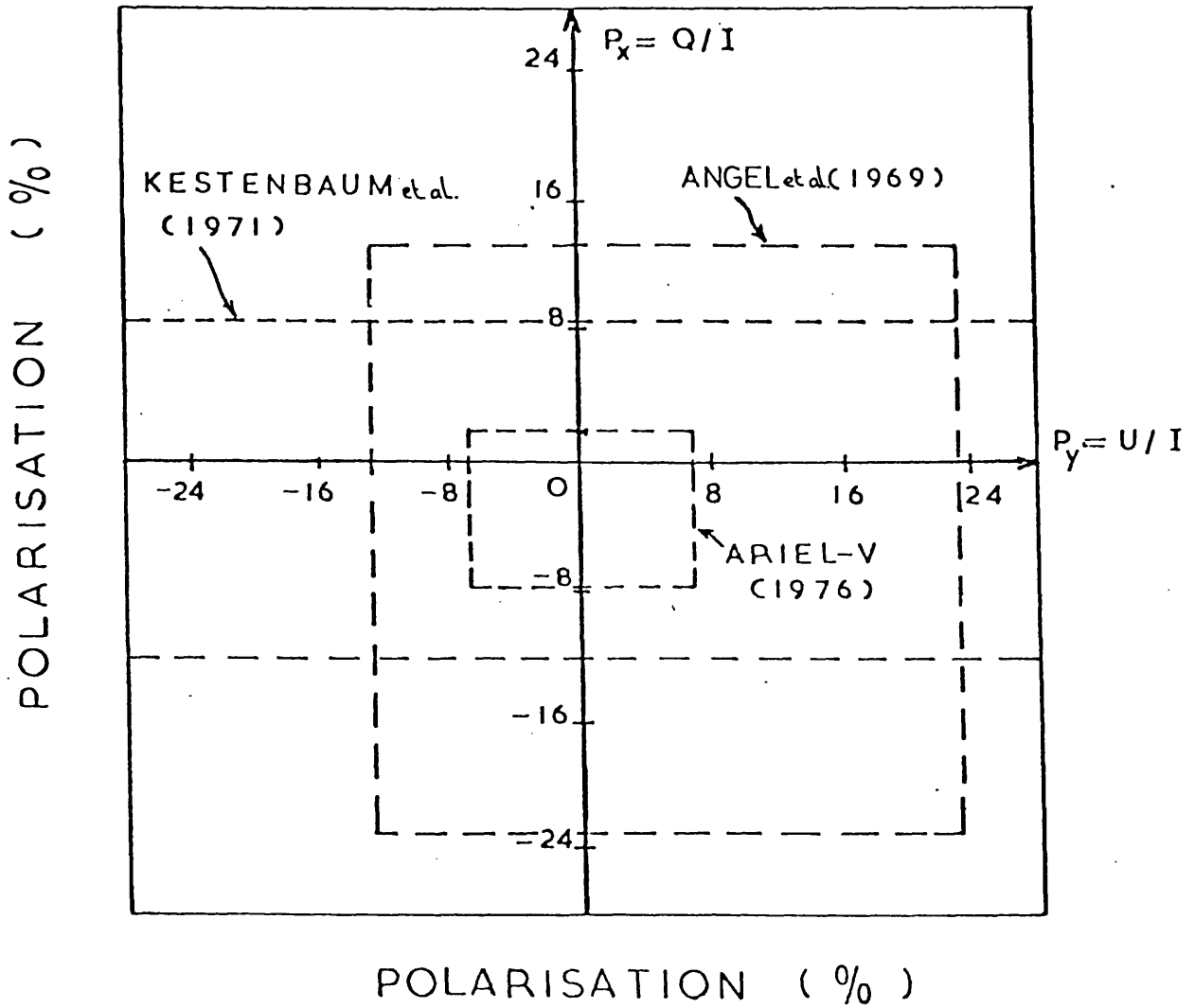
where the errors shown are 1-sigma. From $\underline{S}'(s)$ a value for the degree of linear polarisation, from use of § 4.2.4c equation (192) and the modulation factor m of 0.973 given earlier, was produced as $p_L = 2.39 \pm 1.78\%$. This gives an upper limit on p_L at 3-sigma confidence of 7.7%. This result has been graphically displayed in Fig. 5.6.7 where the previous results of Angel et al. (1969) and Kestenbaum et al. (1971) are also displayed.

The coordinate axes are p_x and p_y , where

$$p_x \equiv \frac{Q_s}{I_s} = p_L \cos 2\theta$$

$$p_y \equiv \frac{U_s}{I_s} = p_L \sin 2\theta$$

FIG.5.6.7. 3-SIGMA UPPER LIMIT CONTOURS OF
THE LINEAR, X-RAY POLARISATION OF SCO X-1



and θ is the position angle of the polarisation.* The calculated value of θ , where the mean position angle of the Sun was calculated as $95.1 \pm 0.7^\circ$, was $90.4 \pm 26.4^\circ$. The values of p_x and p_y were determined as $-2.39 \pm 1.78\%$ and $-0.03 \pm 2.21\%$ respectively where the errors are again one-standard deviation.

§ 5.6.3 Interpretation of Result

This upper limit result, depicted in Fig. 5.6.7, was more sensitive than all previous X-ray polarisation measurements on Sco X-1, and sensitive enough to have relevance to current theories concerning the X-ray emission from Sco X-1.

Specifically, the present result, consistent with Sco X-1 as an unpolarised X-ray source, was compatible with the two previous measurements reported by Angel et al. (1969) and Kestenbaum et al. (1971). This observation also reduced the previous upper limit to the degree of X-ray linear polarisation of Sco X-1 in any direction, at 2.6 keV, to 7.7% at ≈ 3 -sigma confidence.

Recent evidence confirming the binary nature of Sco X-1 (Gottlieb, Wright and Liller 1975; Wright, Gottlieb and Liller 1975; Cowley and Crampton 1975) had increased the probability of expecting linear polarisation associated with emission from a thin accretion disk. Calculations made by Chandrasekhar (1960) and confirmed by Angel (1969), for the limiting case where the optical depth $\tau \gg 1$, imply degrees of linear polarisation for thin accretion disk emission from 0 to 12% dependent upon the viewing angle i between the accretion disk and the plane of the sky. The present upper limit of 7.7%, for this case where $\tau \gg 1$, produced an independent upper limit of $i < 85^\circ$, consistent with a

* Q_s , U_s and I_s represent rotated Stokes parameters so that the positive p_x axis represents linear polarisation in the North-South direction.

recent upper limit reported by Hutchings (1975) of $i < 65^\circ$ from considerations concerning the absence of X-ray eclipse features from Sco X-1. However, this present upper limit is far from achieving the accuracy of a more recent result yet, published by Perrenod (1976) of $i < 30^\circ$, obtained from comparison of light curves of Sco X-1 with predictions from a model in which the photosphere of a non-degenerate star is heated by X-rays from a degenerate companion.

For an accretion disk which is not thin, and has more realistic values for τ , Angel (1969) has published values of polarisation for averaged situations where $60^\circ < i < 120^\circ$. However, in view of Perrenod's result it would now seem desirable that Angel's calculations should be repeated for particular values of $i < 30^\circ$.

Also, from Perrenod's estimate of the likely value of i of $\approx 10^\circ$, Chandrasekhar's calculations indicate that the polarisation expected will only be $\approx 0.1\%$. Thus it can be clearly seen that if future X-ray polarisation measurements are to have relevance to accretion-disk models and confirming Perrenod's result, it is likely that they need to have a much greater sensitivity than the present observation. Also, higher degrees of X-ray polarisation associated with flare emission from Sco X-1 are not excluded, although for this case a short observation time would be required, therefore, again requiring a polarimeter of high sensitivity.

§ 5.6.4 Discussion and Conclusions

The adoption of the conclusions which resulted from the 1975 Sco X-1 observation analysis clearly led to the attainment of this much improved polarisation sensitivity from 17.8% to 7.7%, since:-

- (i) The background modulation amplitude and phase were estimated and subtracted from the 'source + background' data, thereby allowing a considerable reduction in error on polarisation

modulation determination.

- (ii) The small spin-axis offset of 0.3° compared with $\approx 3^\circ$ for the 1975 Sco X-1 observation:-
- a) Resulted in an increased signal count rate by a factor of ≈ 1.5 , which reduced the effects of background level and modulation errors being propagated as uncertainties in the polarisation modulation, and also allowed an increased MDP sensitivity for equal observation durations.
 - b) Allowed relaxation of error estimates for a spurious modulation which might be caused by the offset, unpolarised, X-ray continuum flux from Sco X-1.
- (iii) Also, the longer observing time on Sco X-1 of 10 days for this 1976 observation helped to further increase the statistical sensitivity from the 4% MDP ($3-\sigma$) for the 1975 Sco X-1 observation to 1%.

It would be expected that a possible future polarisation observation of Sco X-1 with the Ariel-V polarimeter could, using a similar observing program to that of this 1976 Sco X-1 observation, together with a slightly longer observation duration on the background (to reduce the statistical error on the background modulation), and also without the disturbing influence of a major solar flare, produce a practical polarisation sensitivity of around 3 to 5%.

However, to obtain a polarisation sensitivity of about 1% using again this method of measuring background modulations, would require a prohibitively long continuous observation duration of about 2 months; or alternatively, achievement of greater sensitivity via accurate theoretical prediction of the complex background modulations would seem a formidable task.

Also, in general, for observation of weak sources, the smallest

modulation error in the background can become greatly magnified via the S_0/B_0 ratio, from of the order of 1 (for Sco X-1) to 10^4 times (for an \approx 1 U.U. source) in terms of the spurious source polarisation produced. It would therefore seem likely that only a new design of polarimeter, one where the S_0/B_0 ratio would be considerably greater, would be able to achieve much more sensitive polarisation measurements. That is, possibly, observation from a focusing polarimeter (see § 4.2.3c).

§ 6	<u>CONCLUSIONS</u>	
		Page
§ 6.1	RECENT RESULTS	271
	1. General	271
	2. Galactic sources	271
	3. Extragalactic sources	282
	4. Unidentified High Galactic Latitude Sources	285
§ 6.2	ARIEL-V POLARIMETER PERFORMANCE	287
	1. General Performance	287
	2. Estimated Instrument Sensitivity	287
	3. Spurious Modulations	289
	4. Capability for Broad Band Polarimetry	294
§ 6.3	FUTURE X-RAY POLARIMETRY	301

§ 6.1 RECENT RESULTS

§ 6.1.1 General

During the $\approx 2\frac{1}{2}$ years since the launch of the Ariel-V satellite in October 1974 to the approximate time of writing these conclusions (mid 1977), the number of X-ray sources discovered has been seen to rise from the 161 sources listed by the 3U catalogue to over 200 (Dailey and Fishman 1977). Some 50 new X-ray sources had been detected (see Pounds 1976a) before the end of 1976 by the Ariel-V experiment B Sky Survey Instrument (SSI), half of which lay well off the galactic plane.

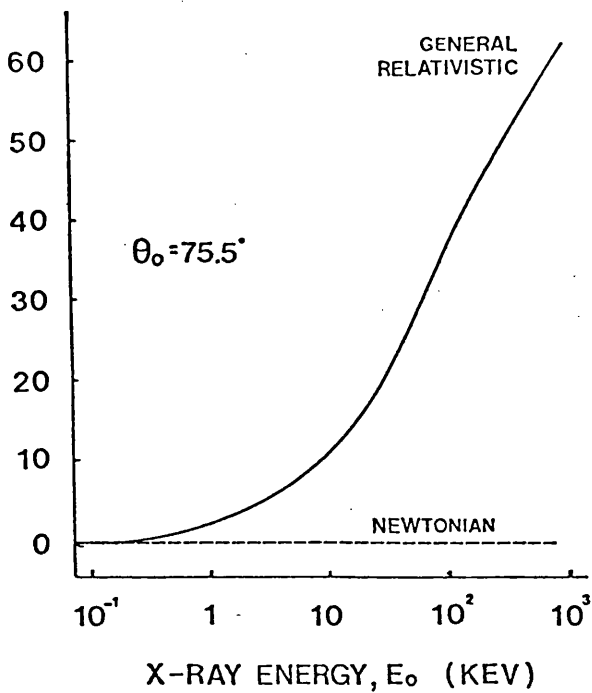
Also during this period a new 'type' of X-ray source had been discovered and termed "burster" sources (see Grindlay 1976).

§ 6.1.2 Galactic Sources

A major advance for the potential understanding of galactic sources has been the publication of several theoretical reports concerning X-ray polarisation properties predicted for the most abundant galactic X-ray emitting group - the binary sources. Rees' (1975) wide ranging report has already been discussed in the review chapter (§ 2). Lightman and Shapiro (1975) note that, in addition to providing information about accretion disk structure and orientation, observation of X-ray polarisation will also be crucial in confirming simply the existence of an accretion disk. Also, Lightman and Shapiro report that the 'standard' instability-free disk model is inapplicable for Cyg X-1, believed to contain a black hole, since for reasonable parameters ($6-10 M_{\odot}$, total luminosity $< 10^{38}$ erg s⁻¹) it does not predict the observed high energy X-ray flux at > 10 keV. Thus, alternatives to the standard disk model for Cyg X-1 must be considered, possibly involving the types of modification suggested by Rees (1975), or others suggested by Lightman and Shapiro. However

recently, Stark and Connors (1977) have reported application of general relativity to the problem of a fast rotating black hole embedded in an accretion disk. This has led to a new potentially very important result that the predicted polarisation effects on the emitted X-rays are large, sufficient, at least for Cyg X-1, to easily distinguish between such a black hole and a neutron star as the compact companion. Furthermore, Stark and Connors (1977) have reported that their general relativistic prediction of the X-ray polarisation properties from an accretion disk around Cyg X-1 would be similar for most disk models. In more detail, the general relativistic effects on the polarisation properties for a fast rotating black hole are predicted an order of magnitude greater than for a slowly rotating black hole or for a neutron star. The general relativistic effects, whilst completely altering the classical Newtonian situation (see Fig. 6.1.1), are also reported to be typically an order of magnitude greater than those due to special relativity. From Fig. 6.1.1a it can be seen that a large variation of the plane of polarisation with energy will be expected, amounting to about a 10° rotation between 1 and ≈ 20 keV, this extending to about a 60° rotation at 10^3 keV for a disc viewed at 75.5° from a normal to the disk. Similarly, from Fig. 6.1.1b, it can be seen that a fairly distinctive peaked behaviour in the degree of polarisation is expected with energy, the peak value being lower than the Newtonian value. Stark and Connors conclude that the opportunity for testing the black hole hypothesis for Cyg X-1 is provided by these large gravitational rotation changes in plane of polarisation with energy, which would be expected for most disk models whether optically thick or thin. Furthermore, in order to observe such effects it was noted that future X-ray satellite polarimeters will need to be more sensitive over a wider range of energy, than has been recently available. At present only a single measurement of the degree of linear polarisation of

ANGLE OF PLANE
OF POLARIZATION,
 Φ (DEGREES)



PERCENTAGE
LINEAR
POLARIZATION, $\bar{\delta}$

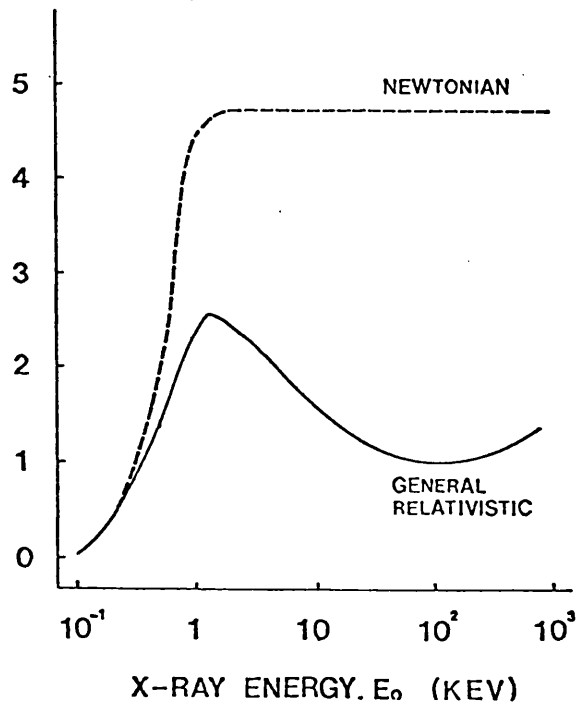


Fig. 6.1.1: Classical and General relativistic predictions for polarisation properties of X-ray emission from an accretion disk surrounding a fast rotating black hole (from Stark and Connors 1977).

- a) Variation of plane of polarisation with energy.
 θ_0 (inclination of disk to observer) = 75.5°
 $(\theta_0$ of 90° would mean an edge-on disk)
 viscosity $\alpha = 0.1$, mass of black hole $M = 9M_\odot$
 mass accretion rate = $7 \times 10^{17} \text{ gs}^{-1}$.
- b) Variation of linear polarisation with energy.

X-rays from Cyg X-1 of 3% has been obtained, at a marginal significance of $2\frac{1}{2}\sigma$. This recent result was obtained from the polarimeter on board the OSO I satellite, and reported by Novick (see Stark and Connors 1977).

As discussed in the previous chapter, observations from the Ariel-V polarimeter has resulted in publishing recent X-ray polarisation results on two galactic X-ray sources. These sources were Sco X-1, recently confirmed to be a binary system, and the powerful X-ray transient (Nova) source A0620-00. $\overline{\sphericalangle}$ An optical counterpart for A0620-00 was discovered, where both the optical and X-ray measurements were consistent with a galactic source at a distance of ≈ 1.5 kpc (see Griffiths et al. 1976b). $\overline{\sphericalangle}$ For both these sources upper limits on X-ray linear polarisation at ≈ 2.6 keV, of 7.7% for Sco X-1 and 2% for A0620-00, were produced. The upper limit on Sco X-1 was also lower than that previously achieved (see § 2). Both these upper limits were interpreted via Angel (1969), Rees (1975) and Chandrasekhar's (1960) works which together relate the degree of polarisation to accretion disk emission according to optical depth, viewing angle i (see § 5) and shape of the accretion disk - all important parameters, which determine major characteristics of the expected emission mechanisms for these objects. The Sco X-1 result was consistent, for a thin, optically thick, accretion disk, with the inclination i of the disk to be $< 85^\circ$, in agreement with independent estimates of i of $\leq 65^\circ$ (Hutchings 1975) and $\approx 10^\circ$ (Perrenod 1976). Thus, clearly, it could be seen that more sensitive X-ray polarisation observations of this source will be useful in providing a more testing confirmation of the expected inclination angle i . It was also noted that higher degrees of X-ray polarisation expected from flare emission were still possible. Also, recently Rees (1977, private communication) had suggested that it might be possible to observe the change in plane of X-ray linear polarisation for different portions of the binary orbit of Sco X-1 due to

the method proposed (Rees 1975), whereby X-rays generated from the suspected accretion disk emission mechanism are reflected off the primary component. From Rees (1975) it would seem that, in general for close binary systems, such polarisation degrees would be expected to be high, of the order of 20-50% for hard X-rays (≥ 8 keV), and also that this polarisation might be expected even at lower energies if the system contains an ionised wind or corona with significant scattering optical depth. Furthermore, specifically for Sco X-1, Tsuruta (1976) had proposed a supercritical accretion model, whereby during the optically "bright" phase (characterised by $B \lesssim 12.8$, and both optical and X-ray flaring) the Eddington luminosity limit is exceeded. This 'bright' phase was argued to correspond to radiation produced from a surrounding gas cloud, whilst the 'dark' phase, not subject to X-ray flaring, is supposed to correspond to radiation from an accretion disk. It is interesting to note that recently Hutchings (1975) had also suggested supercritical accretion for Sco X-1. From Tsuruta's paper it appears that her above model can be hoped to naturally explain the major characteristics of Sco X-1 reported from X-ray, optical and radio observations (explaining, in general terms, the existence of the two radio lobes associated with Sco X-1 by mass flow outwards approximately along the rotation axis of the accreting object, due to the least resistance offered for those directions. This outward flow, or 'wind', would be supported by the high radiation pressure caused by accretion from the disk). Thus, if Tsuruta's model for Sco X-1 is valid, then it may be expected that the X-ray polarisation properties of Sco X-1 could depend upon its intensity state. Then, X-ray polarisation associated with accretion disk emission would be expected during the dark phase, whilst during the bright phase X-ray polarisation properties would become associated with the proposed surrounding gas cloud for which production of a comparable additional component of X-ray emission is expected. For a

spherical cloud, or nearly so, little or no polarisation would be expected, though many uncertainties associated with the bright phase model could easily change this expectation.

From a recent X-ray linear polarisation observation of the Crab Nebula supernova remnant from the OSO I satellite, Weisskopf et al. (1976b) have reported a result of a much improved accuracy compared with the $15.4 \pm 5.2\%$ at a position angle of $156 \pm 10^\circ$ obtained from the previous rocket flight observations (see § 2). The new observation was for 6 days from 1976 March 11 to 17-th from which 15 "quick-look" orbits data were analysed. At 2.6 keV and 5.2 keV, degrees of linear X-ray polarisation of $15.7 \pm 1.5\%$ at $161.1 \pm 2.8^\circ$ and 18.3 ± 4.2 at $155.5 \pm 6.6^\circ$ were obtained respectively, consistent with the X-ray polarisation being independent of energy. These results, as Weisskopf et al. reported, confirmed the previous measurement and also, with much higher confidence, that synchrotron radiation is responsible for the Crab Nebula X-ray emission.

At present only preliminary X-ray polarisation results for two other sources have been reported concerning observations from the OSO I satellite. Upper limits to the degree of linear polarisation from GX5-1 (3U1758-25) and Cen X-3 (3U1118-60) of 12% and 28% respectively, were obtained at 99% confidence for the integrated X-ray emission from narrow bands about 2.6 keV and 5.2 keV (Weisskopf et al. 1976). It was stressed that these results assumed no large effects from spurious background modulations that might be present, particularly the Cen X-3 data for which the signal to background ratio was approximately unity. Table 6.1.2 lists the 4 binary sources, for which Weisskopf et al. expects that OSO I observations will have been completed by the end of 1975, together with the X-ray polarisation sensitivities hoped to be achieved. As yet only the already discussed result on Cyg X-1 has been available, though it may be expected that more will soon be forthcoming, providing new, and also

Sensitivity to Polarization of Binary Sources

Source	Minimum Detectable Polarization		
	First Order (%)	Second Order (%)	Combined (%)
Cen X-3	5.0	8.7	4.4
Her X-1*	10.2	13.2	8.1
Cyg X-1 [†]	5.0	12.8	4.8
Cyg X-3 [§]	5.7	12.1	5.3

*Observation time known; source strength estimated.

[†]Observation time known; Poisson statistics assumed; source strength estimated.

[§]Observation time and source strength estimated.

Table 6.1.2: The 4 binary X-ray sources hoped to have been observed by the end of 1975 by the OSO I polarimeter, together with the 3- σ sensitivities hoped to be achieved (from Weisskopf et al. 1976).

improved results, before the next generation of polarimeters are flown.

Concerning 'transient' X-ray sources (see § 2) an unexpectedly large number had been recently discovered lying close to the galactic plane and reaching considerable peak intensities. The 5 'bright' transient sources known before the launch of the Ariel-V satellite, had been increased to 12 by April 1976 (Pounds 1976b) and these are listed in Table 6.1.3. Pounds reports that these transients, having a sky distribution concentrated along the galactic plane, are clearly a galactic population with typical distances ranging from 1-10 kpc. Some other transients observed to be fainter and at high galactic latitude, Pounds reports as being of an apparently different class, and these are discussed in the section concerning unidentified sources, § 6.1.4. It was reported that the observation of the bright galactic transients has also led to several important advances, in particular the discovery of 2 sources A118-61 and A0535+26 which exhibit strongly pulsed X-rays, and also the first secure identification of a transient source, i.e. A0620-00. Furthermore, the spectra of the two above pulsating sources were amongst the "hardest" of any cosmic X-ray source, and unlike most of the others in Table 6.1.3 which exhibited "soft" spectra. The high degree of sky coverage by the Ariel-V sky survey experiments together with the observed rate of transient discoveries, has also allowed a prediction to be made of the expected rate of transients for the total galaxy as less than approximately 40 per year (Pounds 1976b). Pounds also reports that though no direct evidence yet exists for any transient to be involved in a binary system, he believes that variable mass transfer in a binary system, containing preferably a neutron star or black hole, remains the most likely explanation for the bright, galactic, X-ray transients. However, some recent reports of the transient source A0620-00 do now provide some direct evidence for a binary nature for this source. Matilsky et al.

Source	Peak (if seen)	Ref.	Peak int. (X Crab)	β_{II}	Rise-Time (10-90%)	Decay (to 10%)	Remarks
1. Cen X-2	Ap 67	1-3	20	0	-	~2 m	-
2. Cen X-4	Jl 69	4-7	25	23	~4 d	2 m	rapid precursor?
3. 3U 1735-28	Mr 71	8	0.6	1.6	<5 d	<1 m	-
4. 3U 1543-47	Jl 71	9, 10	4	5.4	-	4.5 m	-
5. Cep X-4	Jn 72	11	(0.15)	3.4	-	-	peak not seen
6. A 1524-62	Ne 74	12	0.9	-4.5	~3 d	3 m	strong precursor
7. A 1246-58	De 74	37	~0.15	3.5	-	-	-
8. A 1118-61	De 74	13-16	0.2	-0.8	3-7 d	0.5-1 m	405 s period Be Star?
9. A 1742-28	Fe 75	17, 18	2	0	-	1 m	radio source?
10. A 0535+26	Ap 75	19-24	1.5	-2.6	6 d	0.5-1 m	104 s period Be star (HDE 245770)?
11. A 0620-00	Au 75	25-36	30	-6.5	4 d	2.5 m	strong precursor optical nova radio and IR source
12. A 1744-36	Fe 76	37	~0.15	-4	-	<1 m	-

Table 6.1.3: The bright, galactic plane transient X-ray sources (from Pounds 1976b).

(1976), Chevalier (1976) and Tsunemi et al. (1977) have all reported evidence for an ≈ 8 day period in the emission from A0620-00. Both optical and X-ray observations were used. Although one report by Duerbeck and Walter (1976) gives evidence for a period of approximately half the above value, the bulk of the present evidence is against this being the primary modulation.

It is also interesting to note that this evidence for a period in the emission from A0620-00 supports Griffiths et al.'s (1976b) polarisation measurement interpretation in terms of an accretion disk associated with a binary system, since Griffiths et al.'s interpretation was largely based on evidence that a model of the plasma associated with A0620-00 had accretion disk characteristics. The $3-\sigma$ upper limit obtained by Griffiths et al. of 2% to the linear X-ray polarisation at 2.6 keV, was taken to imply an upper limit to the inclination angle i of $< 57^\circ$ for a physically thin accretion disk which is optically thick, or conversely, parameters for a thicker disk (see § 5).

The new type of X-ray source, discovered since the launch of the Ariel-V satellite and termed "burster" sources, were first discovered from observations by the ANS satellite in September 1975 (see Pounds 1976a, Grindlay 1976); and within several months of this first report, over a dozen further sources were reported, together with tentative lists for many more (Grindlay 1976). The main distinguishing characteristics of these sources are that the bursts, are typically at least an order of magnitude more intense than variations of known sources on similar time scales, and display rise times at least two orders of magnitude faster than comparably large "flares". Burst intensities several times greater than the Crab Nebula intensity have been observed, and typical rise-times of ≈ 1 s are reported (Grindlay 1976). Other characteristics of these sources (Grindlay 1976) are that their spectra often hardens during the

decay, and that a given burst source is only active for a fraction $\approx 10\%$ of the time, for which during these relatively brief active periods the bursts recur (quasi-periodically) with reasonably well defined intervals $\approx 10^3$ times as long as the burst duration. Also, some bursters have been detected as "steady" X-ray sources.

Grindlay reports that although no positive identifications have yet been made, the early indications are that these bursters are a galactic population with the distribution of sources concentrated in the disk and central bulge of the galaxy. Also, a number of bursters have been possibly identified with galactic globular clusters, and as yet there are no sources which could definitely not be associated with a globular cluster. Furthermore, none of these sources has yet revealed regular pulsations or eclipses which would directly connect them with binary stars.

Grindlay further argues that, given the strong evidence that the bursters are somehow linked to systems like globular clusters, that perhaps the same mechanisms that operate in globular clusters to produce d.c. X-ray sources could also lead to bursters. He notes that there are 5 quite certain identifications of normal X-ray sources with globular clusters (i.e. NGC 1851, 6440, 6441, 6624 and 7078) all of which display high central densities $\approx 10^5 M_{\odot} \text{pc}^{-3}$ and that for 2 of these the X-ray emission has been shown to lie with the central core. He reviews that in support of binary models for bursters are models invoking magnetic instabilities for the rapid burster relaxation oscillator, and a burst scattering model with a dense cloud around a few solar mass X-ray sources. The alternate hypothesis concerns spherical accretion onto a massive black hole. He further argues that the high observed luminosities and required magnetic fields begin to strain neutron star binary models; though a black hole, either starved of gas, or spherically accreting near an Eddington type limit ≈ 100 times lower than normal (because of radiative

heating of infalling gas giving molecules thermal velocities $>$ escape velocity) could explain the observed luminosities, and such a mechanism could also lead to unstable flow thereby producing a relaxation oscillator which, in turn, could explain the quasi-periodicities of the bursts.

X-ray polarisation from these intense burst sources could be hoped to provide information on the mechanism producing the bursts, since presumably a high degree of linear polarisation would be likely if most of a burst X-ray emission arises from a highly directional flow of material. However, in order to be able to measure the linear X-ray polarisation of a burst, future polarimeters will be required to possess a very large increase in sensitivity compared with those at present in operation. (The Ariel-V polarimeters had an effective area of $\approx 46 \text{ cm}^2$ for the graphite panel at $\theta_B = 45^\circ$, and required $\approx 3 \times 10^5 \text{ s}$ to obtain a 14% (3- σ) M.D.P. for the Crab Nebula, and therefore an effective area $\approx 10^3$ to 10^4 times greater (i.e. $A_e \gtrsim 50,000 \text{ cm}^2$) would be required to measure the polarisation of a burst of several times the Crab intensity, but lasting only 10 s.)

§ 6.1.3 Extragalactic Sources

While no X-ray polarisation measurements have yet been performed for any extragalactic sources, much general information has been recently gathered and reported by Pounds (1977).

For the division of extragalactic sources concerned with individual galaxies (or objects), the most dramatic increase in number of discovered sources was reported to occur for the Seyfert galaxies. From only one (NGC 4151) listed in the 3U catalogue this had been increased to 12 (see table 6.1.4), so these Seyferts now almost certainly represent a 'class' of X-ray emitters which furthermore dominate the whole group of 'active' galaxy X-ray sources. It was reported that it would now seem

Table 6.1.4: X-ray sources identified with Seyfert galaxies (from Pounds 1977).

3U catalogue identifications	(2)	NGC 4151, NGC 1275
3U identifications confirmed		
by 2A position	(1)	NGC 5506
or Copernicus	(1)	3C 390.3
New 2A identifications	(8)	NGC 3783
		NGC 5548
		NGC 7469
		IC 4329A
		Mk 79
		Mk 279
		Mk 376
		Mk 509

Table 6.1.5: X-ray sources identified with clusters of galaxies (from Pounds 1977).

3U catalogue identifications (12)	Virgo, Coma, Perseus, Centaurus, Cygnus A, 3C129, A161, 262, 401, 1367, 2256, 2319
3U identifications confirmed by 2A position (6)	A478, 754, 1060, 2142, 2147, 2199
Kellogg* list confirmed by 2A observations (2)	A496, 576
New cluster identifications (9)	A85, 119, 1146, 1795, Vidal Cluster, CA 0340-538, Sersic 40/6, Anon 0316-44, Klem 44

unlikely that the powerful emission from these Seyfert galaxies would not be associated with their nucleus. Also, it was noted that this Seyfert dominance be even more enhanced if Weedman's (1976) argument, assuming cosmological redshifts, that QSO's may be simply distant Seyferts with $z > 0.1$ is true, which would then involve another discovered QSO PKS 0349-14 in X-rays, and also 3C273, being incorporated into the Seyfert group.

The number of extragalactic sources whose X-ray emission has been reported to vary on timescales of months or less now includes Cen A, NGC 4151, 3C 390.3, and probably 3C 273. In addition X-ray emission from a new source probably associated with the galaxy BL Lac Mk421 has also been observed to be highly variable.

Concerning the other division of extragalactic sources, the clusters of galaxies, a further 9 were reported as identified from Ariel-V observations. Pounds lists 29 clusters for which identifications have been made and have been seen by the Ariel-V SSI (see Table 6.1.5). Pounds (1976a) reports the gathering strength of the hot intra-cluster gas emission mechanism for X-rays from these sources.

§ 6.1.4 Unidentified High Galactic Latitude Sources

Concerning the 56 unidentified high galactic latitude sources (UHGLS) listed in the 3U catalogue with a galactic latitude $> 10^\circ$, Pounds (1977) reports that the Ariel-V survey, together with the new 4U analysis, has now revealed that 11 have been identified with Seyferts or clusters, and 5 more recently identified as 3C 120, AM Her, NAB 0137-01, A 2204 and θ^2 Ori. Others still have large error boxes for which Pounds considers that many may be additional members of established classes, e.g. distant clusters or nearby low luminosity star systems such as AM Her. Also, 11 sources are not confirmed by the Ariel-V survey and are listed as doubtful

in the revised Uhuru analysis. Thus, it is reported that there does not seem to be a strong case for any new class of extreme X-ray emitter.

Pounds (1976b) reports observations of an apparently different class of transient X-ray source than the bright (> 150 Uhuru Flux Units, (UFU)) sources detected at low galactic latitude. It was reported that 5 examples of these high galactic latitude transients had been detected by the Ariel-V SSI, one apparently twice. They were observed to be characteristically less bright, reaching peaks of only 50-60 UFU, and also more brief, remaining bright in all but one case for ≈ 1 day. (c.f. the bright galactic transients which remain bright for \approx few days to several months). The only exception to this characteristic behaviour for the high galactic latitude transients was A1103+38, for which Pounds (1976b) noted a proposed identification with the BL Lac type galaxy Mk 421, and in a later paper (1977) reported a communication from Ricketts where an error box reduced by a factor of 3 still contained this object.

§ 6.2 ARIEL-V POLARIMETER PERFORMANCE

This section discusses the performance of the Ariel-V polarimeter with respect to its initial aims; focuses attention on those aspects which limited its sensitivity and usefulness; and includes suggestions where major improvements would be appropriate for future instrument design.

§ 6.2.1 General Performance

This first serious attempt to detect X-ray polarisation of extra-solar sources from a satellite experiment was to take advantage of the long observing time available, compared with that from the previous short duration rocket flights, and to learn from this attempt.

Indeed, the reduced statistical fluctuations obtained because of a long observation on Sco X-1 were directly responsible for the improved X-ray polarisation upper limit, more sensitive than previous observations had managed to achieve. The opportunity for this satellite experiment to observe, and obtain a sensitive polarisation measurement on a powerful transient source A062-00, was also a result of the long observation times available.

The low signal to background ratio, together with the unexpected discovery of spurious modulations in the background data, were seen to be major factors which prevented further advantage being taken of the long observing times.

§ 6.2.2 Estimated Instrument Sensitivity

The observations discussed in § 5 verified that the reported (Peacock 1975) difficult estimate of the expected background levels at ≈ 0.8 and 1.0 counts s^{-1} for the graphite and LiF crystal systems were reasonably accurate. The observed background count rates normally ranged from 0.7 to 1 counts s^{-1} for the graphite system and from about 0.5 to 1.2 counts s^{-1} for the LiF system.

The observations on Cyg X-3 (Peacock 1975), and on Sco X-1 during 1975 confirmed the close agreement with the observed and expected signal count rates. For the 1975 Sco X-1 observation, the instrument was predicted to produce $0.7 \text{ counts s}^{-1}$ for the graphite system, and a reasonable $0.6 \text{ counts s}^{-1}$ were observed. Peacock confirmed that the expected graphite count rate from Cyg X-3 was consistent with that observed, and, after taking an improved background count rate, the signal count rate from the LiF system.

The accuracy of these predicted background and signal count rates was reflected by the accuracy of the predicted M.D.P. sensitivities (given in Fig. 4.2.15). Scaled down for a ≈ 4 day observation on Sco X-1 (allowing for the reduced visibility of Sco X-1 (see § 5.1), and number of discarded orbits data) and a ≈ 6 day observation on Cyg X-3, the respective expected polarisation sensitivities of 3.7% and 100% were close to the achieved theoretical M.D.P.'s of 4.1% for Sco X-1 and 100% for Cyg X-3.

The long observation times (≈ 10 days) required to obtain sufficient sensitivity (even on a strong source ≈ 1000 UFU) was due to the small effective area of the instrument; only $\approx 40 \text{ cm}^2$ for each crystal panel. (The actual surface area of the crystal panel was $\approx 200 \text{ cm}^2$, approximately a factor of 5 greater than the effective area.) An increased effective area, for example 4000 cm^2 , would allow observation times to be reduced by a factor of 10^2 (i.e. a 10 day observation from the Ariel-V polarimeter could be performed in only 0.1 day with the larger instrument. Or, conversely, a source 100 times as weak could be observed to a comparable polarisation sensitivity in the original 10 days). This increased effective area could be expected to require a surface collecting area of $\approx 10,000 \text{ cm}^2$ (i.e. $1 \text{ m} \times 1 \text{ m}$) though, of course, when projected to a Bragg angle of 45° the linear dimensions of a box capable of containing

the instrument would be $\approx 85 \times 85 \times 85 \text{ cm}^3$. This relatively low estimate of $10,000 \text{ cm}^2$ is taken, since I have assumed that the proportional effects of experiment support structure reducing the collecting area of a large instrument, could be significantly reduced from those required for the small Ariel-V polarimeter. Large areas can also be obtained using grazing incidence mirrors (see Novick 1975).

It may also be noted that a value for R_c could be approximately twice as great as that for the Ariel-V polarimeter, thereby doubling the detected signal, if trade-offs for use of such an instrument as a spectrometer do not need to be made. See § 3.2.3.

However, for this Bragg crystal type of polarimeter, it is concluded that only via increased effective area, is a conceivable, practical method that will allow:-

- (i) Weak X-ray sources to be observed to sufficient polarisation sensitivity in a reasonable (≈ 10 day) observation time, and
- (ii) Polarisation determination of short lived events, for example, flares and the recently discovered burst phenomena.

Thus, it is advised that increased effective area be a prime consideration for future instruments.

§ 6.2.3 Spurious Modulations

Possible sources of spurious modulation were divided into 3 categories in § 4.2.3c and discussed in detail. They were those due to:-

- (i) An offset source.
- (ii) Time variations in the intensity of the observed source.
- (iii) Background radiation.

i) Offset Source Modulations

The calibration curves for the Ariel-V instrument indicated that

these would be small for small offsets. (It is expected that there would be some residual modulation even at zero offset due to small internal misalignments of the instrument.) However, since no laboratory calibration was carried out on the Ariel-V assembled instrument before flight, this meant that an inconvenient and perhaps somewhat inaccurate method had to be adopted whereby such modulations for various offsets had to be estimated from calibration graphs concerning only limited portions of the experiment. However, the estimated spurious modulation at the polarisation frequency, dependent upon the Bragg angle, of $\approx 1\%$ for the offset range used of, ≈ 0.3 (for nominal zero degree offset observations) to 3° , was negligible for the Ariel-V data compared with other sources of error.

This insignificance of such a source of offset produced error, however, may not be so for future polarimeters, and it is therefore advised, that either careful thought, or much preferably a laboratory calibration is performed on any future, assembled instrument before flight. A laboratory calibration is envisaged where an assembled instrument is subjected to an offset source of X-rays of known intensity and polarisation state. Then, either the X-ray source is moved at constant offset about the line of sight to the instrument, or the instrument is rotated. Results from such a laboratory calibration may also give further information on the desired pointing accuracy required of the instrument; for example, an offset of only a few arc minutes may be sufficient to reduce these spurious modulations to an acceptable level.

Also, as future instruments are likely to be observing sources in the galactic plane where the density of sources is great, it is realised that there will be a much higher probability for more than one source to be in an instrument's f.o.v. than has been at present. Then, the presence of secondary sources in the f.o.v., offset from the pointing direction,

will mean that spurious modulations will be likely to be produced. Future instruments should be able to avoid this situation if they are equipped with suitably narrow f.o.v. collimators.

ii) Time variations in the intensity of the observed source

The Ariel-V polarimeter was not specially equipped with the means to measure or eliminate time variations likely to produce spurious polarisation measurements (see § 4.2.3c). It may be recalled that the Sco X-1 observations relied upon a previous search for periodic time variations in order to eliminate a possible large component of spurious modulation.

However, spurious polarisation modulations arising from irregular, unknown, or unpredictable, time variations (possibly flare type), cannot be eliminated in the above way. Also, the time variation nature of a source may not have been extensively, or sensitively, established prior to an X-ray polarisation measurement (e.g. a transient source (A0620-00)).

A solution, as set out in § 4.2.3c, which completely eliminates the effect of such time modulations, is to measure, for example, orthogonal components of polarisation simultaneously. Then, time modulations appear as in phase modulations in the two simultaneous measurements, and polarisation appears as 180° out of phase (see Novick 1974, Clark and Grainger 1971). This solution can be achieved by the provision of two, or more, separate crystal faces fixed at different rotation phase angles, the outputs being fed into separate detectors.

iii) Background radiation

Spurious modulations in the background data were considered the greatest cause for loss of polarisation sensitivity with the Ariel-V polarimeter.

It was noted in § 5 that 2-nd harmonic modulations in the

background data from ≈ 2 to 8% for both crystals were observed, capable of producing spurious polarisation measurements. It could also be seen that the low signal to background ratios obtained (≈ 0.1 for a 1000 UFU source), acted to considerably magnify the effect of even small spurious background modulations into large spurious effects in the source data, from which a search for polarisation is made.

A high signal to background ratio would considerably reduce the effects of possible spurious background modulations for future instruments.

It has been stated by Schnopper and Kalata (1969) and Novick (1974), (see § 4.2.3) that large signal to background levels may be achieved by use of a focusing instrument. The polarimeter at present being flown on OSO I is an example of this idea. The signal to background for this OSO I instrument was estimated at ≈ 100 times better than for the Ariel-V polarimeter (see § 4.2.3c).

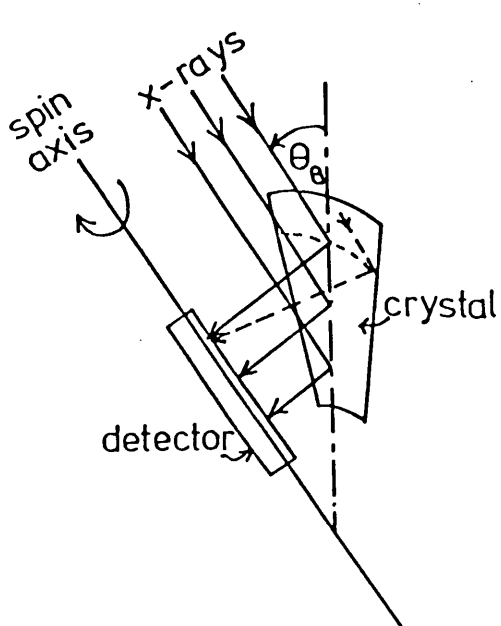
By fixing many small flat crystals onto a curved surface (plate), such focusing may be achieved. This focusing allows the use of a very small detector, for which the background count rate is expected to be very low (since the background level is largely expected to be proportional to the surface area of a detector).

If the curvature is as shown by Fig. 6.2.1a (e.g. in the spin-plane), then some loss of polarisation resolution may be expected.

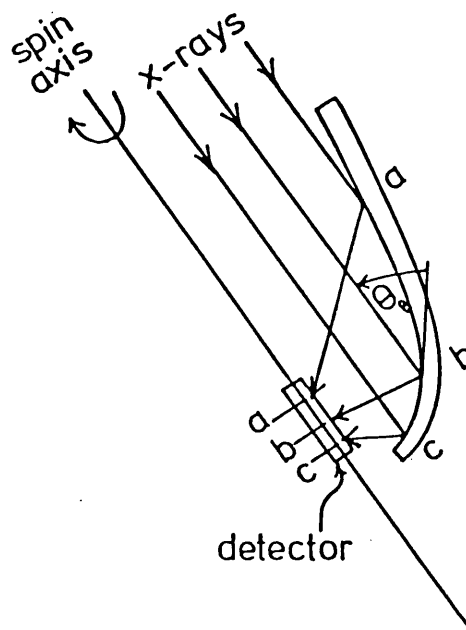
If the curvature is in the dispersive plane, as shown by Fig. 6.2.1b (e.g. perpendicular to the spin-plane) then several Bragg angles will be selected simultaneously, and therefore also several energies.

If, for example, we assume that only modest increases in background to signal sensitivities of about 20 can be reasonably obtained for each of these curvatures, then a doubly curved crystal polarimeter shown in Fig. 6.2.1c would be expected to have a considerable gain of ≈ 400 compared with a flat crystal experiment.

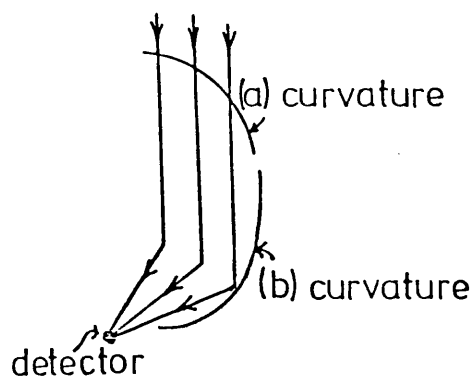
Fig. 6.2.1: Focusing curvatures for a Bragg crystal polarimeter.



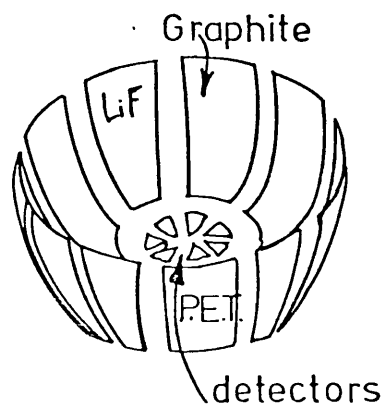
a) Curvature in spin-plane.



b) Curvature perpendicular to spin-plane.



c) Double curved system.



d) Circular, curved crystal, segmented polarimeter.

Whilst theoretically the possible gain in signal to background is infinite with use of focusing instruments, and in practice, compared with the Ariel-V polarimeter, enormous gains should be achieved, it is expected that some limitations will become evident. Ability concerning accuracy of focusing, limiting small size of detectors, and largeness of collecting area, are envisaged as some practical gain constraints.

(Some considerations with respect to prevention of possible spurious modulations caused by adoption of a focusing system are discussed in § 4.2.3c(i).)

§ 6.2.4 Capability for Broad Band Polarimetry

For the Ariel-V polarimeter, the capability to perform polarisation measurements at different energies was not considered a primary objective. The instrument was basically designed to perform polarisation measurements at only $\theta_B = 45^\circ$ for which the sensitivity to polarisation was greatest. However, as one crystal panel was constructed from graphite crystals and the other from LiF crystals, this naturally gave a small broad band capability, since at $\theta_B = 45^\circ$ the graphite panel reflected 2.6 keV X-rays and the LiF panel 4.4 keV X-rays. It may also be noted that the Ariel-V crystal panels were steerable so that a range of Bragg angles (from ≈ 25 to 70°) could be obtained. This facility allowed detection of X-ray energies, according to the position of the crystal from ≈ 2 to 3.5 keV for the graphite system, and from ≈ 3.5 to 7.7 keV for the LiF system. Only the low polarisation sensitivity (i.e. small m , effective area, and signal to noise ratio) prevented this small broad band potentiality from becoming a practical proposition for the Ariel-V polarimeter.

It is interesting to speculate, with the publication of Stark and Connors (1977) requirements for broad band polarimetry to test for a black hole (and also general relativity) (see § 6.1), that future

polarimeters with the desired characteristics discussed here in § 6.2, might be capable of a suitable broad band sensitivity. From Stark and Connors' paper it seems that even a moderate energy band from about 2 to 20 keV, or perhaps less, would be adequate to perform significant tests (see § 6.1).

Two different potential methods for such broad band polarimetry have already been revealed:-

- i) Use of different crystal materials, and
- ii) Use of a scan range of Bragg angles.

Also, not previously discussed here, is the possibility of

- iii) Use of higher orders of reflection.

i) Use of different crystal materials

For this method, a simple configuration of adjacent segments of different crystal materials around a circle may be envisaged, as depicted in Fig. 6.2.1d. At the most sensitive Bragg angle of 45° , the energy range of 1st order Bragg reflected X-rays is limited by suitable crystal materials. Novick (1975), from a selection of many crystal materials, gives some calculated and measured R_c values for crystals having the highest reflectivities and for some commonly used in X-ray analysis. He gives an energy range for the calculated values from Mica at 0.88 keV to LiF at 4.4 keV. However, it may be possible that this quite severe high energy limit could be extended to near 10 keV by other crystal materials (Evans 1977, private communication).

The energy range made available by this method also provides a base from which it may be extended by use of the Bragg angle scan and higher order reflection methods discussed below.

ii) Use of a scan range of Bragg angles

Theoretically, from § 3 equation (3) that

$$E = \frac{nhc}{2d} \frac{1}{\sin \theta_B} \left[\frac{1}{10^3 e} \right] \quad (\text{keV}) ,$$

no limit exists for the achievable energy range from use of this method.

However, several practical problems can be immediately envisaged:-

- 1) A decrease in modulation factor m , for Bragg angles away from 45° .
- 2) A decrease in projected collection area for decreasing Bragg angles.
- 3) The capability of a detector to operate efficiently over a large energy range (see Novick 1975).

The above losses in instrument sensitivity are also likely to be compounded by large decreases in source flux as measurements at higher energies are attempted.

The extent to which these problems become serious will largely depend upon how much the demands of energy range can be satisfied by capabilities for increased collecting area and signal to background ratio.

It can be seen from Fig. 6.2.1a that mechanical movement of this curved crystal panel to different Bragg angles will give some capacity for 'broad band' polarimetry.

Also, Fig. 6.2.1b depicts a somewhat natural broad band polarimeter since several Bragg angles are simultaneously selected. Then, if the points a, b and c are not chosen to be coincident it may be envisaged that a position sensitive detector will enable polarisation measurements to be performed simultaneously at different energies. Conversely, if a, b and c are coincident, then it may be envisaged that pulse height analysis from the detectors will re-separate the data into discrete energy levels. Comparison between position sensitive detection and pulse height analysis,

based upon optimisation of signal to background and required energy resolution, would be desirable for choice of the most efficient. However, for this dispersive focusing system, it can be foreseen that further scanning by mechanical means analogous to that proposed for the curvature depicted in Fig. 6.2.1a would create problems, since the curvature-focusing geometry would become distorted.

iii) Use of higher orders of reflection

From use of $n = 2, 3$ etc., in § 3 equation (3), it can be seen that the energy of reflected X-rays will be respectively double, and triple etc., that for 1-st order reflection. Usually, however, the integrated reflectivity R_c is only large for 1-st order reflection (Evans et al. 1977), though Weisskopf et al. (1976) has reported a relatively large value of R_c of 5×10^{-4} radians for graphite at $n = 2$ (c.f. 9×10^{-4} at $n = 1$) suitable for practical X-ray astronomical polarisation measurements using a large area focusing polarimeter. If similar R_c values exist at other than 1-st order reflection for other crystal materials, where the 1-st order reflection energy is relatively high, then this method would be useful for much greater energy polarisation measurements than has been previously possible with a Bragg crystal instrument (e.g. if a crystal such as LiF has a suitable reflection at $n = 2$, then polarisation measurements at ≈ 9 keV could be performed).

In summary, from the 3 methods of broad band polarimetry discussed, it would seem that use of different crystal materials and also 2-nd order reflection could produce a useful energy range from, say, 1 to 9 keV. This moderate energy range, even without further extension, would be useful for performing tests of Stark and Connors' theory.

Also, re-orientation of crystal surfaces to different Bragg angles could expand the above energy range if the curvature shown in Fig.

6.2.1a is employed. Also, a similar extension to energy range using both types of curvature shown by Fig. 6.2.1c should be possible.

A quantitative estimate of a practical size of Bragg crystal instrument required to achieve reasonable broad band sensitivities of $\approx 0.67\%$ for observation of Cyg X-1 was made. Such polarisation sensitivities should be sufficient to provide a test of a black hole model for this source. It was assumed for convenience, that the required observation time should be suitable for operation on board a space shuttle flight of duration 7 to 14 days. Experiment parameters compatible with Ariel-V's, and a background level reduction compared with the Ariel-V polarimeter of $1/20$ by use of non-dispersive focusing only, were also assumed. Then, with these assumptions, it was found that by collection of 2-nd order reflected X-rays from a 'LiF' crystal system of projected area $\approx 9000 \text{ cm}^2$ at $\theta_B = 45^\circ$, that only a total of 7 days continuous observation would be required for polarisation measurements of the above sensitivity at 9, 12 and 18 keV. For occurrence of 50% Earth eclipse, say, then ≈ 14 days would be required. Collection of the 1-st order reflected X-rays also, would simultaneously provide measurements at 4.5, 6 and 9 keV and possibly at greater sensitivities. Such a projected collection area of $\approx 9000 \text{ cm}^2$ could be contained within a cylinder of radius and depth $\approx 54 \text{ cm}$. The estimated experiment parameters, Cyg X-1 intensity, and the calculated observation durations and expected signal to noise ratios for each of the 9, 12 and 18 keV observations are set out in Table 6.2.2. The expected signal to noise ratios of 10, 8.5 and 4.5 for the 9, 12 and 18 keV observations respectively are healthy values, although independent observation of the background to determine the extent of any background modulations would be necessary. With the envisaged low background count rate of $0.05 \text{ counts s}^{-1}$ an ≈ 0.5 day background observation would be required to be able to reduce any possible background induced spurious

Table 6.2.2: Estimate of broad band capability of 9000 cm² projected area, Bragg crystal, polarimeter observing the black hole candidate X-ray source Cyg X-1.

Energy (keV)	θ_B	$I(E)^*$ Cyg X-1 $\left(\frac{n}{Crab} = \frac{2}{2.6 \text{ keV}}\right)$	m	**** R_C (LiF, n=2) $\left(\frac{\text{Graphite}}{n=1}\right)$	** rel. eff.	*** S_0 (n=2) cts s ⁻¹	Reqd. obs. time for 1- σ error (n=2) + 0.67%	S_0/B_0 (n=2)	
4.5	9	45°	0.11	1	0.22	≈ 1.5	.51	1.5d	10
6	12	30°	0.095	0.6	0.22	1.3	.43	1.8d	8.5
9	18	20°	0.08	0.26	0.22	0.8	.22	3.8d	4.5
Total =								7.1d	

* Units (keV keV⁻¹ cm⁻² s⁻¹)

** Estimate of relative efficiency of detector for 2-nd order reflected X-rays compared with Ariel-V at 2.6 keV, which was ≈ 0.6.

*** Calculated from § 4.2.3 equation (130b).

**** Assumes crystal material LiF or similar, exists with appropriate R_c value ratio of 5/9 for n = 2 c.f. n = 1. Ratio taken, as example, from Weisskopf et al. (1976).

polarisation modulation to less than about $\pm 0.67\%$ for the worst case 18 keV observation.

In general, for other sources, the achievable polarisation sensitivities will depend upon the source intensity at high X-ray energies. For Cyg X-1 at 18 keV its intensity ($\text{keV keV}^{-1} \text{ cm}^{-1} \text{ s}^{-1}$) was estimated at ≈ 0.08 of that of the Crab Nebula at 2.6 keV, and therefore equivalent to observing X-rays at an intensity of ≈ 70 UFU centred at the appropriate Bragg reflection energy.

Finally, it is to be remembered that there are types of polarimeter other than Bragg reflection. Novick (1974, 1975) refers to a Lithium scattering polarimeter capable of achieving high sensitivity over a large range of energies. Novick also refers, amongst other possibilities, to multilayer reflector systems from which it is reported that high degrees of reflectivity may be obtained at even normal incidence. This seems an intriguing possibility for which future work, even of a preliminary nature, would be welcomed.

§ 6.3 FUTURE X-RAY POLARIMETRY

Already mentioned in § 2 were two small NRL polarimeters scheduled to be flown on forthcoming DOD 'Solrad' missions.

However, recently, Novick (1975) has described a large X-ray polarimeter designed to study solar flares, which has been proposed for the new NASA Solar Maximum Mission. This polarimeter is a sophisticated scattering device using LiF, and reported capable of attaining MDP values around 5% for 20 s of data for a class 1B solar flare over a broad energy range $\approx 8 - 50$ keV, and only slightly less sensitive for the integrated bands 5 - 8 keV and 50 - 100 keV. Similar sensitivity is predicted for X-ray polarisation measurements in only 1 s during rapid time variations of the impulsive phase of a hard X-ray burst. Such a polarimeter should be capable of performing sensitive measurements relevant to theories of solar flare emission for which the predicted energy dependence varies considerably.

Novick (1975) also reported a large Bragg crystal polarimeter that might be flown on an Aries rocket, an explorer satellite, or the Shuttle. This instrument, depicted in Fig. 6.3.1, consists of a 1 m diameter circle of crystal panels, with a multi-anode proportional counter at the focal point. (Further descriptive details are contained in Novick (1975)). The predicted performance of this instrument is illustrated by Figs. 6.3.2a and b. If this polarimeter is flown it could certainly provide good polarimetric data on a large number of interesting and important sources.

Andresen et al. (1976) describe European designs of spectrometer/polarimeters for photon energies above 2 keV, suitable for use on Spacelab via the forthcoming Shuttle launch facility. Such instruments, it is expected, will be flown on short duration (10 - 30 day) missions. Three

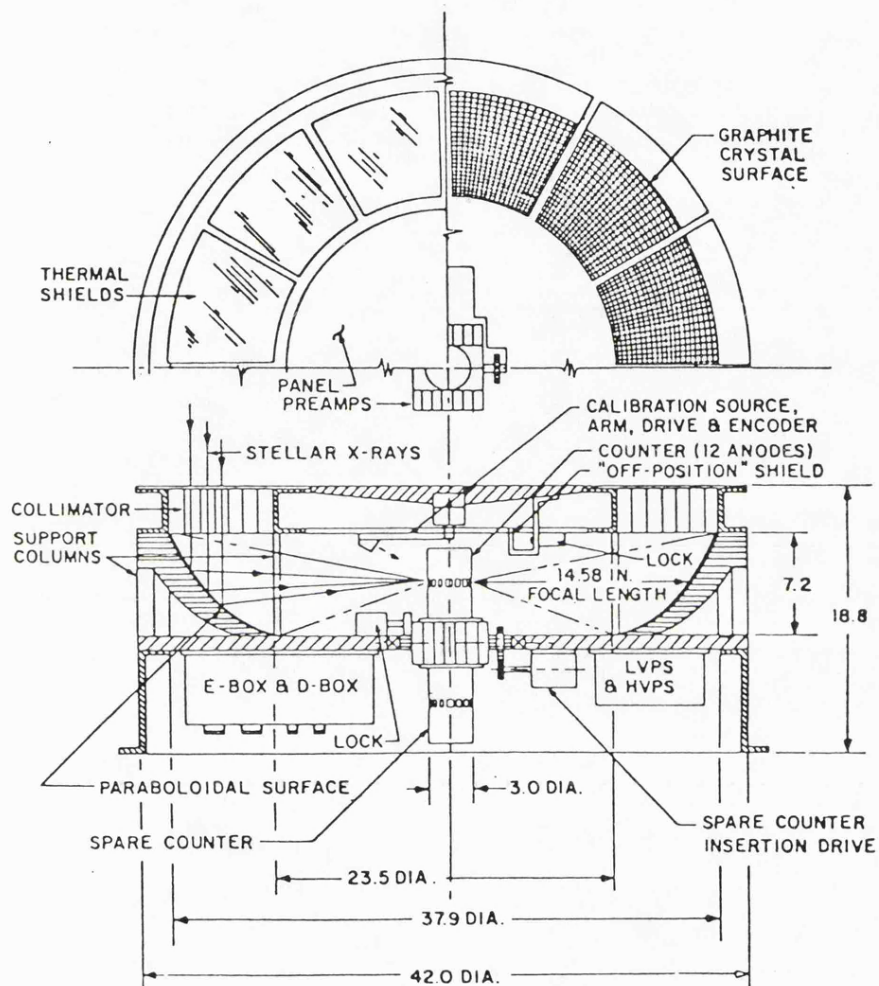
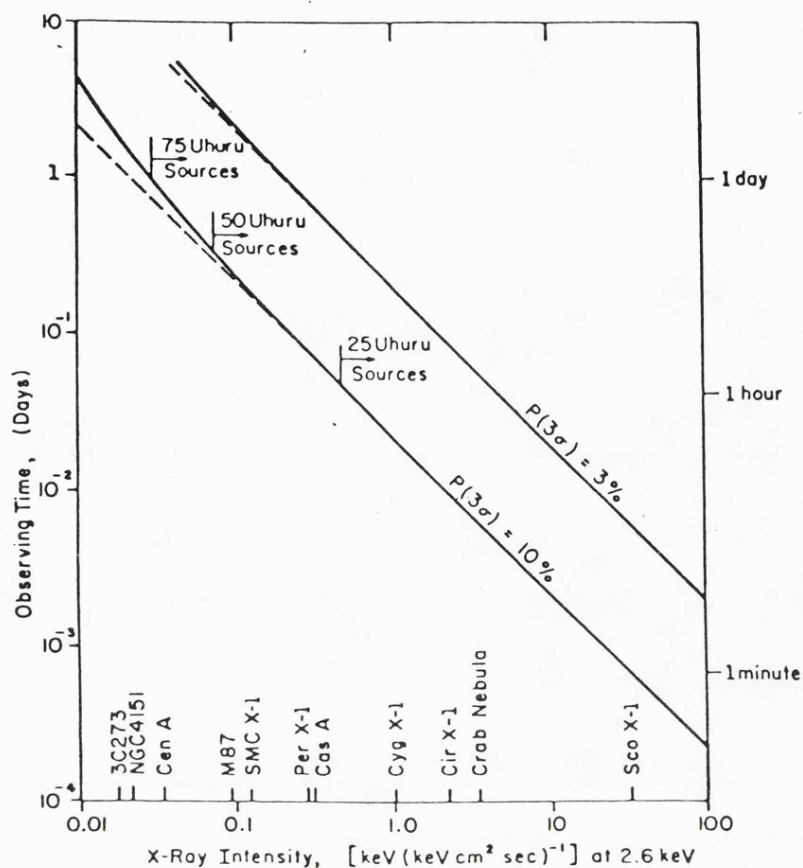
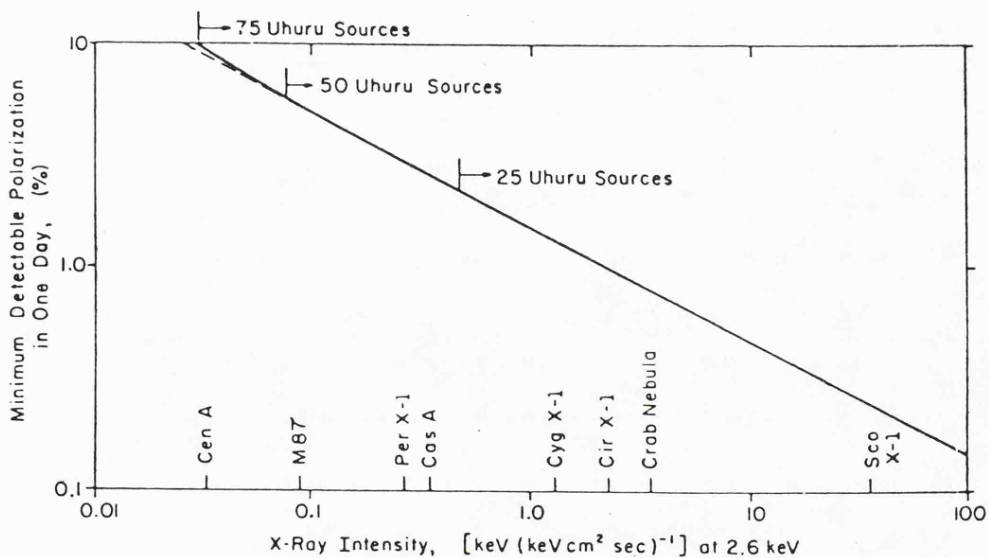


Fig. 6.3.1: Columbia university 12-segment, graphite, Bragg crystal polarimeter which might be flown on an Aries rocket, Explorer satellite or the Shuttle (from Novick 1975).

Fig. 6.3.2: Predicted performance of (Fig. 6.3.1) Columbia university polarimeter (from Novick 1975).



(a) Sensitivity curves for the 12-segment focusing graphite crystal polarimeter. The ordinate corresponds to the observing time in days required to reach either 3% or 10% ($3\text{-}\sigma$) limits on the polarization for sources having 2.6-keV intensities shown on the abscissa. The strengths of a number of interesting sources are given on the abscissa, and the number of *Uhuru* sources that can be studied at three different intensity levels are shown on the 10% curve.



(b) Sensitivity curve for the 12-segment focusing graphite crystal polarimeter showing the minimum detectable polarization at the $3\text{-}\sigma$ level in one day of observing time as a function of the source intensity at 2.6 keV. Shown on the abscissa are the intensities of a number of interesting and important X-ray sources. Also shown on the curve are the number of *Uhuru* sources that can be observed at three different intensity levels.

different instruments are described. The first is a doubly curved focusing instrument consisting of 6 separate panels, each curved analogously to that illustrated by Fig. 6.2.1c, and set in a circle. With this instrument a total projected area of $15,600 \text{ cm}^2$ could be made available for polarisation studies at $\theta_B = 45^\circ$ (an increase of ≈ 100 compared with the Ariel-V polarimeter.) The predicted signal to background ratio for an observation of the Crab Nebula of ≈ 260 makes this ≈ 3500 times greater than that for the Ariel-V instrument. Thus, the vast increase in sensitivity for this instrument is such that for only an 8 UFU source it is reported that an X-ray polarisation of 5% could be registered in an observing time of 10^4 s ($\approx 3\text{h}$). A collimator of 5° FWHM is to be used with this instrument, though if observations are to be made of sources lying in the galactic plane such a coarse collimator could mean difficulty in excluding more than one source from the f.o.v., with the possible consequences of resulting spurious modulations (see § 4.2.3). Secondly, a conical focusing crystal spectrometer is described which forms part of the previous instrument (see Fig. 6.3.3 for the layout of these two instruments). The crystal panels for this instrument have a total projected area of $14,400 \text{ cm}^2$ but are only curved in the non-dispersive ("spin") plane, therefore not allowing such potential for a reduced background and hence consequent loss of possible polarisation sensitivity, especially for observation of weak sources. The third instrument is described as a bent crystal spectrometer designed to study Fe line emission ($\approx 6.65 - 6.69 \text{ keV}$) using graphite crystals at Bragg angles around 16° , and this together with a 1500 cm^2 total projected area would make this instrument relatively insensitive to polarisation.

Also, perhaps, a more modest but sensitive polarimeter with broad band capabilities such as I have described earlier in § 6.2, flown aboard the Shuttle on an early 14 day mission and pointed at Cyg X-1

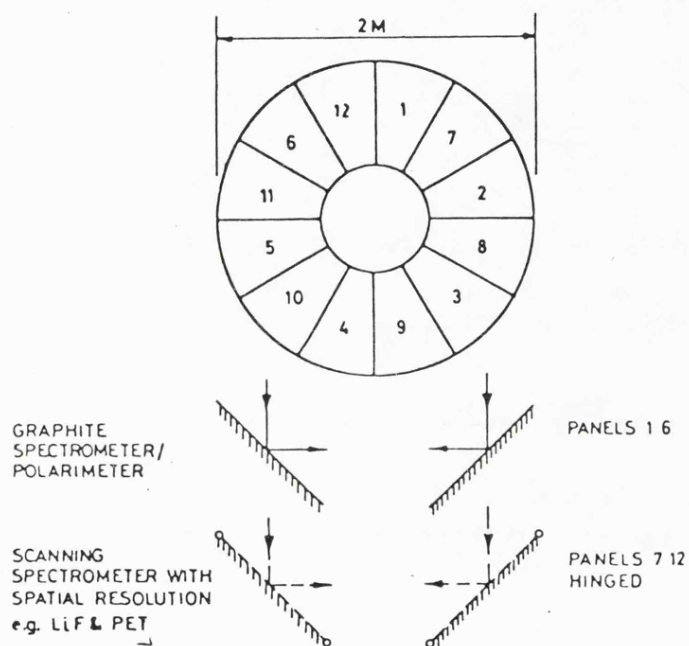


Fig. 6.3.3: European design of a medium energy spectrometer/polarimeter showing the layout of crystal panels for both doubly curved spectrometers/polarimeters and conically focusing scanning spectrometer (from Andresen et al. 1976).

could detect Stark and Connors' (1977) large, recently predicted general relativistic effects for a black hole believed to exist in this system. Such a polarimeter would also be capable of other highly sensitive measurements well beyond the capabilities of the Ariel-V and OSO-I instruments presently in flight.

These highly sensitive proposed instruments described here in § 6.3, when flown, would be eminently suitable for a vast expansion of X-ray polarisation measurements.

BIBLIOGRAPHY

- Anderson, T.W., 1971, "The Statistical Analysis of Time Series", Pub. by John Wiley and Sons, Inc., New York, U.S.A., pp. 102-110.
- Andresen, R.D., Brinkman, A.C., Beuermann, K., Culhane, J.L., Griffiths, R., Manno, V., Rocchia, R. and Whitcomb, G., 1976, Space Sci. and Instrumentation, 2, 325-337.
- Angel, J.R.P., 1969, Astrophys. J., 158, 219.
- Angel, J.R.P., Novick, R., Vanden Bout, P. and Wolff, R., 1969, Phys. Rev. Lett., 22, No. 16, 861.
- Angel, J.R.P., 1974, "Planets, Stars and Nebulae: Studied with Photopolarimetry". Ed. by Gehrels, T. Pub. University of Arizona Press, Tucson, Arizona, p. 54.
- Bahcall, J.N., 1975, "International Conference on 'X-rays in Space'" held at Univ. of Calgary, Aug. 14-21, 1974, Alberta, Canada T2N 1N4, Vol. 1, 147-162.
- Berthelsdorf, R., Linke, R.A., Novick, R., Weisskopf, M.C. and Wolff, R.S., 1973, Astrophys. Lett., 14, 171.
- Bevington, P.R., 1969, "Data Reduction and Error Analysis for the Physical Sciences", Pub. by McGraw Hill Inc., New York, U.S.A.
- Bowyer, S., Byram, E.T., Chubb, T.A. and Friedman, H., 1964, Nature, 201, 1307-1308.
- Burbidge, G.R., 1973, "X- and Gamma-Ray Astronomy", Ed. by Bradt, H. and Giacconi, R. Pub. by D. Riedel, Dordrecht-Holland/Boston-U.S.A., pp. 199-207.
- Burnight, T.R., 1949, Phys. Rev., 76, 165.
- Chandrasekhar, S., 1960, "Radiative Transfer", Dover Publications, N.Y.
- Charles, M.W. and Cooke, B.A., 1968, Nuclear Instr. and Methods, 61, 31.
- Chevalier, C., 1976, IAU Circular, No. 2957.
- Clarke, D., 1974, "Planets, Stars and Nebulae: Studied with Photopolarimetry". Ed. by Gehrels, T. Pub. University of Arizona Press, Tucson, Arizona, pp. 45-53.
- Clarke, D. and Grainger, J.F., 1971, "Polarised Light and Optical Measurement". Published by Pergamon Press.
- Coffeen, D.L. and Hansen, J.E., 1974, in "Planets, Stars and Nebulae: Studied with Photopolarimetry". Ed. by Gehrels, T., University of Arizona Press, Tucson, Arizona, p. 550.
- Compton, A.H. and Allison, S.K., 1935, "X-Rays in Theory and Experiment", Pub. by D. Van Nostrand Company, Inc., Princeton, New Jersey, U.S.A.

- Cowley, A.P. and Crampton, D., 1975, *Astrophys. J. Lett.*, 201, L65-68.
- Dailey, C.C. and Fishman, G.J., 1977, Reprint from March 1977 "NASA Report to Educators".
- Duerbeck, H.W. and Walter, K., 1976, *Astr. Astrophys.*, 48, 141-144.
- Eadie, G., 1977, Ph.D. Thesis, unpublished.
- Elvis, M., Griffiths, R.E., Turner, M.J.L. and Page, C.G., 1975a, *I.A.U. Circ.* 2814.
- Elvis, M., Page, C.G., Pounds, K.A., Ricketts, M.J. and Turner, M.J.L., 1975b, *Nature*, 257, 656-657.
- Evans, K.D. and Leigh, B., 1976, "The Absolute Calibration of the Reflection Integral of Bragg X-ray Analyser Crystals - Single Reflection Methods", *Space Sci. and Instr.*, in press.
- Evans, K.D., Hall, R., Lewis, M., Underwood, D. and Cooke, B.A., 1976, "Calibration Data for the Ariel 5 Bragg Spectrometer", *Sp. Sci. and Instr.*, in press.
- Evans, K.D., Hall, R. and Lewis, M., 1977, "The Calibration of Bragg X-ray Analyser crystals for use as Polarimeters in X-ray astronomy", *Sp. Sci. and Instr.*, 3, 163-169.
- Feynman, R.P., Leighton, R.B. and Sands, M., 1963, "The Feynman Lectures on Physics", pub. by Addison-Wesley, Vol. 1.
- Friedman, H., 1964, *Sci. Am.*, 210, No. 6, 36.
- Friedman, H., 1969, *Proc. Roy. Soc. London*, 313, 301.
- Friedman, H., Fritz, G., Henry, R.C., Hollinger, J.P., Meekins, J.F. and Sadeh, D., 1969, *Nature Phys. Sci.*, 221, 345.
- Gehrels, T., 1974, in "Planets, Stars and Nebulae: Studied with Photopolarimetry". Ed. by Gehrels, T. Pub. University of Arizona Press, Tucson, Arizona, p. 3.
- Giacconi, R., Gursky, H., Paolini, F.R. and Rossi, B.B., 1962, *Phys. Rev. Lett.*, 9, 439.
- Giacconi, R., 1973, *Phys. Today*, May Issue, pp. 38-47.
- Giacconi, R., 1974, "X-Ray Astronomy", ed. by Giacconi, R. and Gursky, H. (*Astrophysics and Sp. Sci. Lib.*, Vol. 43). Pub. D. Riedel, Dordrecht-Holland, pp. 155-168.
- Giacconi, R., Murray, S., Gursky, H., Kellogg, E., Schreier, E., Matilsky, T., Koch, D. and Tananbaum, H., 1974, *Astrophys. J. Suppl.*, 237, 27.
- Gibson, E.G., 1973, "The Quiet Sun", NASA Publication SP-303, Ch. 6, 297.
- Gnedin, Yu. N. and Sunyaev, R.A., 1974, *Ast. and Astrophys.*, 36, 379.

- Gorenstein, P. and Tucker, W.H., 1974, "X-ray Astronomy". Ed. by Giacconi, R. and Gursky, H. (Astrophysics and Sp. Sci. Lib., Vol. 43). Pub. D. Riedel, Dordrecht-Holland, pp. 155-168.
- Gottlieb, E.W., Wright, E.L. and Liller, W., 1975, *Astrophys. J. Lett.*, 195, L33-L35.
- Gould, R.J., 1967, *American J. of Phys.*, 35, 376.
- Griffiths, R.E., Cooke, B.A., Peacock, A., Pounds, K.A. and Ricketts, M.J., 1976a, *Mon. Not. R. astr. Soc.*, 175, 449.
- Griffiths, R.E., Ricketts, M.J. and Cooke, B.A., 1976b, *Mon. Not. R. astr. Soc.*, 177, 429-440.
- Grindlay, J.E., 1976, *Comments Astrophys.*, 6, No. 6, 165-175.
- Gursky, H., Giacconi, R., Paolini, F.R. and Rossi, B.B., 1963, *Phys. Rev. Lett.*, 11, 530.
- Gursky, H. and Schwartz, D., 1974, "X-Ray Astronomy". Ed. by Giacconi, R. and Gursky, H. (Astrophysics and Sp. Sci. Lib., Vol. 43). Pub. D. Riedel, Dordrecht-Holland, pp. 26-98.
- Gursky, H., 1975, "Workshop Papers for a Symposium on X-ray Binaries", Goddard Space Flight Centre, Greenbelt, Maryland, U.S.A., 353-361.
- Hiltner, W.A., Mook, D.E., Ludden, D.J. and Graham, D., 1967, *Astrophys. J.*, 148, L47.
- Hiltner, W.A. and Mook, D.E., 1970, *Ann. Rev. of Astr. and astrophys.*, 8, 139.
- Hutchings, J.B., 1975, "Proceedings of the Enrico Fermi Summer School", to be published.
- Kellogg, E.M., 1973, "X- and Gamma Ray Astronomy". Ed. by Bradt, H. and Giacconi, R. Pub. by Riedel, D., Dordrecht-Holland/Boston-U.S.A., 171-183.
- Kellogg, E.M., 1974, "X-Ray Astronomy". Ed. by Giacconi, R. and Gursky, H. (Astrophysics and Sp. Sci. Lib., Vol. 43). Pub. D. Riedel, Dordrecht-Holland, pp. 321-357.
- Kestenbaum, H., Angel, J.R.P., and Novick, R., 1971, *Astrophys. J.*, 164, L87.
- Korchak, A.A., 1967, *Soviet Phys.-Doklady*, 12, 192-194.
- Kristian, J., Visvanathan, N., Westphal, J.A. and Snellen, G.H., 1970, *Astrophys. J.*, 162, 475.
- Landstreet, J.D. and Angel, J.R.P., 1971, *Nature*, 230, 103.
- Lightman, A.P. and Shapiro, S.L., 1975, *Astrophys. J.*, 198, L73.

- Longaire, M.S. and Willmore, A.P., 1974, Mon. Not. R. astr. Soc., 168, 479-490.
- Matilsky, T., Bradt, H.V., Buff, J., Clark, G.W., Jernigan, J.G., Joss, P.C., Laufer, B., McClintock, J. and Zubrod, D., 1976, Astrophys. J., 210, L127-L131.
- Novick, R., Weisskopf, M.C., Berthelsdorf, R., Linke, R. and Wolff, R.S., 1972, Astrophys. J., 174, L1.
- Novick, R., 1974, "Planets, Stars and Nebulae: Studied with Photopolarimetry". Ed. by Gehrels, T. Pub. University of Arizona Press, Tucson, Arizona, p. 262.
- Novick, R., 1975, Sp. Sci. Revs., 18, 389.
- Page, C., 1976, Private Communication, Department of Physics, University of Leicester.
- Peacock, A., 1975, Ph.D. Thesis.
- Perrenod, S.C., 1976, Astrophys. J., 206, 876-882.
- Peterson, L.E., 1975, A. Rev. Astr. Astrophys., 13, 423.
- Pounds, K.A., 1970, Sci. J., 6, 61.
- Pounds, K.A., 1976a, Q.J. R. astr. Soc., 17, 218-220.
- Pounds, K.A., 1976b, Comments Astrophys., 6, No. 5, 145-156.
- Pounds, K.A., 1977, "The Ariel-V High Latitude Catalogue". To be published. Univ. of Leicester, England.
- Rees, M.J., 1975, Mon. Not. R. astr. Soc., 171, 457.
- Rees, M.J., 1977, Private Communication.
- Ricketts, M.J., 1976, Private Communication, Department of Physics, University of Leicester.
- Sargent, W.L.W., 1973, "X- and Gamma Ray Astronomy". Ed. by Bradt, H. and Giacconi, R., Pub. by D. Riedel, Dordrecht-Holland/Boston-U.S.A., pp. 184-198.
- Sartori, L. and Morrison, P., 1967, Astrophys. J., 150, 385-403.
- Schnopper, H.W. and Kalata, K., 1969, Astron. J., 74, 854.
- Shklovskij, I.S., 1960, "Cosmic Radio Waves", Pub. by Cambridge Mass.: Harvard Univ. Press, pp. 292-316.
- Silk, R.S., 1976, Ph.D. Thesis, University of Leicester.
- Skinner, G., 1976, Private Communication, University of Birmingham, England.
- Solar Geophysical Data 380 part 1, 26-29, April 1976, U.S. Department of Commerce, (Boulder, Colorado, U.S.A. 80302).

- Stark, R.F. and Connors, P.A., 1977, *Nature*, 266, 429-430.
- Tananbaum, H., Tucker, W.H., 1974, "X-ray Astronomy". Ed. by Giacconi, R. and Gursky, H. (*Astrophysics and Sp. Sci. Lib.*, Vol. 43). Pub. D. Riedel, Dordrecht-Holland, pp. 207-266.
- Tindo, I.P., Ivanov, V.D., Mandel'stam, S.L. and Shuryghin, A.I., 1970, *Solar Phys.*, 14, 204.
- Tindo, I.P., Ivanov, V.D., Mandel'stam, S.L. and Shuryghin, A.I., 1972, *Solar Phys.*, 24, 429.
- Tsunemi, H., Matsuoka, M. and Takagishi, K., 1977, *Astrophys. J.*, 211, L15-L18.
- Tsuruta, S., 1974, "Some Observational Tests for Possible Models of Her X-1: Pulse Shape and Polarisation", Preprint.
- Tsuruta, S., 1976, "Supercritical Accretion Model of Sco X-1". To be published. Max-Planck-Institut für Physik und Astrophysik, 8 München 40, Föhringer Ring 6, Germany.
- Turner, M.J.L., 1976, Private Communication, Department of Physics, University of Leicester.
- "UK-5 Flight Qualification Review", May 1973, Marconi Space and Defense Systems, Portsmouth.
- Underwood, J.H. and Neupert, W.M., 1974, *Solar Phys.*, 35, 241.
- Vaiana, G., Tucker, W., 1974, "X-Ray Astronomy". Ed. by Giacconi, R. and Gursky, H. (*Astrophys. and Sp. Sci. Lib.*, Vol. 43). Pub. D. Riedel, Dordrecht-Holland, pp. 169-205.
- Wampler, E.J., Scargle, J.D. and Miller, J.S., 1969, *Astrophys. J.*, 157, L1.
- Weisskopf, M.C., Cohen, G.G., Kestenbaum, H.L., Novick, R., Wolff, R.S. and Landecker, P.B., 1976, "The X-Ray Polarisation Experiment on the OSO-8", submitted for publication in "Proceedings of Symposium on X-Ray Binaries, held at NASA Goddard Space Flight Centre, Greenbelt, Maryland, U.S.A., October 20-22, 1975.
- Weisskopf, M.C., Cohen, G.G., Kestenbaum, H.L., Long, K.S., Novick, R. and Wolff, R.S., 1976b, *Astrophys. J.*, 208, L125-L128.
- Wolff, R.S., Angel, J.R.P., Novick, R. and Vanden Bout, P., 1970, *Astrophys. J.*, 160, Lett. 21.
- Wright, E.L., Gottlieb, W.E. and Liller, W., 1975, *Astrophys. J.*, 200, 171-176.

An upper limit to the linear X-ray polarization of Sco X-1

R. A. Gowen, B. A. Cooke, R. E. Griffiths
and M. J. Ricketts *X-ray Astronomy Group, Physics Department,
The University, Leicester*

Received 1976 October 11; in original form 1976 August 17

Summary. Sco X-1 was observed in a narrow band of X-ray energies centred on 2.6-keV from 1976 March 31 to April 10 with the *Ariel V* satellite, Bragg crystal spectrometer/polarimeter. This search for linear, X-ray polarization of Sco X-1 produced an upper limit of 7.7 per cent at three-sigma confidence. Modulations in the data which could lead to a spurious measurement of polarization were observed, and are discussed.

1 Introduction

Evidence confirming the binary nature of Sco X-1 (Gottlieb, Wright & Liller 1975; Wright, Gottlieb & Liller 1975; Cowley & Crampton 1975) increases the probability of expecting linear polarization associated with emission from a thin accretion disk, which can range up to ≈ 12 per cent (Chandrasekhar 1960; Rees 1975). Less aspherical models of Sco X-1, involving hot gas clouds, may be expected to exhibit degrees of polarization of about 1–5 per cent (Angel 1969). Tsuruta (1976) considers a binary model of Sco X-1 involving supercritical accretion, where candidates for the compact companion star are either a neutron star or a black hole. For this model, the X-ray generating mechanism is dominated by emission from the accretion disk during Sco X-1's optically dark phase ($B \gtrsim 12.8$) while during the bright phase (flaring, $B \lesssim 12.8$), a significant contribution may arise from an enveloping hot gas cloud. Thus, the degree of polarization could be dependent upon the intensity state of Sco X-1 during an observation.

Two previous observations of the linear X-ray polarization of Sco X-1 have been made. Angel *et al.* (1969) has reported a 20 per cent upper limit at \approx three-sigma confidence, and Kestenbaum, Angel & Novick (1971) measured the north–south component of polarization P_x as -1.7 ± 3.4 per cent, also consistent with Sco X-1 as an unpolarized source.

The more sensitive measurement described here produces a result which is in agreement with the two previous observations, and such that constraints can begin to be made on models of Sco X-1 which involve accretion-disk emission.

2 The spectrometer/polarimeter

The spectrometer polarimeter is of the Bragg crystal type and is mounted to view along the

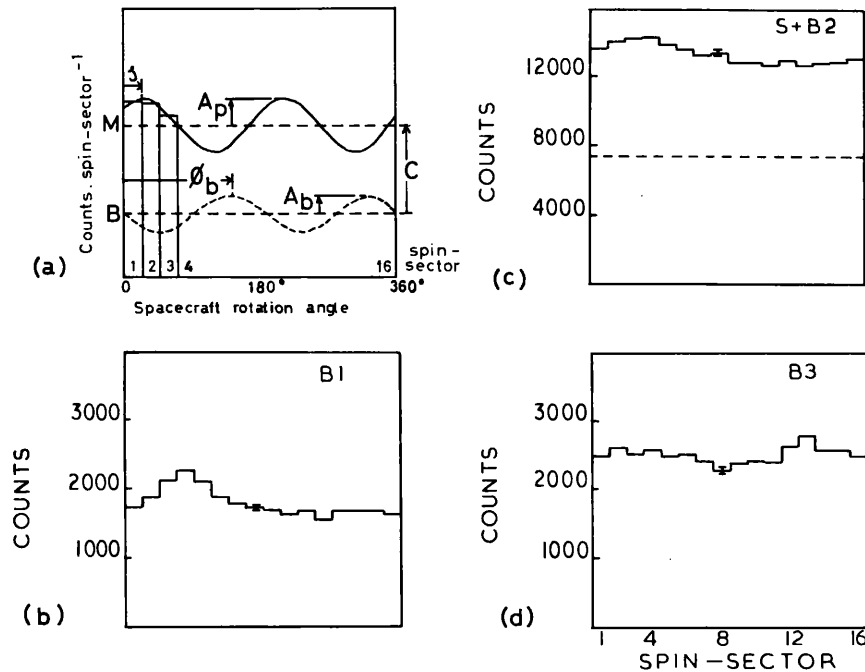


Figure 1. (a) Expected data format for an observation of a polarized X-ray source where a spurious 2nd-harmonic modulation A_b is present. (The observed amplitude A_{obs} is not shown, and is the superposition of the modulations A_b and A_p allowing for their respective phase differences.) (b), (c) and (d) Variation of summed data as a function of the spacecraft rotation angle. (Only data from that part of the satellite orbit, Sun-sectors S1–S4, for which the view to Sco X-1 is unobscured by the Earth is included in the summation.) The summed data from the first background observation (B_1) are depicted in (b), the source plus 2nd background data ($S+B_2$) in (c), and the third background observation (B_3) data in (d).

after the observation of Sco X-1. These were determined as $B_1 = 0.9235 \pm 0.0116$ count/s and $B_3 = 1.0336 \pm 0.0252$ count/s respectively, giving a value for B_0 of 0.9785 ± 0.0139 count/s. (A check that the background level did not vary significantly during the observation intervals was provided by data obtained from a part of the satellite orbit for which the Earth obscured the view to Sco X-1. Background levels from these regions remained constant to within one standard deviation).

From the calculated background count rate B_0 , the estimated background contribution during the source observation is shown by the dashed line in Fig. 1(c).

4.2.2 Estimation of spurious modulation amplitudes and phases

Modulation amplitudes and phases at the 2nd harmonic are illustrated for both the source and background data in Figs 2 and 3. (The source observation data has been divided into three equal sections SA, SB and SC to enable a clearer indication of any time variations. The summed data labelled Sun-sectors S1 to S4 arises from that part of the satellite orbit where there is a clear view of the celestial sky for the background observations, and to Sco X-1 for the source observation. For the Sun-sector S6–S11 summed data this view is obscured by the Earth so that all data from that region is background data.)

An interpolation procedure was used to obtain the background modulation amplitudes

SCO X-1 OBSERVATION, APRIL 1976

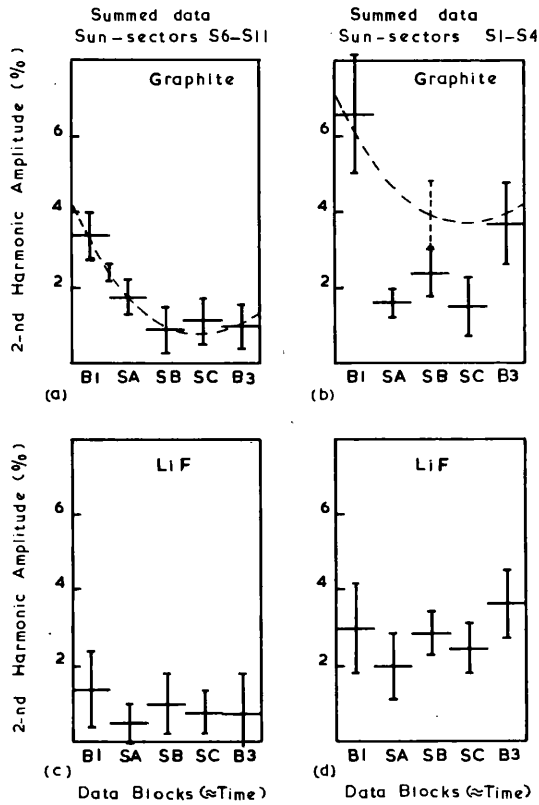


Figure 2. 2nd harmonic amplitude modulations plotted in chronological order of observation. (Dashed lines indicate best fit 2nd-order polynomials to the data. Error bars are one-sigma standard deviations).

and phases which existed during the source observation. Polynomials were fitted to the data time variations, and these are shown in Figs 2 and 3 as dashed lines with appropriate one-sigma error bars for each fit. (Data from the LiF crystal panel is shown since its low sensitivity to polarization is such that X-rays from Sco X-1 would only be expected to produce a modulation ≈ 4.5 times less than in the graphite data, and therefore provides an independent and more sensitive observation of background variations).

From the polynomial fits to the data, a background modulation amplitude of $A_B = 4.12 \pm 0.09$ per cent at a phase angle of $\phi_B = 1.30 \pm 0.23$ rad was obtained. (Information concerning the expected cause of the background data modulations may be obtained from Griffiths *et al.* (1976a).)

Other effects which could produce spurious modulations have been considered and found unlikely to be large enough to have had any significant effect upon the present observation. These considerations included; sources of X-rays in the instrument fov but offset from the satellite spin-axis, including the unpolarized component from Sco X-1; and also a periodic component in the intensity from Sco X-1. Friedman *et al.* (1969) has given an upper limit of 1 per cent to pulsed X-ray emission from Sco X-1 for periods ranging from 0.07 to 4 s which includes the half spin-period of the *Ariel V* satellite. Also, apart from Sco X-1, no other known X-ray source was in the instrument fov during the observations, and evidence from

SCO X-1 OBSERVATION, APRIL 1976

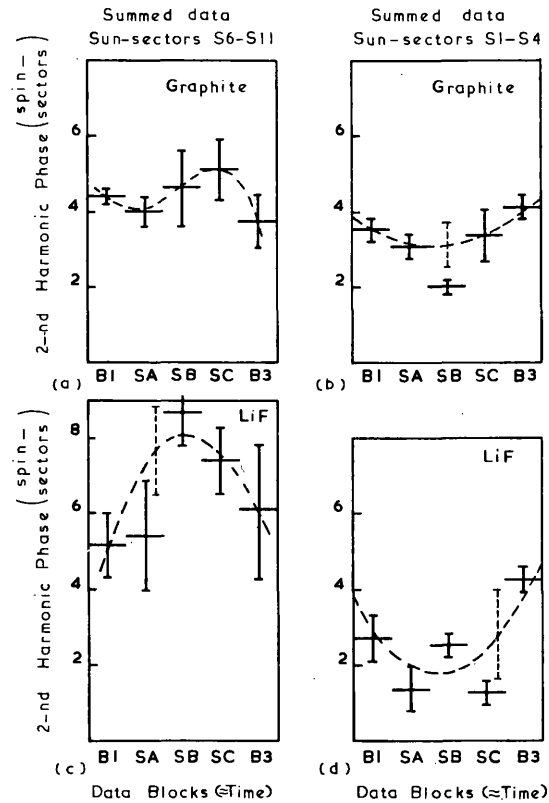


Figure 3. 2nd harmonic phase variations plotted in chronological order of observation. (Dashed lines indicate best fit polynomials to the best-fit 3rd order polynomial to (a), and 2nd order to (b), (c) and (d) data. Error bars are one-sigma standard deviations.)

other *Ariel V* data (Griffiths, Ricketts & Cooke 1976b) indicates that no significant modulation from the unpolarized component from Sco X-1 at a mean offset of 0.4° should arise.

4.3 CALCULATION OF THE POLARIZATION PARAMETERS FOR THE SOURCE SCO X-1

By subtracting the Stokes parameters for the background $S(b)$ from those of the background plus source measurement, the Stokes parameters $S(s)$ concerning the source were determined as

$$S(s) = \begin{pmatrix} I_s \\ Q_s \\ U_s \end{pmatrix} = \begin{pmatrix} 11974.64 \pm 217.78 \\ 274.97 \pm 204.95 \\ 45.93 \pm 260.62 \end{pmatrix}$$

where the errors given, as before, are one-sigma. These give a value of p , from equation (2), of 2.39 ± 1.78 per cent. Thus, an upper limit on p at three-sigma confidence is 7.7 per cent. This polarization result has been graphically displayed in Fig. 4 where the previous results of Angel *et al.* (1969) and Kestenbaum *et al.* (1971) are also displayed. The coordinate axes are

3-SIGMA UPPER LIMIT CONTOURS OF THE LINEAR, X-RAY POLARISATION OF SCO X-1

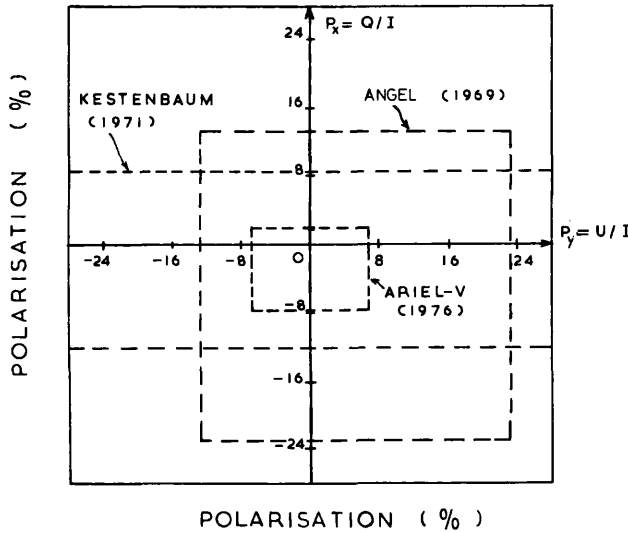


Figure 4. Three-sigma upper limit contours for the linear, X-ray polarization of Sco X-1.

P_x and P_y , where

$$P_x = Q_s/I_s = p \cos 2\theta$$

$$P_y = U_s/I_s = p \sin 2\theta$$

where θ is the position angle of the polarization. The calculated value of θ , where the mean position angle of the Sun was calculated as $95.1 \pm 0.7^\circ$, was $90.4 \pm 26.4^\circ$. The values of P_x and P_y were determined as -2.39 ± 1.78 per cent and -0.03 ± 2.21 per cent respectively, where the errors given are one-sigma.

5 Conclusions and discussion

The present result, consistent with Sco X-1 being an unpolarized X-ray source, is compatible with the two previous results from Angel *et al.* (1969) and Kestenbaum *et al.* (1971). This observation also reduces the previous upper limit to the degree of X-ray, linear polarization of Sco X-1 in any direction, to 7.7 per cent at \approx three-sigma confidence.

For binary system models of Sco X-1, calculations made by Chandrasekhar (1960) and confirmed by Angel (1969), for the limiting case where the optical depth $\tau \gg 1$ imply degrees of linear polarization for thin accretion-disk emission from 0 to 12 per cent dependent upon the viewing angle i between the accretion disk and the plane of the sky. The present upper limit of 7.7 per cent, for this case where $\tau \gg 1$, produces an independent upper limit of $i < 85^\circ$, consistent with Hutchings (1975) upper limit of $i < 65^\circ$ from considerations concerning the absence of X-ray eclipse features from Sco X-1. However, it is far from achieving the accuracy of the recent upper limit to i of 30° , produced by Perrenod (1976) who compares the light curve of Sco X-1 with predictions from a model in which the photosphere of a non-degenerate star is heated by X-rays from a degenerate companion. For an accretion disk which is not thin, and has more realistic values for τ , Angel (1969) has published values of polarization for averaged situations where $60 < i < 120^\circ$. However, in view of Perrenod's

result it would now be desirable, in the case of Sco X-1, to repeat Angel's calculations where i has particular values $< 30^\circ$. Also, from Perrenod's estimate of the likely value for i of $\approx 10^\circ$, Chandrasekhar's calculations indicate that the polarization expected will be only ≈ 0.1 per cent. Thus, it can be clearly seen that if future X-ray polarization measurements of Sco X-1 are to have relevance to accretion-disk models and confirming Perrenod's result, then they need to have a much greater sensitivity than the present observation. Also, higher values of X-ray polarization associated with flare emission from Sco X-1 are not excluded.

Acknowledgments

RAG, REG and MJR would like to thank the Science Research Council for their financial support.

References

- Angel, J. R. P., Novick, R., Vanden Bout, P. & Wolff, R., 1969. *Phys. Rev. Lett.*, **22**, 861.
Angel, J. R. P., 1969. *Astrophys. J.*, **158**, 219.
Chandrasekhar, S., 1960. *Radiative transfer*, Dover Publications, New York.
Clarke, D. & Grainger, J. F., 1971. *Polarized light and optical measurement*, Pergamon Press.
Cowley, A. P. & Crampton, D., 1975. *Astrophys. J. Lett.*, **201**, L85.
Evans, K. D., Hall, R. & Lewis, M., 1977. The calibration of Bragg X-ray analyser crystals for use as polarimeters in X-ray astronomy, *Sp. Sci. Instr.*, **3**, No. 2.
Friedman, H., Fritz, G., Henry, R. C., Hollinger, J. P., Meekins, J. F. & Sadeh, D., 1969. *Nature Phys. Sci.*, **221**, 345.
Gottlieb, E. W., Wright, E. L. & Liller, W., 1975. *Astrophys. J. Lett.*, **195**, L33.
Griffiths, R. E., Cooke, B. A., Peacock, A., Pounds, K. A. & Ricketts, M. J., 1976a. *Mon. Not. R. astr. Soc.*, **175**, 449.
Griffiths, R. E., Ricketts, M. J. & Cooke, B. A., 1976b. *Mon. Not. R. astr. Soc.*, **177**, 429.
Hutchings, J. B., 1975. *Lecture given at Enrico Fermi Summer School*, Varenna, Italy.
Kestenbaum, H., Angel, J. R. P. & Novick, R., 1971. *Astrophys. J. Lett.*, **164**, L87.
Novick, R., 1974. *Planets, stars and nebulae: studied with photopolarimetry*, p. 262, ed. T. Gehrels, University of Arizona Press, Tucson, Arizona.
Perrenod, S. C., 1976. *Astrophys. J.*, **206**, 876.
Rees, M. J., 1975. *Mon. Not. R. astr. Soc.*, **171**, 457.
Schnopper, H. W. & Kalata, N., 1969. *Astr. J.*, **74**, 854.
Stokes, G. G., 1852. *Trans. Camb. phil. Soc.*, **9**, 399; see also 1901, *Mathematical and physical papers*, vol. 3, Cambridge University Press.
Tsuruta, S., 1976. *Supercritical accretion model of Sco X-1*, Preprint.
Wright, E. L., Gottlieb, E. W. & Liller, W., 1975. *Astrophys. J.*, **200**, 171.

STELLAR X-RAY POLARIMETRY FROM THE ARIEL-V SATELLITE

ABSTRACT

X-ray polarisation observations from the Ariel-V satellite are described. Notably, an upper limit to the X-ray polarisation of Sco X-1 was produced, more sensitive than previous results had managed to achieve, and for which constraints could be placed upon models for the X-ray emission mechanism.

Analysis of the data provided strong empirical confirmation of the desirability for future polarimeters to incorporate some previously proposed design features. These include utilisation of focusing methods to allow a smaller detector, and hence a reduced background level; increased area of collection, so that much weaker X-ray sources may be usefully observed; and also sufficiently accurate pointing, narrow f.o.v. and a capability for simultaneous measurement of more than one component of linear polarisation, all to suppress possible spurious modulations. It would be expected that the advantages obtained by following the advocated design features would result in a polarimeter sufficiently sensitive to be able to measure X-ray polarisation from weak X-ray sources, and to achieve accuracies that have not yet been remotely approached.

Characteristics of a Bragg crystal instrument capable of a sufficient degree of broad band X-ray polarimetry to test for the existence of a fast rotating black hole in the Cyg X-1 system, are also described.

Finally, the need for X-ray polarisation measurements throughout the field of current X-ray astronomy is illuminated.